REALIZATION CALCULUS

Special Functions

Expanded visual guide

Packets, sequences, polyphase channels
and exact mathematical examples

Komorebi P.

How to use this guide

This guide develops the pictures into a sequence of worked mathematical lessons. It accompanies the consolidated manuscript and the eight original papers. Each lesson has one central figure, a formula, directions for reading the figure, a worked example, and a source-and-scope note.

The figures are produced by Python and Matplotlib from explicit formulas, finite matrices, declared quadrature, or bounded arithmetic sums. Vector diagrams describe exact relationships; numerical curves are labeled with their parameter ranges and approximation limits. Original source statements are interpreted through the correction register in the consolidated manuscript.

Route	What to follow
Foundations	Coefficient addresses, refinement, carry, detail banks, truncation, interference, moments, and parameter domains.
Papers I–III	Analytic packet reconstruction, Bernoulli–Hurwitz refinement, arithmetic depth, positive measures, Gamma limits, and spectral reduction.
Papers IV–VI	Time-average Gram lifts, signed rational models, log-Gamma windows, Fourier geometry, and continuous shape refinement.
Papers VII–VIII	Finite lowest-weight spaces, Casimir atlases, signed recoupling amplitudes, measurement channels, tree consistency, and q-deformation.
Synthesis	The precise bridges between the three kinds of packets, with examples that retain the hypotheses.
Sequence and signal atlases	OEIS families and transforms, exact polyphase operations, finite taps, filter banks, and streaming execution.
Bridges and capstone	Seeds, pole cancellation, operator contracts, complete residual calculations, information loss, model-based repair, and the streaming phase clock.

A first pass. Read the eight foundations, then the first three lessons of each paper. Return to the later lessons for the asymptotic, spectral, and representation-theoretic developments. The contents list every lesson so the guide also works as a reference.

Evidence scope. A plot illustrates a statement within its declared range. It does not prove an unbounded claim. The signed arithmetic obstruction remains open. The scalar-to-matrix q-Racah comparison remains a separate normalization task. Full analytic Lean formalization is not established by the available source evidence. These distinctions are taught at the points where they matter.

Contents

Foundations: Read the packet language **1**
1 An exponent becomes an address . . . 1
2 Refinement preserves every address . . . 2
3 Multiplication carries between packets . . . 3
4 A detail bank separates average and variation . . . 4
5 Separate routing error from truncation error . . . 5
6 Positive energy does not retain interference . . . 6
7 One measure creates a sequence of moments . . . 7
8 Parameters have different mathematical jobs . . . 8

Paper I: Exact lifts, Bernoulli refinement, and signed transfer **9**
9 A scalar germ has exact coefficient addresses . . . 9
10 Multiplication creates a carry . . . 10
11 The Euler operator remembers the full exponent . . . 11
12 A differential equation survives the lift . . . 12
13 Integer Bernoulli values sit inside an entire family . . . 13
14 A parent is exactly the sum of its children . . . 14
15 Detail phases preserve complete information . . . 15
16 Bernoulli and Euler share one channel bank . . . 16
17 A Wronskian can reject a broad conjecture . . . 17
18 Third-root norms remember parity . . . 18
19 Scale filters select an arithmetic window . . . 19
20 Coherence has a proved scale and an open estimate . . . 20

Paper II: Local germs, positive moments, and character geometry **21**
21 Stieltjes constants encode a detail's local slope . . . 21
22 A character packet returns an L-value . . . 22
23 Detail variance measures child disagreement . . . 23
24 A resultant compresses primitive detail channels . . . 24
25 The energy is a positive moment measure . . . 25
26 Every alternating difference layer is positive . . . 26
27 Hankel positivity is a Gram-space statement . . . 27
28 Positive mass gives a zero-free slit resolvent . . . 28
29 A zeta-ratio stencil exactly recovers the energy . . . 29
30 Squarefree counting fixes the energy scale . . . 30
31 The active coordinate approaches a Gamma law . . . 31
32 Distinct characters decohere at a fixed modulus . . . 32

Paper III: Jacobi models, endpoint limits, and the spectral edge **33**
33 The zero packet belongs to the positive contraction . . . 33
34 Generalized Hankel minors are strictly positive . . . 34
35 One measure determines a Jacobi recurrence . . . 35
36 A Gaussian node can lie between arithmetic atoms . . . 36

37 Four nodes preserve exactly eight moments . . . 37
38 Positive spectral weights have negative z-residues . . . 38
39 The two Gamma coordinates share all moment limits . . . 39
40 Fixed-degree packet polynomials become Laguerre . . . 40
41 The scaled Jacobi coefficients have a fixed point . . . 41
42 A shifted determinant has an explicit leading constant . . . 42
43 The kernel and Gaussian rule share the same limit . . . 43
44 The edge cusp follows conditionally from energy decay . . . 44

Paper IV: Arithmetic depth, time, and signed coordinates **45**
45 Keep the signs while changing depth . . . 45
46 Compute one coefficient in two coordinates . . . 46
47 Watch finite time extract the diagonal . . . 47
48 The positive kernel is a complex Gram matrix . . . 48
49 Use Beta to connect depth with Gamma . . . 49
50 Remove the carrier before comparing limits . . . 50
51 An exact envelope can have non-Gaussian tails . . . 51
52 Center the logarithmic frequency law . . . 52
53 Compare depth ratios before absolute depths . . . 53
54 Use the actual character modulus . . . 54
55 Change generating coordinates without losing signs . . . 55
56 State the signed Padé contract precisely . . . 56

Paper V: The log-Gamma phase-space atlas **57**
57 Normalize the log-Gamma window . . . 57
58 Build an ambiguity integral . . . 58
59 Separate magnitude from wrapped phase . . . 59
60 Raise shape and read its differential equation . . . 60
61 Transform the window into a Gamma envelope . . . 61
62 Read depth overlap as a characteristic function . . . 62
63 Resolve the negative Wigner lobes . . . 63
64 Project Wigner onto its probability marginals . . . 64
65 Compare uncertainty with orbit geometry . . . 65
66 Create orthogonal Laguerre packets . . . 66
67 Keep Fourier phases in the common ladder . . . 67
68 Extend the arithmetic depth continuously . . . 68

Paper VI: Shape composition and transfer **69**
69 Read shape through the logarithmic coordinate . . . 69
70 Separate shape affinity from local curvature . . . 70
71 Keep magnitude and phase in cross ambiguity . . . 71
72 Factor energy into two independent laws . . . 72
73 Add shapes by convolution . . . 73
74 Continuous shape produces jumps and cumulants . . . 74
75 Split one polynomial without losing energy . . . 75
76 Choose a refinement tree freely . . . 76

77 Read conditional transfer from its singular values . . . 77
78 A continuous coherent orbit resolves identity . . . 78
79 Positive smoothing can have unstable inversion . . . 79
80 Rescale shape toward a Gaussian heat kernel . . . 80

Paper VII: Classical recoupling packets **81**
81 A ladder begins with a positive shape . . . 81
82 Project a large excitation simplex . . . 82
83 See the lowest-weight plane . . . 83
84 Two observables select two atlases . . . 84
85 The middle shape controls a beam splitter . . . 85
86 An exact three-channel transform . . . 86
87 Phase changes a measured output . . . 87
88 A positive recurrence needs its own gauge . . . 88
89 A fixed measured channel spreads a law . . . 89
90 Tree coordinates have joint addresses . . . 90
91 What a pentagon check actually certifies . . . 91
92 Compile in the reduced dimension . . . 92

Paper VIII: q-deformation and scalar bridges **93**
93 Replace a linear number by a q-number . . . 93
94 The coproduct routes lowering events . . . 94
95 A q-Hahn seed keeps signs and weights . . . 95
96 Deform both a spectrum and an atlas . . . 96
97 An exact q-coordinate reaches a swap . . . 97
98 Two-channel mixing has a monotone gap . . . 98
99 Higher-level row entropy can decrease . . . 99
100 Differentiate a complete coordinate transform . . . 100
101 Approach the classical atlas carefully . . . 101
102 q-trees need more than loop closure . . . 102
103 A scalar table is a separate comparison . . . 103
104 Check a shifted Askey–Wilson operator . . . 104

Synthesis: Connections across the eight papers **105**
105 Three reconstruction contracts . . . 105
106 Arithmetic parameters become a shape . . . 106
107 A diagonal lift removes arithmetic signs . . . 107
108 A binary refinement becomes a tree . . . 108
109 Positivity needs a specified measure . . . 109
110 Match the evidence to the question . . . 110

Sequence atlas: OEIS families and exact transforms **111**
111 Two seeds, one Fibonacci recurrence . . . 111
112 Longer recurrence memory . . . 112
113 Jacobsthal separates two modes . . . 113
114 A Pell pair shares one unit . . . 114

115 Normalize central binomial coefficients . . . 115
116 Catalan convolution rebuilds the next term . . . 116
117 Bell numbers are Stirling row sums . . . 117
118 Factorial weights order the blocks . . . 118
119 Derangements show signed cancellation . . . 119
120 Secant and tangent interleave . . . 120
121 Bernoulli data need both coordinates . . . 121
122 Partitions multiply reciprocal factors . . . 122
123 Apéry uses taps that depend on the index . . . 123
124 Divisor convolution changes the address rule . . . 124
125 One binary statistic creates three families . . . 125
126 Sums and differences form a polynomial ladder . . . 126

Polyphase atlas: Channels, refinement, and transfer **127**
127 Split Fibonacci into three actual streams . . . 127
128 Weave the three streams back together . . . 128
129 Two Fibonacci channels share one denominator . . . 129
130 Every Fibonacci stride has a jump recurrence . . . 130
131 Complex phases select one residue . . . 131
132 Refine even and odd into six coefficient streams . . . 132
133 Different refinement orders reach the same coefficient . . . 133
134 Three carries produce one block delay . . . 134
135 Polynomial multiplication has visible residue carries . . . 135
136 An exponential generating function changes the weights . . . 136
137 Parity separates secant and tangent counts . . . 137
138 Thue–Morse refines by copying and complementing . . . 138
139 Binary weight keeps the affine increment . . . 139
140 A Haar bank preserves average and detail together . . . 140
141 One retained channel cannot identify the original . . . 141
142 A complete operation agrees along both routes . . . 142

Tap atlas: Finite weights and exact execution **143**
143 Read a tap as a delayed contribution . . . 143
144 Execute the taps on Fibonacci numbers . . . 144
145 Turn three taps into a two-phase matrix . . . 145
146 Locate the delay when a tap wraps a block . . . 146
147 Route a finite filter through four phases . . . 147
148 Compose filters before or after phase splitting . . . 148
149 Use signed taps as finite differences . . . 149
150 Let recurrence taps expose initial data . . . 150
151 Give the two Fibonacci phases different numerators . . . 151
152 Separate finite taps from an infinite reciprocal response . . . 152
153 Read frequency response from the tap polynomial . . . 153
154 Expose the delay carried by symmetric taps . . . 154
155 Reconstruct exactly with Haar analysis and synthesis . . . 155

156 Reverse signed prediction and update steps . . . 156
157 Resample at rate three over two by exact routing . . . 157
158 Carry the needed state across chunk boundaries . . . 158

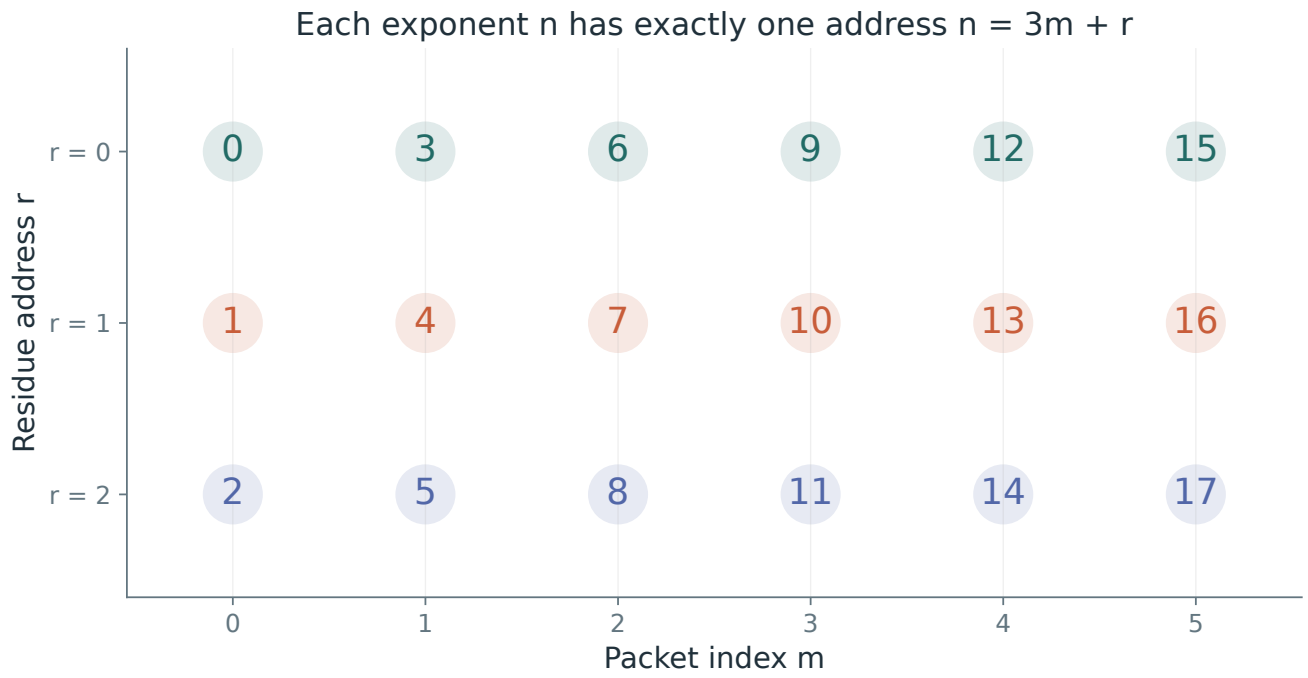
Operator bridges: Seeds, responses, and coefficient transforms 159
159 Seeds choose which modes survive . . . 159
160 Compile taps against an exact recurrence . . . 160
161 A formal reciprocal need not be a stable filter . . . 161
162 Coefficient division becomes an area average . . . 162

Operator contracts: Normalization, translation, and boundaries 163
163 Transport the operator with the normalization . . . 163
164 Bernoulli resolves a discrete antiderivative . . . 164
165 The boundary changes what an inverse can recover . . . 165

Worked capstone: One record through channels, residuals, and repair 166
166 A finite record leaves endpoint impulses . . . 166
167 Transfer the whole residual into three channels . . . 167
168 An interior perturbation has its own signature . . . 168
169 A discarded channel returns through the next operation . . . 169
170 Repair with a declared recurrence model . . . 170
171 Keep the history and the phase clock . . . 171

FOUNDATIONS / 01 **LESSON 1**

An exponent becomes an address



$$n = Mm + r, \qquad F_{M,r}(u) = \sum_{m \geq 0} a_{Mm+r} u^m$$

Read the figure. Read each row as a residue class and each column as its internal index. The figure lists the first eighteen exponents at modulus three. Every number occurs once. The row selects a packet; the column tells that packet where the coefficient belongs.

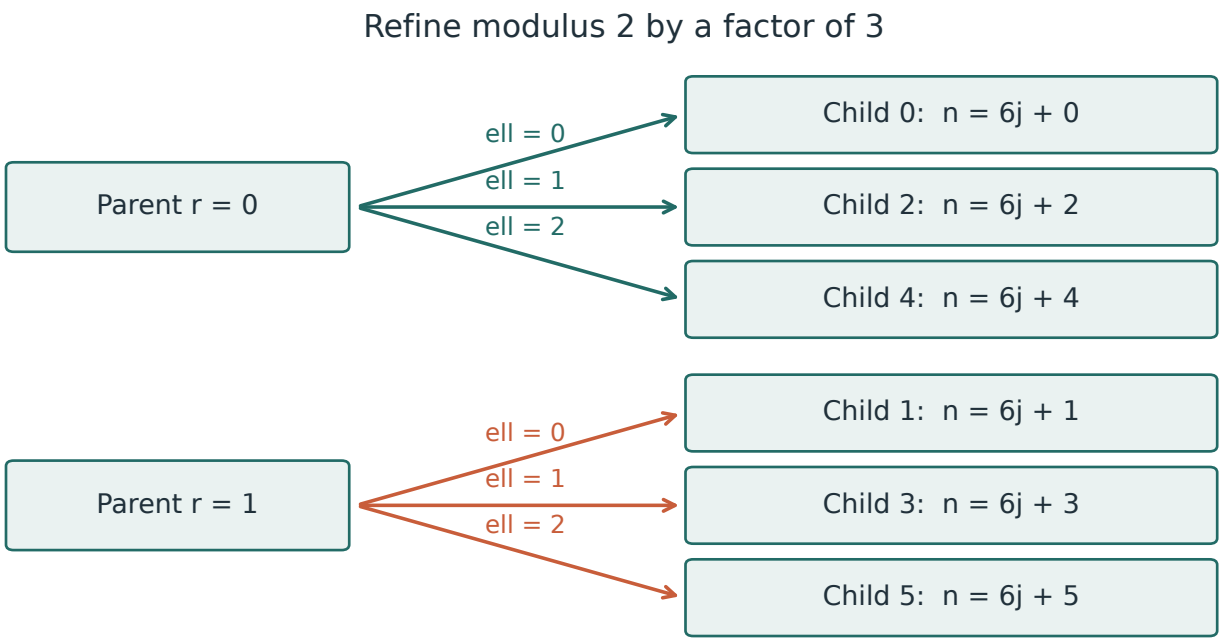
Work an example. For exponent 14, divide by three: $14 = 3 \cdot 4 + 2$. Its coefficient is the coefficient of u^4 in $F_{3,2}$. Multiplying this term by z^2 and substituting $u = z^3$ restores $a_{14} z^{14}$. No coefficient has been averaged or discarded.

Carry forward. A packet address is a reversible coordinate for a coefficient. It is useful before any special-function identification is made.

Source and scope. Paper I, "Residue-section functions" and "Exact polyphase reconstruction." The displayed address table is exact integer arithmetic.

FOUNDATIONS / 02 **LESSON 2**

Refinement preserves every address



$$F_{M,r}(u) = \sum_{\ell=0}^{L-1} u^{\ell} F_{LM,r+M\ell}(u^L)$$

Read the figure. Start at either parent on the left and follow its three arrows. Refining modulus two by three produces modulus six. The children of the even parent are addresses $0, 2, 4$; those of the odd parent are $1, 3, 5$. The factor u^{ℓ} keeps the child offset.

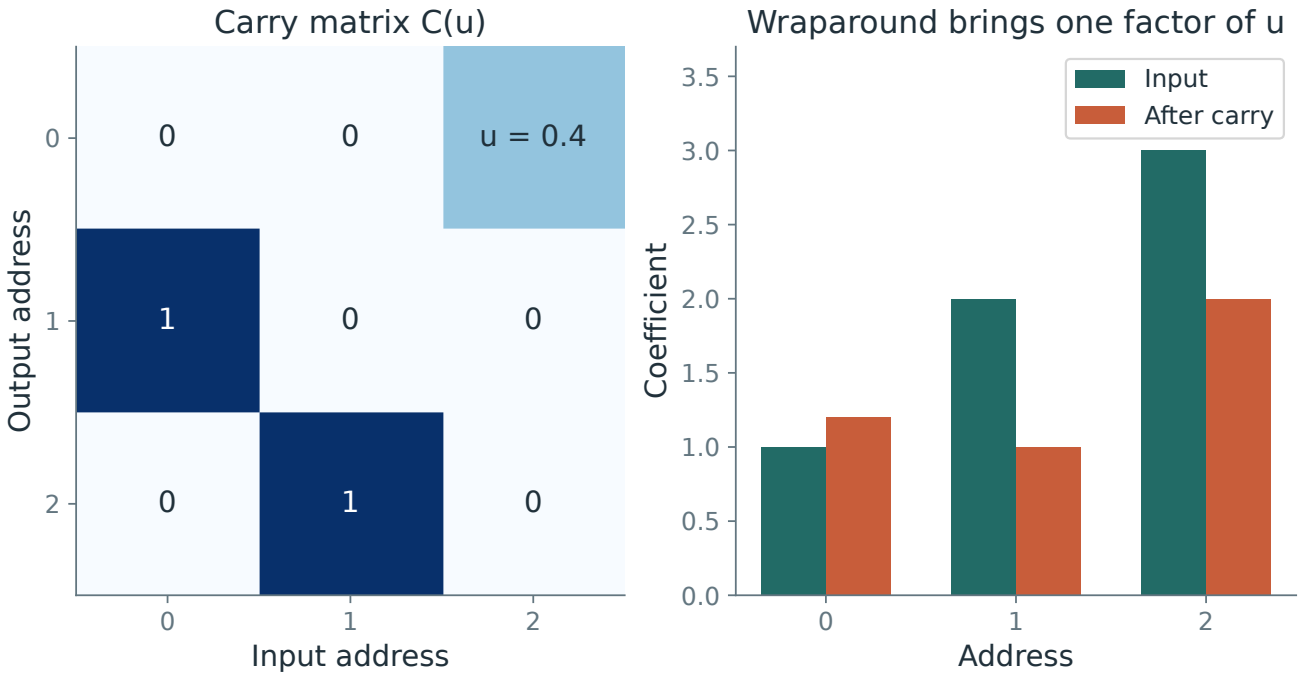
Work an example. Take $M = 2$, $r = 1$, and parent index $m = 7$. Split $7 = 3 \cdot 2 + 1$. The original exponent is $2 \cdot 7 + 1 = 15$, and its refined address is $6 \cdot 2 + 3 = 15$. The coefficient passes to child $r + M\ell = 3$ at internal index two.

Carry forward. Refinement reorganizes the same coefficients. Parent and child indices must be tracked together.

Source and scope. Paper I, "Parent-child refinement" and the coefficient refinement identity in the consolidated manuscript. This diagram uses $M = 2$, $L = 3$.

FOUNDATIONS / 03 **LESSON 3**

Multiplication carries between packets



$$C_3(u) = \begin{pmatrix} 0 & 0 & u \\ 1 & 0 & 0 \\ 0 & 1 & 0 \end{pmatrix}, \qquad \mathcal{S}_3(C_3 f) = z\mathcal{S}_3(f)$$

Read the figure. Read matrix columns as input addresses and rows as output addresses. Multiplication by z advances addresses zero to one and one to two. Address two wraps to zero, bringing one factor of $u = z^3$. The right panel evaluates this carry at $u = 0.4$.

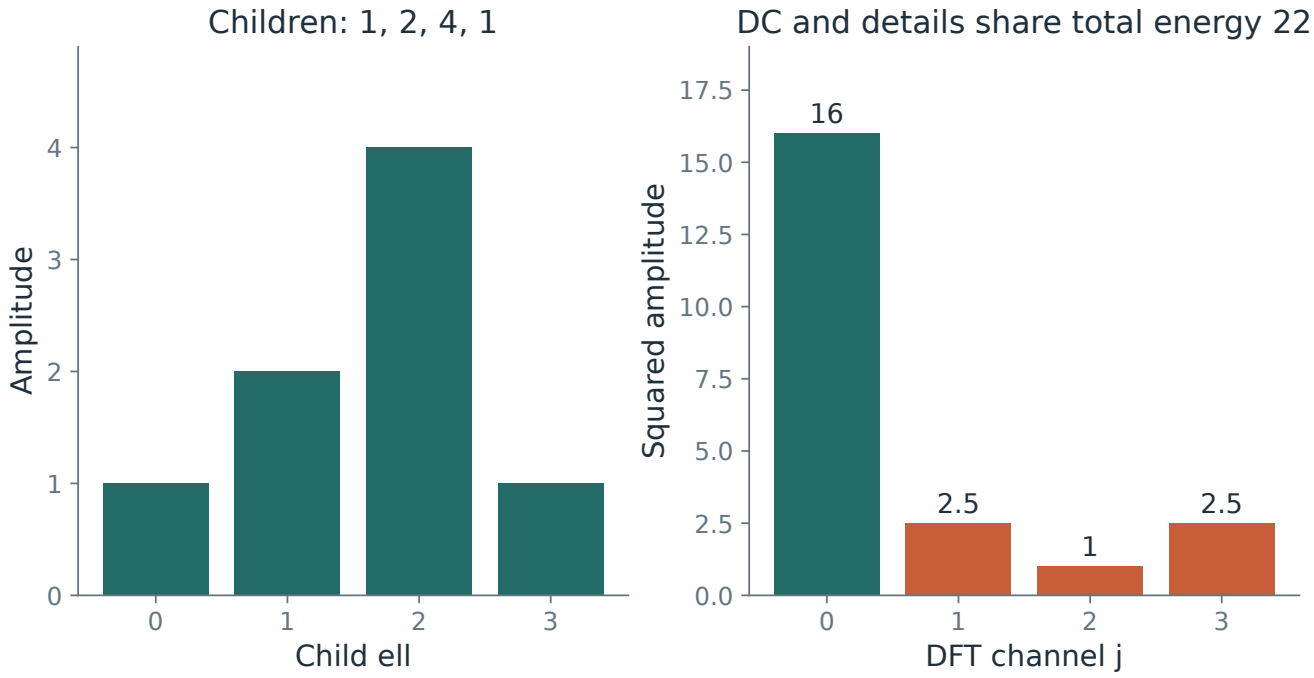
Work an example. For the constant packet vector $(1,2,3)^T$, synthesis gives $1 + 2z + 3z^2$. The carried vector is $(3u,1,2)^T$, whose synthesis is $3z^3 + z + 2z^2$. This is exactly $z(1 + 2z + 3z^2)$. At $u = 2/5$, its entries are $(6/5,1,2)$.

Carry forward. A scalar operation can become a small matrix operation, with the wrap recorded explicitly.

Source and scope. Paper I, "Intertwining laws." The matrix and polynomial identity are exact; the bars evaluate one rational parameter.

FOUNDATIONS / 04 **LESSON 4**

A detail bank separates average and variation



$$W_j = L^{-1/2} \sum_{\ell=0}^{L-1} e^{-2\pi i j \ell / L} b_\ell, \qquad \sum_j |W_j|^2 = \sum_\ell |b_\ell|^2$$

Read the figure. The left panel has four child amplitudes. The right shows their unitary discrete Fourier channel energies. Channel zero is the aggregate; the other channels encode variation among children. Because the transform is unitary, energy is preserved, even though the original real amplitudes can become complex.

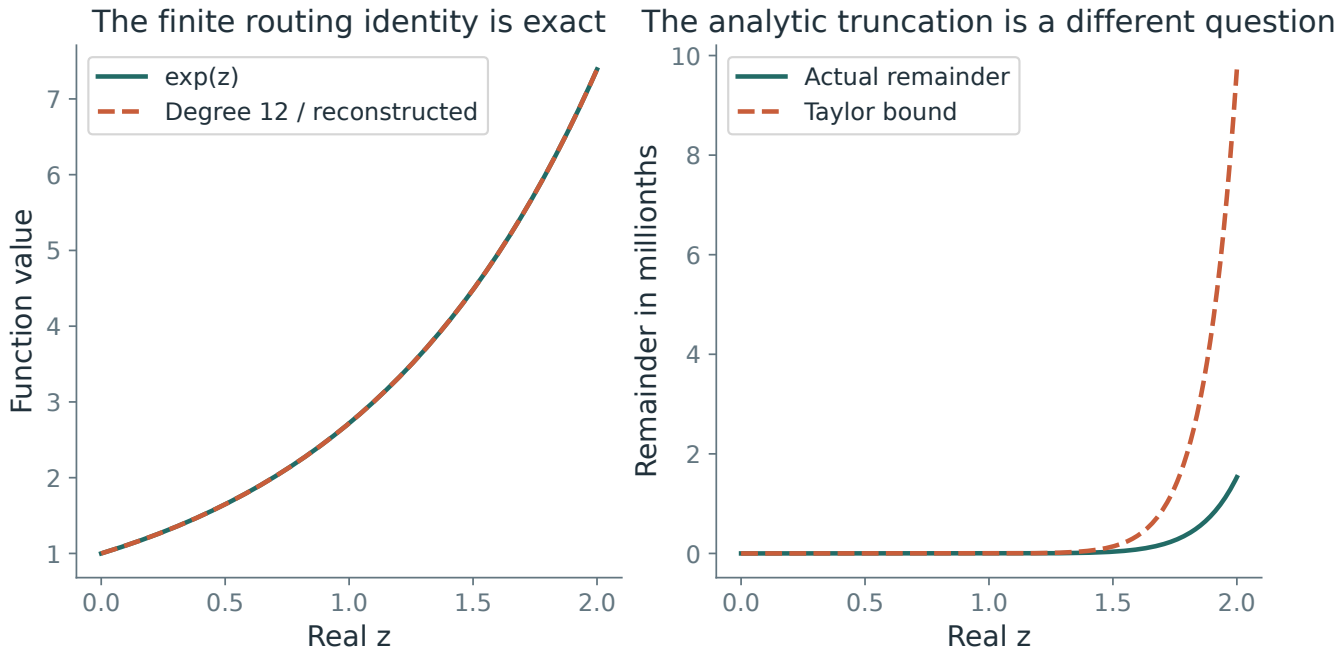
Work an example. For $b = (1, 2, 4, 1)$, the channels are 4, $(-3 - i)/2$, 1, and $(-3 + i)/2$. Their energies are 16, $5/2$, 1, and $5/2$, totaling 22. The inverse transform restores all four children. Keeping only channel zero would discard the details.

Carry forward. A reversible detail bank needs all channels. Aggregation alone is a projection.

Source and scope. Paper I, the unitary child bank. This four-child example uses exact integer inputs and algebraic DFT values; numerical Parseval is also checked.

FOUNDATIONS / 05 **LESSON 5**

Separate routing error from truncation error



$$P_{12}(z) = \sum_{n=0}^{12} \frac{z^n}{n!}, \qquad |e^z - P_{12}(z)| \le e^2 \frac{2^{13}}{13!} \quad (0 \le z \le 2)$$

Read the figure. The first panel overlays the exponential and its degree-twelve truncation. The second enlarges the small remainder and its Taylor bound. Reconstructing the finite polynomial from three packets introduces no mathematical routing error. Approximating the infinite exponential by that polynomial does introduce a remainder.

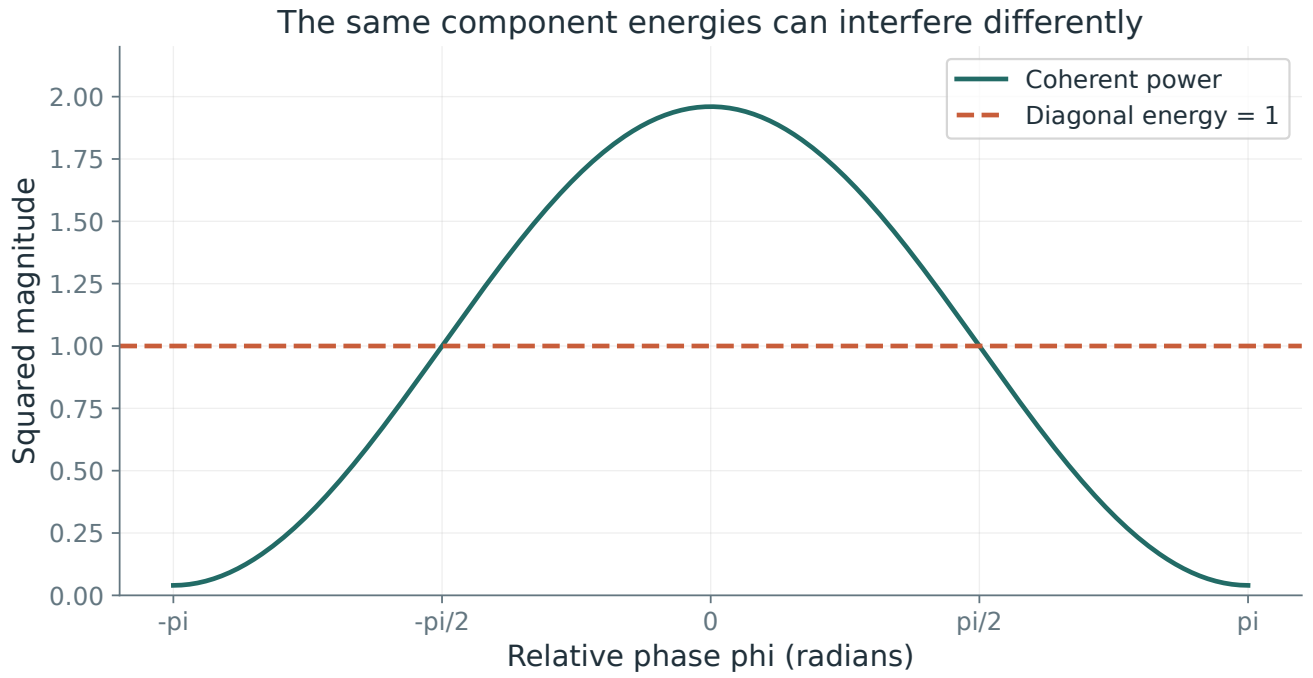
Work an example. The three finite packets use exactly the coefficients with $3m + r \le 12$. Their synthesized sum is P_{12}. At real $z = 2$, Taylor's theorem bounds the omitted tail by $e^2 2^{13}/13!$, about 9.72×10^{-6}. The figure plots the actual remainder in millionths.

Carry forward. An exact coordinate identity can coexist with a numerical approximation. Report the approximation at the stage where it enters.

Source and scope. Paper I reconstruction, illustrated with $F = e^z$. Degree twelve, real domain $[0, 2]$; the remainder bound is the elementary Taylor bound.

FOUNDATIONS / 06 **LESSON 6**

Positive energy does not retain interference



$$\left|\frac{4}{5}+\frac{3}{5}e^{i\phi}\right|^2 = 1+\frac{24}{25}\cos\phi$$

Read the figure. The solid curve is coherent power as the relative phase changes. The dashed line keeps only the sum of the two component energies. The latter is constant, while the coherent value can be almost canceled or almost doubled. Removing cross terms changes the information being represented.

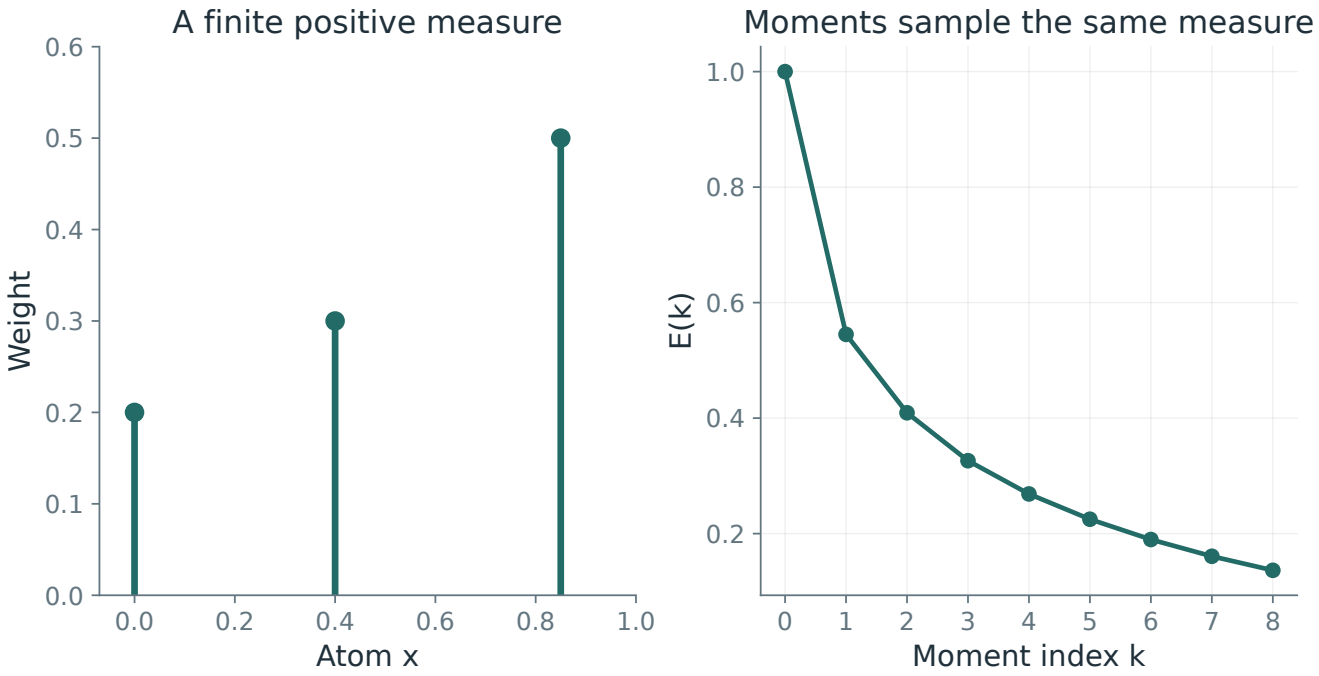
Work an example. Both component energies sum to $(4/5)^2+(3/5)^2=1$. At phase zero the coherent power is $49/25$. At phase π it is $1/25$. Averaging uniformly over a full phase period gives one because the cosine term has zero mean.

Carry forward. A positive diagonal lift is valuable, but a bound on it alone does not recover a signed or coherent cancellation estimate.

Source and scope. An exact two-component teaching model for the distinction used in Papers I, IV, VII, and VIII. It is not an arithmetic cancellation theorem.

FOUNDATIONS / 07 **LESSON 7**

One measure creates a sequence of moments



$$E_k = \sum_j w_j x_j^k, \qquad c^T H c = \sum_j w_j \left(\sum_r c_r x_j^r \right)^2 \geq 0$$

Read the figure. The left panel shows three atoms and their positive weights. The right plots nine moments of this same measure. Higher powers favor atoms nearer one. The zero atom contributes to E_0 and disappears from positive moments, so discarding it would change the starting value.

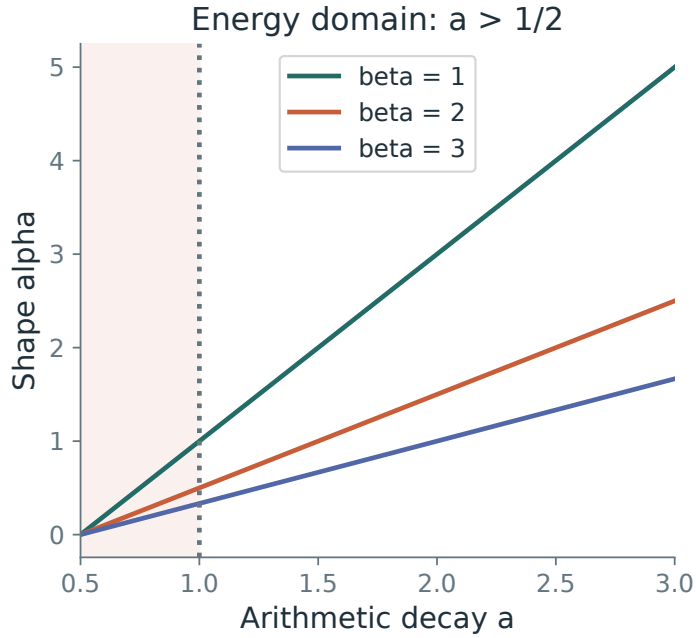
Work an example. Use nodes $(0, 2/5, 17/20)$ and weights $(1/5, 3/10, 1/2)$. Then $E_0 = 1$, $E_1 = 109/200$, and $E_2 = 1637/4000$. The three-by-three Hankel matrix is positive definite because a nonzero quadratic cannot vanish at all three distinct atoms. The four-by-four matrix is singular because this toy support has only three points.

Carry forward. Strict positivity at every size requires enough support. The arithmetic source measure has infinitely many distinct atoms.

Source and scope. Papers II–III positive-moment construction. This explicitly finite teaching measure has rank three; its moments and determinant are computed with rational arithmetic.

FOUNDATIONS / 08 **LESSON 8**

Parameters have different mathematical jobs



Shape bridge
alpha = 2 kappa

a	beta	alpha	kappa
2	2	3/2	3/4
3/2	1	2	1
5/4	3	1/2	1/4

$$\alpha = \frac{2a-1}{\beta} > 0, \qquad \kappa = \frac{\alpha}{2}$$

Read the figure. The curves convert arithmetic decay a and scale exponent β into a positive Gamma shape. The shaded strip marks $1/2 < a \leq 1$: positive energy is defined there, while the absolutely convergent signed transfer uses $a > 1$. The table continues each shape to its ordinary ladder label.

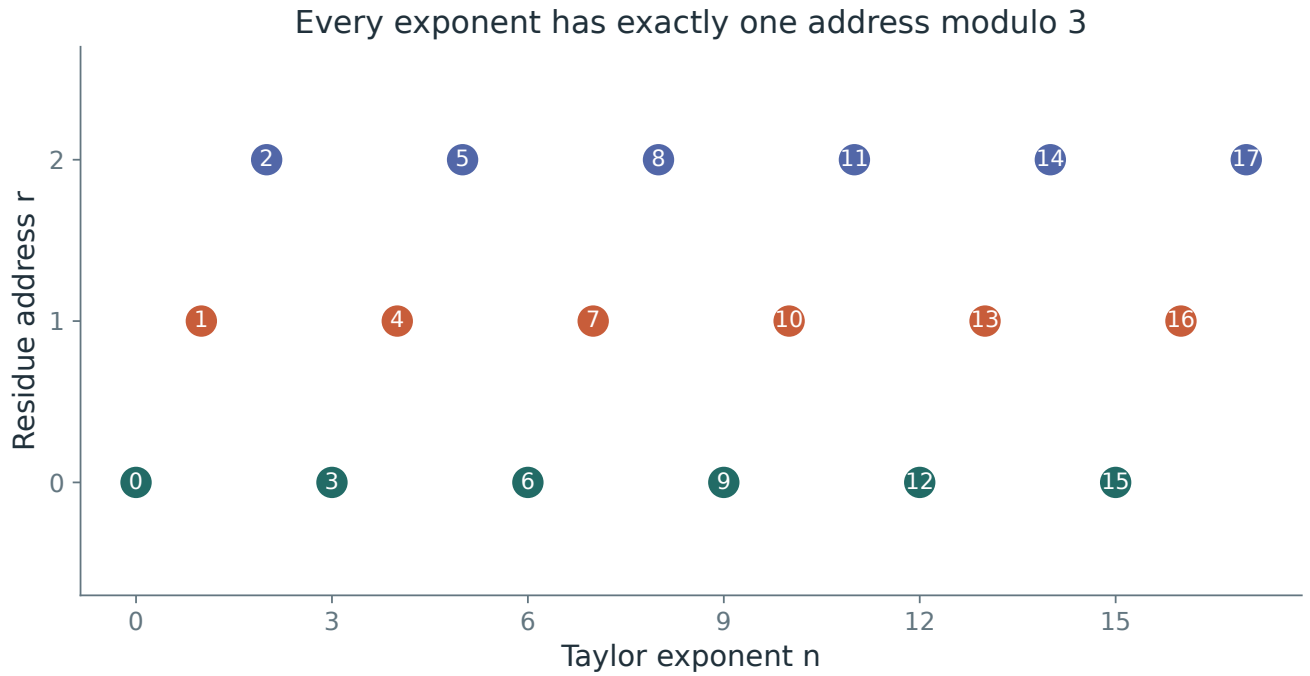
Work an example. For $a = 2$ and $\beta = 2$, the shape is $\alpha = 3/2$ and the ladder parameter is $\kappa = 3/4$. This parameter choice differs from the half-shape recoupling example $\kappa = 1/2$. Also distinguish an integer character modulus from the real deformation parameter $0 < q \leq 1$ used in Paper VIII.

Carry forward. Follow the declared parameter domain whenever a formula crosses from arithmetic packets to continuous shapes or finite recoupling.

Source and scope. Consolidated Chapters 1–3; Papers II, V, and VII. The table is exact rational arithmetic, and the curves show the stated parameter map.

PAPER I / 01 **LESSON 9**

A scalar germ has exact coefficient addresses



$$F(z) = \sum_{r=0}^{M-1} z^r F_{M,r}(z^M), \qquad F_{M,r}(u) = \sum_{m \geq 0} a_{Mm+r} u^m.$$

Read the figure. Follow each colored row horizontally. The label on a dot is the original Taylor exponent, while its row is the residue address. The three rows cover every exponent once. Moving from the scalar function to packets changes coordinates and preserves all coefficients; synthesis restores each packet's residue factor. This diagram shows addresses, not the magnitudes of the coefficients.

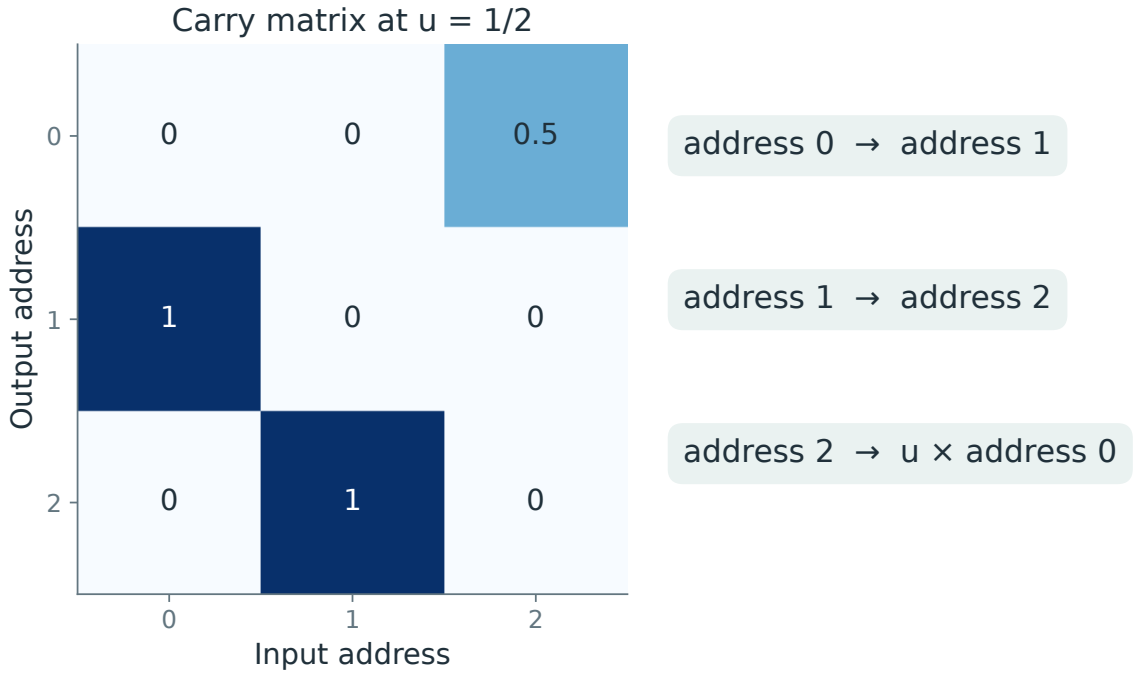
Work an example. For e^z and $M = 3$, the first packets begin $E_{3,0} = 1 + u/6 + \cdots$, $E_{3,1} = 1 + u/24 + \cdots$, and $E_{3,2} = 1/2 + u/120 + \cdots$. The term $u/120$ in address 2 reconstructs to $z^2 z^3/120 = z^5/5!$.

Carry forward. An exact packet is a coefficient address together with its synthesis rule.

Source and scope. Volume I, Chapter 1, Definition 1.1 and Theorem 1.2, "Exact polyphase reconstruction." Analytic germs at zero; the series identities hold in their convergence domains.

PAPER I / 02 **LESSON 10**

Multiplication creates a carry



$$C_3(u) = \begin{pmatrix} 0 & 0 & u \\ 1 & 0 & 0 \\ 0 & 1 & 0 \end{pmatrix}, \qquad \mathcal{S}_3(C_3 f) = z\mathcal{S}_3 f.$$

Read the figure. Read a matrix column as an input address and a row as an output address. Multiplication advances addresses 0 and 1 by one position. Address 2 wraps to address 0 and acquires a factor u. The left panel evaluates that matrix at $u = 1/2$ only to make its entries visible; the algebraic matrix retains the variable u.

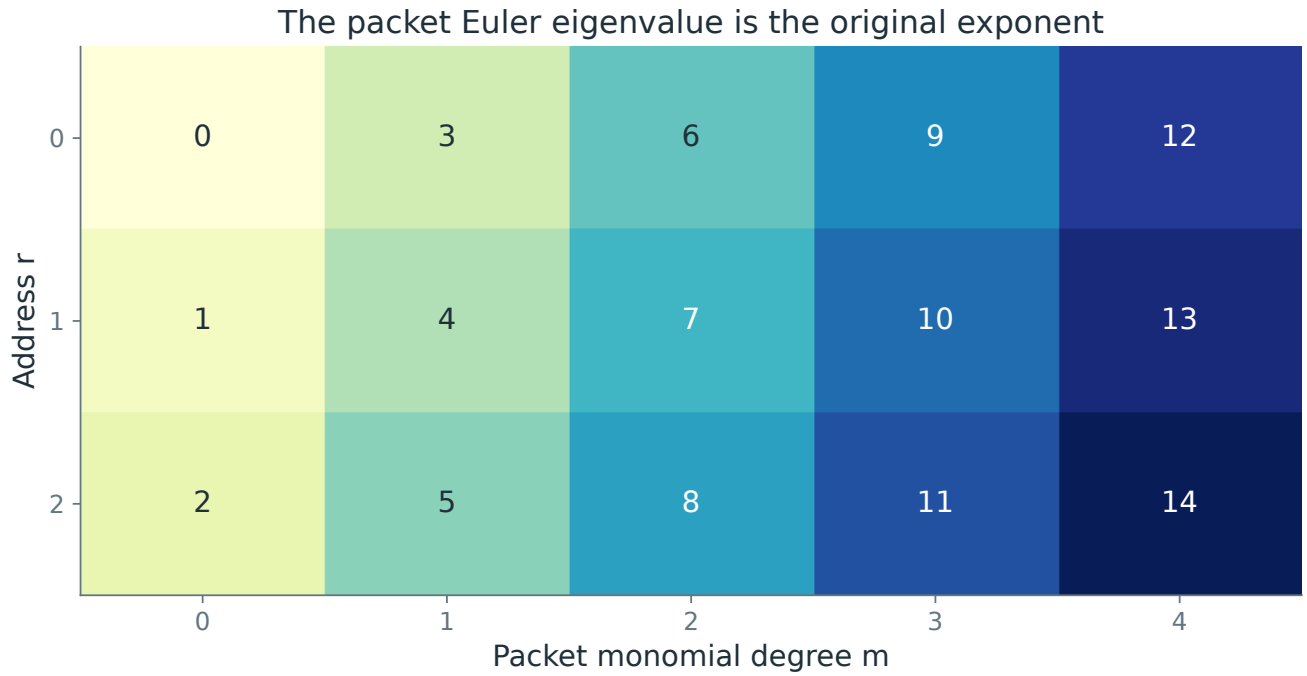
Work an example. The scalar term z^2u^m represents exponent $3m + 2$. After multiplication it becomes $z^3u^m = u^{m+1}$ in address 0. The factor u at the matrix's upper-right corner records exactly this carry. Without it, the exponent and coefficient reconstruction would both fail.

Carry forward. Carry is part of multiplication, so it must be transported with the packets.

Source and scope. Volume I, Chapter 2, Proposition 2.1, "Intertwining laws." The matrix acts on analytic packet germs. The displayed numerical heatmap is an illustrative evaluation, not a fitted operator.

PAPER I / 03 **LESSON 11**

The Euler operator remembers the full exponent



$$\Theta_M = Mu\frac{d}{du}I_M + \operatorname{diag}(0,\dots,M-1), \qquad \Theta_M(u^m e_r) = (Mm+r)u^m e_r.$$

Read the figure. Choose a column to fix the packet degree m, then move between rows to change address r. Each cell returns the original scalar exponent $3m + r$. Differentiating only in u would recover $3m$ and lose the address contribution. The diagonal term restores it. The table is exact integer arithmetic.

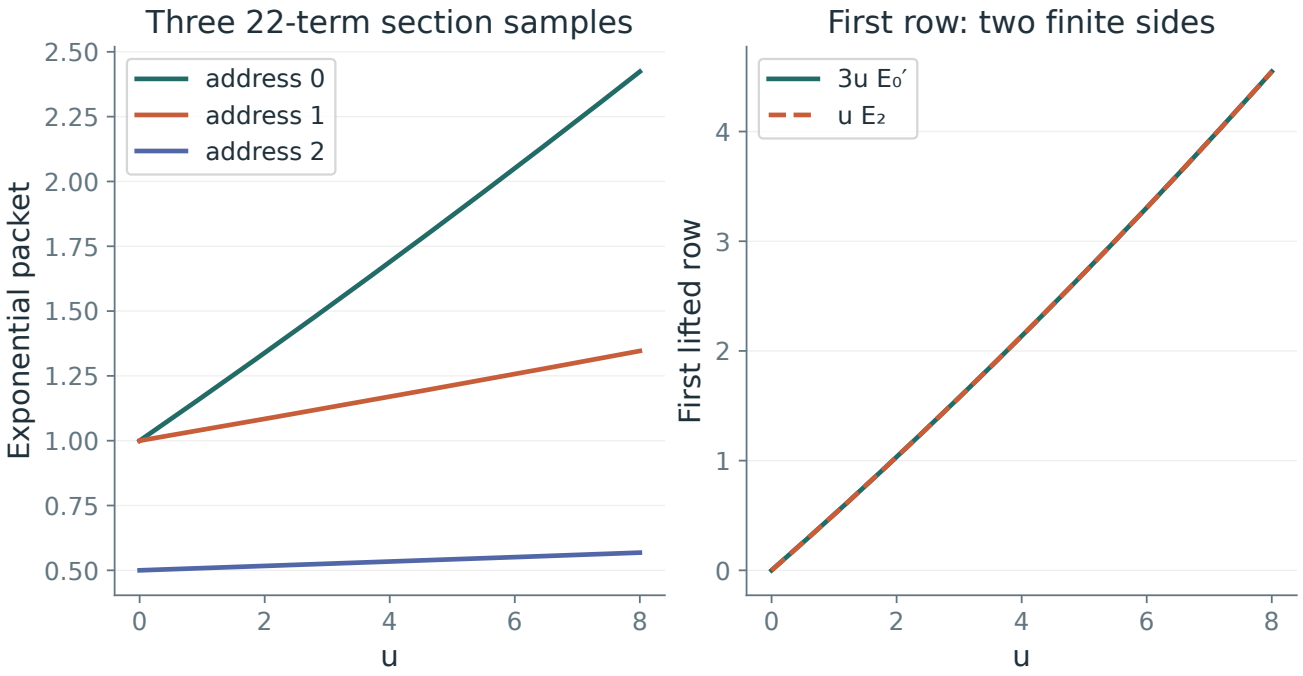
Work an example. For $m = 2$ in address $r = 1$, synthesis gives $z^1(z^3)^2 = z^7$. The operator $3u\,d/du + 1$ multiplies that packet monomial by $3 \cdot 2 + 1 = 7$, just as $z\,d/dz$ multiplies z^7 by 7. Apply multiplication once more and the eigenvalue rises to 8.

Carry forward. The transported Euler and carry operators satisfy $[\Theta_M, C_M] = C_M$.

Source and scope. Volume I, Chapter 2, Proposition 2.1 and Corollary 2.2, "Weyl commutator." Addresses and packet degrees are nonnegative integers; operator ordering is retained.

PAPER I / 04 **LESSON 12**

A differential equation survives the lift



$$\Theta_3 \boldsymbol{E}_3 = C_3 \boldsymbol{E}_3, \qquad 3uE'_{3,0}(u) = uE_{3,2}(u).$$

Read the figure. The left panel plots 22-term samples of the three exponential sections. The right panel compares the two sides of the first lifted row. Their agreement expresses a coefficient identity inherited from $\theta e^z = ze^z$. The scalar differential equation becomes a coupled matrix system, with the same ordered operator products.

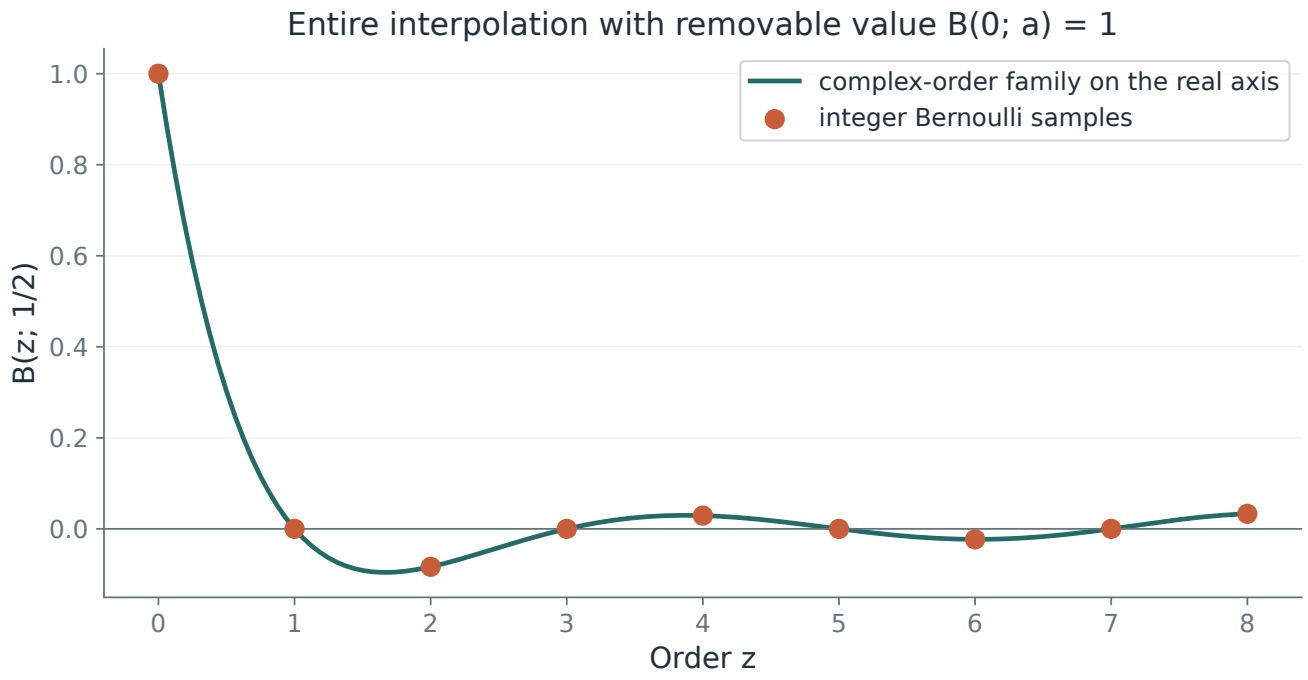
Work an example. For $m \geq 1$, a term $u^m/(3m)!$ in $E_{3,0}$ contributes $3m\,u^m/(3m)! = u^m/(3m-1)!$. This is the term obtained from $uE_{3,2}$ by using packet degree $m-1$. At $u = 0$ both sides of this row vanish.

Carry forward. Transport an equation by intertwining its ordered operators, rather than approximating its solutions.

Source and scope. Volume I, Chapter 2, Theorem 2.3, "Differential lift," and Chapter 3, exponential example. On $0 \leq u \leq 8$, each 22-term packet tail is below 10^{-60}; recorded bounds also include the unmatched last finite row term. Floating-point rounding is separate.

PAPER I / 05 **LESSON 13**

Integer Bernoulli values sit inside an entire family



$$\mathfrak{B}(z;a) = -z\zeta(1-z,a), \quad \mathfrak{B}(0;a) = 1, \quad \mathfrak{B}(n;a) = B_n(a)\ (n \geq 1).$$

Read the figure. The curve varies the order continuously while keeping $a = 1/2$. The dots mark positive-integer Bernoulli-polynomial samples and the removable value at zero. A family indexed by complex order carries more local information than its integer samples. The order-zero value is defined by removal of the zeta pole, not by evaluating an undefined product directly.

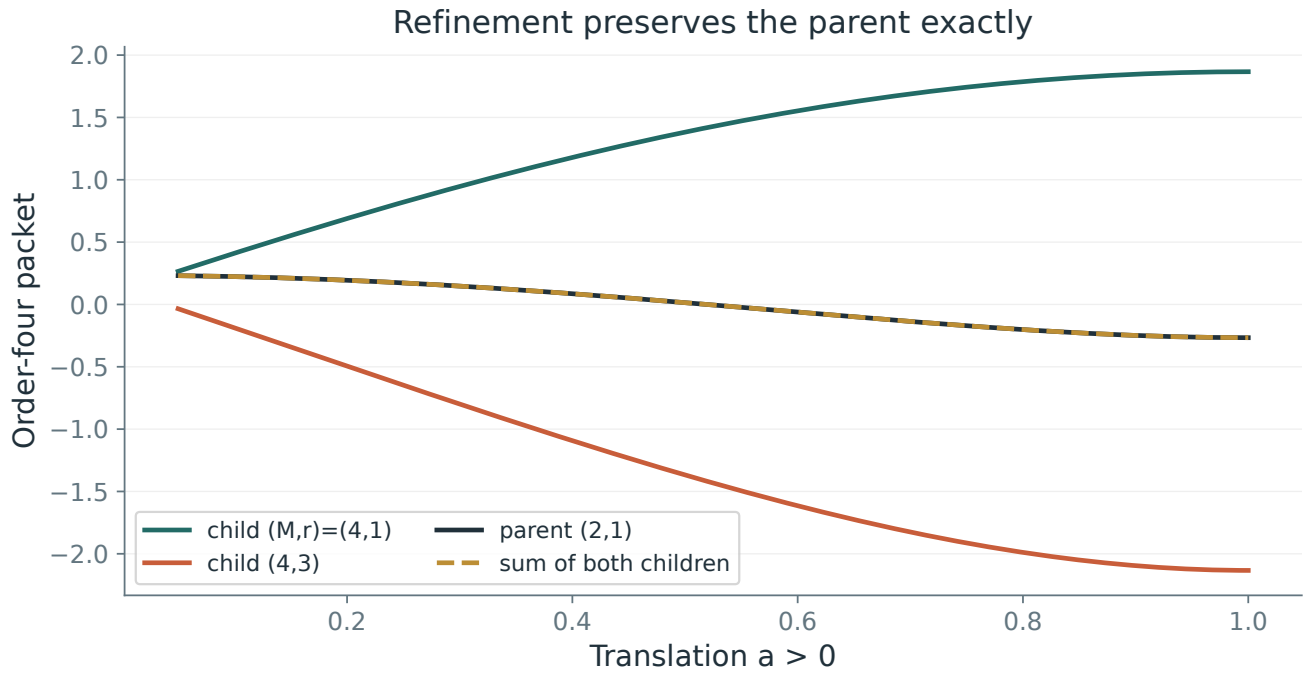
Work an example. At order four, $B_4(1/2) = 7/240$. At every odd integer $n \geq 3$, reflection symmetry gives $B_n(1/2) = 0$. These isolated samples fit inside the continuous curve. The order-one value is also zero at this translation parameter.

Carry forward. Keep the translation parameter and order variable distinct when taking derivatives or refinements.

Source and scope. Volume I, Chapter 4, "Complex-order Bernoulli interpolation." The complex-order family requires $a > 0$; the plot uses 100-digit function evaluations at sampled real orders. Classical Hurwitz special values supply the integer interpolation.

PAPER I / 06 **LESSON 14**

A parent is exactly the sum of its children



$$\mathfrak{B}_{M,r}(z;a) = \sum_{\ell=0}^{L-1} \mathfrak{B}_{LM,r+\ell M}(z;a).$$

Read the figure. The parent curve and the dashed sum coincide, although the two child curves differ substantially. Here the parent has address $(M, r) = (2, 1)$ and is refined to addresses $(4, 1)$ and $(4, 3)$ at integer order four. Refinement does not approximate the parent or reduce its size; it exposes an exact decomposition that later supports detail channels.

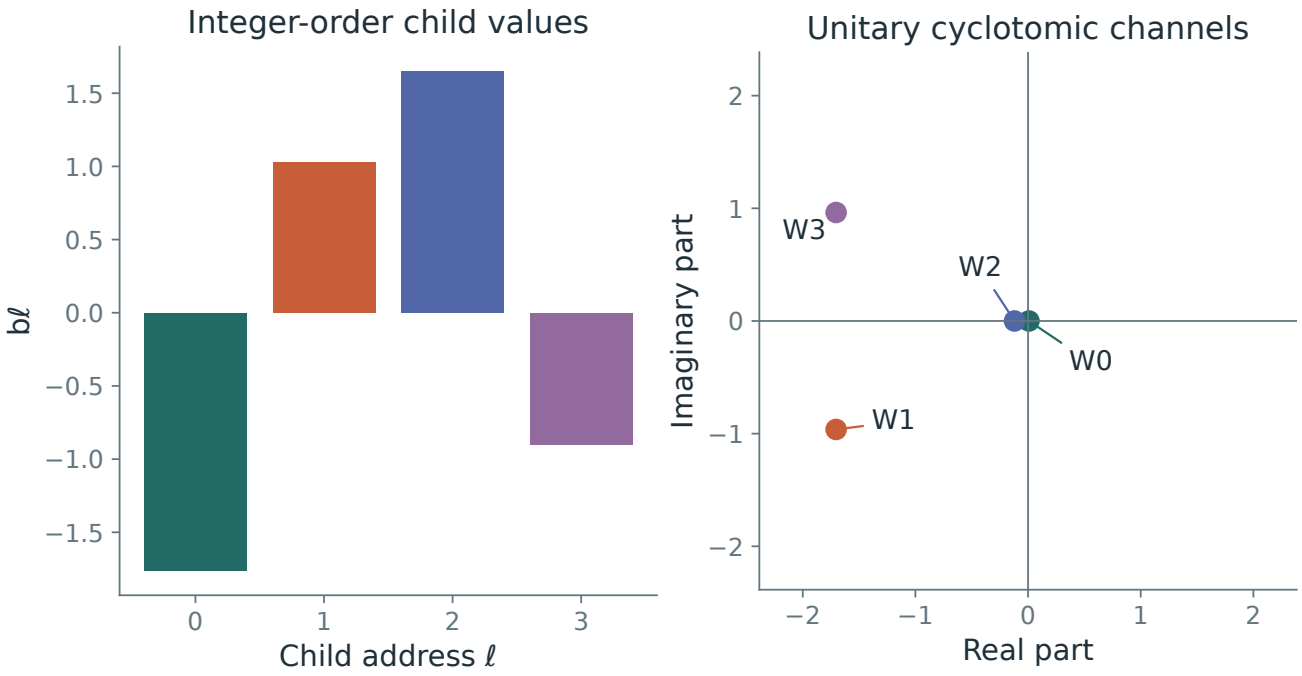
Work an example. At $a = 1/3$, the parent is $8B_4(2/3) = 52/405$. Its children are $64B_4(1/3) = 416/405$ and $64B_4(5/6) = -364/405$. Their exact rational sum is $52/405$. The larger child magnitudes show why complete reconstruction matters.

Carry forward. Information in separate children can disappear when only their parent sum is retained.

Source and scope. Volume I, Chapter 5, Theorem 5.1, "Parent-child refinement," with Theorem 5.2, "Integer samples." The general complex-order identity uses $a > 0$ and the classical Hurwitz multiplication formula.

PAPER I / 07 **LESSON 15**

Detail phases preserve complete information



$$W_j = L^{-1/2} \sum_{\ell=0}^{L-1} \omega_L^{-j\ell} b_\ell, \qquad \sum_j |W_j|^2 = \sum_\ell |b_\ell|^2.$$

Read the figure. The left panel shows four real child values. The right panel places their transformed channels in the complex plane. A nonreal channel is a phase coordinate, not a lost child. The normalized Fourier transform has an inverse and preserves the total squared magnitude. The DC channel is the parent divided by $\sqrt{L}$; the other channels record differences between children.

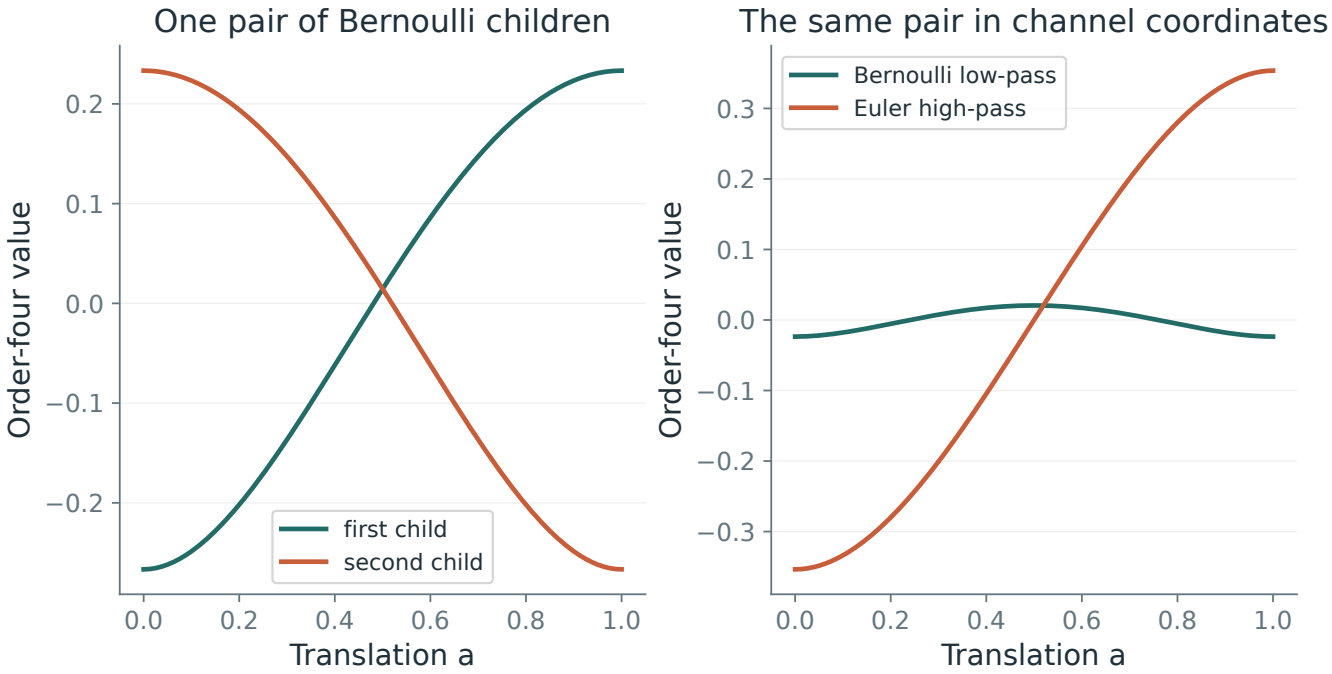
Work an example. Here $L = 4$, $n = 4$, and $a = 1/3$. Applying the inverse formula $b_\ell = L^{-1/2} \sum_j \omega_L^{j\ell} W_j$ reconstructs each individual child. Real input also gives conjugate channels $W_3 = \overline{W_1}$, while the DC and Nyquist channels are real.

Carry forward. A detail bank should come with inverse synthesis and a normalization certificate.

Source and scope. Volume I, Chapter 6, Definition 6.1, "Cyclotomic detail," and the subsequent inverse-transform and Parseval identities. Finite integer-order polynomial data; the figure uses normalized channels, not unnormalized resultant evaluations.

PAPER I / 08 **LESSON 16**

Bernoulli and Euler share one channel bank



$$W_{2,0}(n;a) = \frac{B_n(a)}{\sqrt{2}}, \qquad W_{2,1}(n;a) = -\frac{n}{2\sqrt{2}} E_{n-1}(a).$$

Read the figure. Compare the two panels at the same translation parameter. The left pair consists of Bernoulli children; the right pair consists of their sum and difference channels. The low-pass output is a Bernoulli polynomial and the high-pass output is an Euler polynomial with the displayed scale factor. Both pairs carry the same information. The plotted curves have order four.

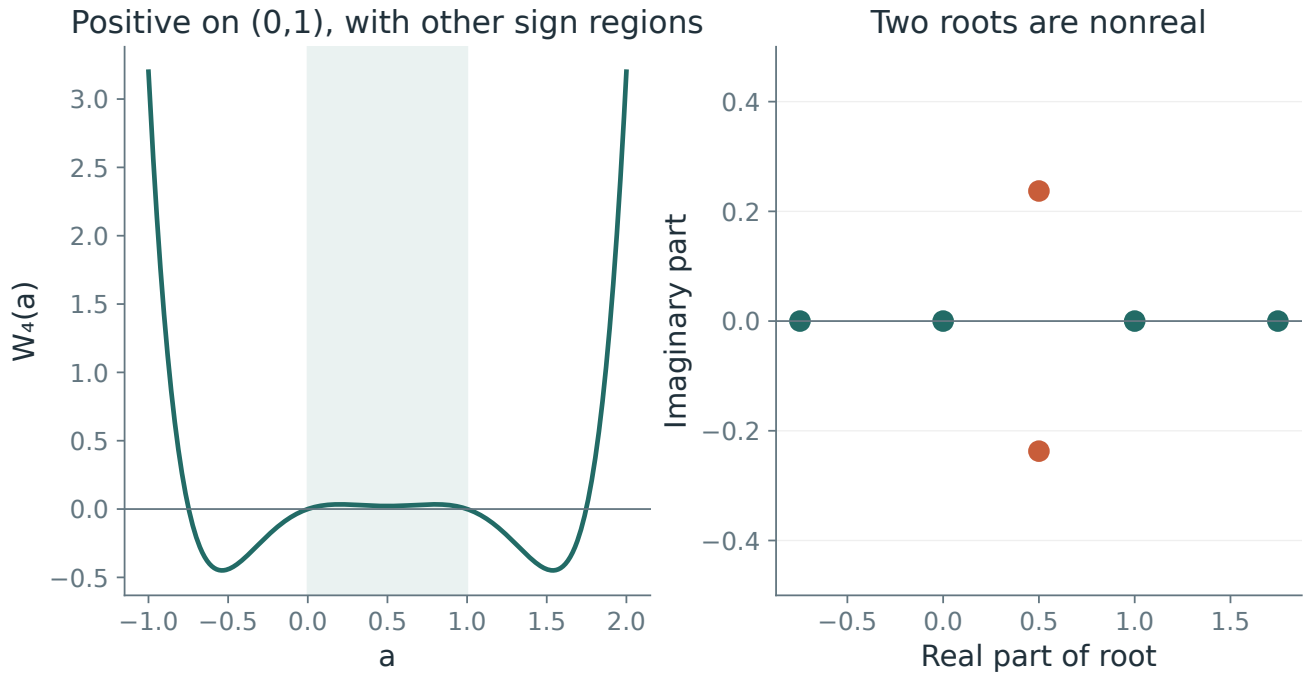
Work an example. At order three and $a = 1/2$, the children are $3/16$ and $-3/16$. Their DC output vanishes and their detail output is $3/(8\sqrt{2})$. This agrees with $E_2(1/2) = -1/4$ in the high-pass formula.

Carry forward. Classical special functions can occur as complementary outputs of one exact refinement.

Source and scope. Volume I, Chapter 8, Theorem 8.1, "Two-channel identity." Positive integer orders; endpoint $a = 0$ in this figure uses the Bernoulli-polynomial extension, not a zero-argument complex-order Hurwitz evaluation.

PAPER I / 09 **LESSON 17**

A Wronskian can reject a broad conjecture



$$\mathcal{W}_4(a) = \frac{a(a-1)}{5}\left(5a^4 - 10a^3 + 5a - 2\right).$$

Read the figure. The real graph is positive between zero and one, but its complete zero set tells a more precise story. The right panel includes two nonreal roots. A favorable sign on one real interval therefore does not imply universal real-rootedness. The shaded interval highlights a valid local feature, while the root plot supplies the negative control against a stronger claim.

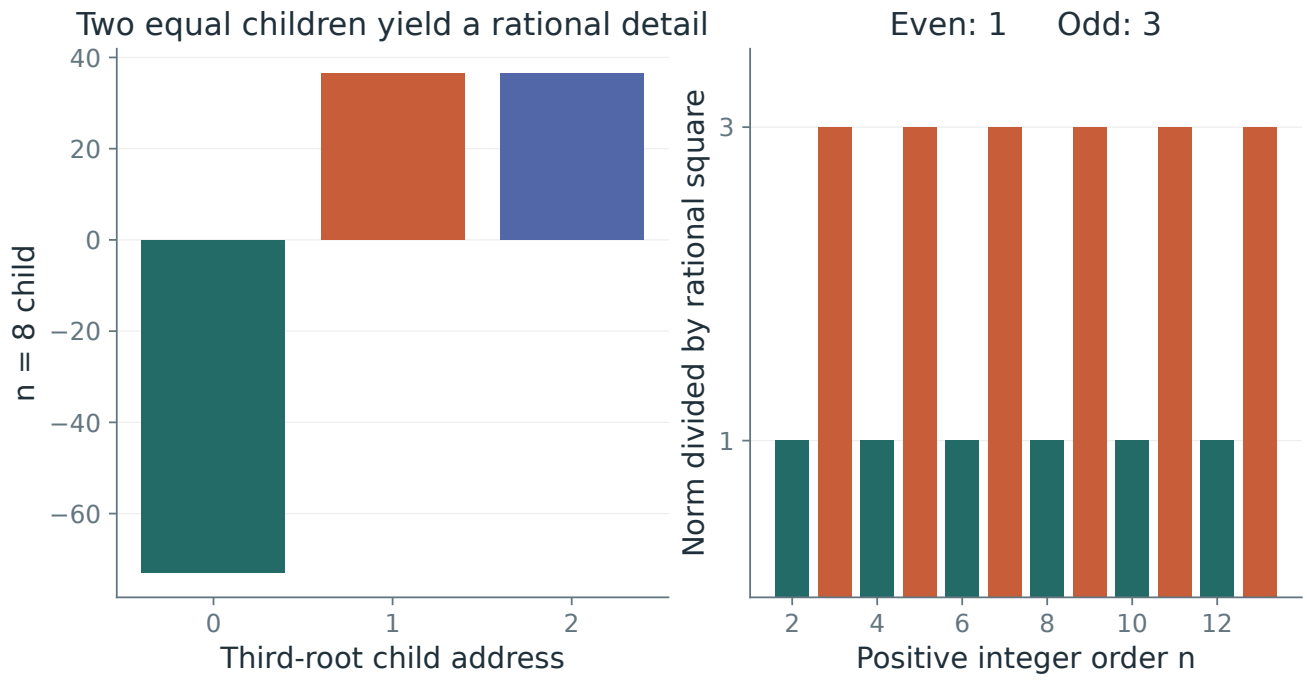
Work an example. The nonreal pair is $\frac{1}{2} \pm i\sqrt{(2\sqrt{65} - 15)/20}$. The other four roots are 0, 1, and $\frac{1}{2} \pm \sqrt{(15 + 2\sqrt{65})/20}$. At $a = 1/2$, the value is $7/320 > 0$. These exact formulas explain both panels.

Carry forward. A zero diagnostic is useful when it records counterexamples as carefully as positive cases.

Source and scope. Volume I, Chapter 9, Worked example 9.2, "Orders two through four," and Boundary 9.3. The plot uses the exact degree-six polynomial and algebraic roots; no general interlacing theorem is inferred.

PAPER I / 10 **LESSON 18**

Third-root norms remember parity



$$N_n = \begin{cases} [3^{n-1}(B_n - B_n(1/3))]^2, & n \geq 2 \text{ even}, \\ 3[3^{n-1}B_n(1/3)]^2, & n \geq 3 \text{ odd}. \end{cases}$$

Read the figure. The equal second and third children in the left panel collapse the even-order primitive detail to a rational number. The right panel divides each norm by its corresponding rational square. The ratio is one at even orders and three at odd orders. The rational square factor has different definitions in the two cases, supplied by Bernoulli reflection.

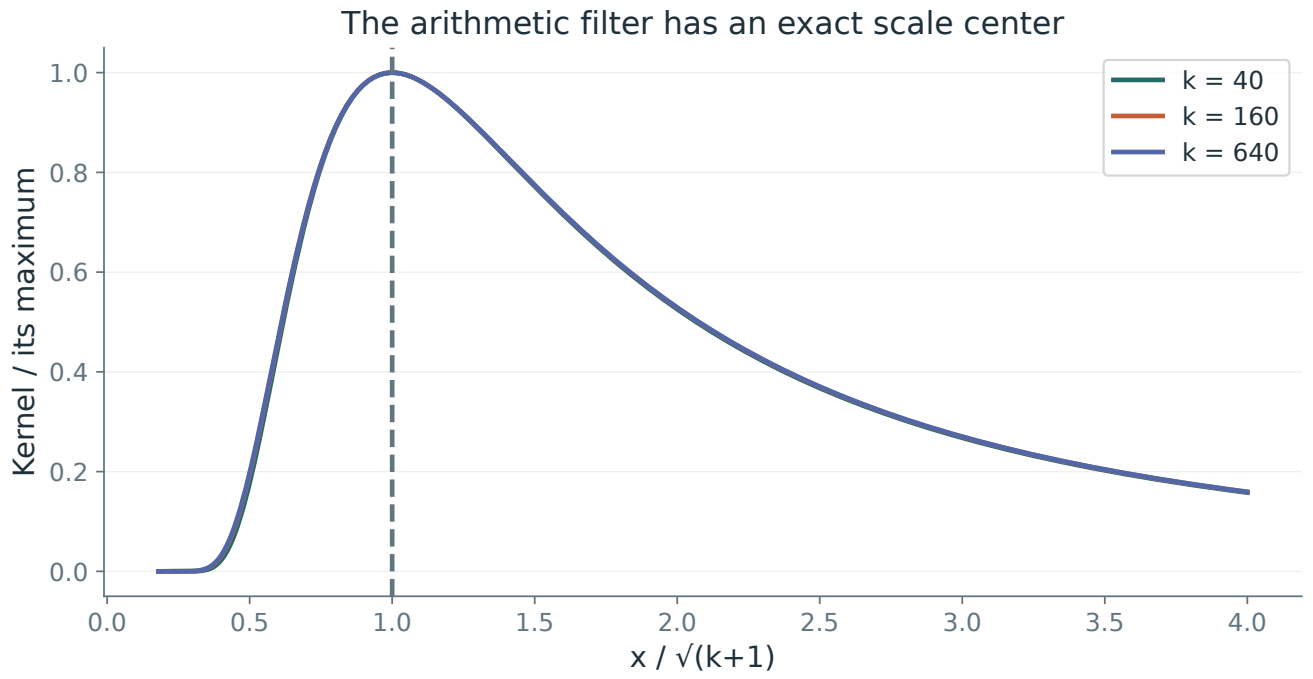
Work an example. At $n = 8$, the children are $-729/10$, $1093/30$, and $1093/30$. Because $\omega_3 + \omega_3^2 = -1$, the unnormalized primitive detail is $-328/3$. Its field norm is $107584/9$. At odd order three, the primitive detail is purely imaginary and its norm is $1/3$.

Carry forward. A cyclotomic norm combines exact arithmetic with the symmetry of its channel orbit.

Source and scope. Volume I, Chapter 10, Theorem 10.1, "Parity law for the third-root detail norm," and Chapter 21, order-eight example. Integer Bernoulli-polynomial samples at $a = 0$; unnormalized details are used.

PAPER I / 11 **LESSON 19**

Scale filters select an arithmetic window



$$f_k(x) = x^{-2}(1 - x^{-2})^k, \qquad x_*(k) = \sqrt{k+1}.$$

Read the figure. Each curve divides the kernel by its own maximum and the horizontal coordinate by its exact maximizing location. The maxima align at one. The curves become similar as the packet order rises, but their finite-order forms remain distinct. Small integers are suppressed by the filter and large integers by the power weight, producing an active window.

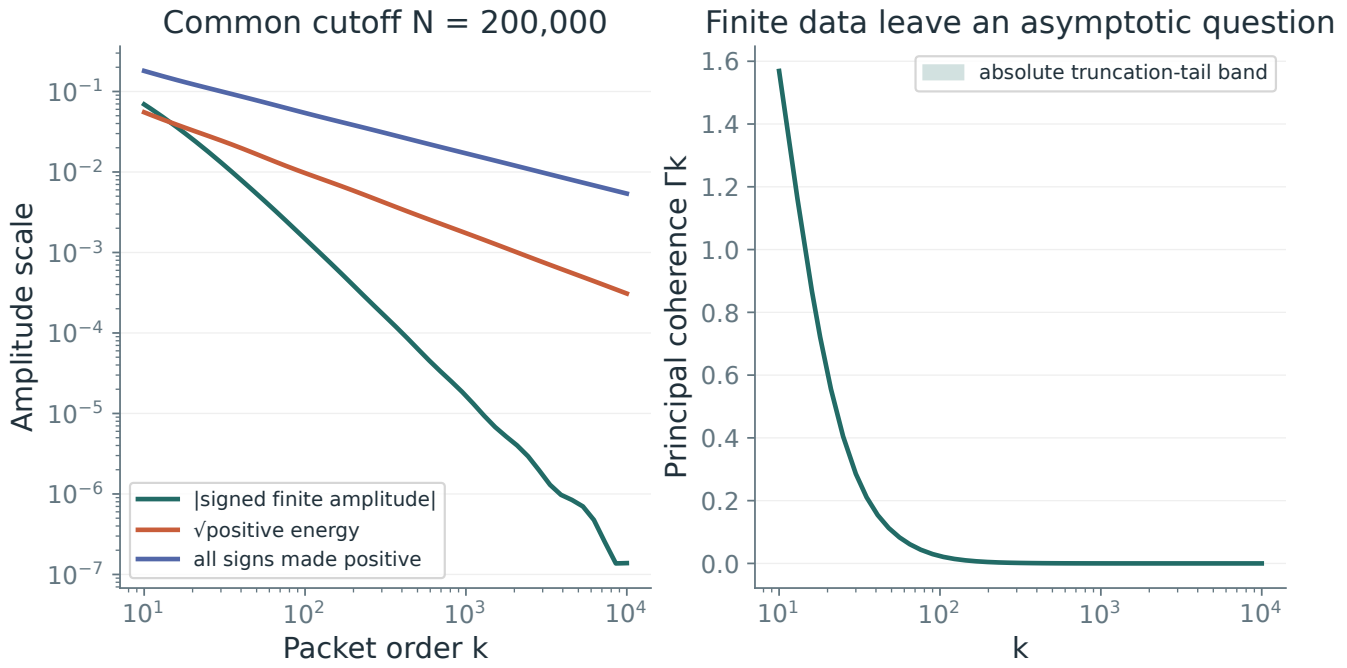
Work an example. For $k = 160$, the center is $\sqrt{161} \approx 12.689$. More generally, the kernel $x^{-a}(1 - x^{-\beta})^k$ has center $(1 + \beta k/a)^{1/\beta}$. Differentiating its logarithm identifies the center directly. Here all plotted points satisfy $x \geq 1$ and the normalized coordinate ranges from 0.18 to 4.

Carry forward. A scale center is a localization statement, not yet a cancellation estimate for signs.

Source and scope. Volume I, Chapter 14, "Scale localization and the Mertens wavelet." Continuous kernels at $k = 40, 160, 640$; this is an exact elementary kernel calculation. Zero-mean wavelet statements in that chapter require $k \geq 1$.

PAPER I / 12 **LESSON 20**

Coherence has a proved scale and an open estimate



$$\Gamma_k = \frac{|c_k|^2}{E_k}, \qquad \text{RH} \iff \Gamma_k = O_\varepsilon(k^\varepsilon) \text{ for every } \varepsilon > 0.$$

Read the figure. The left panel compares the signed amplitude, the square root of positive energy, and the amplitude with all arithmetic signs made positive. These are different quantities. The right panel plots finite principal coherence and an absolute truncation-tail band. Finite small values do not establish the required asymptotic bound. The denominator scale is proved; the remaining assertion concerns Möbius cancellation.

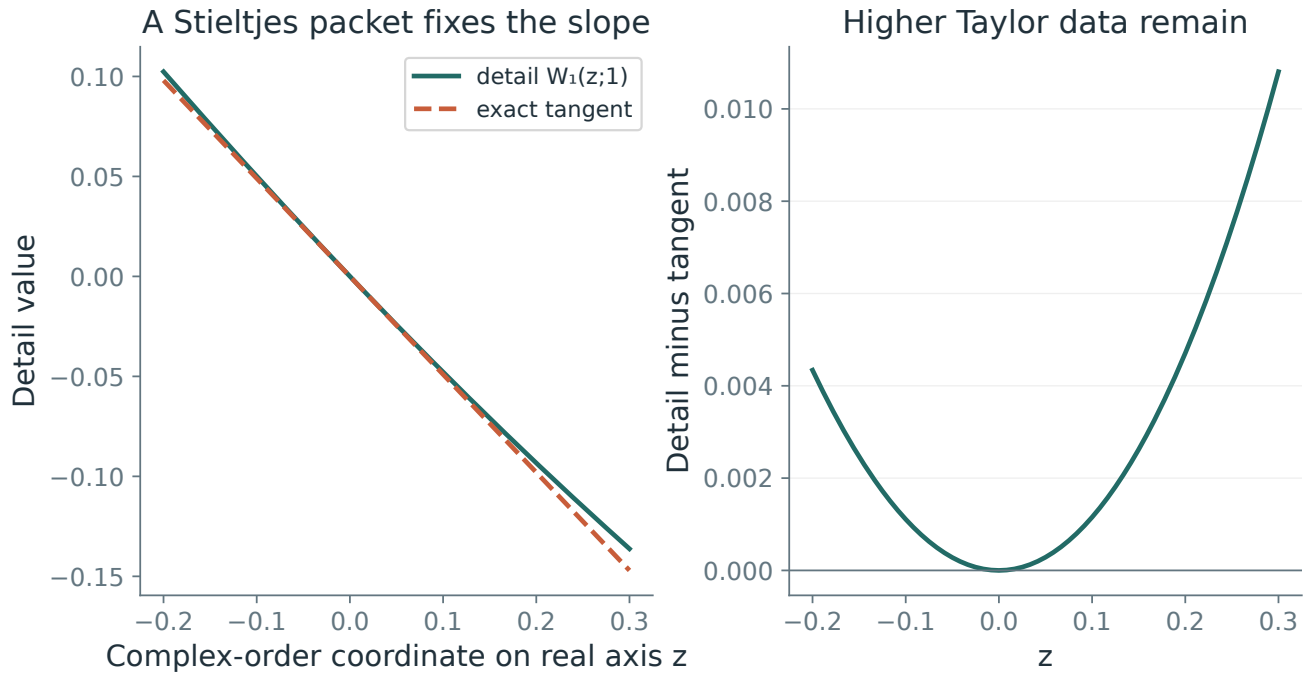
Work an example. At $k = 1200$ and cutoff $N = 200000$, the finite calculation gives $|c_k| \approx 1.1153 \times 10^{-5}$ and $E_k \approx 2.3091 \times 10^{-6}$. Their ratio is about 5.3868×10^{-5}. The omitted amplitude is bounded absolutely by $1/N$, and the omitted energy by $1/(3N^3)$.

Carry forward. Positive energy controls normalization; the signed estimate remains RH-equivalent.

Source and scope. Volume I, Theorems 15.1 and 16.1; Chapter 22's finite example. The RH equivalence imports the classical Báez-Duarte theorem. Bands control truncation only, not interval-certified floating-point rounding.

PAPER II / 01 **LESSON 21**

Stieltjes constants encode a detail's local slope



$$G_{1,0}(1) = \sqrt{2}\log 2, \qquad W_1'(0;1) = -\frac{\log 2}{\sqrt{2}}.$$

Read the figure. The first panel compares the two-channel detail near its removable zero with its exact tangent. The second removes the tangent and displays the remaining curvature. Generalized Stieltjes constants are Taylor data for the Hurwitz-zeta Laurent expansion. Their finite Fourier transform therefore supplies the local expansion of a Bernoulli detail, rather than just its integer values.

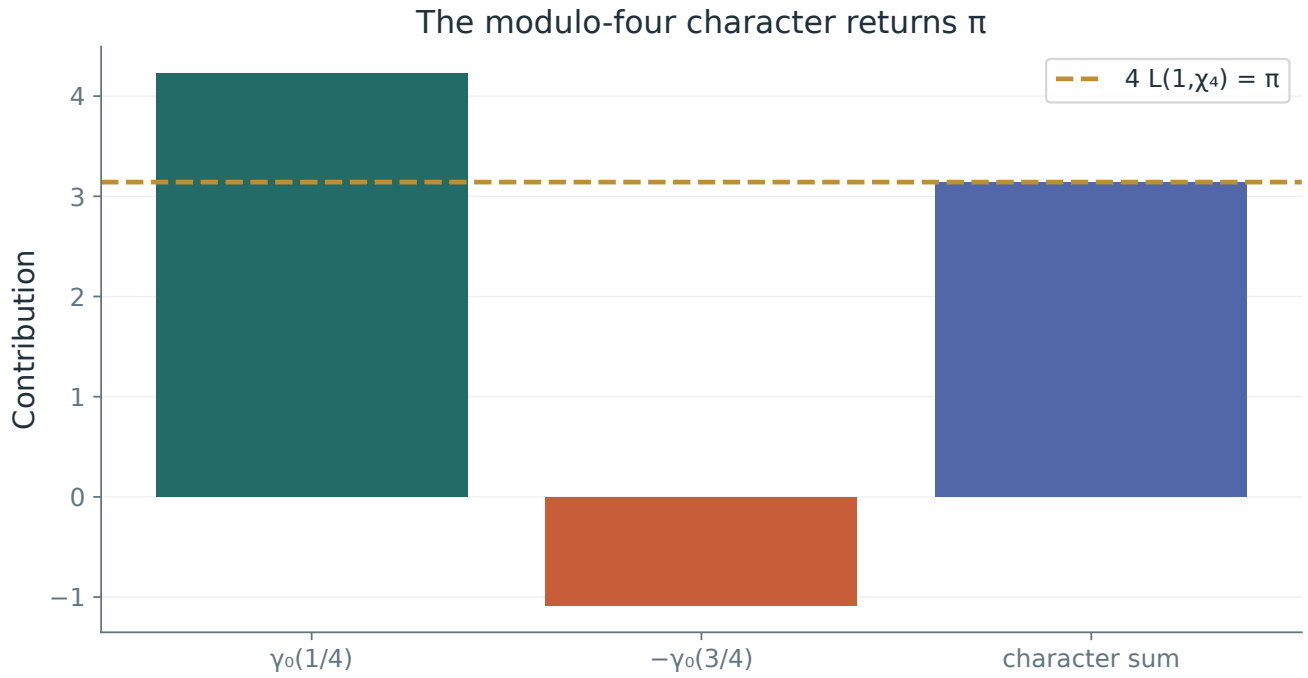
Work an example. For $L = 2, M = 1, a = 1$, the child Hurwitz arguments are $1/2$ and 1. Their zeroth Stieltjes difference is $\gamma_0(1/2) - \gamma_0(1) = 2\log 2$. Dividing by $\sqrt{2}$ gives $G_{1,0}$. The derivative formula adds the factor $-1/2$, giving the slope about -0.490129.

Carry forward. Local derivatives and integer samples probe different information in the same entire function.

Source and scope. Volume II, Chapter 2, Theorem 2.2, "Complete local packet expansion," and Example 2.3. Fixed $a = 1 > 0$; sampled real orders $-0.2 \le z \le 0.3$ evaluated at 100-digit precision.

PAPER II / 02 **LESSON 22**

A character packet returns an L-value



$$\sum_{r=1}^{q} \chi(r)\gamma_0(r/q) = qL(1,\chi) \qquad (\chi \text{ nonprincipal}).$$

Read the figure. The first two bars are signed contributions and the third is their sum. The character removes the pole term of the Hurwitz-zeta representation. What remains is a finite transform of local constants that equals the value of the nonprincipal L-function at one. Cancellation of the common pole is essential to this formula.

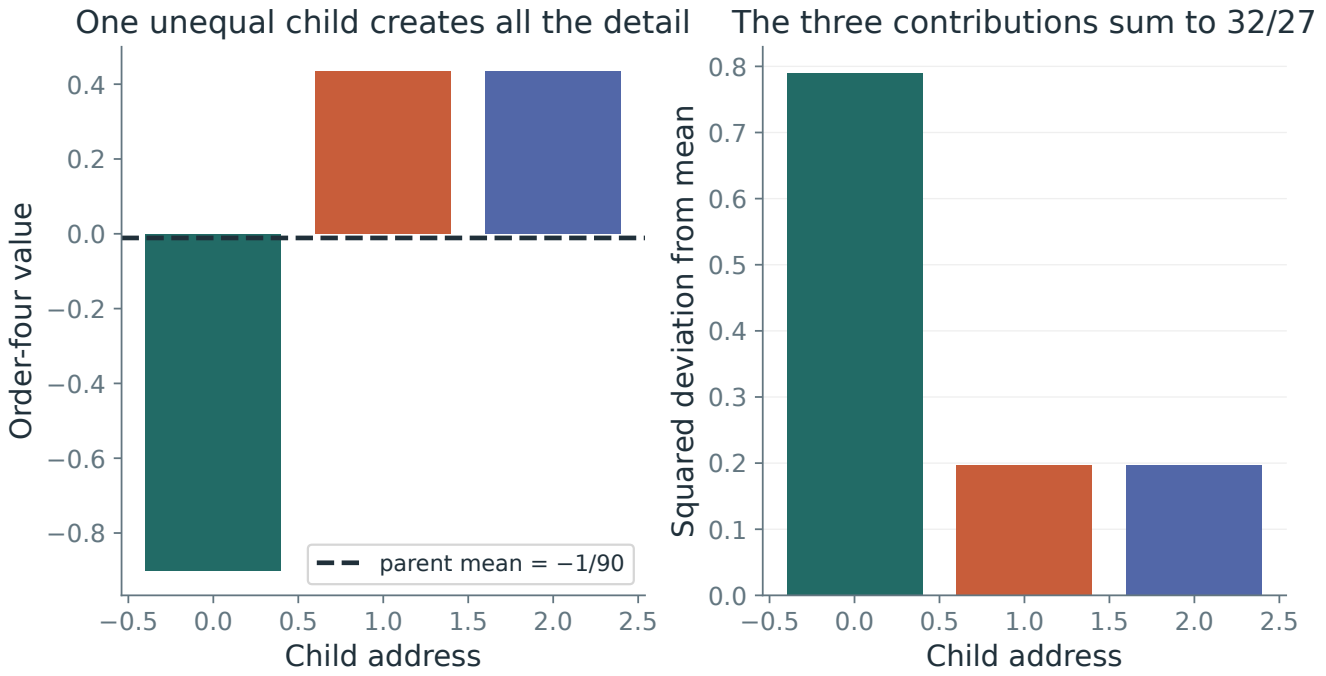
Work an example. For the character modulo four, $\chi_4(1) = 1$, $\chi_4(3) = -1$, and the even residues contribute zero. Since $\gamma_0(x) = -\psi(x)$, digamma reflection gives $\gamma_0(1/4) - \gamma_0(3/4) = \pi$. Thus $4L(1,\chi_4) = \pi$, agreeing with the classical Dirichlet-beta value.

Carry forward. The higher Stieltjes packets recover the whole derivative sequence $L^{(m)}(1,\chi)$.

Source and scope. Volume II, Chapter 3, Theorem 3.2, "Character transform at $s = 1$." This example fixes actual modulus $q = 4$ and a nonprincipal character; the principal character needs separate pole treatment.

PAPER II / 03 **LESSON 23**

Detail variance measures child disagreement



$$\mathcal{V}_L = \sum_{\ell}(b_\ell - \bar{b})^2 = \frac{1}{L}\sum_{\ell<m}(b_\ell - b_m)^2, \quad \bar{b} = L^{-1}\sum_{\ell} b_\ell.$$

Read the figure. The first panel compares three real child values with their common mean. The second shows their squared deviations. Replacing the complete child vector by its mean removes exactly these deviations. For real children the variance also equals the summed squared magnitudes of non-DC unitary channels. For complex children, the holomorphic formula uses squares and paired channels, not absolute values.

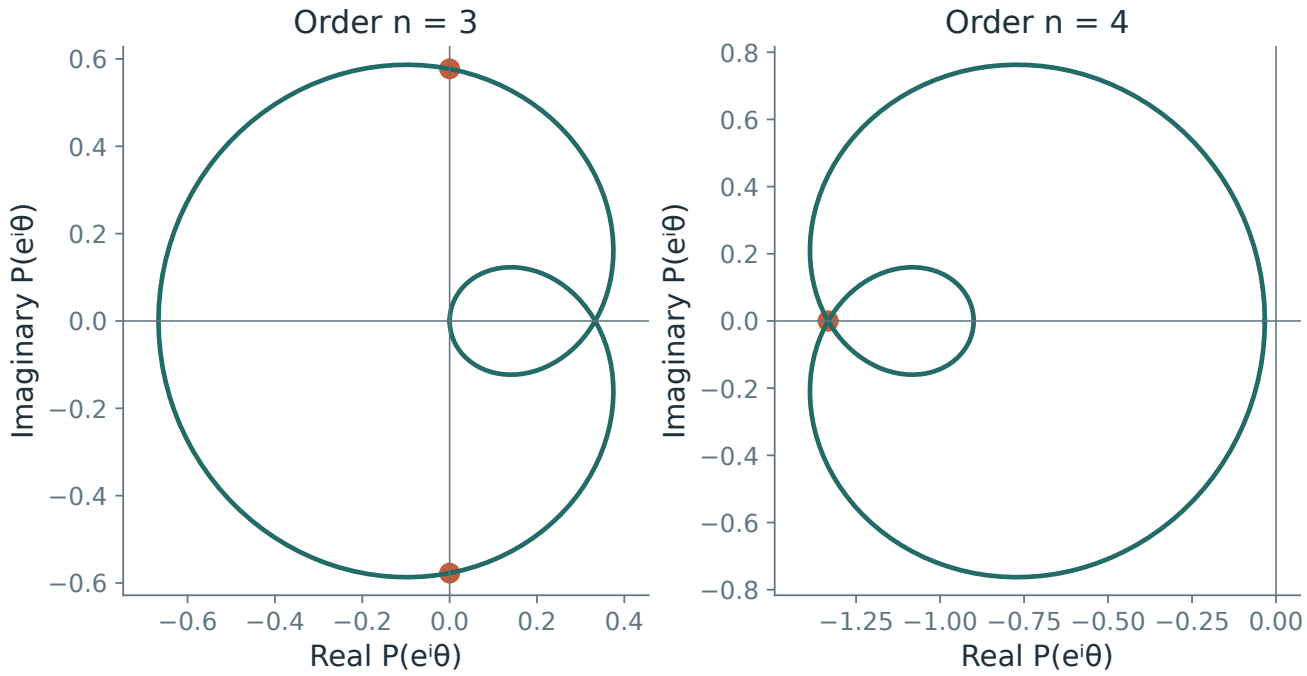
Work an example. At $L = 3, n = 4, a = 0$, the integer-polynomial children are $-9/10, 13/30, 13/30$, with mean $-1/90$. The pairwise form has two nonzero differences of magnitude $4/3$. Hence $\mathcal{V}_3 = (1/3) \cdot 2(4/3)^2 = 32/27$.

Carry forward. A scalar invariant can quantify lost detail while complete synthesis retains every child.

Source and scope. Volume II, Chapter 4, Theorem 4.2, "Three exact forms," and Chapter 5, Example 5.2. The displayed children are real integer-order polynomial samples; complex holomorphic variance is not a positive norm.

PAPER II / 04 **LESSON 24**

A resultant compresses primitive detail channels



$$\mathcal{N}_3 = \mathrm{Res}(X^2 + X + 1, P(X)) = P(\omega_3)P(\omega_3^2) = 3W_1W_2.$$

Read the figure. Each curve evaluates the child polynomial on the entire unit circle. Highlighted points evaluate it at primitive third roots. Their product is the resultant. The order-three pair is imaginary and conjugate; the order-four pair coincides on the real axis. The construction compresses the primitive orbit into one scalar, while the plotted curve retains more detail.

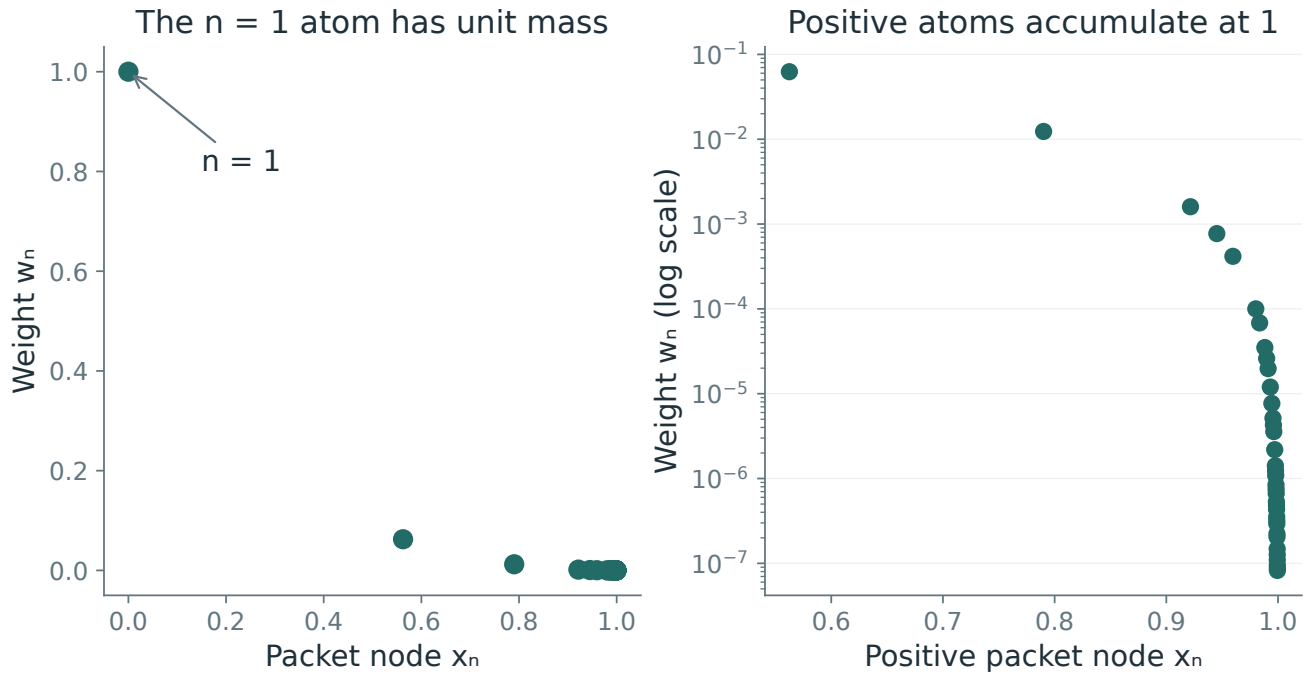
Work an example. At order three, $P(X) = (X - X^2)/3$ and the primitive product is $1/3$. At order four, $P(X) = -9/10 + (13/30)(X + X^2)$; each primitive value is $-4/3$, so the resultant is $16/9$. The factor 3 appears because W_j is normalized by $1/\sqrt{3}$.

Carry forward. Separate field-resultant normalization from unitary-channel normalization.

Source and scope. Volume II, Chapter 6, Definition 6.1 and Theorem 6.2, "Primitive collapse criterion." Here $a = 0$ is used only for positive-integer Bernoulli-polynomial samples. No complete global zero classification is claimed.

PAPER II / 05 **LESSON 25**

The energy is a positive moment measure



$$\nu = \sum_n w_n \delta_{x_n}, \quad w_n = \mu(n)^2 n^{-4}, \quad x_n = (1 - n^{-2})^2, \quad E_k = \int x^k \, d\nu.$$

Read the figure. The left panel retains the large atom at $x_1 = 0$. The right magnifies the remaining weights on a logarithmic scale. The weights are positive at squarefree integers and vanish elsewhere. Atom locations approach one while their masses decay. This produces a finite measure with infinite support, the structural source of the later positivity and spectral results.

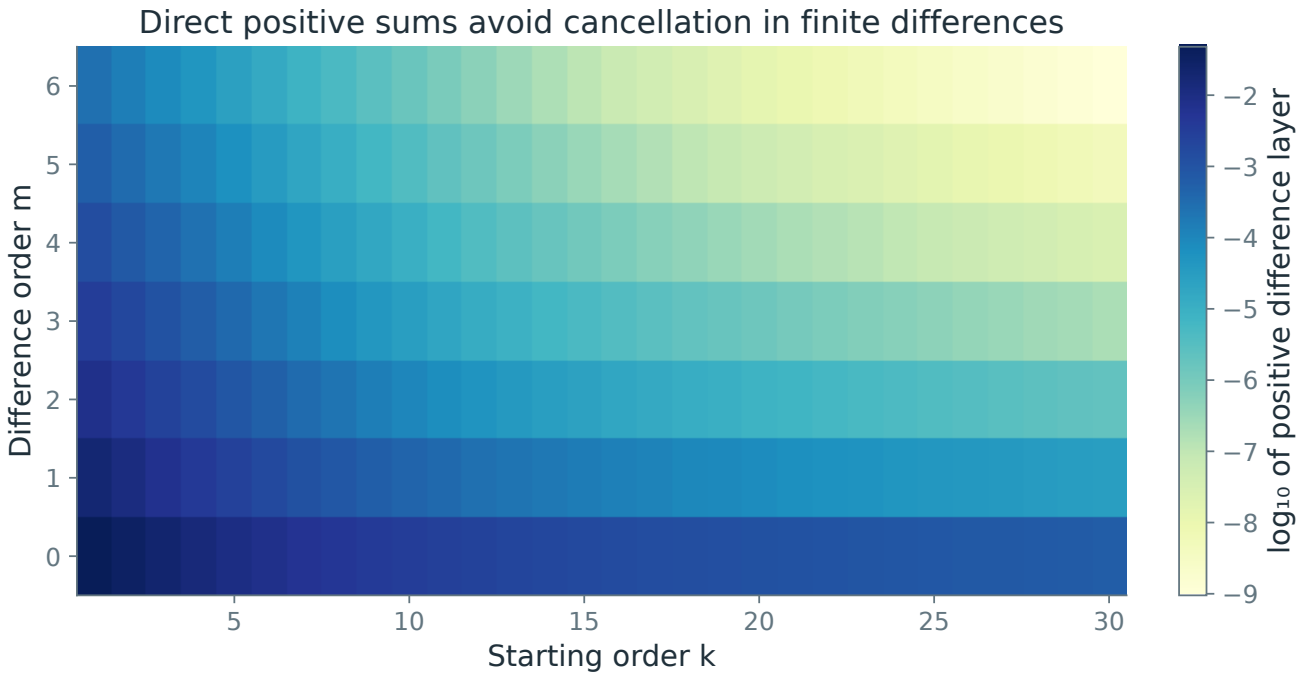
Work an example. At $n = 1$, the atom has weight 1 and contributes to E_0 under the moment convention $0^0 = 1$. At $n = 2$, $x_2 = 9/16$ and $w_2 = 1/16$. The total mass is exactly $E_0 = \zeta(4)/\zeta(8) = 105/\pi^4$.

Carry forward. Keep the zero atom when forming moments and the resolvent.

Source and scope. Volume II, Chapter 7, "The squarefree packet energy." Principal parameters $a = \beta = 2, q = 1$. The picture shows positive atoms through $n = 60$; the mathematical measure has infinitely many atoms.

PAPER II / 06 **LESSON 26**

Every alternating difference layer is positive



$$(-1)^m \Delta^m E_k = \sum_n w_n x_n^k (1 - x_n)^m \geq 0.$$

Read the figure. The horizontal direction changes packet depth and the vertical direction changes difference order. Color records the logarithm of a direct positive sum. The figure does not form large differences of nearly equal numerical energies. The moment representation supplies the positive expression first, making the sign transparent at every displayed depth and difference order.

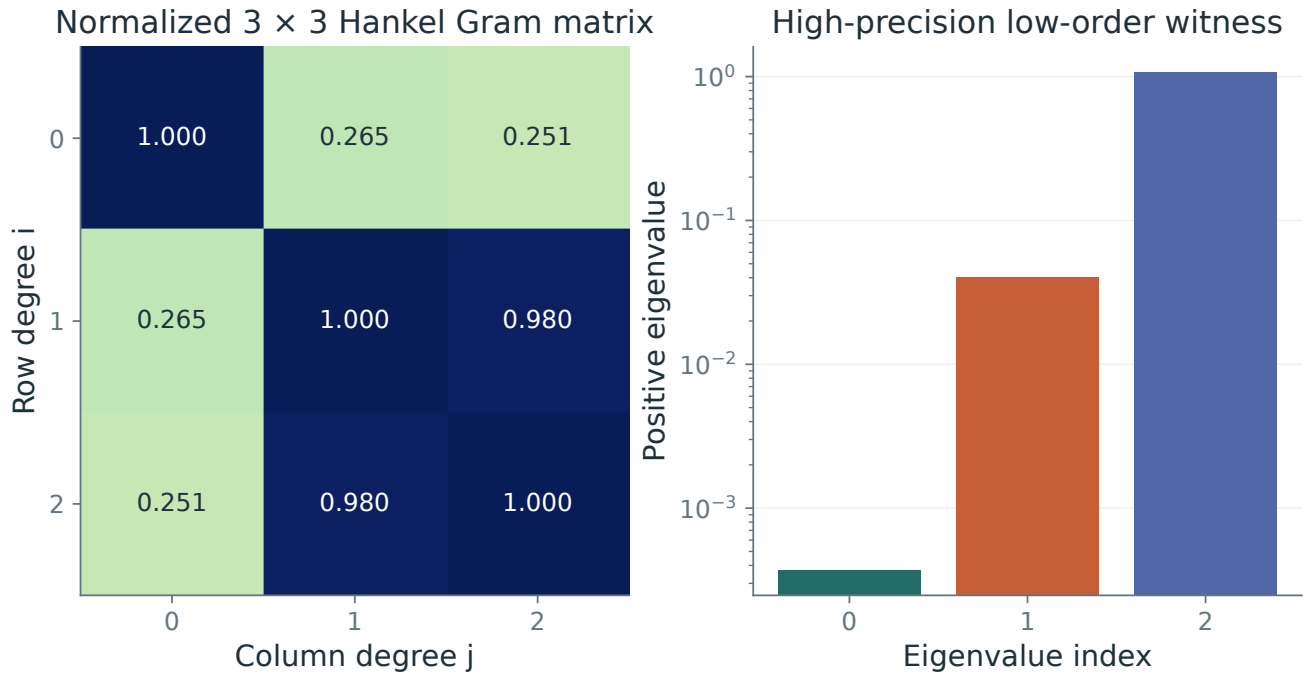
Work an example. For $m = 1$, $E_k - E_{k+1} = \sum_n w_n x_n^k (1 - x_n)$. For $m = 2$, $E_k - 2E_{k+1} + E_{k+2} = \sum_n w_n x_n^k (1 - x_n)^2$. Both are positive because the measure has positive mass away from the endpoints. The same mechanism continues to every integer $m \geq 0$.

Carry forward. Complete monotonicity is an exact representation, not a pattern inferred from a heatmap.

Source and scope. Volume II, Chapter 7, Theorem 7.1, "Complete monotonicity." Plot: $1 \leq k \leq 30$, $0 \leq m \leq 6$, $N = 200000$. Omitted layer m is at most $2^m / [(3 + 2m) N^{3+2m}]$; rounding is separate.

PAPER II / 07 **LESSON 27**

Hankel positivity is a Gram-space statement



$$c^{*}H_{d}c=\int\left|\sum_{j=0}^{d}c_{j}x^{j}\right|^{2}d\nu(x)>0\qquad(c\neq 0).$$

Read the figure. The first panel normalizes the entries of a three-by-three Hankel matrix to show correlations among monomials. The second plots its positive eigenvalues using high-precision low-order moments. Very unequal eigenvalues do not contradict positivity. The proof uses infinitely many distinct atoms: a nonzero polynomial cannot vanish at all of them.

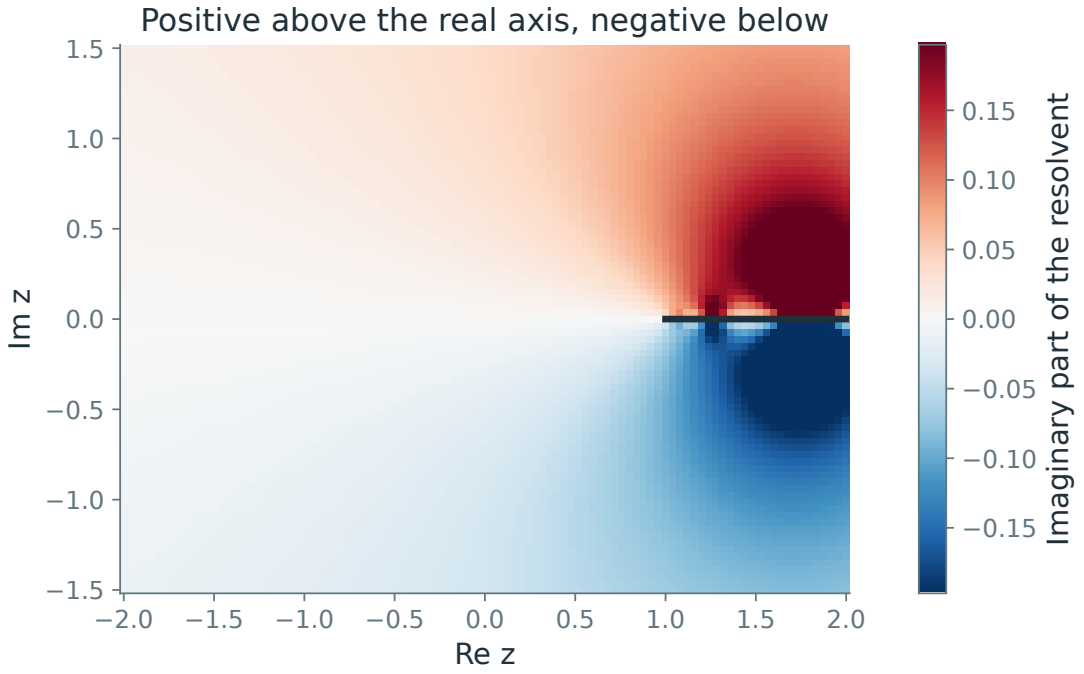
Work an example. For the two-by-two matrix, strict positivity reads $E_0E_2 - E_1^2 > 0$. With principal parameters it is about 0.03026887920. This follows from the nonconstant function x having positive variance under the normalized measure, and independently agrees with the exact zeta-ratio evaluations.

Carry forward. Finite numerical eigenvalues illustrate an exact Gram argument and must respect conditioning.

Source and scope. Volume II, Chapter 8, Theorem 8.1, "Strict finite Hankel positivity." Displayed moments and eigenvalues use 100-digit arithmetic. The claim is strict positivity for every finite degree, not just the displayed matrix.

PAPER II / 08 **LESSON 28**

Positive mass gives a zero-free slit resolvent



$$\operatorname{Im} \mathcal{E}(z) = \operatorname{Im} z \int \frac{x \, d\nu(x)}{|1 - zx|^2}, \qquad z \notin [1, \infty).$$

Read the figure. The upper half-plane has positive imaginary part and the lower half-plane negative imaginary part. The dark segment marks the excluded physical cut, not a line of proved zeros. On the real axis below one, the resolvent is positive. These three regions exclude zero everywhere in the slit domain. The proof uses positive mass on $x > 0$, not signed Möbius cancellation.

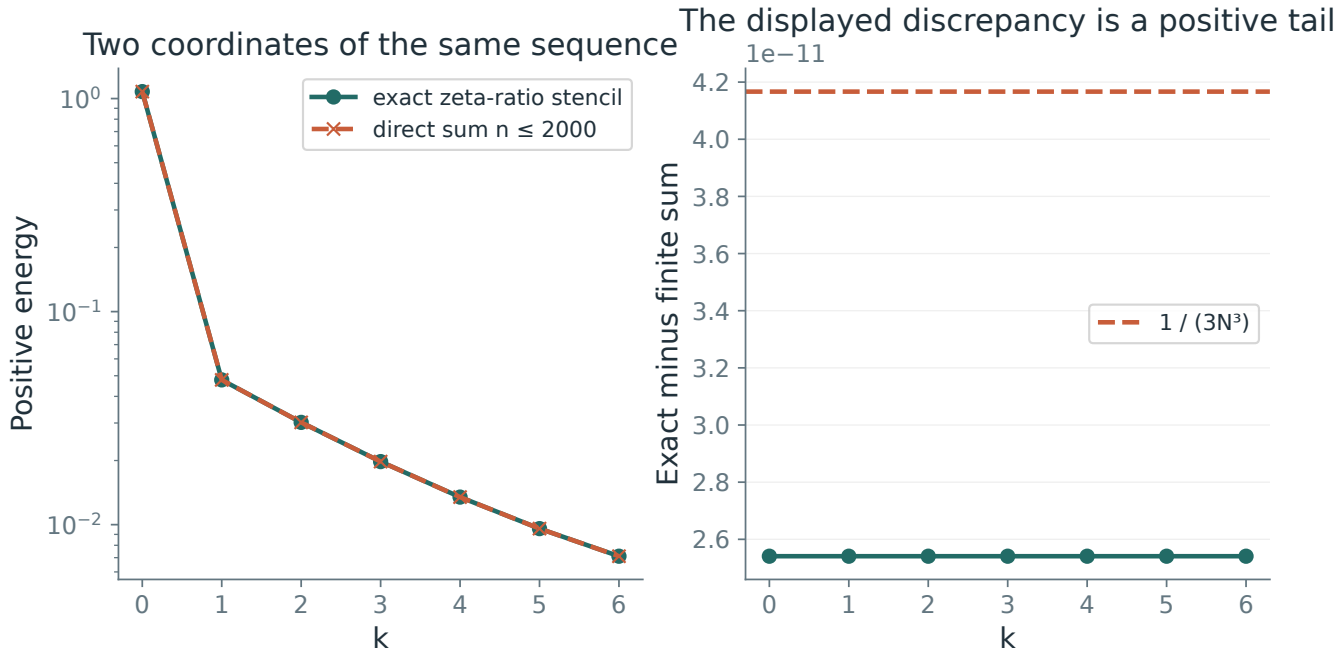
Work an example. At $z = 0$, $\mathcal{E}(0) = E_0 > 0$. At $z = i$, every positive atom contributes a positive imaginary part $w_n x_n / (1 + x_n^2)$. The zero atom adds a real constant and therefore cannot cancel that imaginary part.

Carry forward. Zero-freeness here belongs to the positive resolvent family.

Source and scope. Volume II, Chapter 8, Theorem 8.3, "Zero-free slit plane." Grid: $-2 \le \Re z \le 2$, $|\Im z| \le 1.5$, $N = 2000$. The audit bounds omitted terms using the minimum denominator distance on each retained sampled point; the cut is masked.

PAPER II / 09 **LESSON 29**

A zeta-ratio stencil exactly recovers the energy



$$E_k = \sum_{j=0}^{2k} (-1)^j \binom{2k}{j} \frac{\zeta(4+2j)}{\zeta(8+4j)}.$$

Read the figure. The first panel overlays the exact finite stencil with a direct truncated positive sum. The second resolves the small difference between them. This difference is the omitted positive tail, not disagreement between two mathematical definitions. The stencil comes from expanding the packet filter and interchanging a finite sum with an absolutely convergent Dirichlet series.

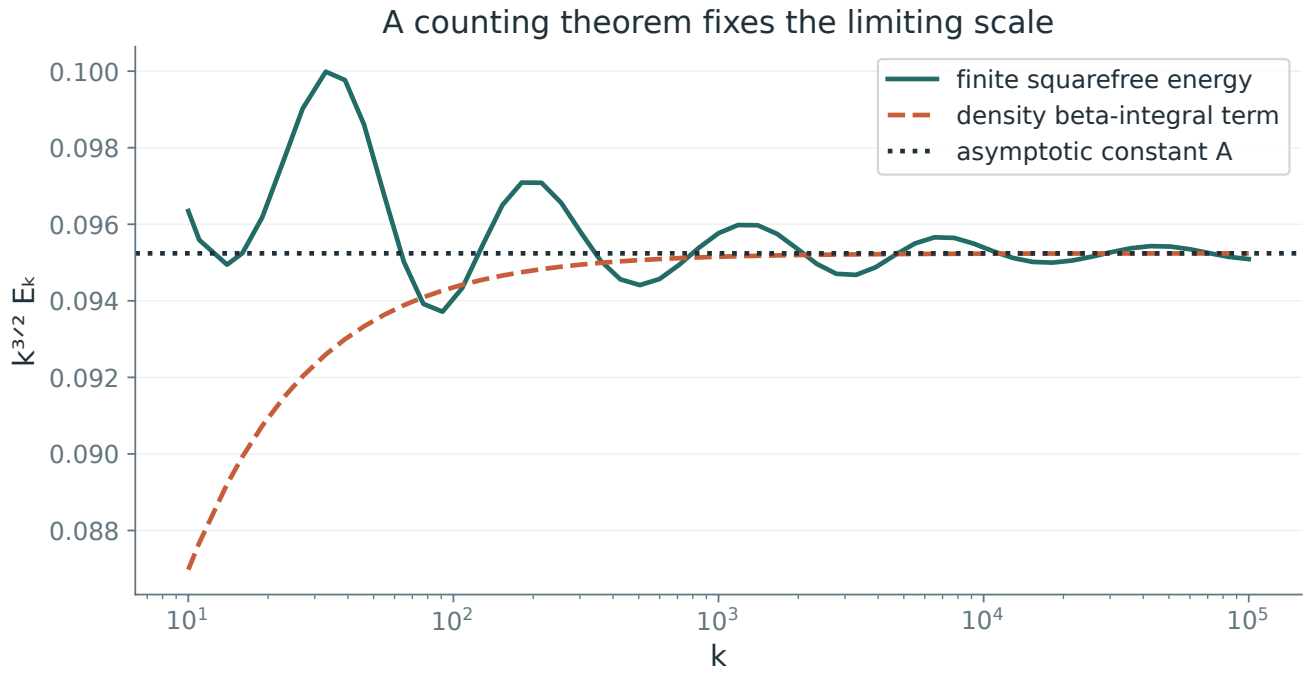
Work an example. At $k = 1$, the stencil has three terms: $E_1 = D(4) - 2D(6) + D(8)$, where $D(s) = \zeta(s)/\zeta(2s)$. It gives approximately 0.04780461034. Direct summation through $N = 2000$ undershoots the infinite value by at most $1/(3N^3)$.

Carry forward. Exact coordinate changes can require extra numerical precision when their coefficients alternate.

Source and scope. Volume II, Chapter 9, Theorem 9.1, "Exact zeta-ratio finite difference." Principal parameters; $0 \le k \le 6$. Stencil values use 100-digit arithmetic, and the finite sums use the explicit absolute tail bound.

PAPER II / 10 **LESSON 30**

Squarefree counting fixes the energy scale



$$E_k \sim Ak^{-3/2}, \qquad A = \frac{3}{2^{5/2}\pi^{3/2}}.$$

Read the figure. Multiplying by $k^{3/2}$ removes the leading power decay. The finite arithmetic curve approaches the horizontal constant. The dashed curve is the density contribution expressed by a beta integral. The remaining difference includes arithmetic counting error. The asymptotic theorem uses the classical squarefree counting estimate; the graph displays its finite behavior.

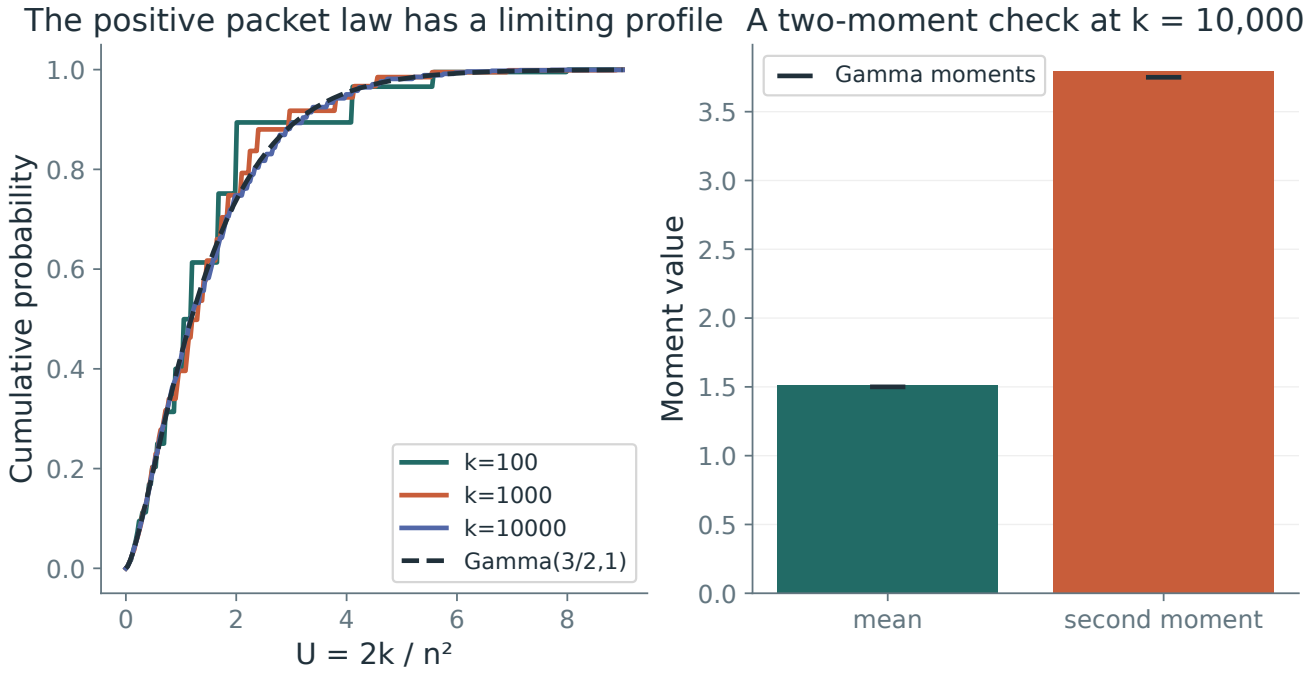
Work an example. For the principal parameters, the density term is $(3/\pi^2)\mathrm{B}(3/2, 2k+1)$. The beta-function asymptotic yields $A \approx 0.09524045390$. At general $a > 1/2, \beta > 0$, the exponent is $\alpha = (2a-1)/\beta$ and the leading constant also contains the coprime squarefree density for the actual modulus.

Carry forward. Record which counting theorem supplies an asymptotic result and which data merely illustrate it.

Source and scope. Volume II, Chapter 10, Theorem 10.1, "Packet-energy asymptotic." Plot: $10 \le k \le 100000$, $N = 200000$; absolute energy tail $\le 1/(3N^3)$. Classical counting and beta asymptotics are source inputs.

PAPER II / 11 **LESSON 31**

The active coordinate approaches a Gamma law



$$U_k = \frac{2k}{n^2} \Longrightarrow \mathrm{Gamma}(3/2, 1), \qquad \mathbb{E}[U^m] = \frac{\Gamma(3/2+m)}{\Gamma(3/2)}.$$

Read the figure. The distribution curves describe where the normalized positive energy lives in inverse-scale coordinates. Different packet depths approach the same Gamma cumulative distribution. The second panel checks two moments at a large finite depth. The law is weighted by packet energy; it is not the unweighted histogram of integers or squarefree labels.

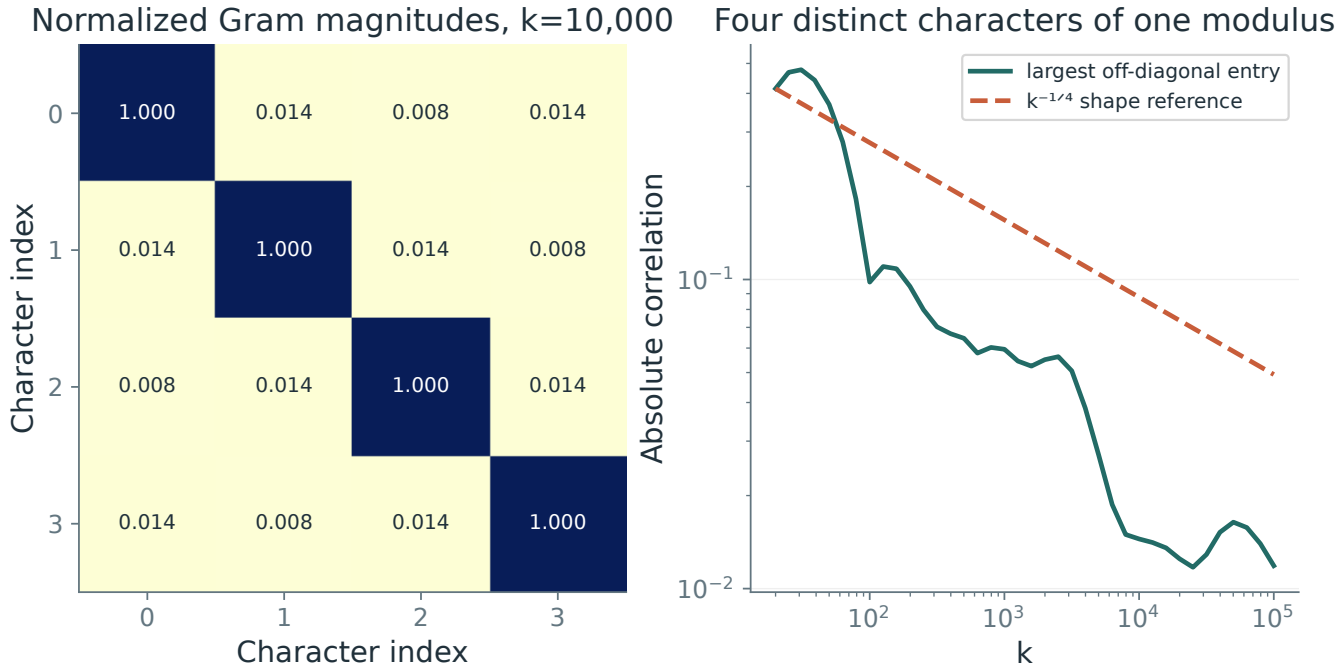
Work an example. The limiting mean is $3/2$ and the limiting second moment is $15/4$. For each integer $m \geq 0$, the finite-depth identity shifts the energy parameter: $\mathbb{E}_k[U_k^m] = (2k)^m E_{2+m,2,1}(k) / E_{2,2,1}(k)$. Applying the energy law gives those Gamma moments.

Carry forward. The moment identity supplies more information than weak convergence alone.

Source and scope. Volume II, Chapter 11, Theorem 11.1, "Gamma scaling limit." $k = 100, 1000, 10000$, $N = 200000$; CDFs sampled on $0 \leq U \leq 9$. Omitted normalized probability is bounded by $1/(3N^3 E_k^{(N)})$.

PAPER II / 12 **LESSON 32**

Distinct characters decohere at a fixed modulus



$$\frac{G_{\chi,\psi}(k)}{E_{a,\beta,q}(k)} = O_{a,\beta,q}(k^{-1/(2\beta)}) \qquad (\chi \neq \psi \bmod q).$$

Read the figure. The diagonal of the normalized character Gram matrix stays one. The off-diagonal entries measure overlap between distinct multiplicative phases. The second panel follows the largest such overlap as depth increases. Its reference line shows the theorem's rate shape, anchored at the first point; it is not a proved numerical upper envelope. All four characters are represented with the same actual modulus five.

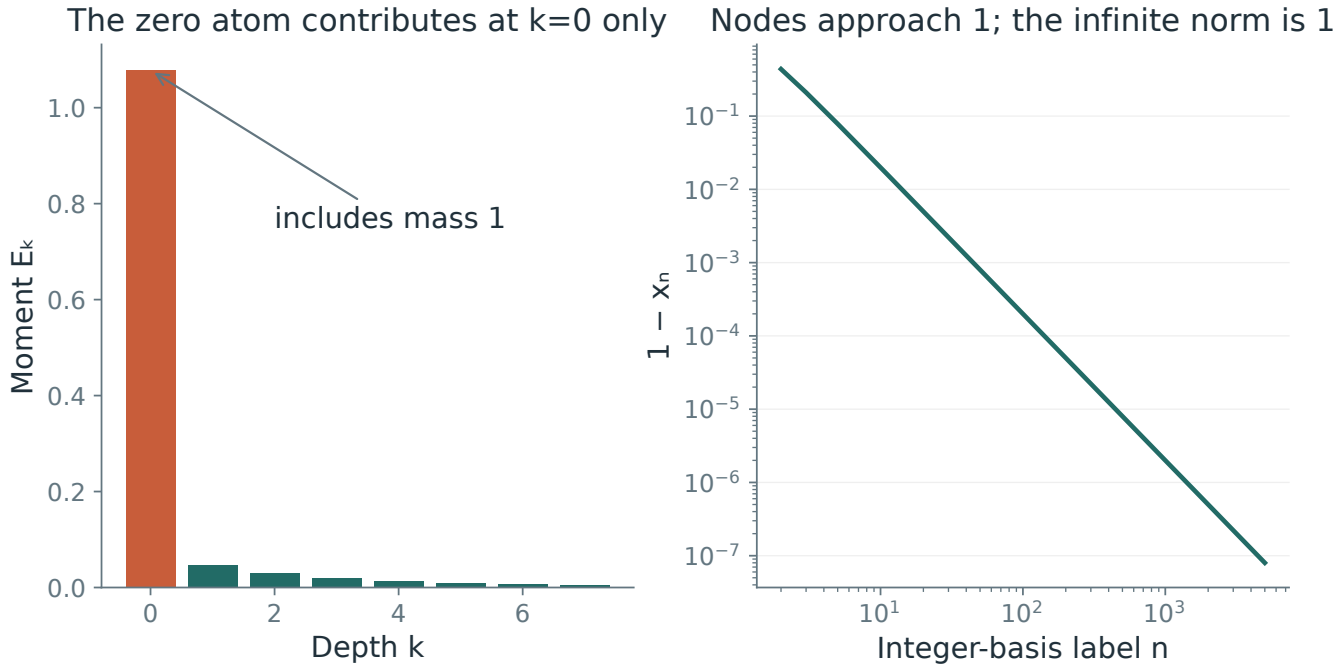
Work an example. Here $a = \beta = 2$, so the normalized source rate is $k^{-1/4}$. The product $\chi\overline{\psi}$ is nonprincipal when the two characters differ. Its squarefree weighted partial sums are $O_q(\sqrt{X})$, which supplies the off-diagonal estimate after partial summation.

Carry forward. Cross-character cancellation differs from cancellation inside the signed principal Möbius amplitude.

Source and scope. Volume II, Chapter 12, Lemma 12.1 and Theorem 12.2, "Character decoherence." $N = 200000$, $20 \leq k \leq 100000$, fixed modulus $q = 5$. The audit records a normalized-entry truncation bound. No character-uniform GRH estimate is inferred.

PAPER III / 01 **LESSON 33**

The zero packet belongs to the positive contraction



$$T|n\rangle = x_n|n\rangle, \qquad E_k = \langle v, T^k v\rangle, \qquad \|T\| = 1.$$

Read the figure. The left panel distinguishes zero depth from positive depth. The atom at $x_1 = 0$ contributes its unit mass to E_0 and vanishes from E_k for $k \geq 1$. The right panel shows the spectral gap of each integer node approaching zero. Individual nodes lie below one, but their supremum is one; there is no uniform gap for the infinite contraction.

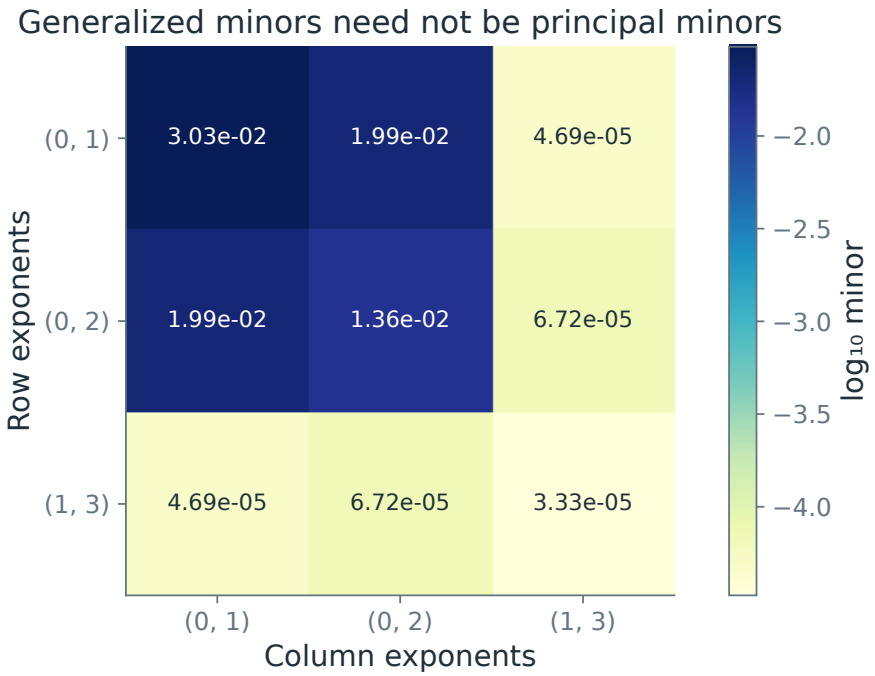
Work an example. At $n = 2$, $x_2 = 9/16$ and $1 - x_2 = 7/16$. Along squarefree primes tending to infinity, $1 - x_n = 2/n^2 - 1/n^4 \to 0$. The logarithmic scale operator $-\log(1 - n^{-2})$ is defined on $n \geq 2$; the zero packet is retained separately.

Carry forward. A zero-depth identity must preserve the endpoint atom and state its convention.

Source and scope. Volume III, Chapters 2 and 13, "Positive contraction realization" and "Number-basis realization." Figure uses principal parameters. The gap panel shows all integer nodes; squarefree nodes select an infinite subsequence with the same limiting norm.

PAPER III / 02 **LESSON 34**

Generalized Hankel minors are strictly positive



$$\det[E_{r_i+s_j}]_{i,j=0}^{d} > 0 \qquad (r_0 < \cdots < r_d,\ s_0 < \cdots < s_d).$$

Read the figure. Choose a row label and a column label to specify two strictly increasing exponent sets. Each colored cell is a two-by-two generalized minor, which need not be a principal minor of a symmetric matrix. High-precision values show several such witnesses. The proof expands the determinant into products of generalized Vandermonde determinants at ordered positive support nodes.

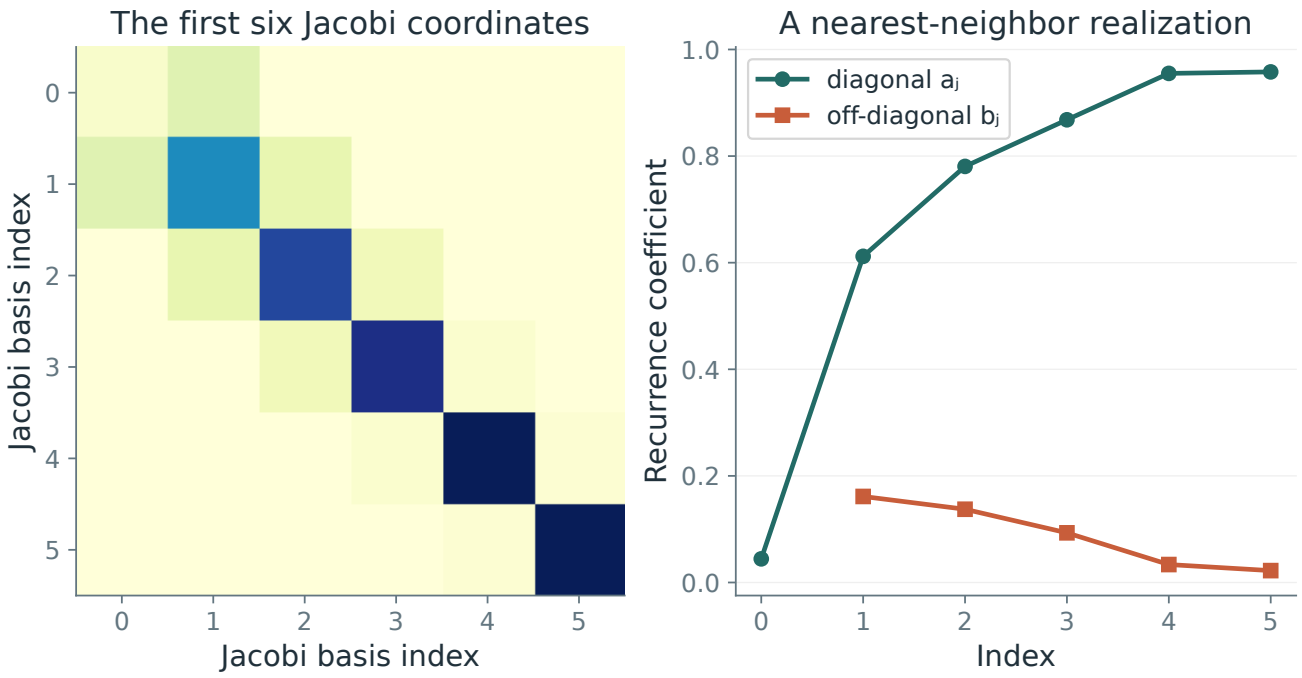
Work an example. For row exponents $(0,1)$ and column exponents $(0,2)$, the minor is $E_0E_3 - E_1E_2$. For rows and columns both $(1,3)$, it is $E_2E_6 - E_4^2$. The infinite support contains enough positive nodes to make the relevant Vandermonde contribution strictly positive.

Carry forward. Total positivity is stronger than positivity of principal Hankel quadratic forms.

Source and scope. Volume III, Chapter 3, Theorem 3.1, "Strict total positivity." Nonnegative, strictly increasing integer exponent sets; low-order values here use 100-digit exact zeta-ratio moments. The theorem covers all finite sizes, not only this grid.

PAPER III / 03 **LESSON 35**

One measure determines a Jacobi recurrence



$$xp_m(x) = b_{m+1}p_{m+1}(x) + a_m p_m(x) + b_m p_{m-1}(x),$$
$$b_m > 0 \ (m \geq 1), \qquad b_0 = 0, \qquad p_{-1} = 0.$$

Read the figure. The matrix panel shows only nearest-neighbor couplings in the orthogonal-polynomial basis. The coefficient panel separates diagonal positions from off-diagonal couplings. This Jacobi system represents the same positive measure that was diagonal in the integer basis. Its coefficients are determined by moments rather than selected as free fitting parameters. The displayed global system is distinct from the later tilted, scaled system.

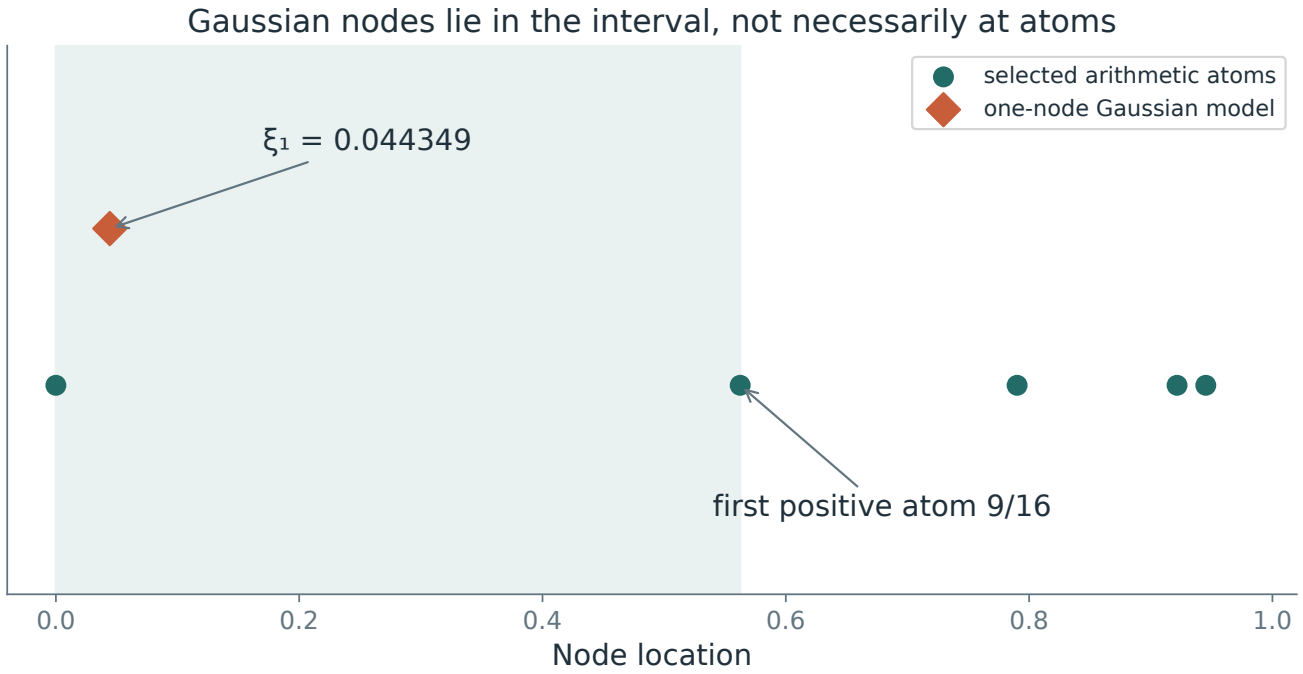
Work an example. The first diagonal coefficient is $a_0 = \int x\,d\nu / \int d\nu = E_1/E_0$. The first off-diagonal coefficient is the square root of the normalized variance of x. Both therefore follow directly from the first three moments. Higher coefficients continue the orthogonalization.

Carry forward. Changing basis makes a diagonal arithmetic operator into a canonical tridiagonal transfer.

Source and scope. Volume III, Chapter 4, "The zero-free Stieltjes-Jacobi function," recurrence and Jacobi matrix after Theorem 4.1. The leading six-by-six block is computed from 100-digit moment data.

PAPER III / 04 **LESSON 36**

A Gaussian node can lie between arithmetic atoms



$$\xi_1 = \frac{E_1}{E_0}, \qquad 0 < \xi_1 < \frac{5}{48} < \frac{9}{16}.$$

Read the figure. The colored atoms lie on the horizontal support line. The diamond is the one-node Gaussian location. It is a weighted mean inside the interval spanned by the measure and lies in a gap of the discrete arithmetic spectrum. Gaussian compression therefore does not preserve the individual atom addresses. The shaded region isolates the simplest exact counterexample to that stronger claim.

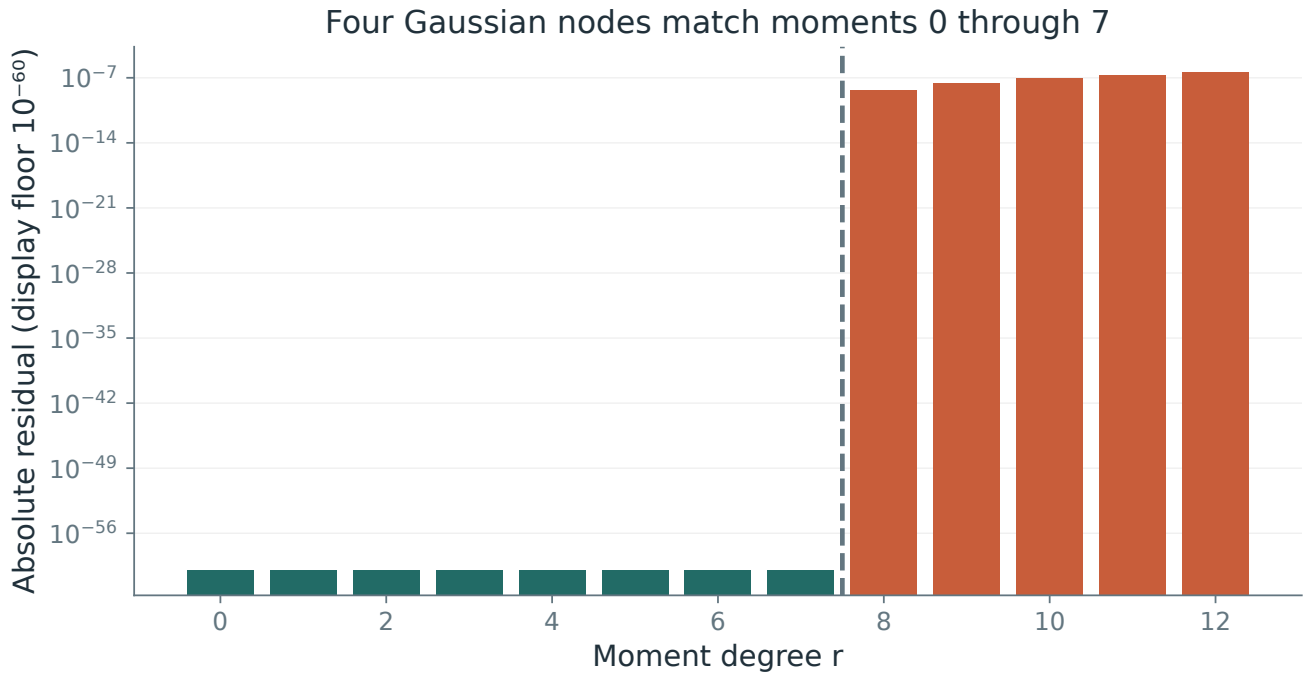
Work an example. For principal parameters, $\xi_1 \approx 0.04434860610$, while the first positive arithmetic atom is $9/16 = 0.5625$. Since $E_0 \geq 1$ and $E_1 < \sum_{n\geq 2} n^{-4} < 5/48$, the gap statement follows without numerical computation. The one-node rule matches moments zero and one.

Carry forward. Use the support interval for Gaussian nodes, rather than claiming membership in the discrete spectrum.

Source and scope. Volume III, Chapter 5, Theorem 5.1, "Moment-exact packet reduction." This is the consolidation correction to the original abstract's spectrum wording. The displayed mean uses 100-digit exact moments.

PAPER III / 05 **LESSON 37**

Four nodes preserve exactly eight moments



$$E_r = E_0 \sum_{j=1}^{m} \lambda_j \xi_j^r = E_0 e_1^T J_m^r e_1, \qquad 0 \le r \le 2m-1.$$

Read the figure. Bars before the vertical divider lie below the display floor; they witness the exact moment contract numerically at high precision. Bars after the divider show the first moments beyond that contract. The divider marks degree seven for a four-node rule. Matching early moments is a precise finite statement, not equality of the complete infinite measure and reduced model.

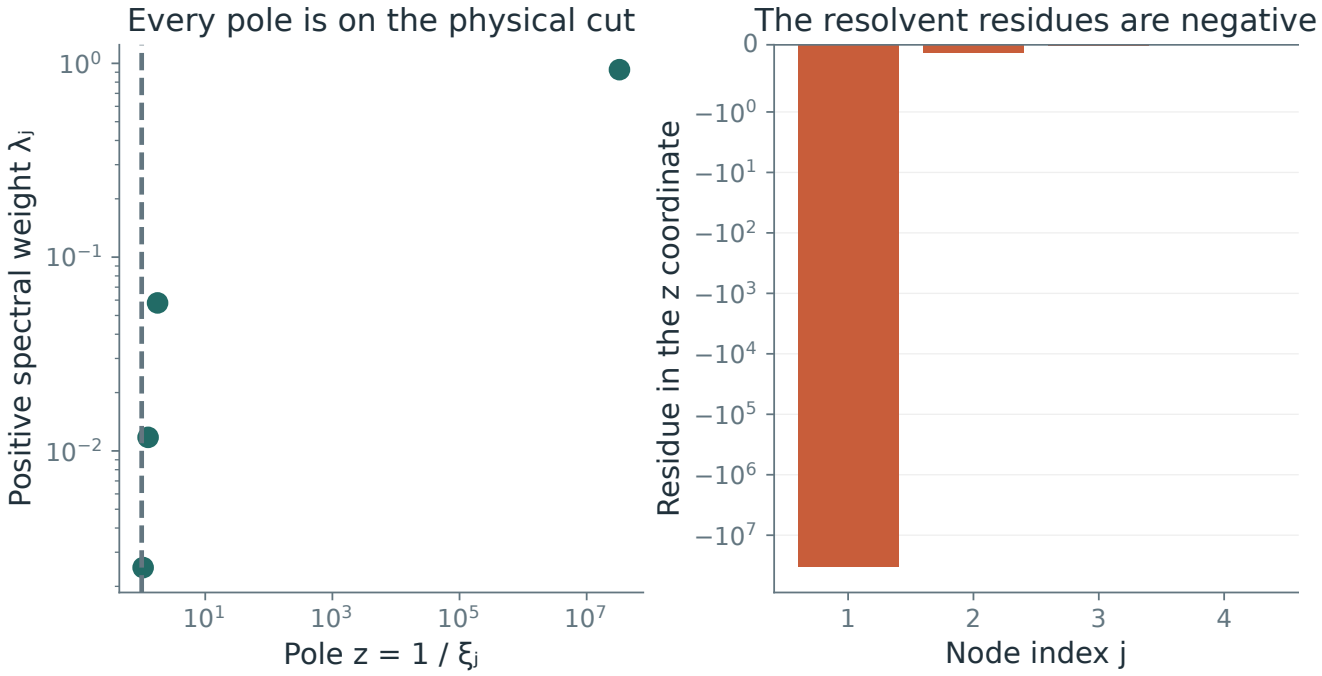
Work an example. With $m = 4$, degrees $0, 1, \ldots, 7$ are exact by Gaussian quadrature. Degree eight is outside that guarantee and displays a nonzero residual. The degree-zero equality states that positive normalized weights sum to one, while the degree-one equality preserves the measure's mean.

Carry forward. State which moments a reduction preserves and where its guarantee ends.

Source and scope. Volume III, Chapter 5, Theorem 5.1, "Moment-exact packet reduction." Gaussian nodes and weights use 100-digit arithmetic; residuals are plotted with floor 10^{-60}. This is a numerical witness of the source theorem, not a new universal proof.

PAPER III / 06 **LESSON 38**

Positive spectral weights have negative z-residues



$$\mathcal{E}_m(z) = E_0 \sum_j \frac{\lambda_j}{1 - z\xi_j}, \qquad \operatorname{Res}_{z=1/\xi_j} \mathcal{E}_m = -\frac{E_0 \lambda_j}{\xi_j} < 0.$$

Read the figure. The first panel places positive weights at their physical-cut poles. The second records the residues in the variable z. Their signs are negative because differentiating the denominator contributes $-\xi_j$. The weights remain positive. This distinction depends on the coordinate and should not be hidden under the word positivity. The logarithmic pole axis keeps distant poles visible.

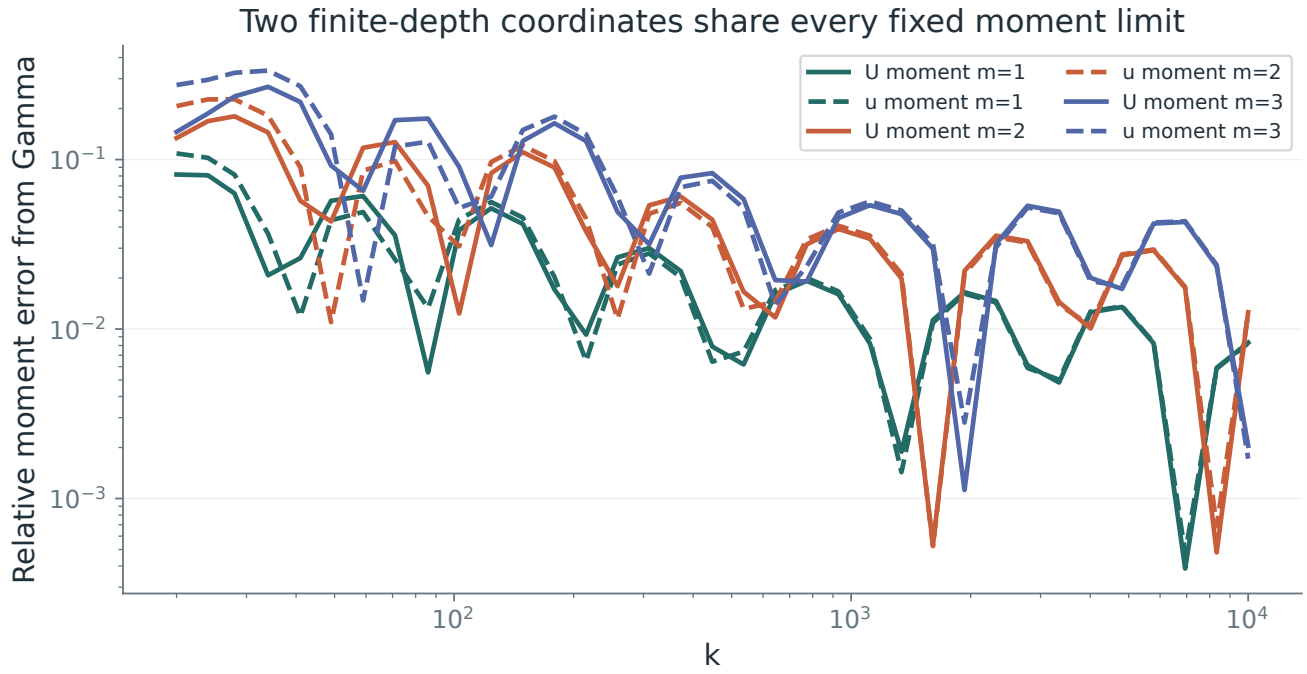
Work an example. For a one-node model, the pole is about 22.54862301 and the residue about -24.30579519. For the plotted four-node model, each node lies strictly in $(0, 1)$, so each pole lies strictly above one. No exact Gaussian node equals the zero atom.

Carry forward. Identify whether positivity refers to weights, moments, or coefficients in a chosen coordinate.

Source and scope. Volume III, Chapter 5, Corollary 5.2, corrected in consolidation. Four-node values use 100-digit moments. The formula repairs the original "positive residues" wording while preserving its positive-measure content.

PAPER III / 07 **LESSON 39**

The two Gamma coordinates share all moment limits



$$u_k = U_k - \frac{U_k^2}{4k}, \qquad 0 \le U_k^m - u_k^m \le \frac{m}{4k} U_k^{m+1} \quad (m \ge 1).$$

Read the figure. Solid and dashed curves use $U_k = 2k/n^2$ and $u_k = k(1 - x_n)$, with $x_n = (1 - n^{-2})^2$, and compare their first three moments with Gamma targets. They approach the same targets without being equal at finite depth. The displayed inequality supplies the bridge: convergence of the next U moment bounds the discrepancy in the current moment. Weak convergence against bounded test functions alone would not provide this conclusion.

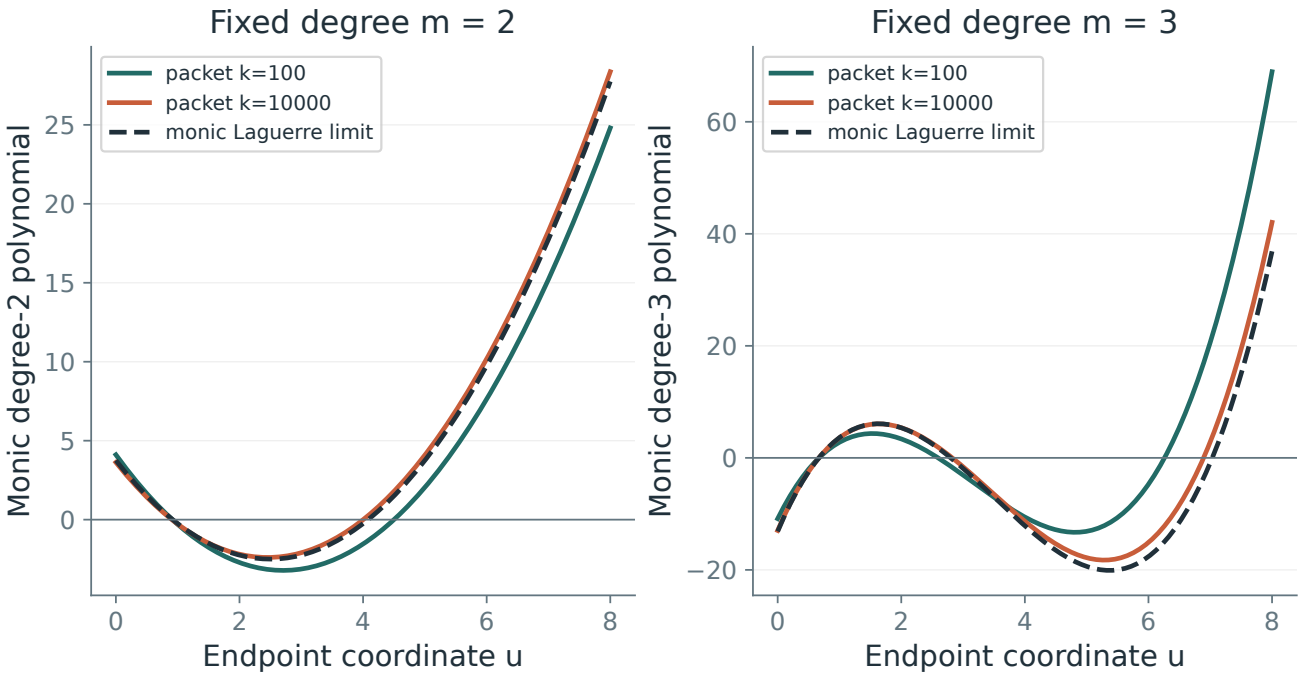
Work an example. For $m = 1$, the exact difference is $\mathbb{E}[U_k] - \mathbb{E}[u_k] = \mathbb{E}[U_k^2]/(4k)$. Its limiting numerator is $15/4$, so the discrepancy is asymptotic to $15/(16k)$. Both means still tend to $3/2$.

Carry forward. All-moment control is the needed input for polynomial and determinant convergence.

Source and scope. Volume II, Theorem 11.1's shifted-energy identity; Volume III, Theorems 6.1 and 7.1; explicit consolidation bridge. $N = 200000$, $20 \le k \le 10000$; the audit records absolute normalized-moment truncation bounds.

PAPER III / 08 **LESSON 40**

Fixed-degree packet polynomials become Laguerre



$$P_m^{(k)}(u) \longrightarrow \Lambda_m(u) = (-1)^m m! L_m^{(1/2)}(u) \quad (m \text{ fixed}).$$

Read the figure. Each panel fixes polynomial degree and changes packet depth. The dashed curve is the classical monic Laguerre limit. The finite packet polynomials are monic and come from the tilted arithmetic measure. They are generally different at finite depth. All-moment convergence gives convergence of their coefficient systems; fixing degree is essential to that implication. The plot does not claim convergence uniform in degree.

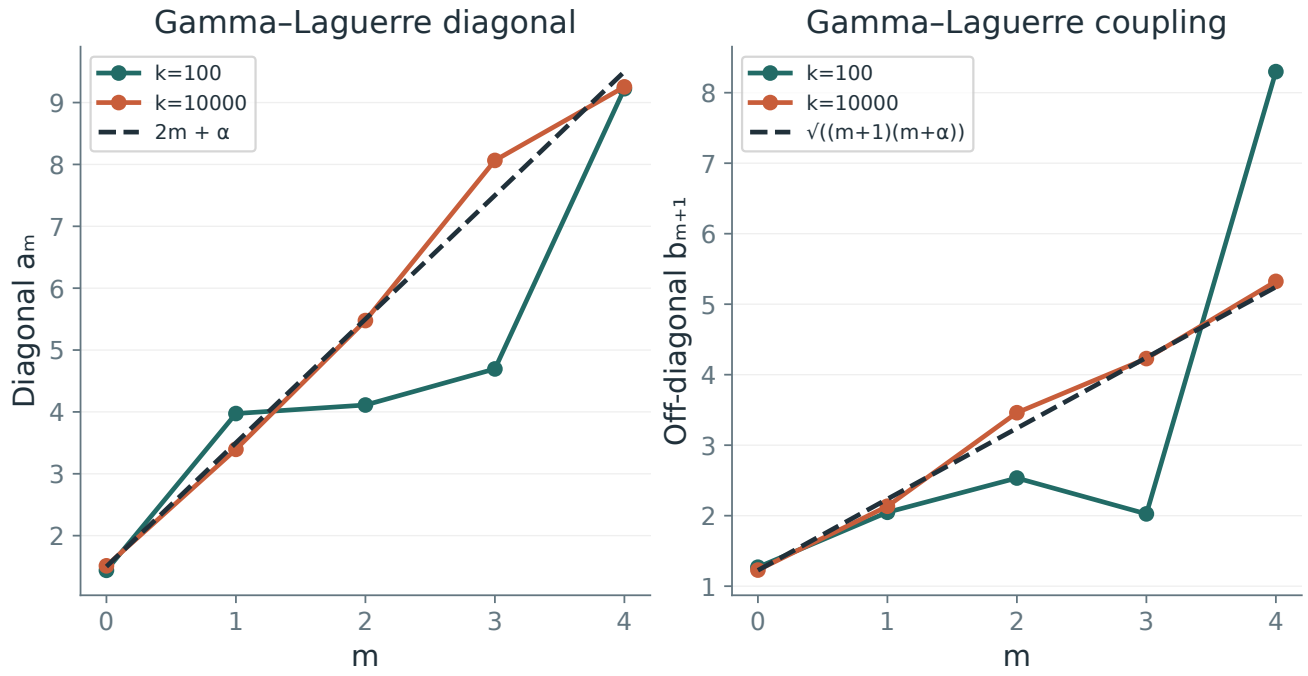
Work an example. At degree two the limit is $u^2 - 5u + 15/4$, with roots approximately 0.91886117 and 4.08113883. At degree three it is $u^3 - (21/2)u^2 + (105/4)u - 105/8$. These coefficients follow from orthogonality under the normalized Gamma-3/2 law.

Carry forward. Polynomial universality follows from a moment bridge and a nonsingular limiting Gram system.

Source and scope. Volume III, Chapter 7, Theorem 7.1, "Fixed-degree Laguerre universality," with the consolidated all-moment justification. Degrees two and three, $k = 100, 10000$, $N = 200000$, displayed on $0 \le u \le 8$.

PAPER III / 09 **LESSON 41**

The scaled Jacobi coefficients have a fixed point



$$a_m(k) \to 2m + \alpha, \qquad b_{m+1}(k) \to \sqrt{(m+1)(m+\alpha)}, \qquad \alpha = 3/2.$$

Read the figure. The left panel follows diagonal recurrence coefficients and the right follows nearest-neighbor couplings. At larger depth the arithmetic Jacobi block approaches the Gamma–Laguerre block. These coefficients belong to the endpoint coordinate u, so they should not be compared directly with the unscaled global Jacobi coefficients on $x \in [0,1]$. Only each fixed leading block is asserted to converge.

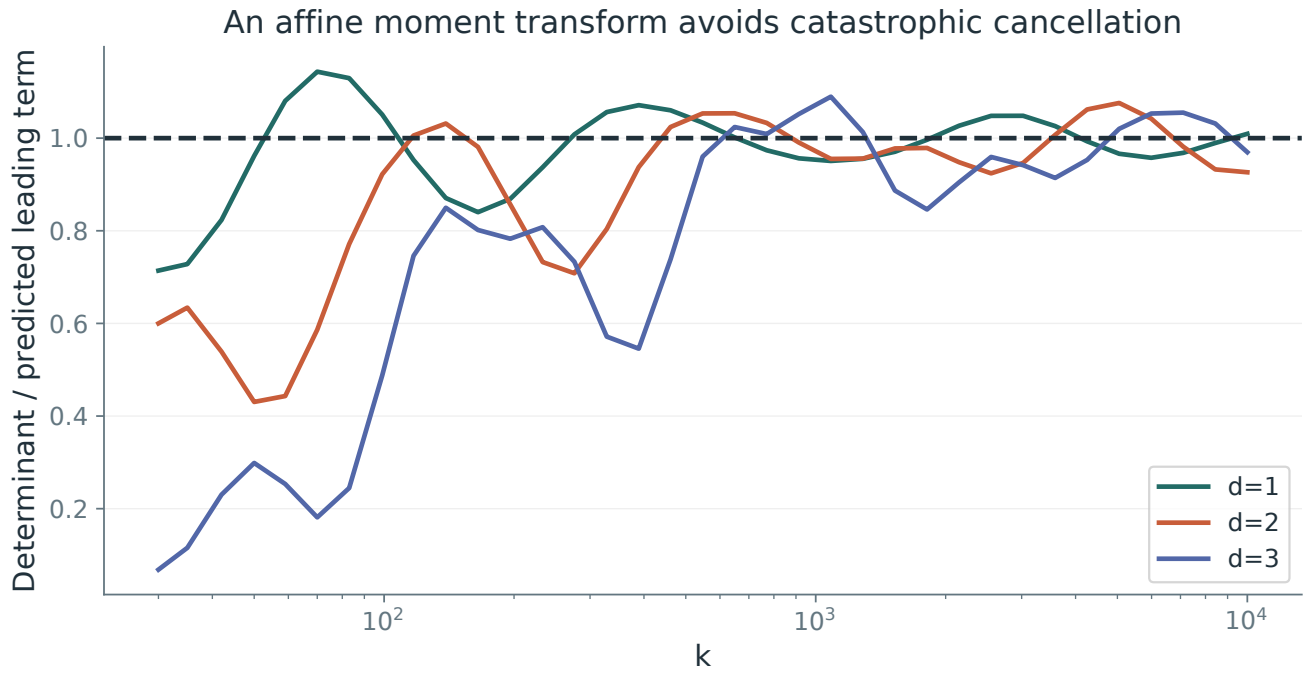
Work an example. For $m = 0, 1, 2$, the limiting diagonal is $3/2, 7/2, 11/2$. The first three off-diagonal entries are $\sqrt{3/2}$, $\sqrt{5}$, $\sqrt{21/2}$. They determine the first leading block and its Gaussian rule.

Carry forward. Specify both the coordinate and the fixed-degree range of a recurrence limit.

Source and scope. Volume III, Chapter 7, Corollary 7.2, "Jacobi fixed point." Principal shape $\alpha = 3/2$; first five coefficients at $k = 100, 10000$, $N = 200000$. Finite Lanczos computations use reorthogonalization.

PAPER III / 10 **LESSON 42**

A shifted determinant has an explicit leading constant



$$\Delta_d(k) \sim A^{d+1} \prod_{j=0}^{d} j!(3/2)_j \, k^{-3(d+1)/2-d(d+1)} \quad (d \text{ fixed}).$$

Read the figure. Each curve divides a shifted Hankel determinant by its predicted leading term. The ratios approach one. The computation changes basis to the endpoint coordinate before evaluating a determinant, avoiding subtraction of nearly equal shifted energies. This numerical method follows the exact affine basis-change argument used in the proof. The plot illustrates fixed determinant orders one, two, and three.

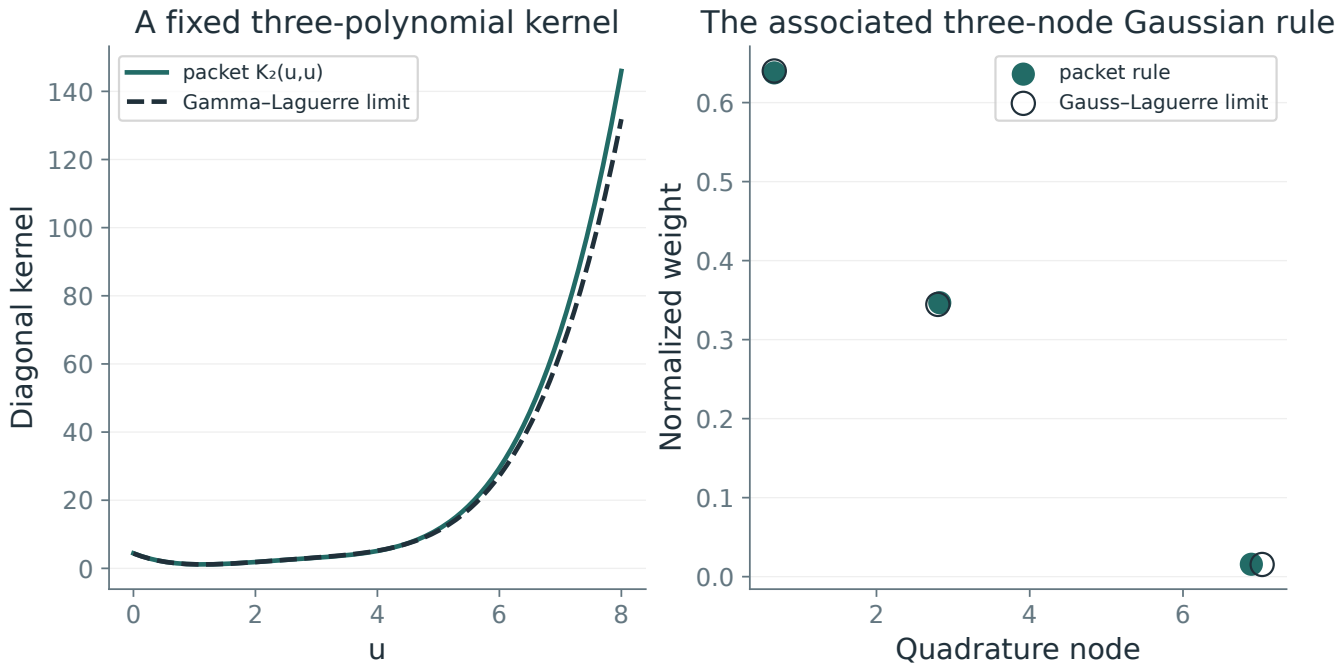
Work an example. For $d = 1$, the determinant is $E_k E_{k+2} - E_{k+1}^2$. Its leading term is $(3/2)A^2k^{-5}$. The factor k^{-2} beyond the two energy factors comes from the affine transformation of the two monomial bases.

Carry forward. Small determinants need a stable coordinate representation as well as an asymptotic formula.

Source and scope. Volume III, Chapter 8, Theorem 8.1, "Complete leading Hankel asymptotic." $30 \le k \le 10000$, $N = 200000$. Underlying moment tails are recorded; this plot is not a certified determinant-error interval.

PAPER III / 11 **LESSON 43**

The kernel and Gaussian rule share the same limit



$$K_d^{(k)} \to K_d^{(3/2)}, \qquad (\xi_j^{(k)}, \lambda_j^{(k)}) \to (\xi_j^{\mathrm{GL}}, \lambda_j^{\mathrm{GL}}) \quad (d, m \text{ fixed}).$$

Read the figure. The left panel sums three orthonormal polynomial squares on the diagonal of a fixed-degree kernel. The right compares the associated three-node Gaussian rule with its normalized Gauss–Laguerre limit. Their common input is the converging finite Jacobi block. Kernel convergence and quadrature convergence are separate outputs of the same moment and recurrence structure.

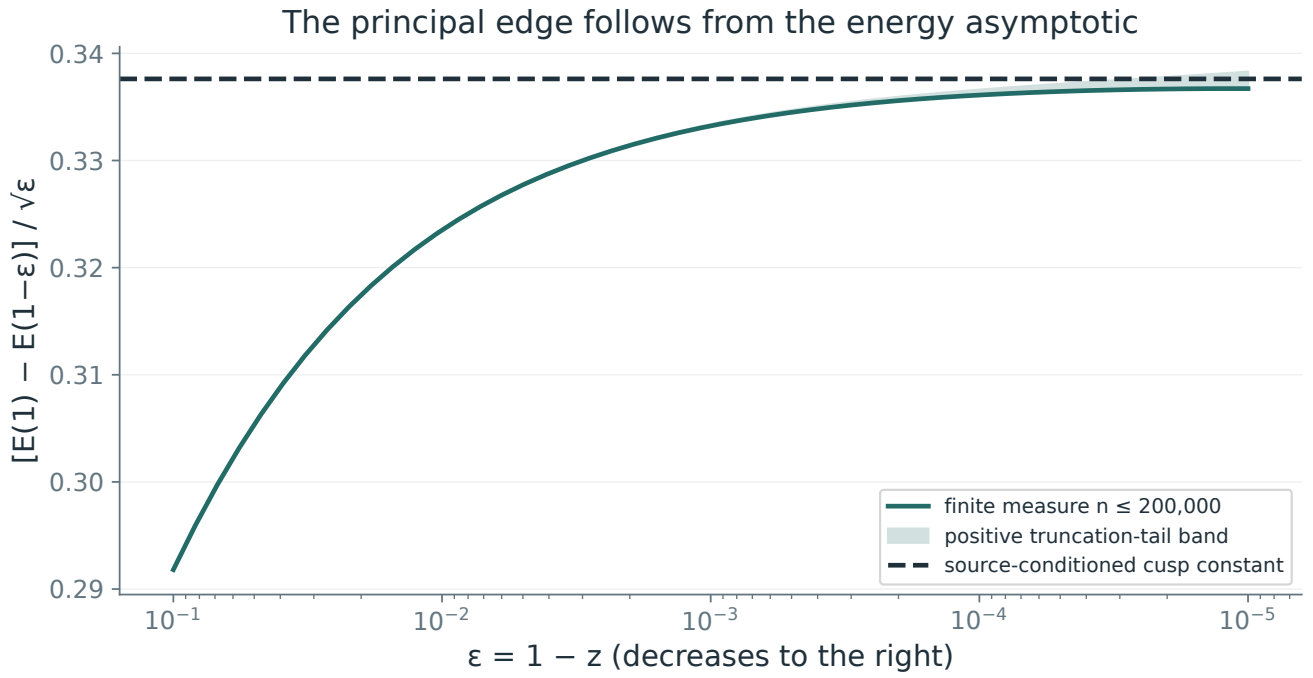
Work an example. The limiting three-node locations are approximately 0.66632591, 2.80077505, and 7.03289904. Their positive weights integrate the normalized Gamma density, so they sum to one. This differs from unnormalized generalized-Laguerre weights, whose sum is $\Gamma(3/2)$.

Carry forward. State the measure normalization when comparing kernels or quadrature weights.

Source and scope. Volume III, Chapters 9–10, Theorems 9.1 and 10.1, "Fixed-degree kernel convergence" and "Quadrature fixed point." $d = 2, m = 3, k = 10000, N = 200000$. Sampled diagonal kernels on $0 \le u \le 8$ illustrate the stronger local-uniform source result.

PAPER III / 12 **LESSON 44**

The edge cusp follows conditionally from energy decay



$$\mathcal{E}(1) - \mathcal{E}(z) \sim 2\sqrt{\pi} A \sqrt{1-z} = \frac{3}{2^{3/2}\pi} \sqrt{1-z} \qquad (z \uparrow 1).$$

Read the figure. Read the horizontal axis toward the right: $\varepsilon = 1 - z$ decreases. Dividing the positive resolvent difference by $\sqrt{\varepsilon}$ exposes the cusp constant. The shaded band adds a positive omitted-tail bound. The asymptotic implication follows from the source energy law through the consolidation's Abelian argument; it does not require an informal continuous density for a discrete measure.

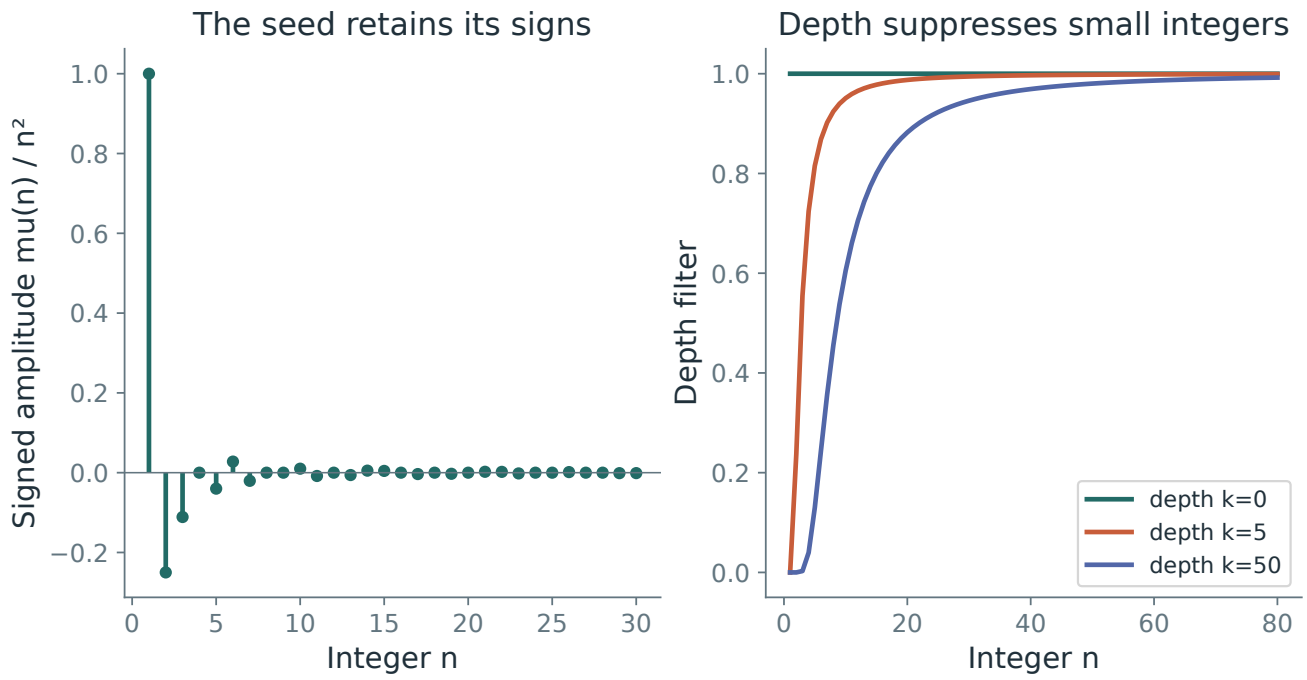
Work an example. Write the difference as $\sum_{k\geq 0} E_k(1 - z^k)$. Conditional on $E_k \sim Ak^{-3/2}$, set $t = -\log z$ and use the integrable profile $u^{-3/2}(1 - e^{-u})$. Its integral is $2\sqrt{\pi}$, giving the displayed constant. Terms away from the endpoint contribute lower-order corrections.

Carry forward. A repaired analytic passage should name its source input and preserve its exact conclusion.

Source and scope. Volume III, Chapter 11, Theorem 11.1, "Principal edge cusp," with the consolidation Abelian repair. $N = 200000$, $10^{-5} \leq \varepsilon \leq 0.1$; omitted difference $\leq 1/N$. The band controls truncation, not interval-certified rounding; no RH bound follows.

PAPER IV / 01 **LESSON 45**

Keep the signs while changing depth



$$C_{a,\beta}(k,t) = \sum_{n\geq 1} \frac{\mu(n)}{n^{a+it}} y_n^k, \qquad y_n = 1 - n^{-\beta}, \quad a > 1,\ \beta > 0$$

Read the figure. The seed panel shows signed amplitudes. Squareful integers vanish, while squarefree integers can contribute either sign. The depth panel displays a separate positive filter. It favors larger integers as depth grows. Filtering does not remove the Möbius signs or replace the signed amplitude with its squared magnitude.

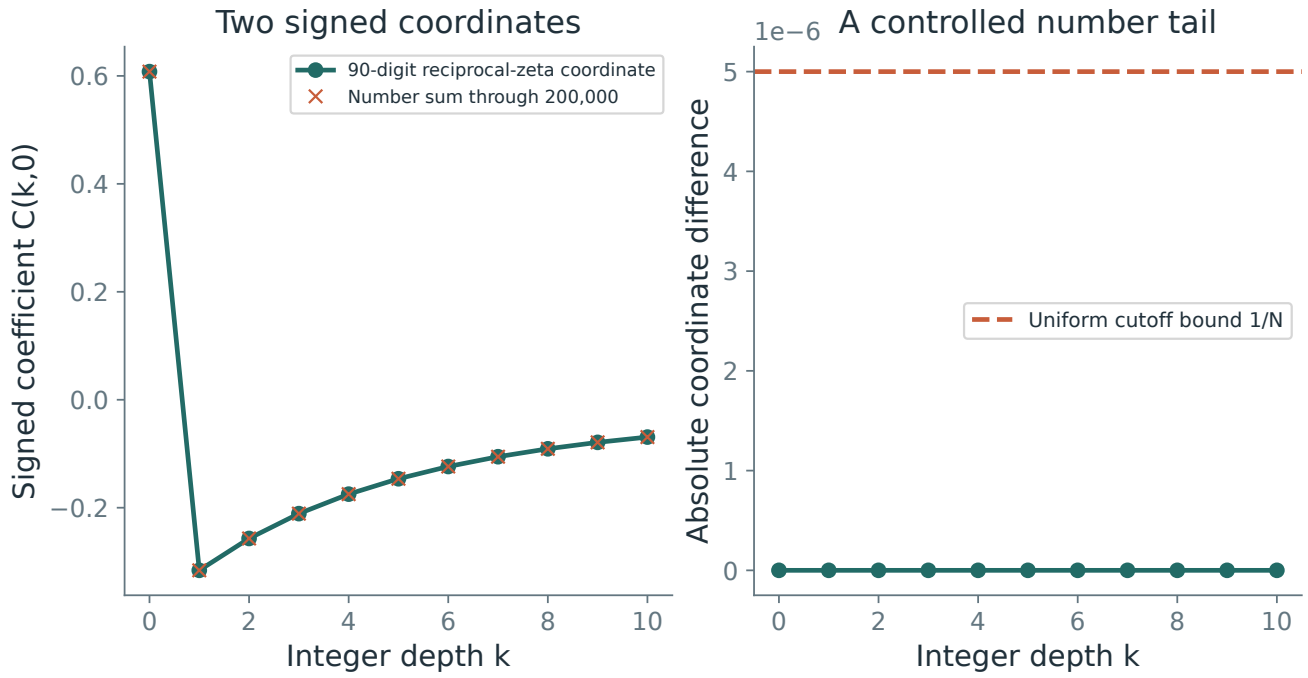
Work an example. Set $a = \beta = 2$. The $n = 1$ amplitude is one at depth zero. Its filter is zero at every positive depth, so this atom disappears immediately. At $n = 2$, the amplitude is $-1/4$ and the depth-five filter is $(3/4)^5$. The complete coefficients begin $C(0,0) \approx 0.607927$ and $C(1,0) \approx -0.316011$.

Carry forward. Arithmetic decay a, scale exponent β, discrete depth k, and logarithmic time t have different jobs.

Source and scope. IV Chapter 1, "One signed seed and two exact evolutions." Seed integers through 30; filters through 80. Subsequent principal calculations use $a = \beta = 2$ and cutoff $N = 200000$.

PAPER IV / 02 **LESSON 46**

Compute one coefficient in two coordinates



$$C_{2,2}(k,0) = \sum_{j=0}^{k} (-1)^j \binom{k}{j} \frac{1}{\zeta(2+2j)}, \qquad |C(k,0) - C_N(k,0)| \le \frac{1}{N}$$

Read the figure. The coefficient panel overlays a direct number sum and a finite difference of reciprocal zeta values. Both retain the signed cancellation. The error panel compares their difference with the number-cutoff bound. This bound concerns the omitted infinite tail. It does not describe rounding in a large alternating finite difference, which needs its own precision choice.

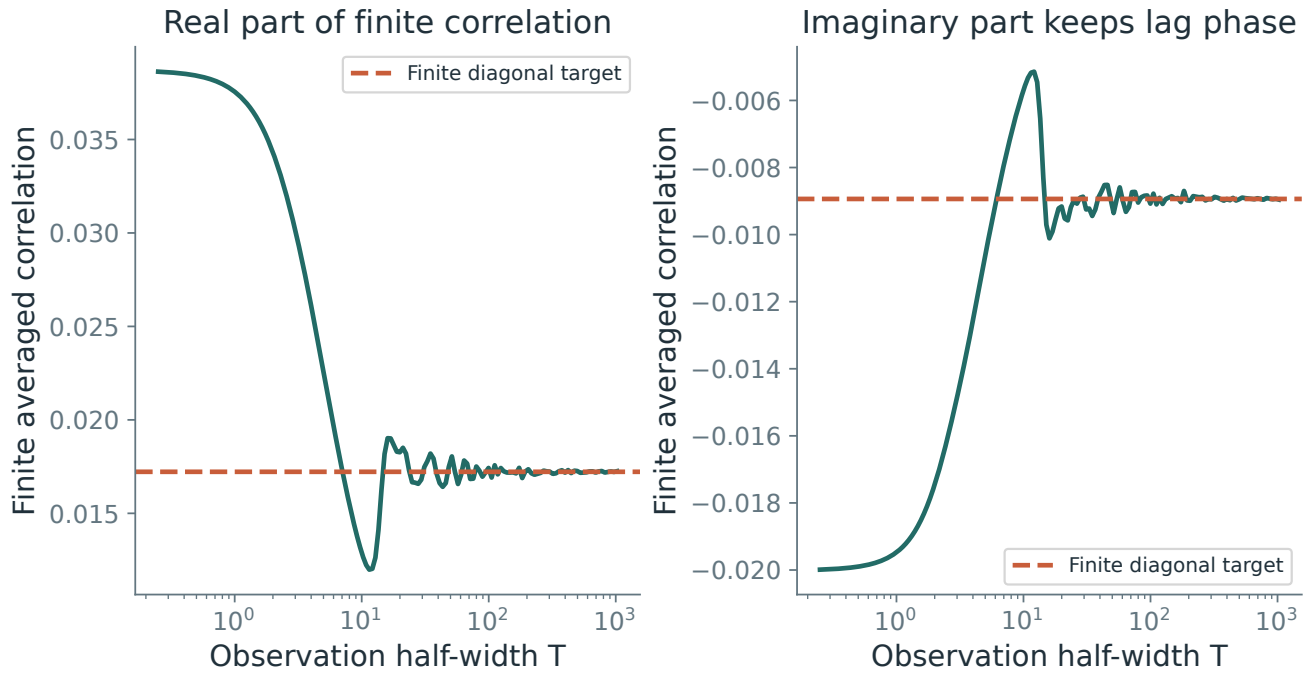
Work an example. At depth one, the filter expansion gives $C(1,0) = \zeta(2)^{-1} - \zeta(4)^{-1}$, about -0.316011. At depth two it gives $\zeta(2)^{-1} - 2\zeta(4)^{-1} + \zeta(6)^{-1}$, about -0.256997. Truncating the number sum at $N = 200000$ introduces at most 5×10^{-6} absolute error, uniformly in every displayed nonnegative integer depth.

Carry forward. Integer depth gives a finite algebraic identity. Infinite number support introduces a separately controlled approximation.

Source and scope. IV Chapter 1 finite-difference identity and Worked example 1.1, "Principal Bernoulli–zeta orbit." Depths 0–10; zeta coordinates use 90-digit arithmetic.

PAPER IV / 03 **LESSON 47**

Watch finite time extract the diagonal



$$\frac{1}{2T}\int_{-T}^{T} C_N(k,t+\tau)\overline{C_N(\ell,t)}\,dt = \sum_{n,m\le N} a_n\overline{b_m}\,\operatorname{sinc}\big(T\log(n/m)\big)$$

Read the figure. Each panel follows one component of an exactly integrated finite correlation. Off-diagonal pairs oscillate through their sinc factors. Diagonal pairs retain the lag phase and form the dashed target. Increasing the observation window need not make the error decrease monotonically. Different logarithmic frequency gaps have different cancellation scales.

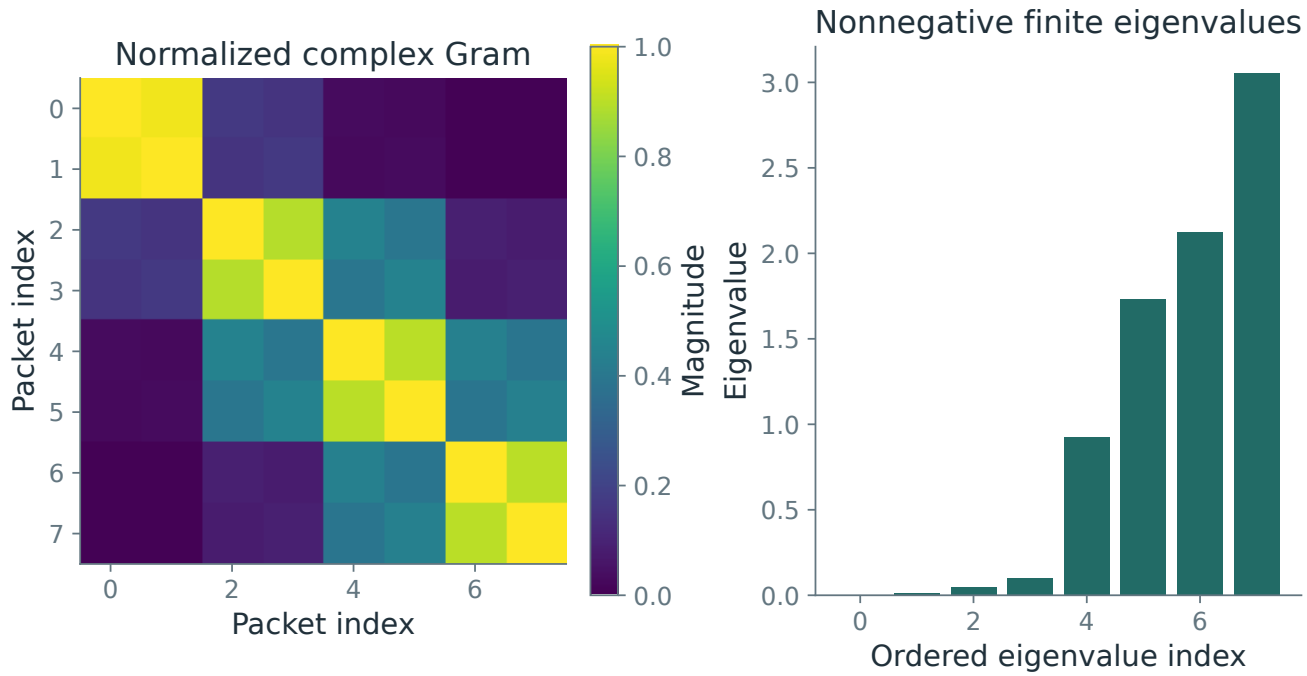
Work an example. For the pair $n = 2$, $m = 3$, the off-diagonal factor is $\sin(T\log(2/3))/(T\log(2/3))$. Its first positive zero occurs at $T = \pi/\log(3/2)$, about 7.748. Other pairs generally remain at that time. The plots keep all 40^2 pairs, use $k = \ell = 3$, and preserve the fixed lag $\tau = 0.5$.

Carry forward. Finite sinc extraction makes the diagonal mechanism explicit. The infinite time-average theorem has an additional absolute-convergence argument.

Source and scope. IV Theorem 2.1, "Exact time-average identity." Here $a_n = \mu(n)n^{-2}y_n^3 n^{-i/2}$ and $b_m = \mu(m)m^{-2}y_m^3$; sinc means $\sin x/x$. No infinite-model finite-time bound is inferred.

PAPER IV / 04 **LESSON 48**

The positive kernel is a complex Gram matrix



$$v_{k,t}(n) = \mu(n) n^{-2} y_n^k n^{-it}, \qquad K_N(k,\ell;t-s) = \sum_{n \le N} v_{k,t}(n)\overline{v_{\ell,s}(n)}$$

Read the figure. The heatmap shows magnitudes of normalized complex overlaps. The underlying matrix still retains complex phases and is Hermitian. The eigenvalue panel tests the displayed finite packet set. Positivity follows from the feature representation: every quadratic Gram sum is a squared norm. The numerical eigenvalues illustrate that identity rather than proving positivity for every possible packet set.

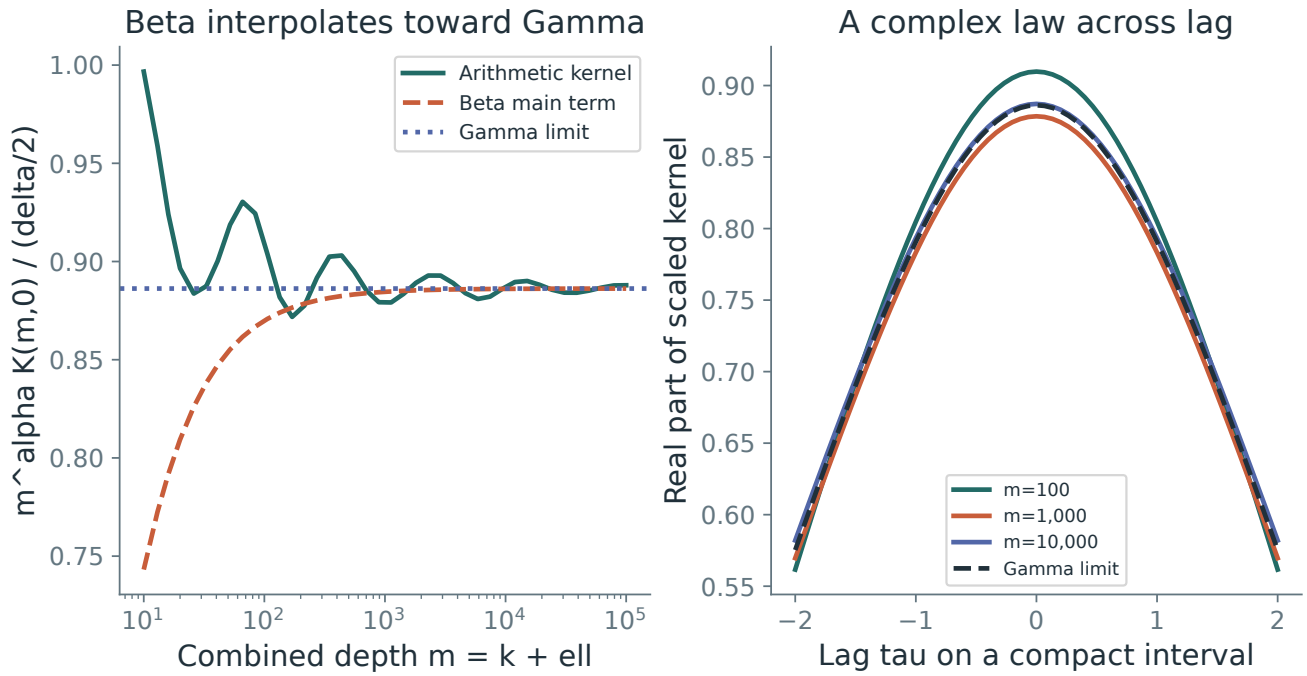
Work an example. Take the eight packets with depths $0, 10, 100, 1000$ and times zero or one. Divide each finite feature vector by its norm. Every diagonal overlap becomes one. For any coefficients c_j, the quadratic form is the norm squared of $\sum_j c_j v_j$, so it cannot be negative, even when individual off-diagonal entries are complex.

Carry forward. Time averaging removes arithmetic interference on the diagonal while leaving a positive depth-time geometry.

Source and scope. IV Theorem 2.2, "Positive-definite packet kernel." Cutoff $N = 200000$; every unnormalized omitted kernel entry is bounded by $1/(3N^3)$. Normalized finite overlaps are displayed.

PAPER IV / 05 **LESSON 49**

Use Beta to connect depth with Gamma



$$K(k,\ell;\tau)=\frac{\delta}{\beta}B(\alpha+i\tau/\beta,k+\ell+1)+O\Big((k+\ell)^{-(2a-1/2)/\beta}\Big),\quad \alpha=\frac{2a-1}{\beta}$$

Read the figure. At zero lag, multiplying out the leading depth power makes the Gamma limit visible. The Beta term retains a finite-depth correction. The second panel restores a compact interval of nonzero lags and their complex exponent. A single real asymptotic at zero lag would not determine this complete complex law.

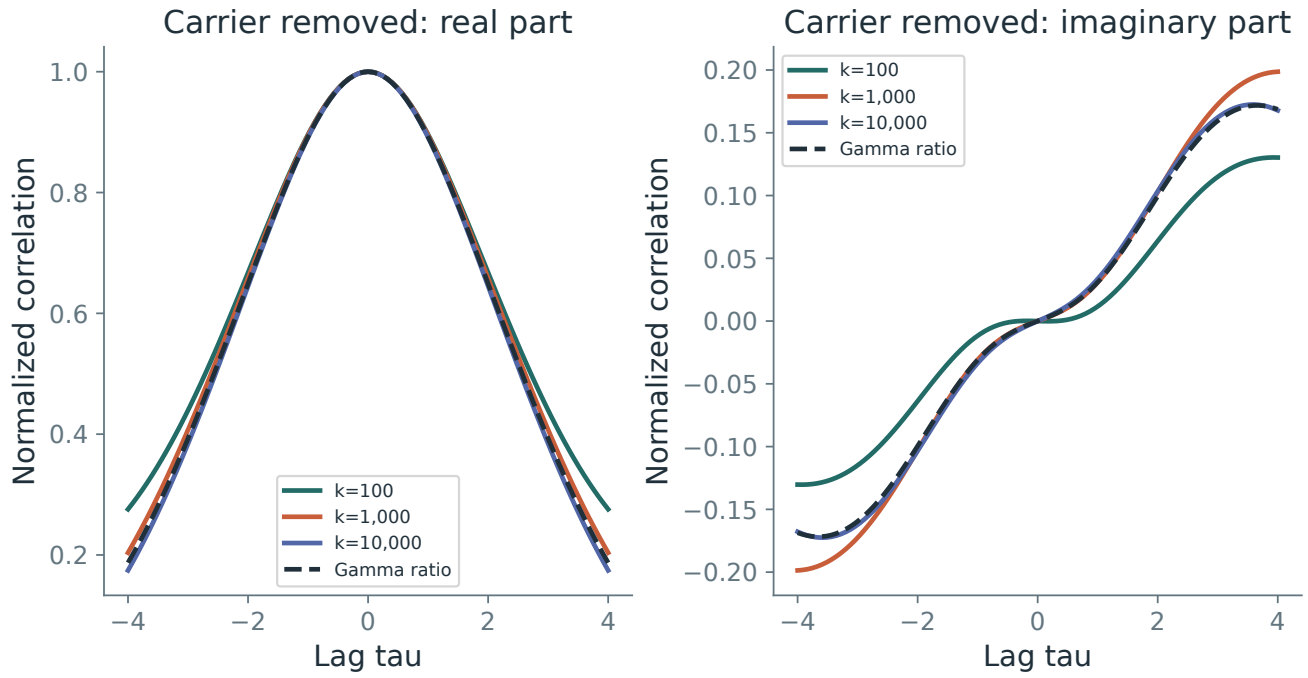
Work an example. For $a=\beta=2$, shape is $\alpha=3/2$ and principal squarefree density is $\delta=6/\pi^2$. Writing $m=k+\ell$, the leading zero-lag kernel is $(3/\pi^2)\Gamma(3/2)m^{-3/2}$. At nonzero lag, the power becomes $m^{-3/2-i\tau/2}$. Removing both parts leaves the Gamma factor, whose real part is shown.

Carry forward. The continuous shape arises from arithmetic decay and scale. Compact lag intervals are part of the uniform theorem.

Source and scope. IV Theorem 4.1, "Uniform complex packet asymptotic." Principal modulus one; $|\tau|\le 2$. Finite-cut data illustrate convergence; the theorem's implicit error constant is not fitted from this plot.

PAPER IV / 06 **LESSON 50**

Remove the carrier before comparing limits



$$A_k(\tau) = \frac{K(k,k;\tau)}{K(k,k;0)}, \qquad (2k)^{i\tau/\beta} A_k(\tau) \longrightarrow \frac{\Gamma(\alpha + i\tau/\beta)}{\Gamma(\alpha)}$$

Read the figure. The two panels compare real and imaginary components after carrier removal. Without that factor, the logarithmic frequency scale keeps drifting with depth. Normalization removes the changing positive energy; the carrier removes the changing phase reference. Both operations are needed to see the same shape-dependent limit across increasing depths.

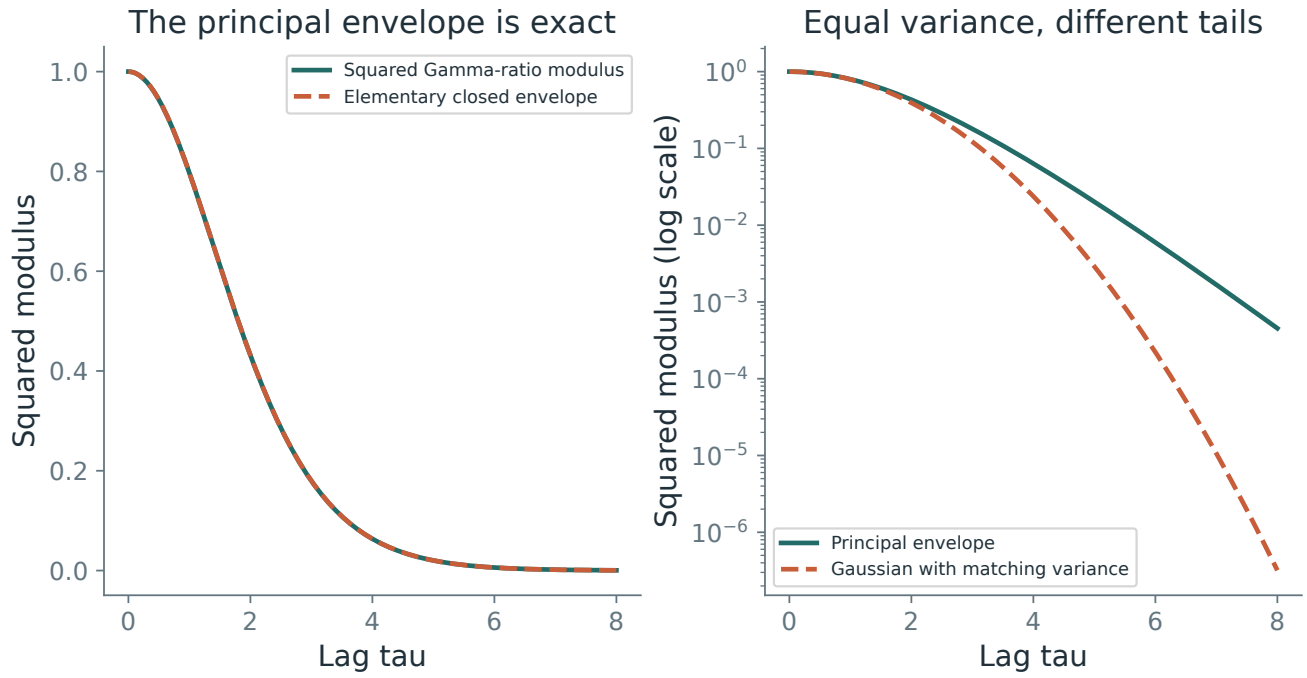
Work an example. Equal depth means the combined depth is $2k$. With $\beta = 2$, the carrier is $\exp(i\tau \log(2k)/2)$, not $\exp(i\tau \log k/2)$. At zero lag the normalized finite kernel and its limit both equal one. For $k = 100, 1000, 10000$, the figures use this same convention and compare against the shape-3/2 Gamma ratio.

Carry forward. Changing the phase reference does not alter modulus. It makes complex correlations at different arithmetic scales comparable.

Source and scope. IV Corollary 5.1, "Equal-depth dephasing." Compact interval $|\tau| \leq 4$; finite energies normalize the displayed kernels. Number-cut errors and normalized bounds are recorded separately.

PAPER IV / 07 **LESSON 51**

An exact envelope can have non-Gaussian tails



$$\left|\frac{\Gamma(3/2+i\tau/2)}{\Gamma(3/2)}\right|^2 = \frac{1+\tau^2}{\cosh(\pi\tau/2)}$$

Read the figure. The first panel overlays the Gamma expression with its elementary closed envelope. The second uses a logarithmic vertical scale to compare its tails with a Gaussian having the same limiting variance. Agreement at the initial curvature does not force agreement farther away. The Gamma recurrence and reflection identity determine the full envelope.

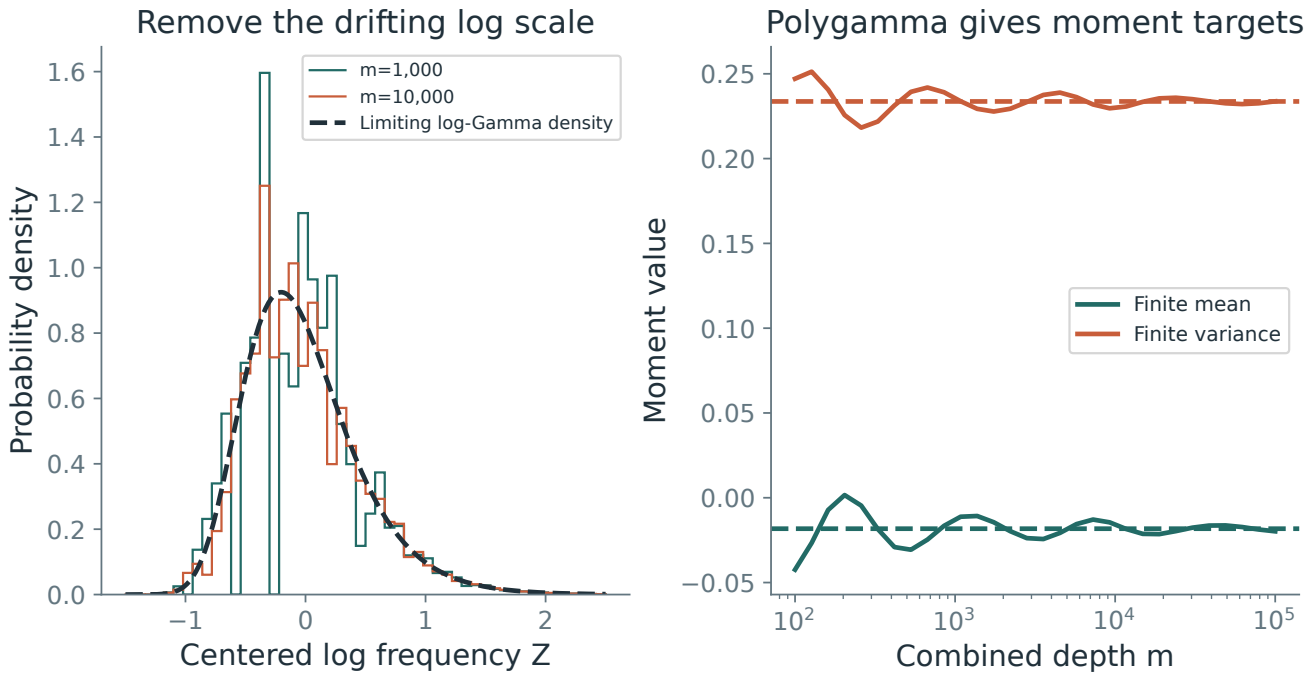
Work an example. At lag one the squared modulus is $2/\cosh(\pi/2)$. At zero it is one. The limiting frequency variance is $\psi_1(3/2)/4 \approx 0.233701$, so the variance-matched Gaussian has squared characteristic modulus $e^{-0.233701\tau^2}$. The exact principal expression instead has an exponential tail multiplied by a quadratic factor.

Carry forward. A few moments determine local behavior. A closed characteristic-function formula determines every displayed lag.

Source and scope. IV Worked example 5.2, "Closed principal envelope." Exact formulas on $0 \le \tau \le 8$. The Gaussian is an explicitly variance-matched teaching comparison, not an asserted approximation theorem.

PAPER IV / 08 **LESSON 52**

Center the logarithmic frequency law



$$Z_m = \log n - \beta^{-1} \log m \Longrightarrow -\beta^{-1} \log U, \qquad U \sim \mathrm{Gamma}(\alpha, 1)$$

Read the figure. The histograms use positive squarefree packet weights after subtracting the drifting log scale. The limiting density remains continuous even though each finite spectrum consists of integer frequencies. The moment panel compares finite means and variances with their polygamma targets. Histogram convergence alone does not justify convergence of every unbounded moment.

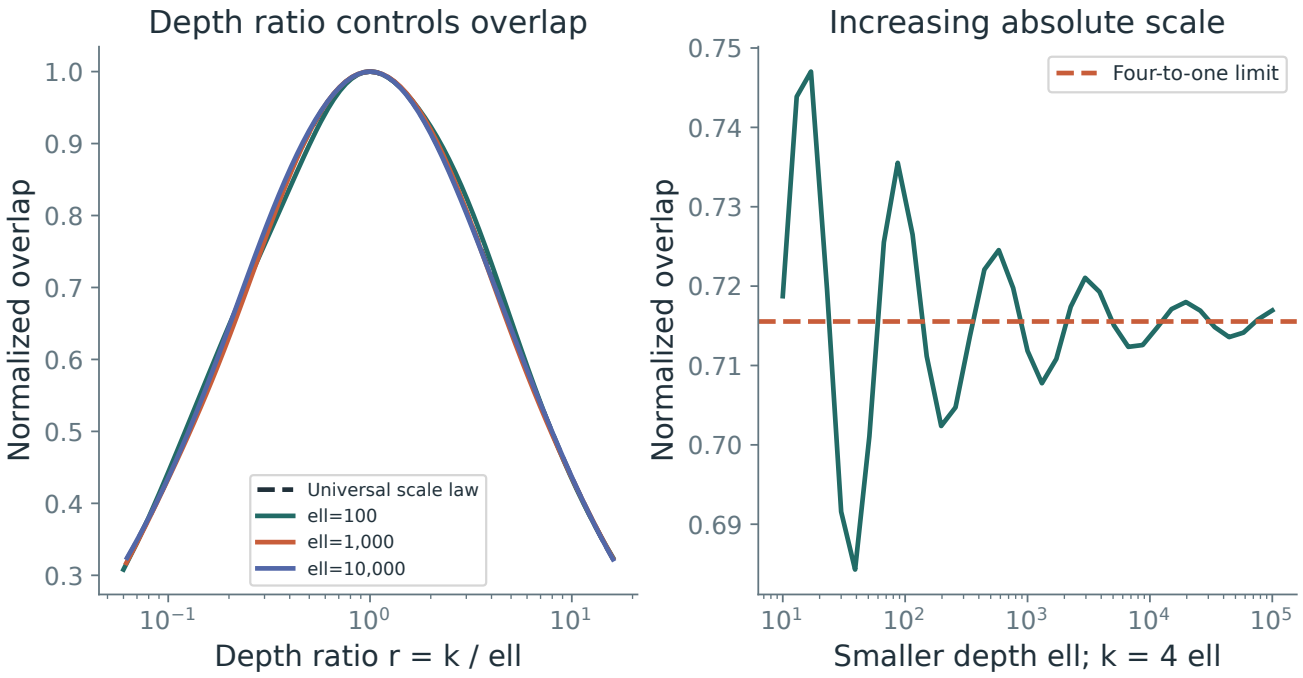
Work an example. For $\alpha = 3/2$ and $\beta = 2$, the limiting density is $2e^{-3z-e^{-2z}}/\Gamma(3/2)$. Its mean is $-\psi(3/2)/2 \approx -0.018244987$ and its variance is $\psi_1(3/2)/4 \approx 0.23370055$. The finite weights are proportional to $\mu(n)^2 n^{-4}(1-n^{-2})^m$, with their full finite mass used for normalization.

Carry forward. Log-frequency centering connects the arithmetic active scale with a fixed log-Gamma probability law.

Source and scope. IV Corollary 6.1, "Polygamma cumulants." Histograms at $m = 1000, 10000$; finite moment records through $m = 100000$. Preserve the source's moment-convergence proviso when claiming cumulant limits.

PAPER IV / 09 **LESSON 53**

Compare depth ratios before absolute depths



$$\mathcal{O}(k,\ell) = \frac{K(k,\ell;0)}{\sqrt{K(k,k;0)K(\ell,\ell;0)}} \longrightarrow \left(\frac{2\sqrt{r}}{1+r}\right)^{\alpha}, \qquad r = k/\ell$$

Read the figure. The first panel compares several absolute depth scales against one ratio profile. Equal depths give overlap one. Exchanging the depths leaves the overlap unchanged, so reciprocal ratios share a value. The second follows a single four-to-one ratio while both depths increase. This separates ratio dependence from finite-depth arithmetic fluctuations.

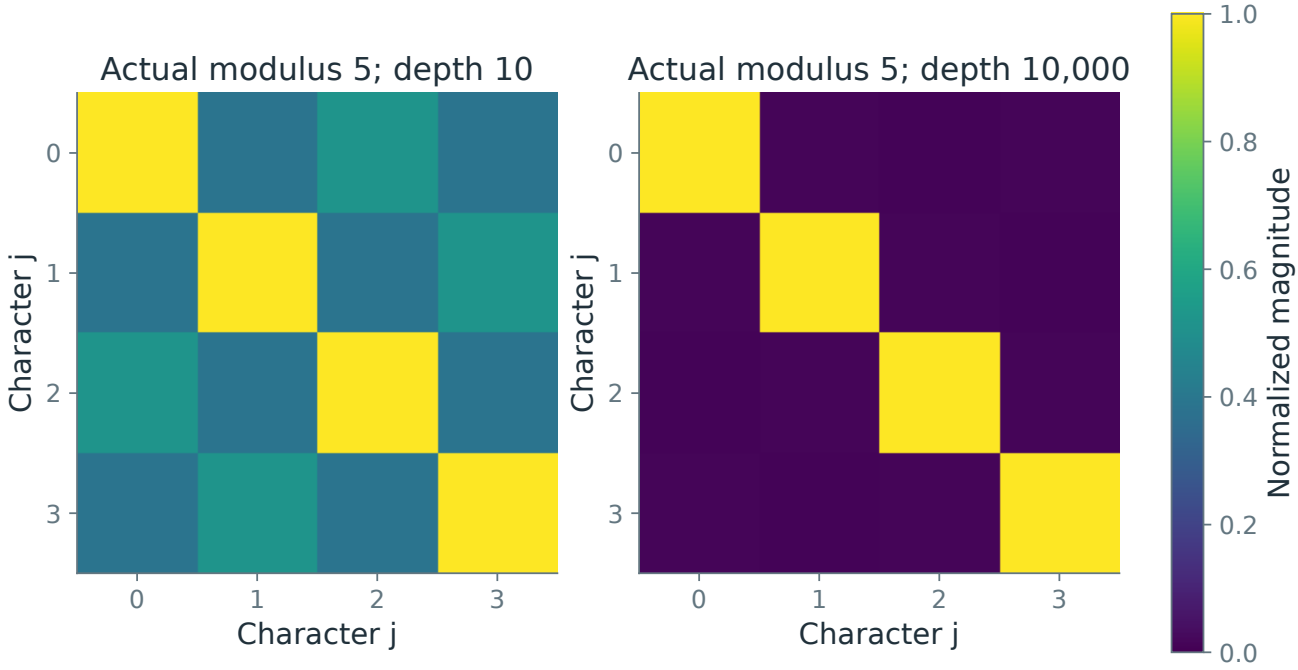
Work an example. Take $\alpha = 3/2$ and $k = 4\ell$. The limiting overlap is $(4/5)^{3/2} \approx 0.715541753$. The same value occurs at ratio $1/4$. At ratio one the limit is exactly one. The displayed comparisons keep ratios between $1/16$ and 16, and round each sampled larger depth to an integer before evaluating the finite kernel.

Carry forward. Comparable depths retain overlap even at large scale. Multiplicative depth separation is measured by a log-depth gap.

Source and scope. IV Theorem 7.1, "Universal scale overlap," and Worked example 7.2, "A four-to-one depth ratio." Compact positive ratio domain; finite number-cut sums are not asymptotic proofs.

PAPER IV / 10 **LESSON 54**

Use the actual character modulus



$$\chi_j(2^r) = i^{jr} \pmod 5, \qquad \chi_j(n) = 0 \text{ if } 5 \mid n, \qquad K_{\chi,\psi} = \sum_n \mu(n)^2 \chi(n) \overline{\psi(n)} n^{-4-i\tau} y_n^{k+\ell}$$

Read the figure. Each matrix compares all four characters modulo five at one equal depth. Diagonal sectors have unit normalized magnitude. Off-diagonal sectors use nonprincipal character products and weaken with depth. The coprimality restriction is determined by the actual modulus. Replacing it with conductor can change even the principal sector's support and normalization.

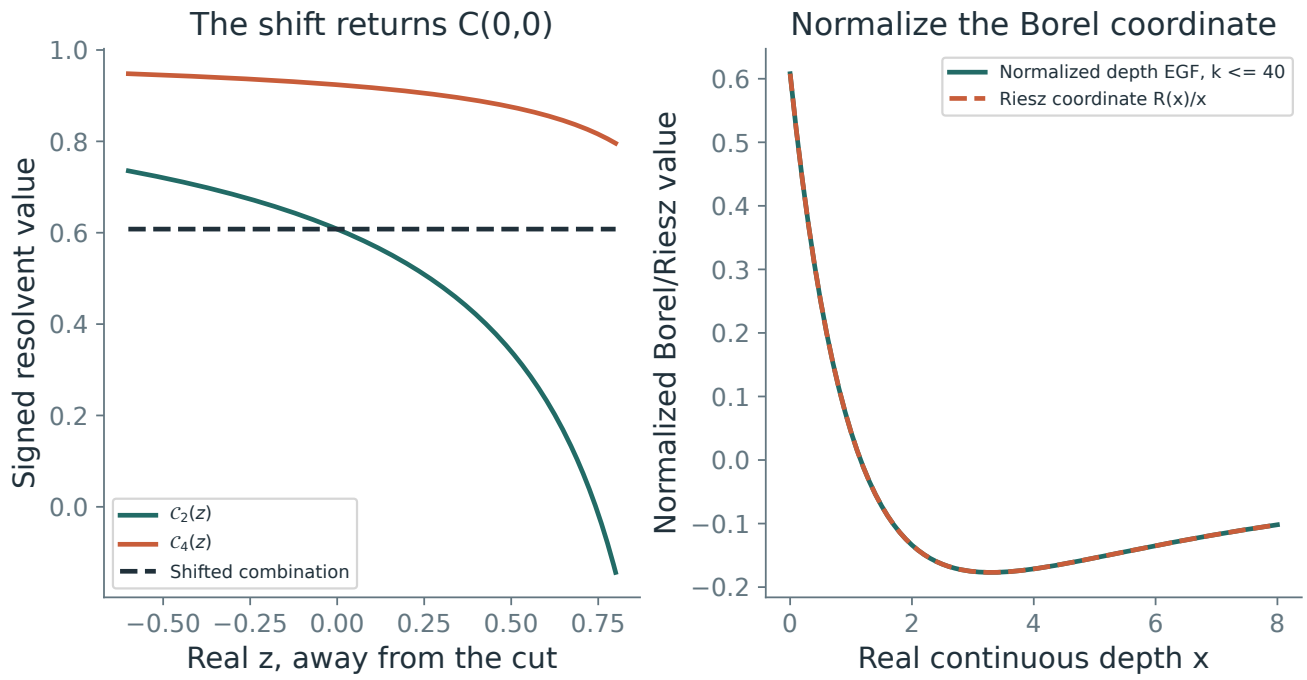
Work an example. The units are the cycle $1, 2, 4, 3$ generated by two. For $j = 1$, their values are $1, i, -1, -i$, while multiples of five have value zero. The principal character modulo five has conductor one but still vanishes at five. Its squarefree density is $(5/6)/\zeta(2)$, not $1/\zeta(2)$.

Carry forward. Distinct characters must share a fixed actual modulus; their product is then nonprincipal and the stated decoherence bound applies.

Source and scope. IV Theorem 8.1, "Character depth-time decoherence," with the consolidation's actual-modulus correction. Depths 10, 10000, zero lag; comparable-depth and compact-lag hypotheses govern the asymptotic theorem.

PAPER IV / 11 **LESSON 55**

Change generating coordinates without losing signs



$$(1-z)\mathcal{C}_a(z,t) + z\mathcal{C}_{a+\beta}(z,t) = L(a+it,\chi)^{-1},$$

$$e^{-x}\sum_{k\geq 0} C_a(k,t)\frac{x^k}{k!} = \mathcal{R}_a(x,t)/x.$$

Read the figure. The first panel combines two signed resolvents using the parameter-shift identity. The result returns the initial signed coefficient. The second changes ordinary discrete-depth coordinates to normalized exponential coordinates. Removing e^x reveals the Riesz companion. These identities retain the signs throughout; positivity or zero-freeness does not follow from a coordinate change.

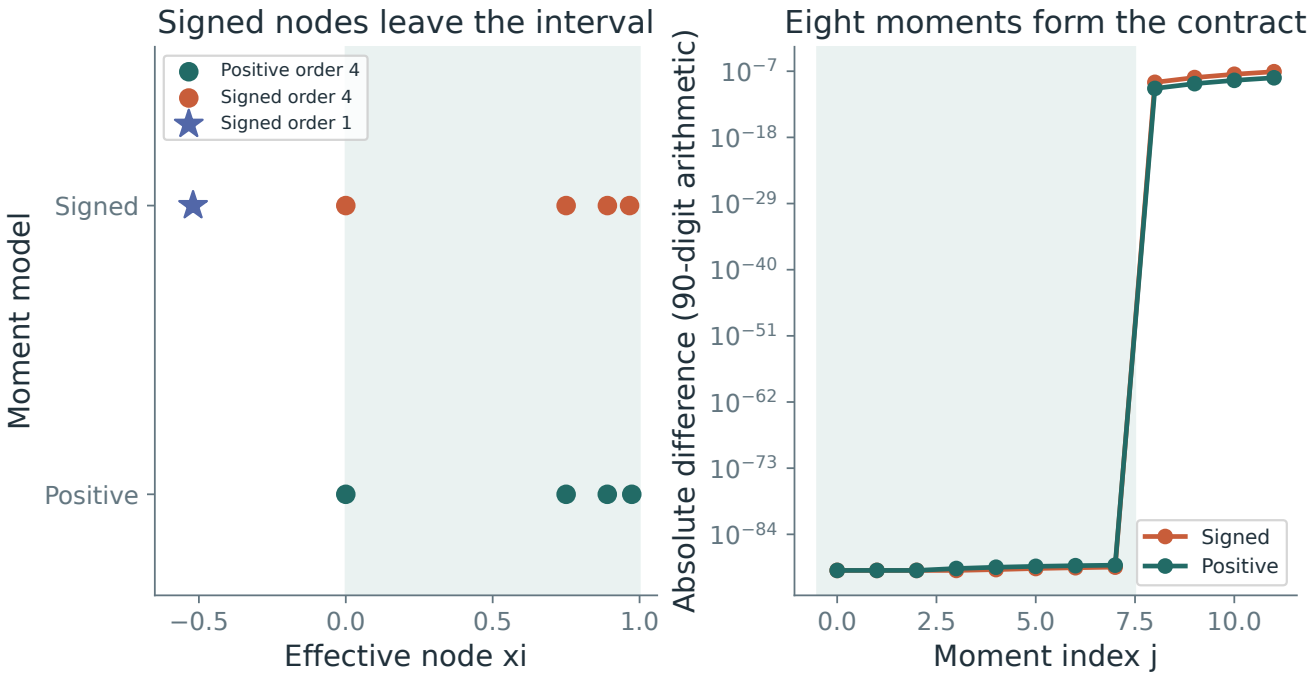
Work an example. For the principal choice $a = \beta = 2$, $t = 0$, the shifted combination returns $1/\zeta(2)$. The normalized Borel value is $\sum_n \mu(n)n^{-2}e^{-x/n^2}$. At $x = 0$, define $\mathcal{R}(x)/x$ by this continuous expression, which returns the same initial coefficient. The finite number cutoff and depth-40 EGF truncation introduce separate errors.

Carry forward. Resolvent shifts and Borel–Riesz normalization are exact transformations of one signed family.

Source and scope. IV Theorem 9.1, "Parameter-shift equation," and Chapter 10, "The Borel–Riesz bridge." Real $z \in [-0.6, 0.8]$, $x \in [0, 8]$; bounds for number support and EGF degree are recorded.

PAPER IV / 12 **LESSON 56**

State the signed Padé contract precisely



$$\Delta_m \neq 0 \implies \mathcal{C} - P/Q = O(z^{2m}), \quad \deg P \leq m-1, \deg Q \leq m,$$
$$\deg Q = m \text{ and simple zeros} \implies m \text{ simple packets.}$$

Read the figure. The node panel contrasts positive and signed effective models. Positive nodes remain in the physical interval; signs can produce a node outside it. The moment panel shades exactly the contracted indices. Later moments are predictions and can differ. Neither numerical nonbreakdown at one order nor this finite contract establishes universal stability.

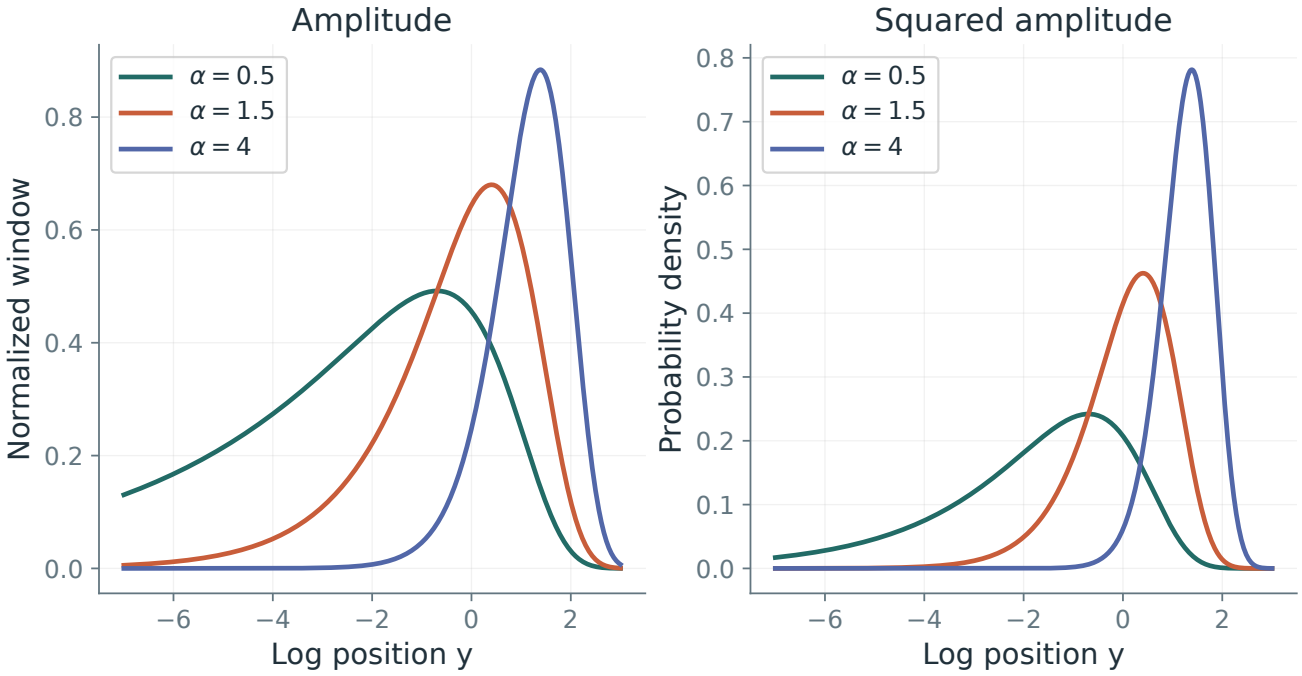
Work an example. The first signed node is $c_1/c_0 \approx -0.519817755$. It already leaves $[0,1)$. Separately, the order-four models use the first eight principal moments evaluated with 90 digits. Their first eight reconstructed moments agree at that precision. Moments eight through eleven have nonzero discrepancies. Full denominator degree and separated simple roots are checked for these displayed models.

Carry forward. Hankel nonbreakdown gives rational matching. A simple-packet expansion also needs full denominator degree and simple zeros.

Source and scope. IV Theorem 11.1, "Finite signed Padé reduction," with the consolidation correction, and Worked example 11.2, "The first signed packet leaves the physical interval." Numerical examples; plotted errors are floored at 10^{-90}.

PAPER V / V01 **LESSON 57**

Normalize the log-Gamma window



$$g_\alpha(y) = \Gamma(\alpha)^{-1/2} e^{\alpha y/2 - e^y/2}, \qquad \int_{\mathbb{R}} |g_\alpha(y)|^2 dy = 1$$

Read the figure. Read amplitude on the left and probability density on the right. A taller curve need not have more total probability. Changing the positive shape moves the active log position and changes its width, while the full squared integral stays one. The curves are unrenormalized crops: the shape 0.5 window has a visible left tail beyond the page.

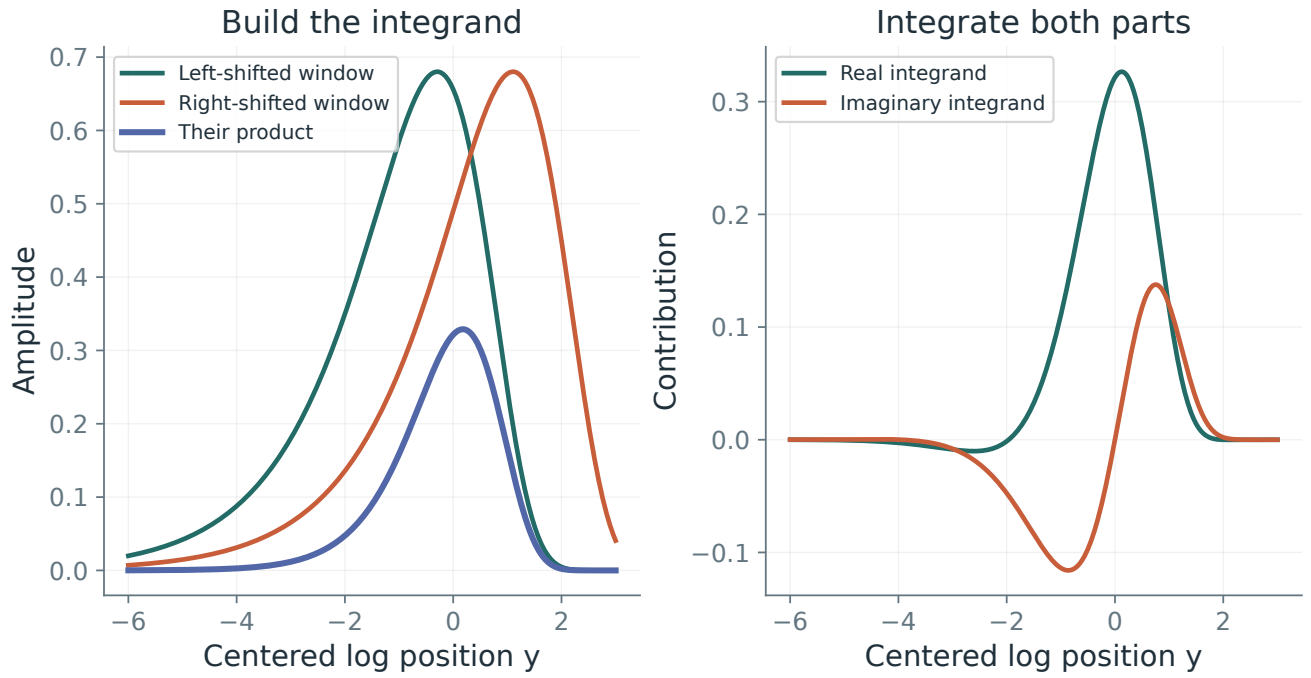
Work an example. For $\alpha = 1.5$, substitute $u = e^y$. The norm becomes $\Gamma(1.5)^{-1} \int_0^\infty u^{0.5} e^{-u} du = 1$. The mode is $y = \log(1.5)$, whereas the mean is $\psi(1.5) \approx 0.036490$. Those two positions differ because the log-Gamma law is asymmetric. Its variance is approximately 0.934802.

Carry forward. Use the normalized window as the common input to every later transform.

Source and scope. V Definition 2.1 and Proposition 2.2, source lines 339 and 369. Shapes $0.5, 1.5, 4$, $y \in [-7, 3]$. Exact Gamma-CDF crop probabilities are recorded in the evidence ledger; the displayed crop is not the full norm.

PAPER V / V02 **LESSON 58**

Build an ambiguity integral



$$A_\alpha(h,\eta) = \int g_\alpha(y+h/2)g_\alpha(y-h/2)e^{i\eta y}dy = \frac{\Gamma(\alpha+i\eta)}{\Gamma(\alpha)}\operatorname{sech}^{\alpha+i\eta}(h/2)$$

Read the figure. First multiply the shifted windows. Their product localizes the integral before modulation is applied. The second panel separates the cosine and sine contributions to its complex value. Negative real or imaginary contributions are phases of the integrand, not negative probability weights. Integrating both components yields one centered ambiguity value.

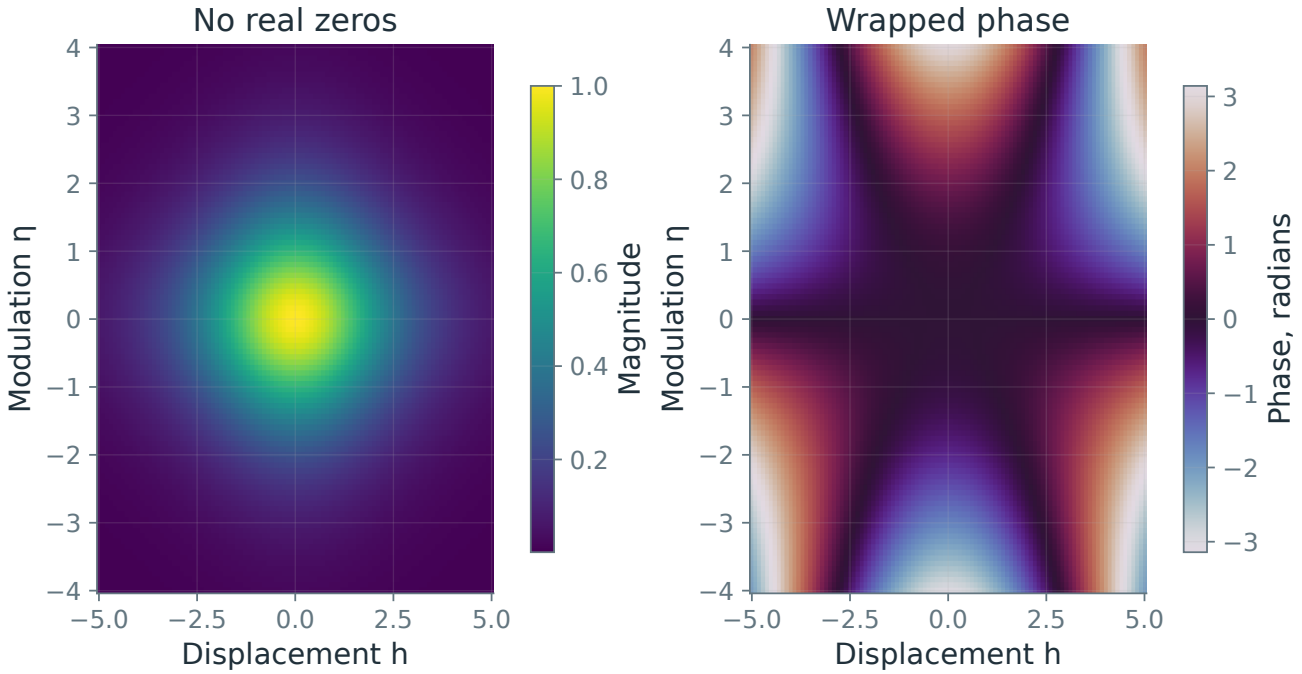
Work an example. Take $\alpha = 1.5$, $h = 1.4$, and $\eta = 0.8$. The closed formula gives approximately $0.536116 - 0.048326i$. Direct quadrature of the displayed definition agrees. At zero modulation the sine contribution vanishes; at zero displacement the two windows coincide and the remaining integral is the log-Gamma characteristic function. Neither operation changes the Fourier convention.

Carry forward. Translation and modulation are joined by one precisely centered integral.

Source and scope. V Theorem 3.1, "Exact ambiguity formula," source line 404. Quadrature uses $y \in [-30, 6]$, tolerance 2×10^{-13}; analytic omitted-amplitude bounds and numerical error estimates are recorded separately.

PAPER V / V03 **LESSON 59**

Separate magnitude from wrapped phase



$$A_\alpha(h,\eta) = \frac{\Gamma(\alpha+i\eta)}{\Gamma(\alpha)} e^{-(\alpha+i\eta)\log\cosh(h/2)} \neq 0 \quad (h,\eta \in \mathbb{R})$$

Read the figure. The left panel measures overlap strength. The right panel records the argument modulo 2π, so its sharp color transitions may be phase wraps. They do not indicate a zero or discontinuity of the complex function. Increasing displacement suppresses magnitude through the hyperbolic factor. Increasing modulation introduces the separate Gamma envelope and its phase.

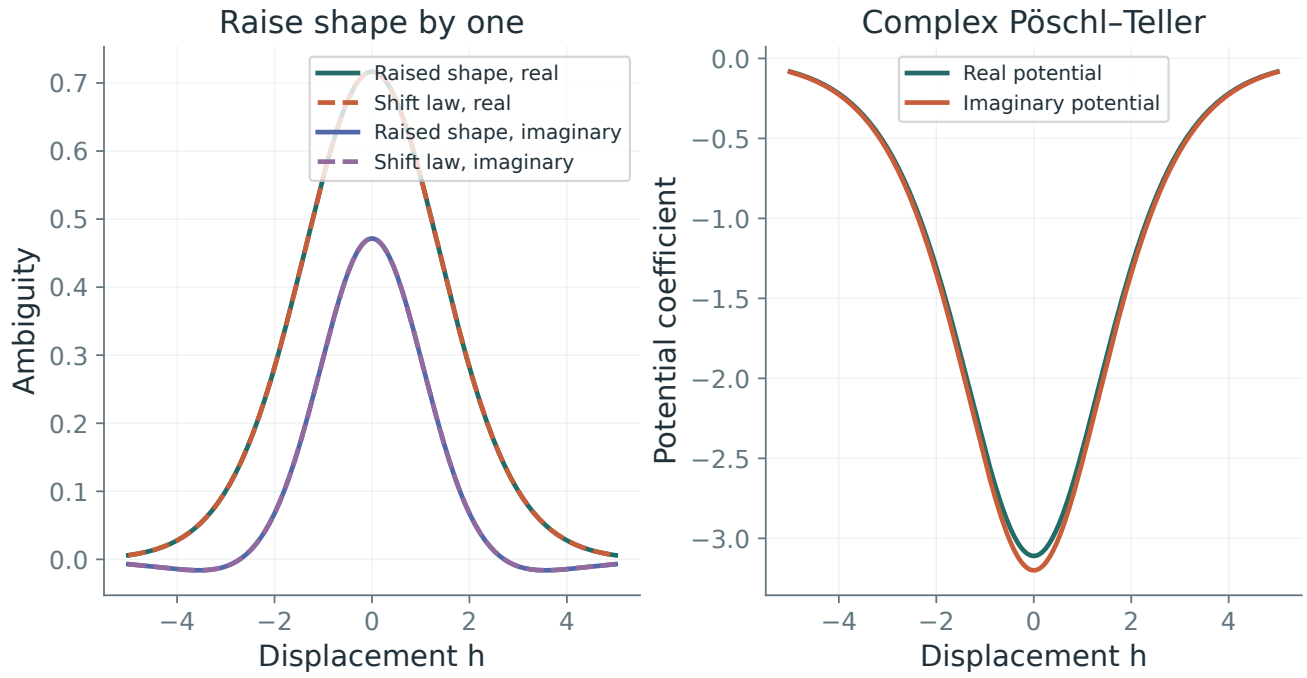
Work an example. At the origin the value is exactly one. At $h = \log 4$ and $\eta = 0$, its value is $(4/5)^{3/2} \approx 0.715542$. At nonzero modulation, use the same formula with a complex exponent. The real logarithm of $\cosh(h/2)$ fixes that exponent without a branch ambiguity on the real plane. The Gamma function has no zeros, which supplies the nonvanishing proof.

Carry forward. A phase wrap is a plotting convention; a zero is a mathematical event.

Source and scope. V Theorem 3.1 and Corollary 3.2, source lines 404 and 447. Shape 1.5; 101-by-101 samples on $[-5,5] \times [-4,4]$. A positive sampled minimum is finite evidence, not the universal nonvanishing argument.

PAPER V / V04 **LESSON 60**

Raise shape and read its differential equation



$$A_{\alpha+1} = \frac{\alpha + i\eta}{\alpha} \operatorname{sech}(h/2) A_\alpha, \qquad \nu = \alpha + i\eta,$$
$$[-4\partial_h^2 - \nu(\nu+1)\operatorname{sech}^2(h/2)]A_\alpha = -\nu^2 A_\alpha.$$

Read the figure. The first panel compares two constructions of the raised shape: direct evaluation and the Gamma recurrence. The second shows the potential coefficient in the differential equation. Both its real and imaginary parts matter when modulation is nonzero. This complex equation should not be silently read as a self-adjoint Hamiltonian with a real energy.

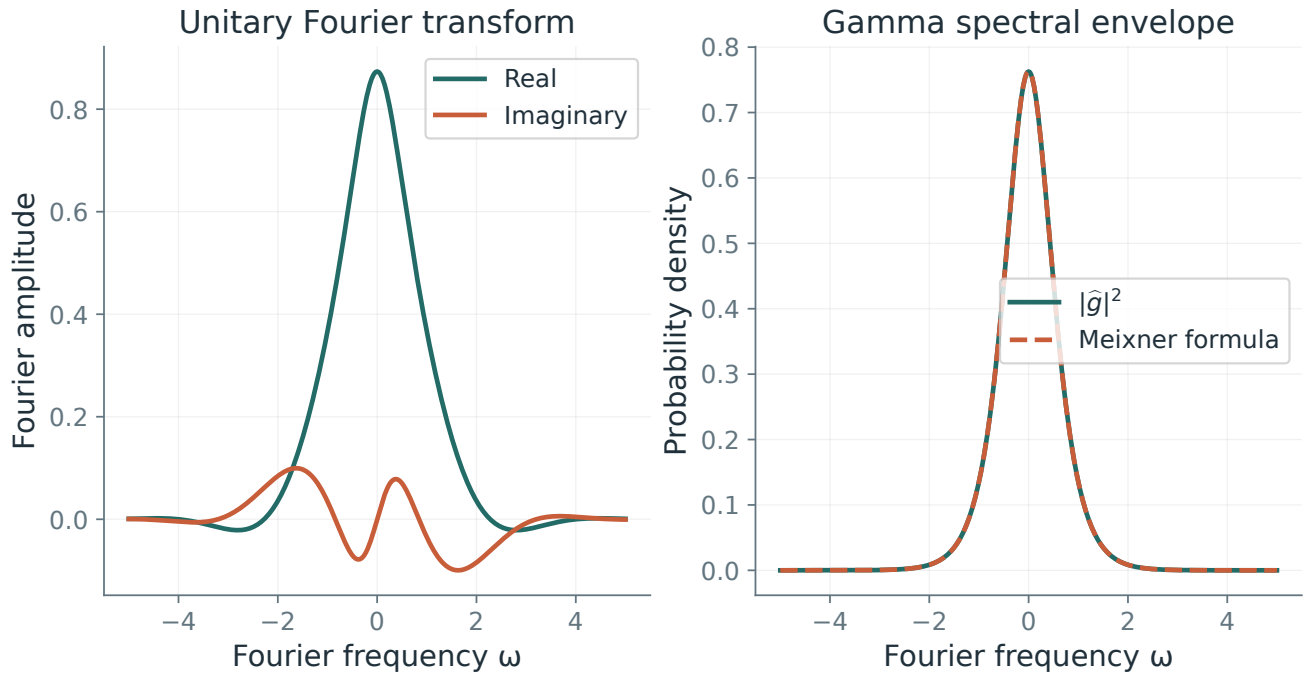
Work an example. For $\alpha = 1.5$ and $\eta = 0.8$, raising shape multiplies the kernel by $(1.5 + 0.8i)\operatorname{sech}(h/2)/1.5$. At $h = 1.4$, the result is approximately $0.447661 + 0.189299i$. Differentiate $\operatorname{sech}^\nu(h/2)$ twice to obtain the displayed equation. The Gamma prefactor is independent of h, so it survives unchanged in this derivative calculation.

Carry forward. One recurrence and one differential equation describe the same kernel.

Source and scope. V Proposition 3.3 and Theorem 3.4, source lines 466 and 491. $h \in [-5, 5]$; derivatives are evaluated analytically. The residual checks floating-point evaluation of the identity, not a discretized spectral problem.

PAPER V / V05 **LESSON 61**

Transform the window into a Gamma envelope



$$\widehat{g}_\alpha(\omega) = \frac{2^{\alpha/2-i\omega}\Gamma(\alpha/2 - i\omega)}{\sqrt{2\pi\Gamma(\alpha)}}, \qquad \rho_\alpha(\omega) = |\widehat{g}_\alpha(\omega)|^2$$

Read the figure. Keep the unitary convention $\widehat{f} = (2\pi)^{-1/2}\int f(y)e^{-i\omega y}dy$ beside the plot. The Fourier amplitude has real and imaginary parts, even though the starting window is real. Squaring its magnitude removes the carrier phase and gives the positive Meixner density. The second panel compares these equivalent density constructions.

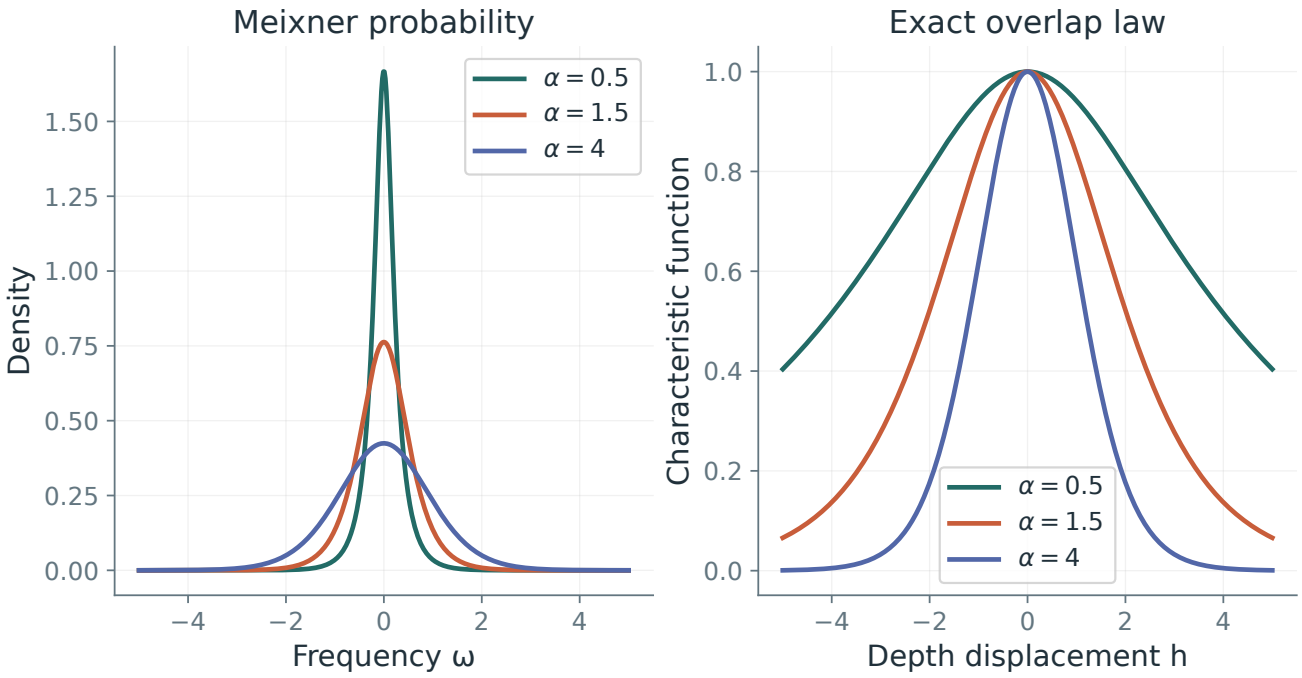
Work an example. Set $u = e^y$. The transform becomes the Gamma integral with exponent $\alpha/2 - i\omega$ and scale $1/2$. For $\alpha = 1.5$, evaluating this integral at frequencies $-2, 0, 2$ agrees with the closed envelope. Conjugating the value at 2 gives the value at -2, as required for a real position window. The positive density is consequently symmetric in frequency.

Carry forward. Preserve the Fourier sign before comparing phases or polynomial bases.

Source and scope. V Theorem 4.1, source line 540. Frequency crop $[-5, 5]$. Independent quadrature uses $y \in [-30, 6]$ with explicit amplitude-tail bounds. The ledger separates the quadrature estimate from the omitted integral.

PAPER V / V06 **LESSON 62**

Read depth overlap as a characteristic function



$$\rho_\alpha(\omega) = \frac{2^{\alpha-1}}{\pi\Gamma(\alpha)}|\Gamma(\alpha/2+i\omega)|^2, \qquad \int \rho_\alpha(\omega)e^{ih\omega}d\omega = \operatorname{sech}^\alpha(h/2)$$

Read the figure. The two panels express one probability law in frequency and characteristic coordinates. Larger shape broadens the frequency density because its variance is $\alpha/4$. Its characteristic function then narrows in displacement. The right curve is also the zero-modulation ambiguity slice, so it has the same depth-overlap interpretation as the arithmetic limit.

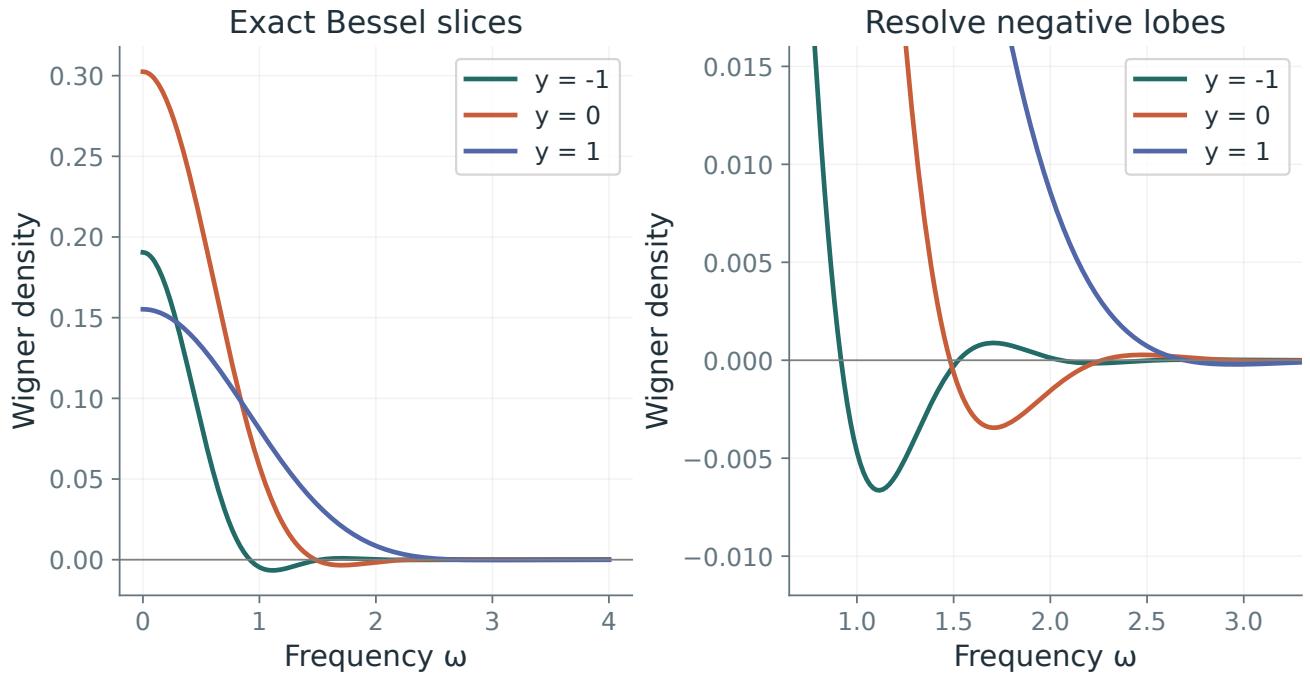
Work an example. Take $\alpha = 1.5$ and a four-to-one depth ratio. Then $h = \log 4$ and $\cosh(h/2) = 5/4$. The exact overlap is $(4/5)^{3/2} \approx 0.715542$. This is a transform identity for the continuous window. A finite squarefree arithmetic packet approaches it under the compact ratio and time hypotheses of V Theorem 1.1; the identity alone does not give a finite-depth error bound.

Carry forward. The arithmetic scale overlap becomes an exact Meixner characteristic law.

Source and scope. V Corollary 4.2, source line 582. Shapes $0.5, 1.5, 4$. Density crop $[-5,5]$ is not renormalized. Full-line adaptive cosine quadrature checks $h = 0, \log 4$ with declared numerical tolerance.

PAPER V / V07 **LESSON 63**

Resolve the negative Wigner lobes



$$W_\alpha(y,\omega) = \frac{1}{2\pi}\int g_\alpha(y+h/2)g_\alpha(y-h/2)e^{-i\omega h}dh = \frac{2e^{\alpha y}}{\pi\Gamma(\alpha)}K_{2i\omega}(e^y)$$

Read the figure. The left panel shows three exact position slices. The right enlarges the small lobes around zero. A negative value is meaningful here: the Wigner function records phase-space interference and is not a pointwise probability density. Its frequency symmetry does not remove those negative regions. Changing position changes where the oscillatory Bessel lobes appear.

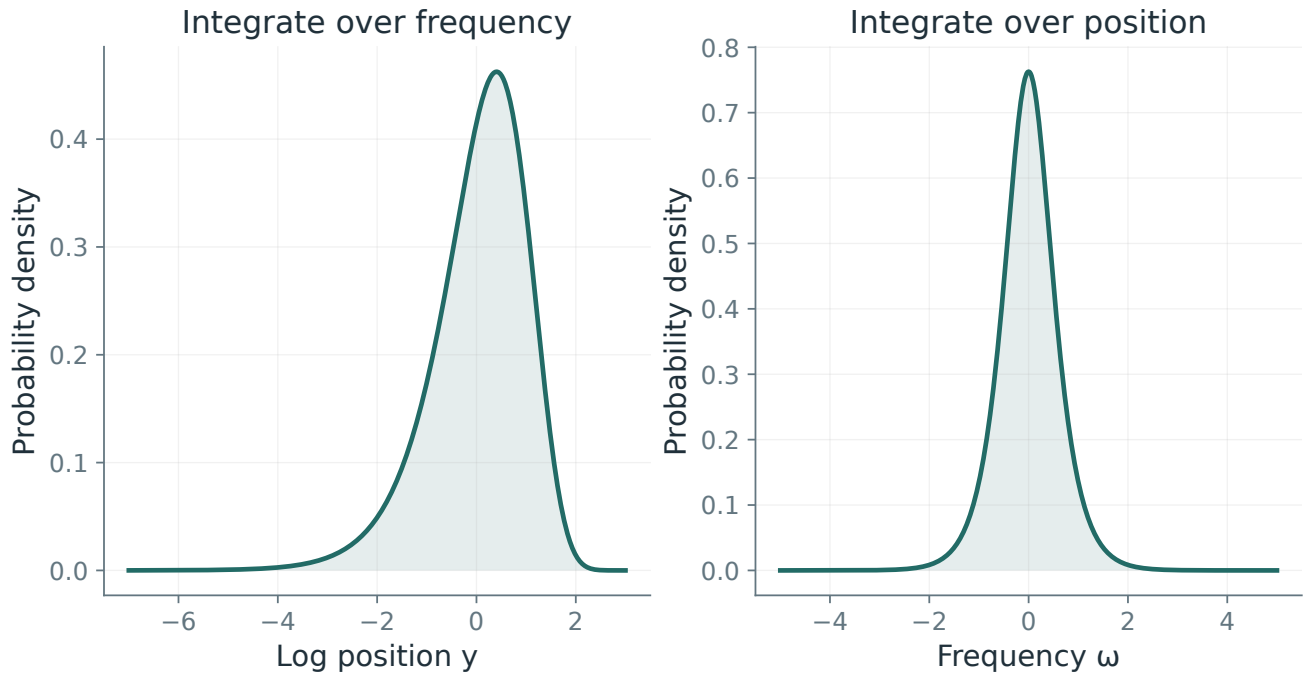
Work an example. For $\alpha = 1.5$, $y = 0$, and $\omega = 2$, the exact expression is $2K_{4i}(1)/(\pi\Gamma(1.5)) \approx -0.00155215$. The integral remains real because its sine part is odd in the displacement variable. Negative phase-space values therefore coexist with real-valued Wigner slices. Integrating over an entire coordinate produces positive marginals, which is the next lesson's separate statement.

Carry forward. Wigner negativity and positive probability marginals are compatible.

Source and scope. V Theorem 5.1, source line 615. Shape 1.5; $y = -1, 0, 1$ and 241 frequency samples on $[0, 4]$. Modified Bessel values use 60-digit working precision; smooth lines connect finite samples.

PAPER V / V08 **LESSON 64**

Project Wigner onto its probability marginals



$$\int_{\mathbb{R}} W_\alpha(y,\omega)d\omega = |g_\alpha(y)|^2, \qquad \int_{\mathbb{R}} W_\alpha(y,\omega)dy = \rho_\alpha(\omega)$$

Read the figure. Integrating over frequency leaves the position density; integrating over position leaves the frequency density. The figure draws these proved exact marginals directly. It does not integrate a cropped Wigner image, which would discard part of an oscillatory integral. The shaded regions show only the probability mass inside the visible windows.

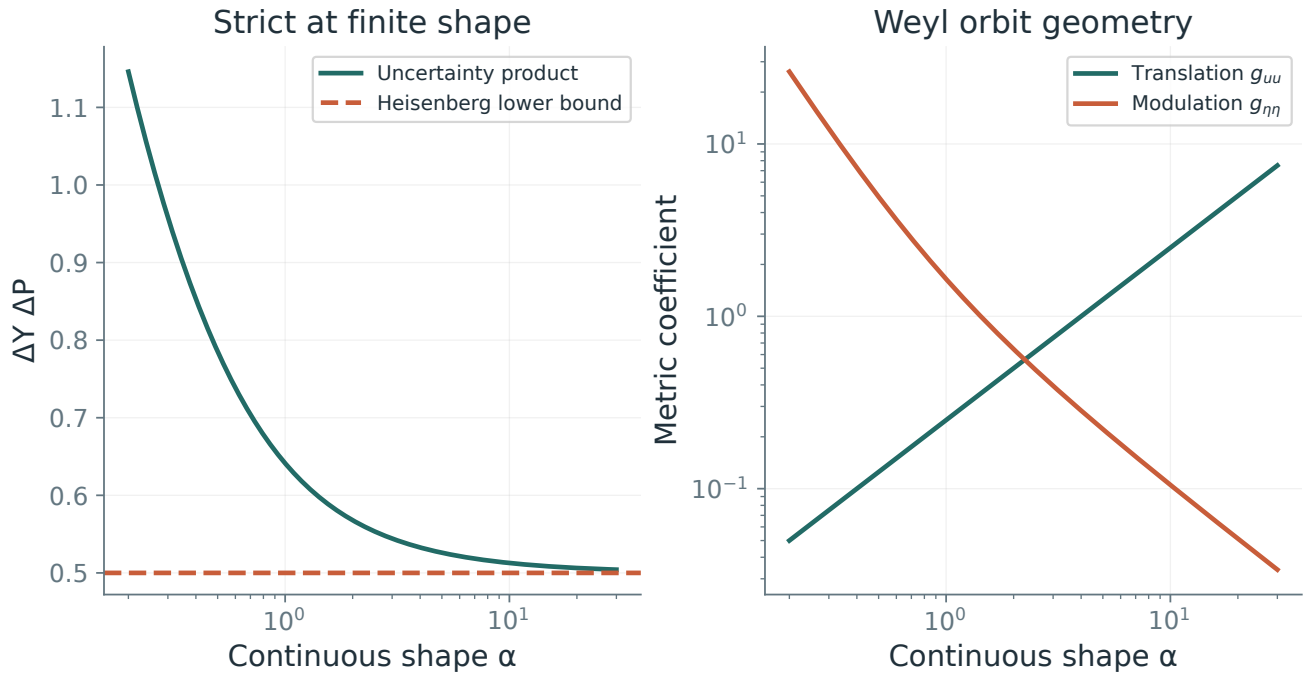
Work an example. At shape 1.5, the position mean is $\psi(1.5) \approx 0.036490$ and the frequency mean is zero. The position variance is $\psi_1(1.5) \approx 0.934802$, while the frequency variance is $1.5/4 = 0.375$. Thus the two marginal widths differ. The negative value from the previous lesson disappears only after complete marginal integration, not because the Wigner function has become pointwise positive.

Carry forward. A projection can be positive even when the joint phase-space representation is not.

Source and scope. V Corollary 5.2, source line 649. Position crop $[-7,3]$, frequency crop $[-5,5]$. Gamma-CDF position mass and adaptively integrated frequency mass are recorded; no truncated-image marginal identity is asserted.

PAPER V / V09 **LESSON 65**

Compare uncertainty with orbit geometry



$$\Delta Y \Delta P = \tfrac{1}{2}\sqrt{\alpha \psi_1(\alpha)} > \tfrac{1}{2}, \qquad g_{uu} = \alpha/4, \qquad g_{\eta\eta} = \psi_1(\alpha)$$

Read the figure. Follow the uncertainty curve toward the dashed lower bound. It approaches that bound with increasing shape but remains strictly above it at every finite shape. The second panel reads the same position and momentum variances as metric coefficients of a fixed-shape Weyl orbit. Translation sensitivity increases while modulation sensitivity decreases.

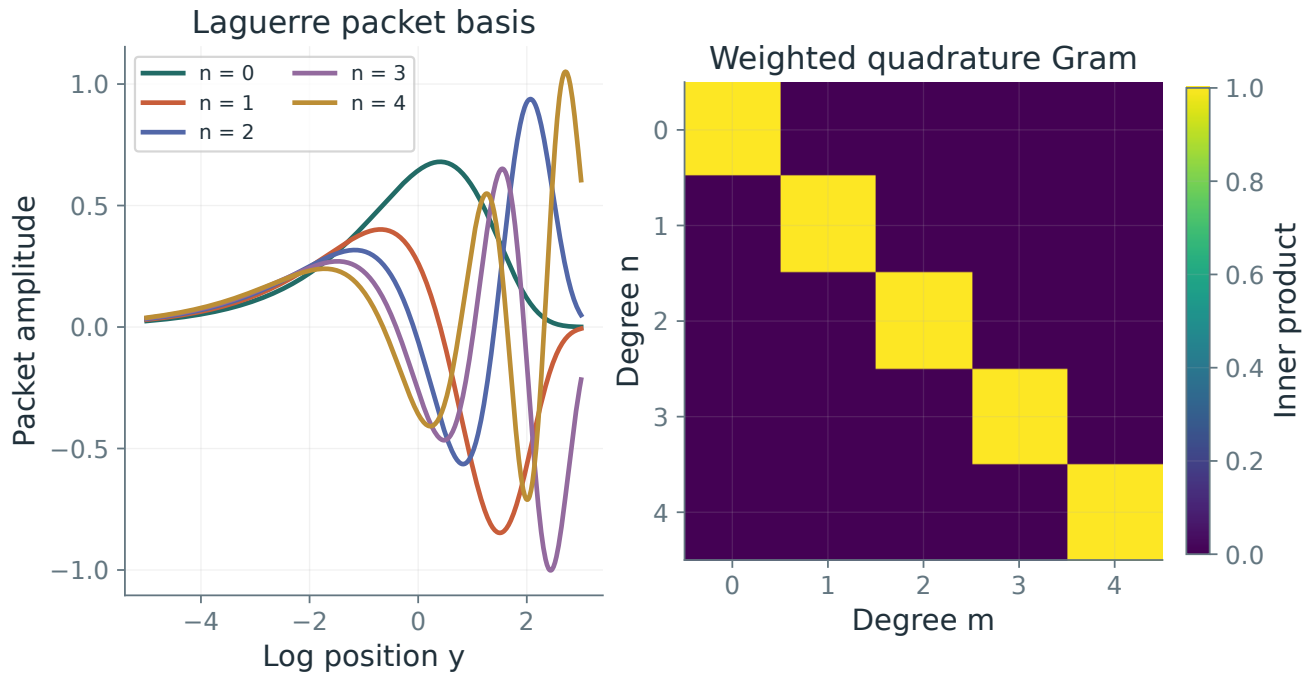
Work an example. At $\alpha = 1.5$, the momentum variance is 0.375 and the position variance is approximately 0.934802. Their square-root product is 0.592073, greater than $1/2$. The quantum Fisher coefficients in these two orbit directions are four times the metric, namely 1.5 and approximately 3.739209. These are local parameter sensitivities, not a claim that the packet is Gaussian at finite shape.

Carry forward. Uncertainty and geometric sensitivity use the same exact packet variances.

Source and scope. V Theorem 6.1 and Proposition 6.2, source lines 678 and 748. Shapes $0.2 \leq \alpha \leq 30$. This is the translation/modulation metric at fixed shape; mixed coefficients involving changing shape are not inferred.

PAPER V / V10 **LESSON 66**

Create orthogonal Laguerre packets



$$\Lambda_{n,\alpha}(y) = \sqrt{\frac{n!}{\Gamma(n+\alpha)}}\, e^{\alpha y/2 - e^y/2} L_n^{(\alpha-1)}(e^y), \qquad \int \Lambda_{n,\alpha}\Lambda_{m,\alpha}\, dy = \delta_{nm}$$

Read the figure. Each degree adds oscillations around the same envelope. A point where two curves cross does not determine their inner product. Orthogonality is the weighted integral over the entire position line. The second panel displays the degree-zero through degree-four Gram matrix, computed in the transformed Gamma coordinate rather than by integrating the cropped curves.

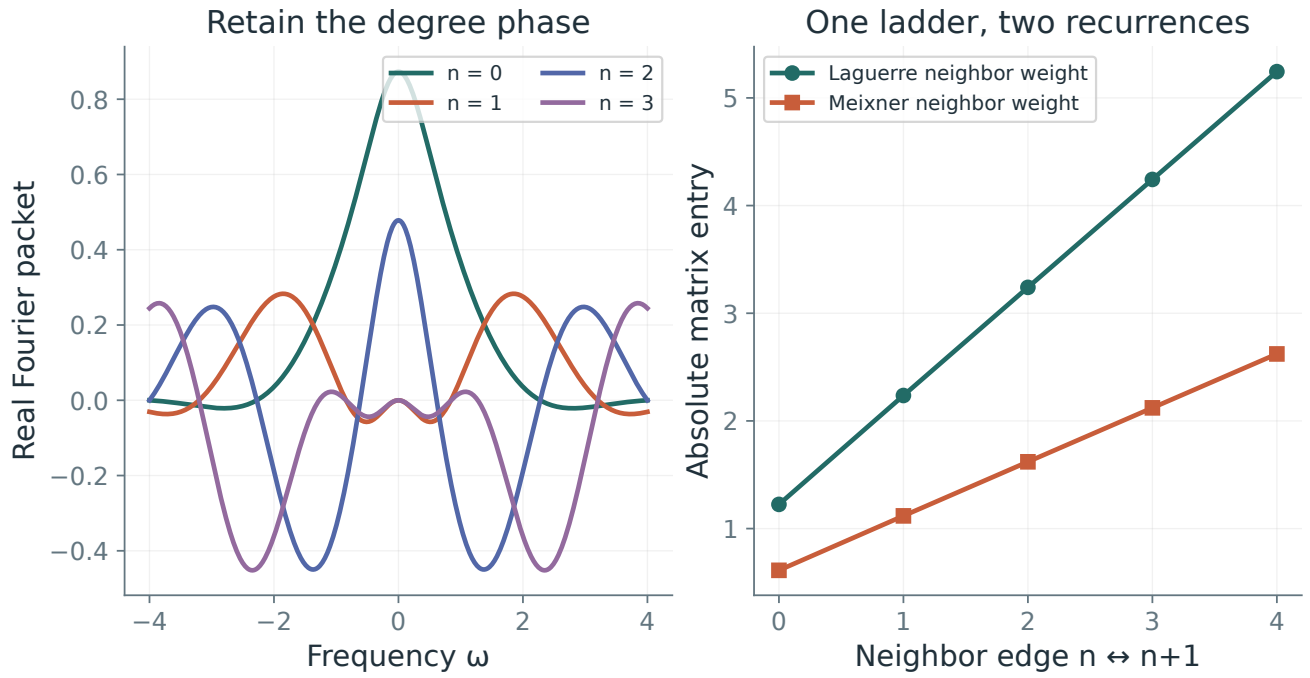
Work an example. Use $u = e^y$. The inner product becomes a generalized Laguerre integral with weight $u^{\alpha-1}e^{-u}$. At $\alpha = 1.5$, products of the shown polynomials have degree at most eight. A 48-node generalized Gauss–Laguerre rule integrates such polynomial products exactly in mathematical arithmetic. Its small recorded residual measures floating-point implementation, whereas the full orthogonality theorem covers all degrees.

Carry forward. A common envelope becomes an orthogonal basis through its natural weight.

Source and scope. V Theorem 7.1, source line 803. Shape 1.5, degrees 0 through 4; position curves cropped to $[-5, 3]$. The Gram uses 48 weighted nodes, whose exact polynomial range extends through degree 95.

PAPER V / V11 **LESSON 67**

Keep Fourier phases in the common ladder



$$\widehat{\Lambda}_{n,\alpha}(\omega) = i^n \widehat{g}_\alpha(\omega) p_{n,\alpha}(\omega),$$
$$J_L = 2K_0 - K_+ - K_-, \qquad J_M = (K_+ + K_-)/2.$$

Read the figure. The first panel retains the degree phase i^n. Dropping it would replace the actual Fourier-transformed position basis with a different frequency basis. The second compares neighbor weights of the two real polynomial recurrences. Their coefficients come from one abstract ladder, although their signs and scaling differ between coordinate realizations.

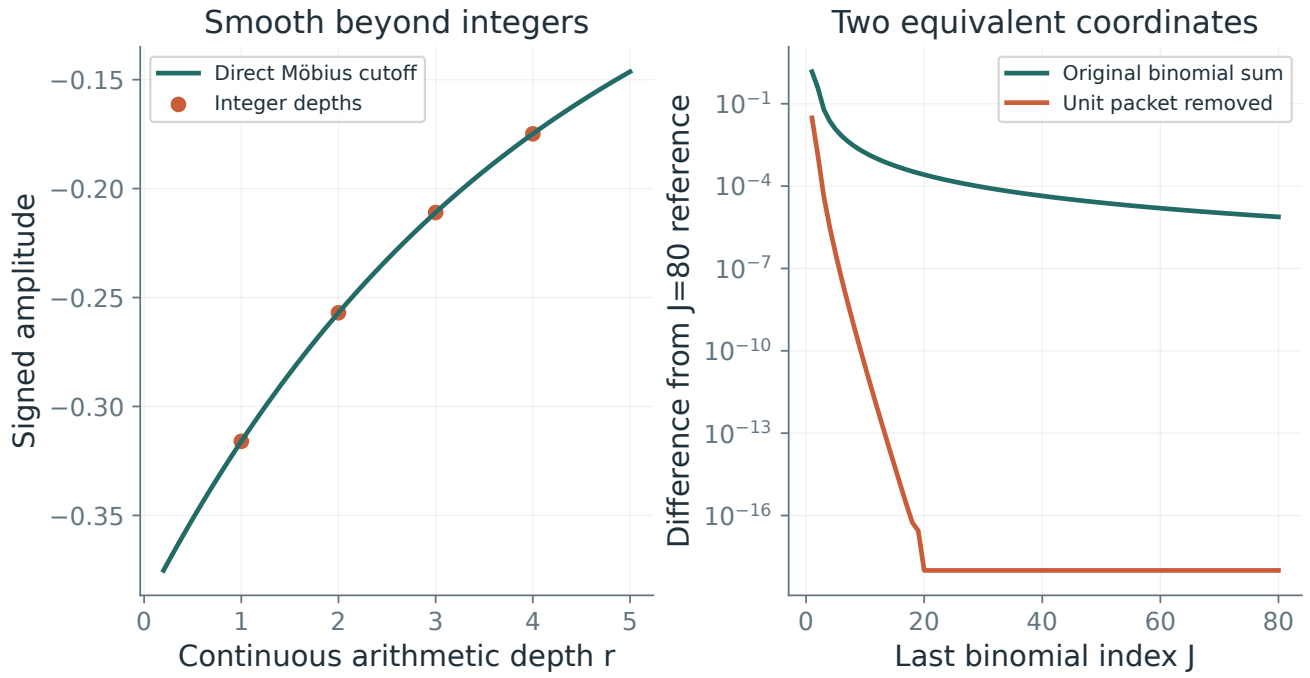
Work an example. At shape 1.5, the first raising coefficient is $\sqrt{1.5}$. The Laguerre neighbor has its negative, while the real Meixner polynomial recurrence uses half that magnitude. Test $[K_-, K_+] = 2K_0$ on a finite-support basis vector below the truncation boundary. A six-dimensional cut satisfies the interior calculation but has a top-row defect because its last raising operation was removed.

Carry forward. Coordinate changes retain degree phases and infinite-basis boundary conditions.

Source and scope. V Theorems 8.1 and 9.1, source lines 855 and 917. Shape 1.5; four Fourier packet curves and a six-dimensional ladder cut. The audit records both the small interior residual and the nonzero top-boundary defect.

PAPER V / V12 **LESSON 68**

Extend the arithmetic depth continuously



$$C_{a,\beta}(r,0)=\sum_{j\ge 0}(-1)^j\binom{r}{j}\zeta(a+\beta j)^{-1}=\sum_{j\ge 0}(-1)^j\binom{r}{j}[\zeta(a+\beta j)^{-1}-1],\quad r>0$$

Read the figure. The left curve embeds the integer signed orbit in a smooth positive-depth parameter. The right measures differences from a finite $J = 80$ reference for two equivalent infinite binomial coordinates. The original finite partial sum retains an artificial remainder from the unit packet. Subtracting one removes that packet and accelerates the displayed finite reconstruction. These are signed amplitudes, not positive densities.

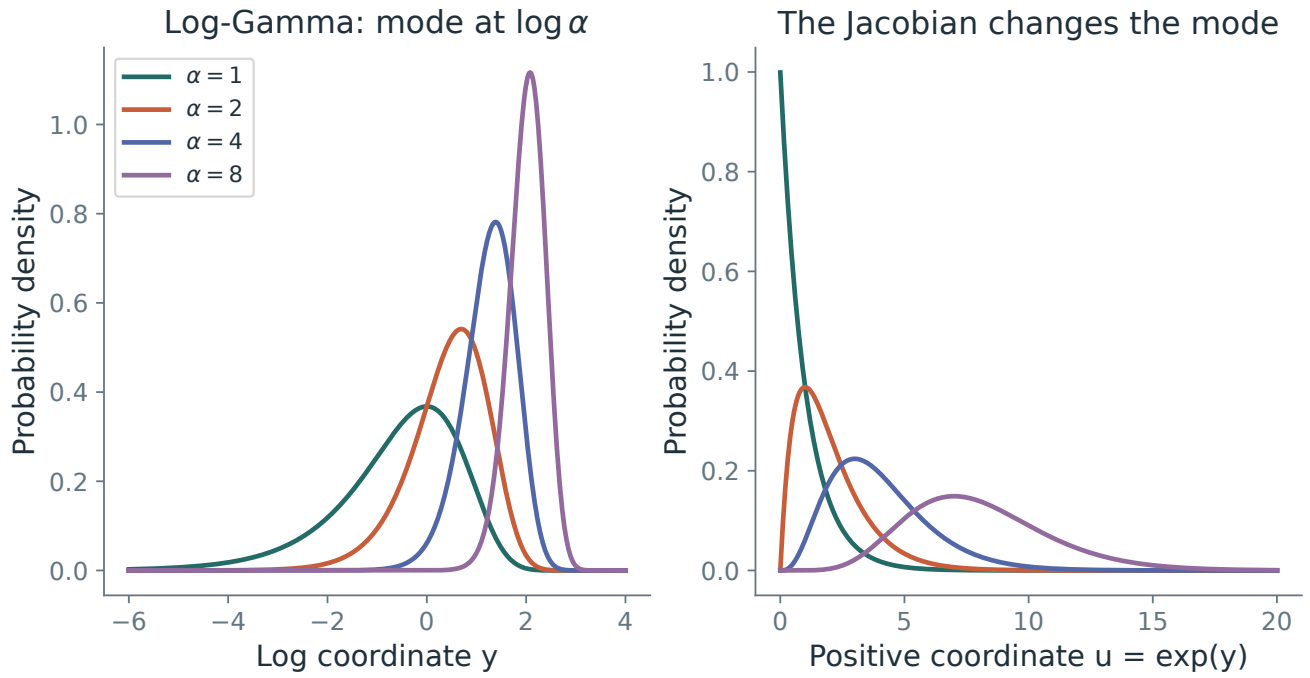
Work an example. Choose arithmetic parameters $a = \beta = 2$ and depth $r = 2.5$. The direct sieve sums $\mu(n)n^{-2}(1-n^{-2})^{2.5}$ through $N = 200000$. For $r > 0$, the full generalized binomial coefficient sum is zero, which justifies the centered reciprocal-zeta series. At integer depths that series terminates. Increasing its last index improves the plotted comparison but does not constitute a universal infinite-series error certificate.

Carry forward. Continuous arithmetic depth preserves the unit-packet boundary and signed character.

Source and scope. V Theorems 10.1 and 10.2, source lines 995 and 1020. $a > 1$ is required for the stated absolute exchanges. Direct cutoff tail is at most $1/N$; the reference is an 80-index binomial sum at 60-digit precision. The log plot floors differences at 10^{-18}.

PAPER VI / 01 **LESSON 69**

Read shape through the logarithmic coordinate



$$g_\alpha(y) = \Gamma(\alpha)^{-1/2} e^{(\alpha y - e^y)/2}, \qquad |g_\alpha(y)|^2\, dy = \frac{u^{\alpha-1}e^{-u}}{\Gamma(\alpha)}\, du$$

Read the figure. The left panel shows probability densities, the squared packet amplitudes. The right shows the same laws after $u = e^y$. Each curve has total mass one on its full domain. The logarithmic Jacobian changes the curve and its mode. Shape therefore does more than move a fixed profile along an axis.

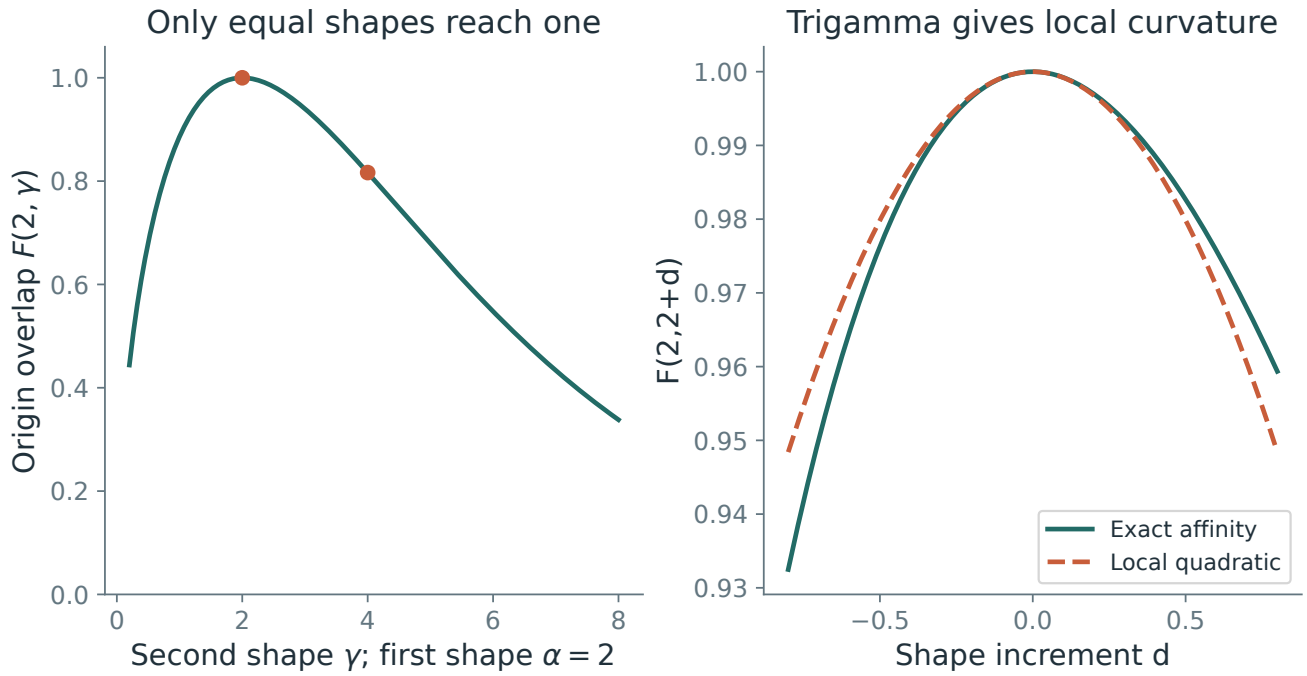
Work an example. For shape two, the log density is e^{2y-e^y}. Its derivative vanishes at $y = \log 2$. The corresponding Gamma density is ue^{-u}, whose mode is $u = 1$. The mean of the log coordinate is $1 - \gamma_{\mathrm{E}}$, about 0.4228, where γ_{E} is Euler's constant; its variance is $\pi^2/6 - 1$.

Carry forward. A change of coordinate preserves probability after including its Jacobian. Packet normalization uses the full real line.

Source and scope. VI Proposition 1.1, "Normalization." Shapes $1, 2, 4, 8$; finite plot windows. Omitted mass is recorded using regularized Gamma functions; no plotted curve is renormalized.

PAPER VI / 02 **LESSON 70**

Separate shape affinity from local curvature



$$F(\alpha,\gamma)=\frac{\Gamma((\alpha+\gamma)/2)}{\sqrt{\Gamma(\alpha)\Gamma(\gamma)}},\qquad F(\alpha,\alpha+d)=1-\frac{\psi_1(\alpha)}{8}d^2+O(d^3)$$

Read the figure. The first panel compares every displayed second shape with the fixed shape two. Only the equal-shape point reaches one. The second enlarges a neighborhood of that point and compares the exact affinity with its quadratic expansion. Their separation away from zero shows why a local expansion should not be used as a global identity.

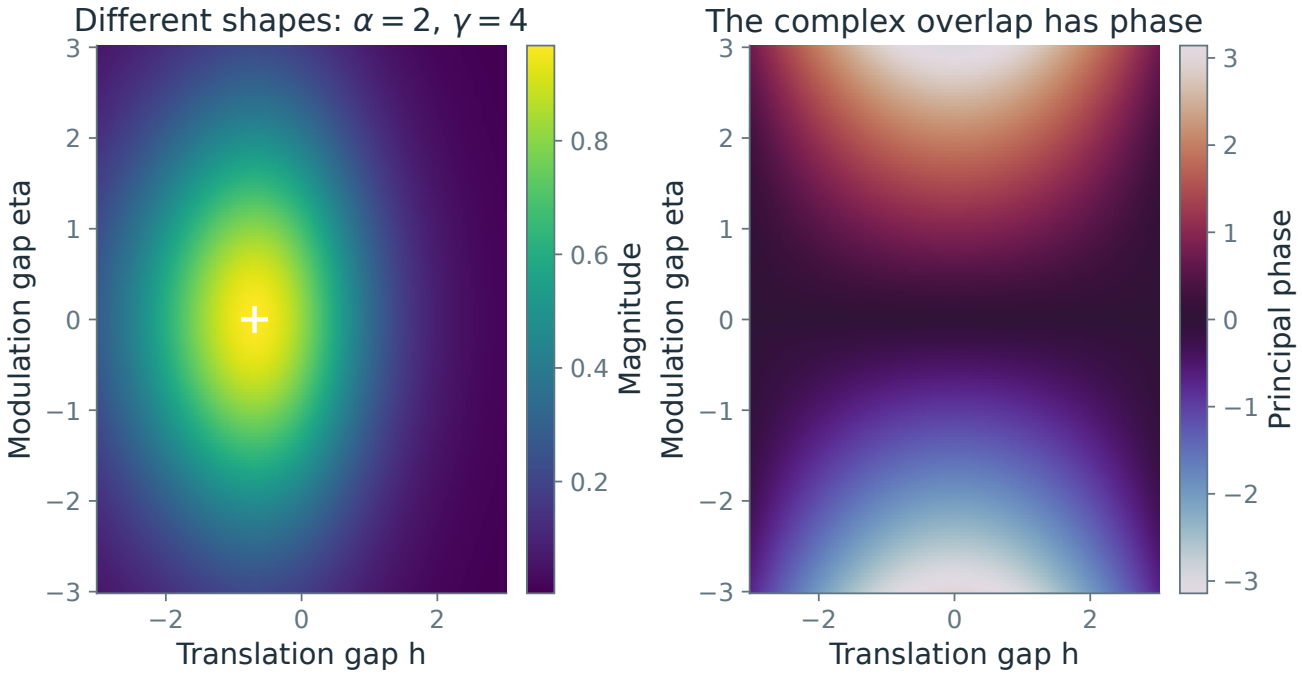
Work an example. For shapes two and four, $F=2/\sqrt{6}=\sqrt{2/3}$. Thus the squared overlap at zero translation and modulation is exactly $2/3$. At increment $d=0.2$, the exact affinity is about 0.996969; the quadratic approximation gives 0.996775. Its curvature comes from $\psi_1(2)=\pi^2/6-1$.

Carry forward. Origin affinity compares shapes at one common coordinate. A later translation can increase their overlap.

Source and scope. VI Proposition 2.2, "Strict shape affinity," and its following local expansion. The local quadratic is displayed as an approximation; the shape metric coefficient is $\psi_1(\alpha)/4$.

PAPER VI / 03 **LESSON 71**

Keep magnitude and phase in cross ambiguity



$$\mathcal{A}_{\alpha,\gamma}(h,\eta) = e^{(\alpha-\gamma)h/4}\frac{\Gamma(\lambda+i\eta)}{\sqrt{\Gamma(\alpha)\Gamma(\gamma)}}\operatorname{sech}^{\lambda+i\eta}(h/2), \quad \lambda=(\alpha+\gamma)/2$$

Read the figure. The two panels represent one complex overlap. Magnitude measures localization; the principal phase records information that a squared magnitude removes. A phase-color jump is a branch wrap, not a zero. Unequal shapes shift the magnitude peak away from zero displacement, while the frequency envelope remains symmetric. The white cross marks the zero-frequency displacement maximum.

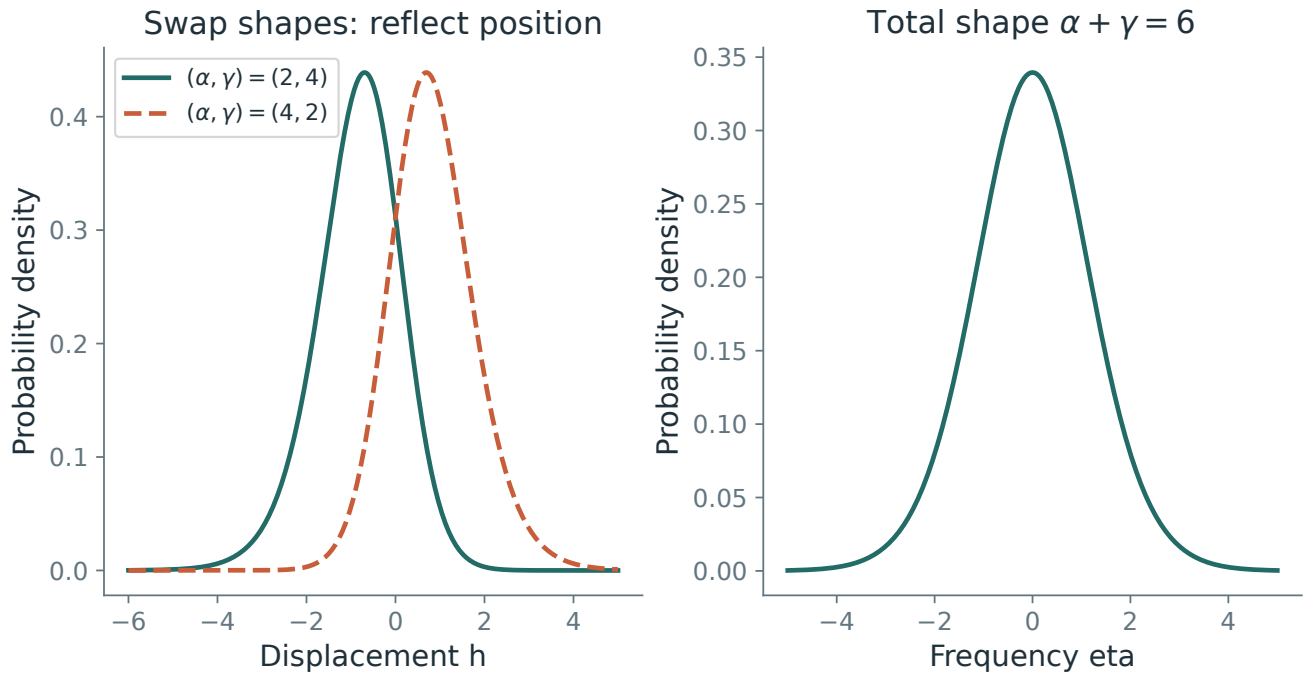
Work an example. Take $\alpha = 2$, $\gamma = 4$. At zero frequency, the magnitude is $\sqrt{2/3}\,e^{-h/2}\operatorname{sech}^3(h/2)$. Differentiating its logarithm gives the maximum at $h = -\log 2$, with value about 0.967700. The origin value is only $\sqrt{2/3}$. At $(h,\eta) = (0,1)$ the squared magnitude is $5\pi/(3\sinh\pi)$.

Carry forward. Translation, modulation, and shape are distinct coordinates. The complex Gamma factor retains their phase relation.

Source and scope. VI Theorem 2.1, "Cross-shape Gamma–sech formula." Shapes 2, 4 on $[-3,3]^2$; exact-formula samples. Independent overlap quadrature is checked separately.

PAPER VI / 04 **LESSON 72**

Factor energy into two independent laws



$$\frac{|\mathcal{A}_{\alpha,\gamma}(h,\eta)|^2}{2\pi} = p_{\alpha,\gamma}(h)\rho_{\alpha+\gamma}(\eta), \qquad \rho_s(\eta) = \frac{2^{s-1}|\Gamma(s/2+i\eta)|^2}{\pi\Gamma(s)}$$

Read the figure. The displacement panel reflects when the two shapes are exchanged. The frequency panel uses only their sum. These are probability marginals of the normalized cross-spectrogram, whose product is its full energy density. Independence here belongs to that product probability law. It does not say that the complex ambiguity factors into two real densities or loses its phase.

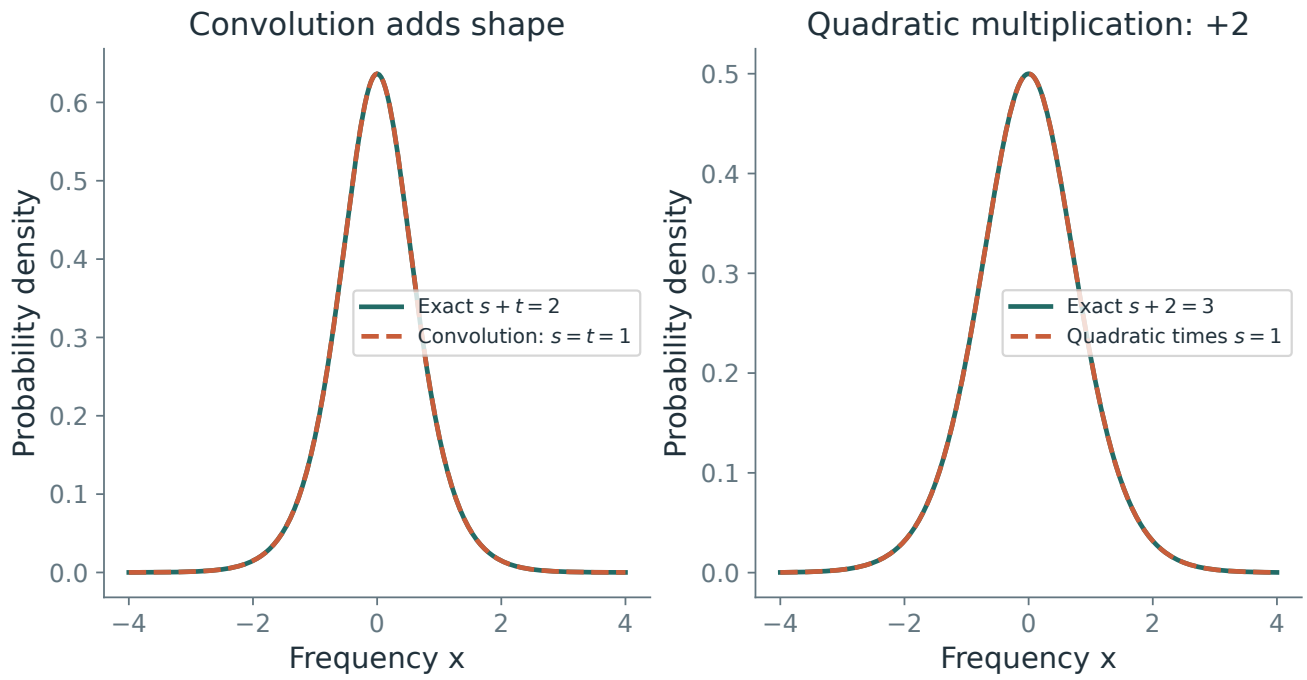
Work an example. With shapes two and four, displacement is the logit of a Beta$(2,4)$ variable. Its mean is $\psi(2) - \psi(4) = -5/6$, while the symmetric shape-six frequency has mean zero and variance $3/2$. At the origin, $p_{2,4}(0) = 5/16$ and $\rho_6(0) = 16/(15\pi)$, so the joint density is exactly $1/(3\pi)$.

Carry forward. A positive two-dimensional energy law can have independent marginals even when its underlying amplitude has nontrivial phase.

Source and scope. VI Theorem 3.1, "Exact cross-spectrogram factorization." Position tails use Beta CDFs; frequency tails use a stated Meixner Chernoff bound. Finite-window mass is not reset to one.

PAPER VI / 05 **LESSON 73**

Add shapes by convolution



$$\rho_{s+t} = \rho_s * \rho_t, \qquad \rho_{s+2}(x) = \frac{s^2 + 4x^2}{s(s+1)}\rho_s(x)$$

Read the figure. The first panel overlays a closed density with an independently integrated convolution. The second uses a different operation: pointwise quadratic multiplication raises shape by two. Both identities change shape, but their inputs and computational costs differ. The convolution adds independent random variables. The ladder changes one density locally at each displayed frequency.

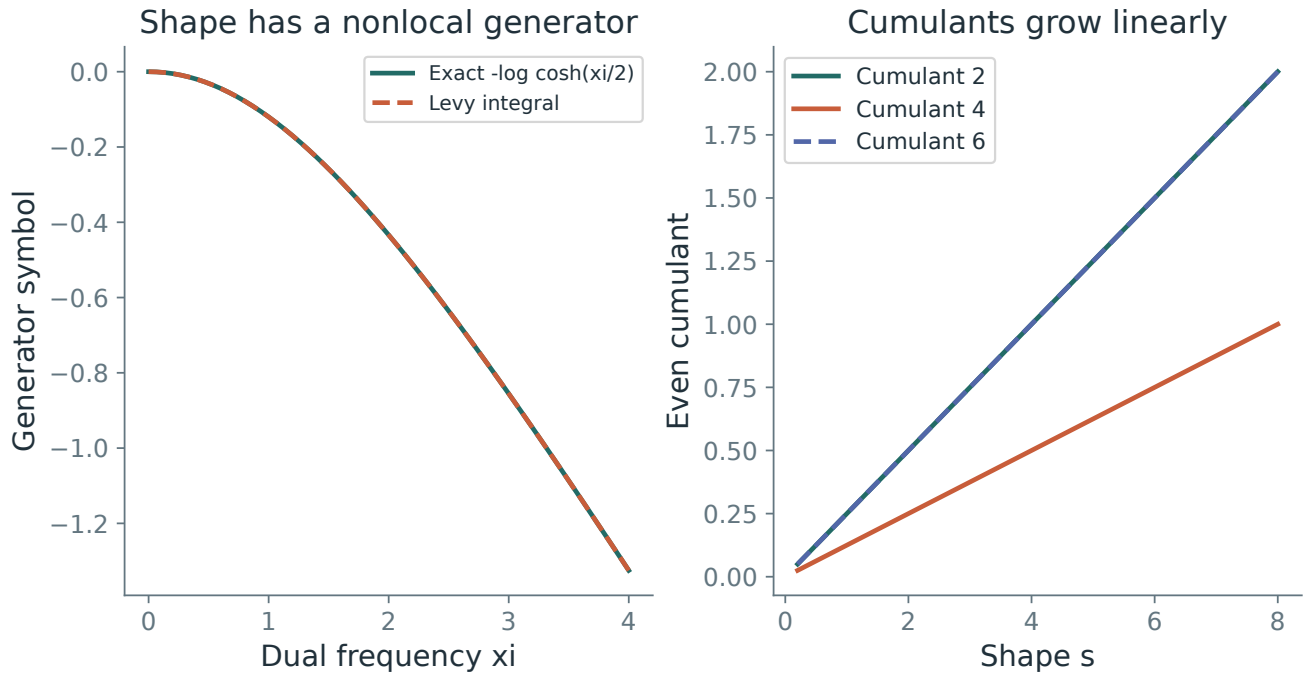
Work an example. Shape one has density $\operatorname{sech}(\pi x)$. Convolving two such laws gives shape two, $2x/\sinh(\pi x)$, with the removable origin value $2/\pi$. Its variance is $1/4 + 1/4 = 1/2$. Separately, multiplying shape one by $(1 + 4x^2)/2$ produces shape three. At $x = 1$, shape two has density about 0.173179.

Carry forward. The characteristic function $\operatorname{sech}^s(h/2)$ turns shape addition into multiplication. The Gamma recurrence gives the ladder.

Source and scope. VI Theorem 4.1, "Meixner shape semigroup," and Proposition 4.2, "Two-step density ladder." Convolution integrates on $[-8, 8]$; its omitted integral is uniformly bounded by 1.55×10^{-11}.

PAPER VI / 06 **LESSON 74**

Continuous shape produces jumps and cumulants



$$-\log\cosh(\xi/2) = \int_0^\infty \frac{\cos(\xi x) - 1}{x \sinh(\pi x)}\, dx, \qquad \kappa_{2m} = s\frac{(2^{2m} - 1)|B_{2m}|}{2m}$$

Read the figure. The generator panel compares its exact Fourier symbol with the Lévy integral. The numerator cancels the apparent origin singularity, so the combined integrand is finite there. The second panel tracks even cumulants through shape. The second and sixth cumulants overlap because both equal $s/4$; their coincidence does not make the distribution Gaussian.

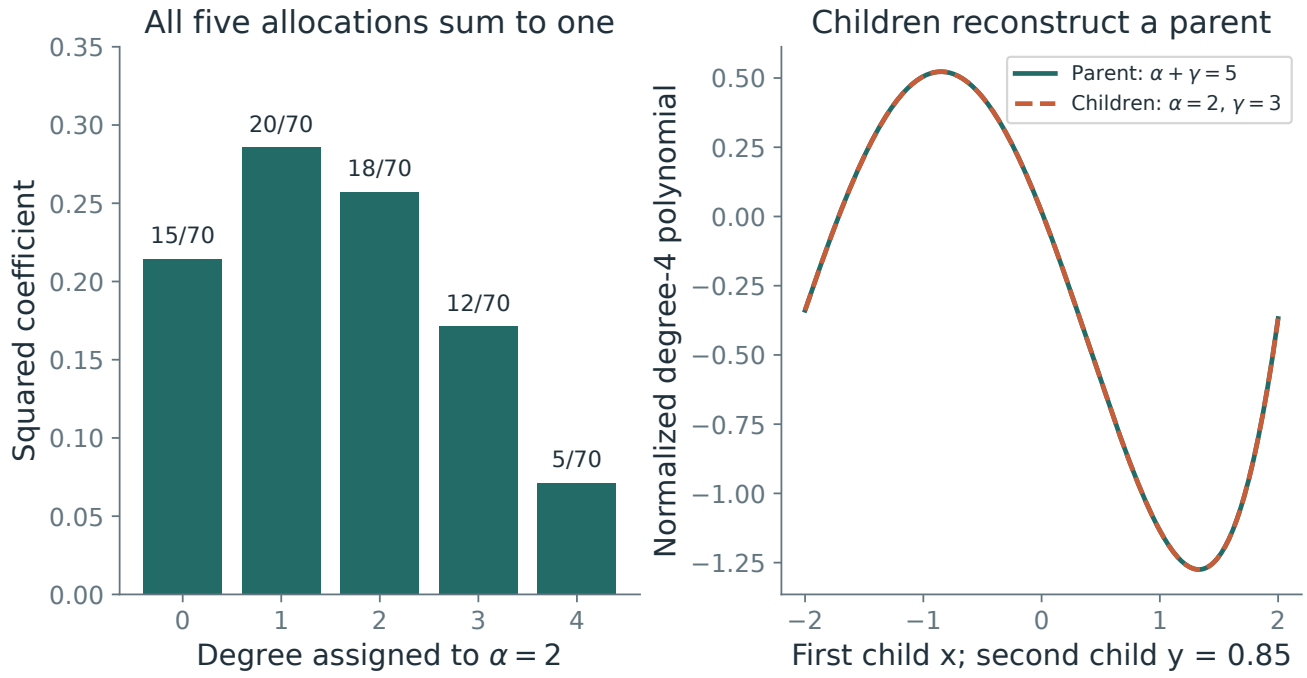
Work an example. At shape four, variance is one, the fourth cumulant is $1/2$, and the sixth is one. A Gaussian with variance one would have both higher cumulants zero. The nonzero values measure departures from Gaussianity. For dual frequency $\xi = 2$, the unit-shape generator symbol is $-\log\cosh 1$, about -0.433781.

Carry forward. The Lévy measure describes infinitesimal shape increments; Bernoulli numbers encode the complete even-cumulant sequence.

Source and scope. VI Theorems 5.1 and 5.2, "Lévy–Khintchine representation" and "Bernoulli cumulant law." Quadrature uses $[0, 10]$, stable sine-squared cancellation, and a tail bound below 2.90×10^{-15}.

PAPER VI / 07 **LESSON 75**

Split one polynomial without losing energy



$$p_{n,\alpha+\gamma}(x+y)=\sum_{r=0}^{n} C_{n,r}^{\alpha,\gamma}\,p_{r,\alpha}(x)\,p_{n-r,\gamma}(y), \qquad (C_{n,r}^{\alpha,\gamma})^2=\binom{n}{r}\frac{(\alpha)_r(\gamma)_{n-r}}{(\alpha+\gamma)_n}$$

Read the figure. Every bar is an allowed degree allocation between two children. Their heights sum to one, so the transfer preserves coefficient energy. The polynomial panel overlays the parent with the sum of all five products. Individual products can be large or signed; the probability bars describe squared transfer coefficients, not pointwise polynomial contributions.

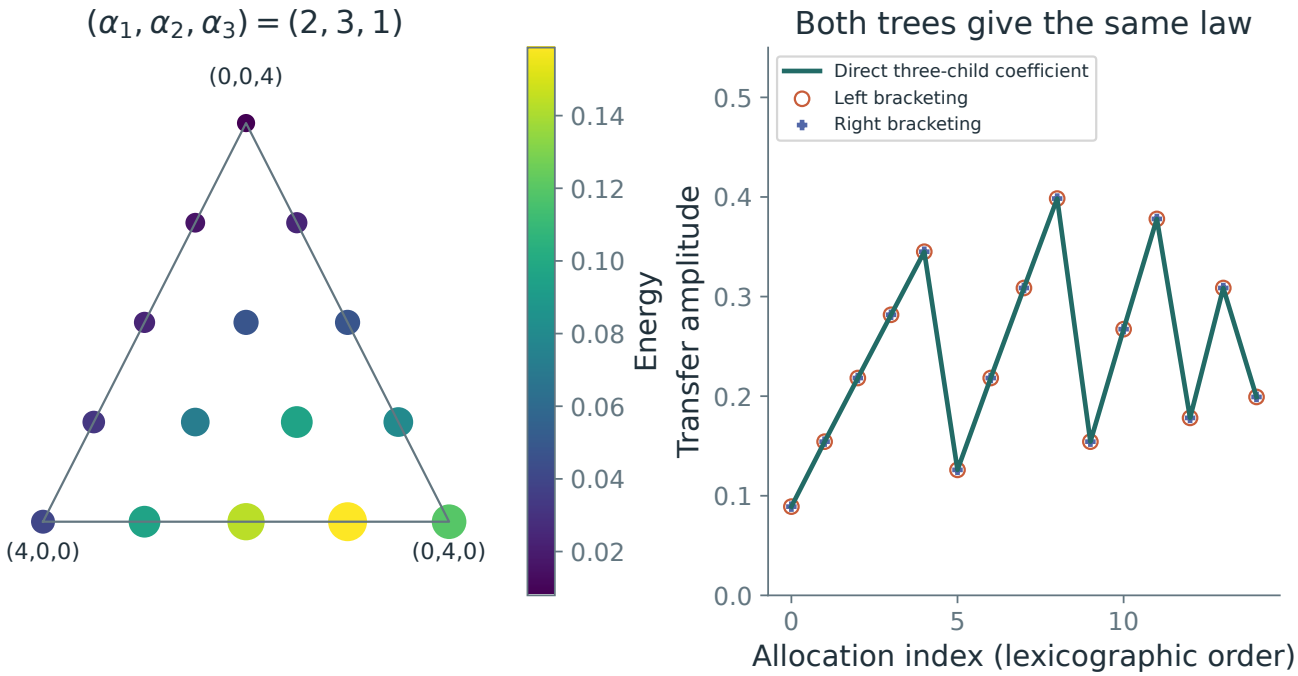
Work an example. Use degree four and child shapes two and three. The energy weights, in order $r = 0, \dots, 4$, are $(15, 20, 18, 12, 5)/70$. Their sum is one and their mean allocation to the first child is $8/5$. At $x = 0.6$, $y = 0.85$, the normalized parent is approximately -0.716400, reproduced by the complete five-term child sum.

Carry forward. An isometric refinement is a complete change of polynomial coordinates. Omitting an allocation changes the reconstruction.

Source and scope. VI Theorem 6.1, "Two-child packet refinement." Degree four, shapes $2, 3$, fixed $y = 0.85$; all five terms are retained. Numerical pointwise reconstruction and coefficient normalization are checked.

PAPER VI / 08 **LESSON 76**

Choose a refinement tree freely



$$C^{\boldsymbol{\alpha}}_{n,\mathbf{r}} = \sqrt{\frac{n!\prod_j (\alpha_j)_{r_j}}{(\sum_j \alpha_j)_n \prod_j r_j!}}, \qquad C^{\alpha_1+\alpha_2,\alpha_3}_{n,r_1+r_2} C^{\alpha_1,\alpha_2}_{r_1+r_2,r_1} = C^{\boldsymbol{\alpha}}_{n,\mathbf{r}}$$

Read the figure. The triangle contains every degree-four allocation among three children. Color encodes energy; marker area increases with it. The second panel lists all fifteen terminal amplitudes and overlays two binary refinement orders. Coincident markers express coassociativity. The geometric arrangement is a degree-allocation simplex, not the phase space used by the ambiguity function.

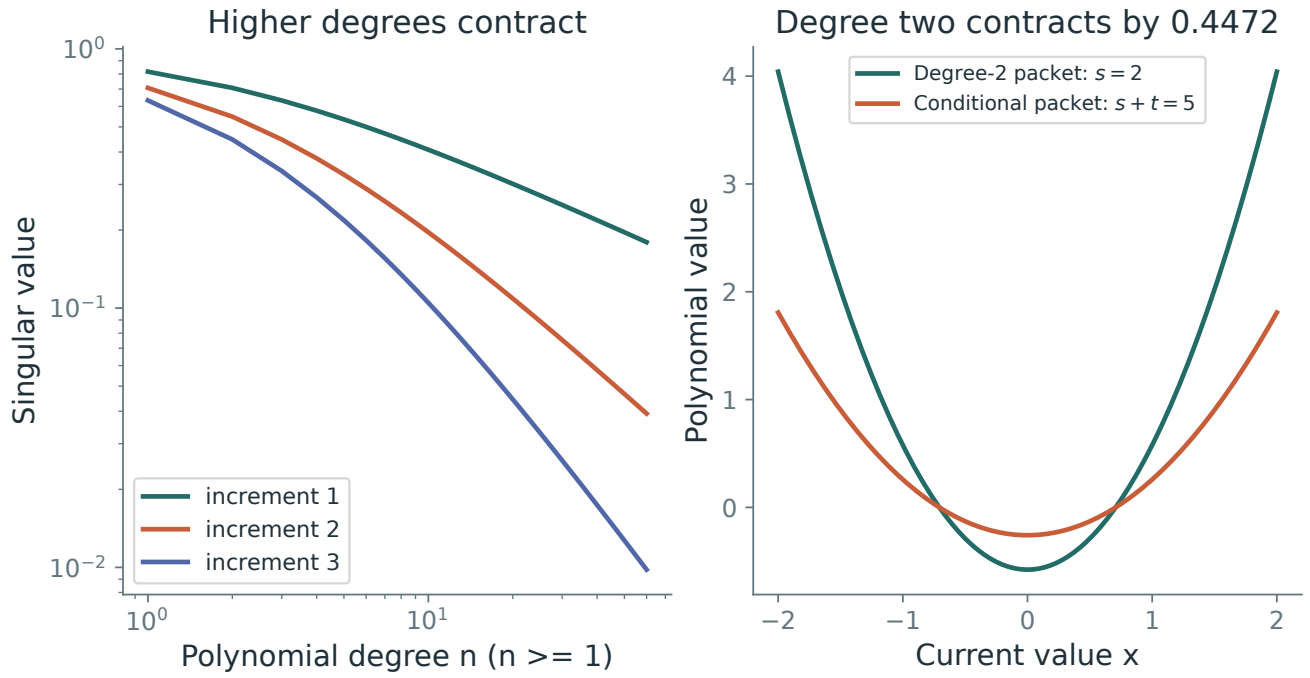
Work an example. Take shapes $(2, 3, 1)$ and allocation $(1, 2, 1)$. The direct squared coefficient is $2/21$. Splitting the first two children first gives squared factors $5/18$ and $12/35$. Splitting the last two first gives $20/63$ and $3/10$. Both products equal $2/21$, and both amplitudes are the positive square root, about 0.308607.

Carry forward. Intermediate shape factors cancel exactly. A deeper binary tree gives the same final many-child coefficients.

Source and scope. VI Theorem 7.1, "Multinomial packet refinement," and Corollary 7.2, "Coassociativity." All fifteen compositions of degree four are shown; both trees and total energy are checked.

PAPER VI / 09 **LESSON 77**

Read conditional transfer from its singular values



$$T_{s,t}p_{n,s+t} = \sigma_n(s,t)p_{n,s}, \qquad \sigma_n(s,t) = \sqrt{\frac{(s)_n}{(s+t)_n}}, \quad \sigma_n(s,t) \sim \sqrt{\frac{\Gamma(s+t)}{\Gamma(s)}}\, n^{-t/2}$$

Read the figure. Each spectral curve measures contraction of one polynomial degree. Larger increments suppress high degrees more strongly. Degree zero, excluded from the logarithmic horizontal axis, remains exactly one. The polynomial panel shows why orthonormal packets contract even though the standard, unnormalized Meixner–Pollaczek polynomials satisfy the martingale identity without a scalar loss.

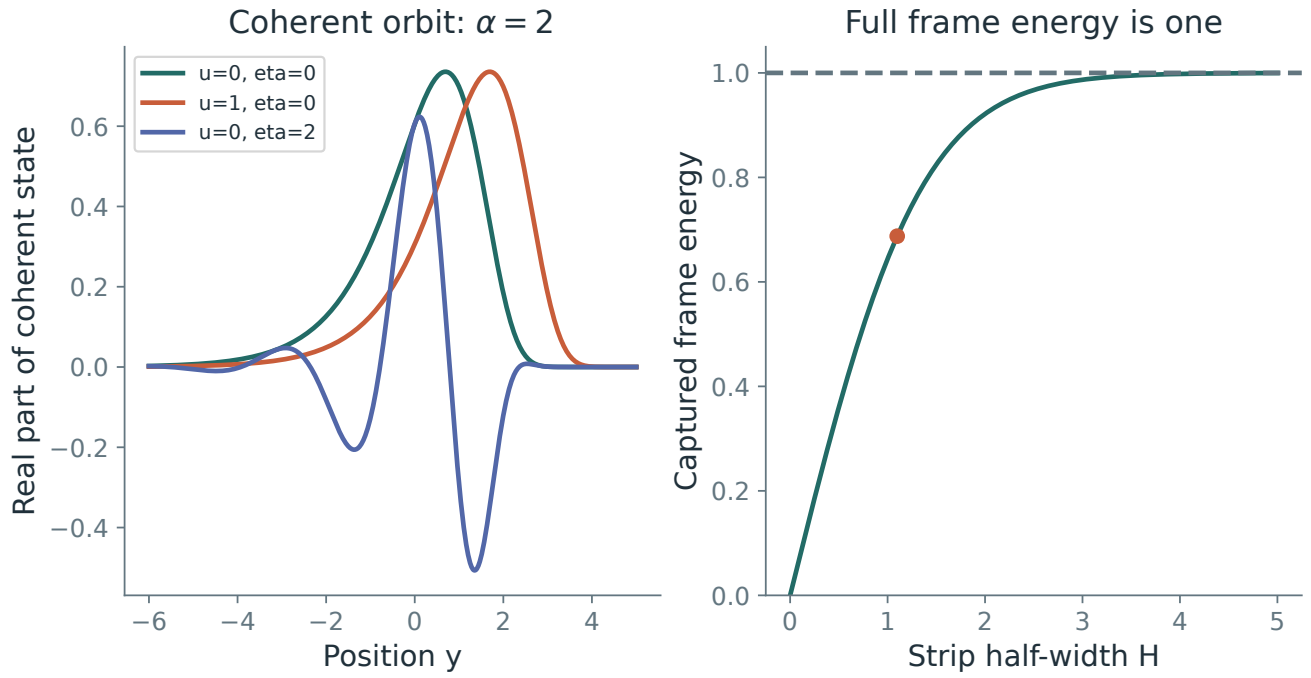
Work an example. For $s = 2$, $t = 3$, the first singular values are 1, $\sqrt{2/5}$, $1/\sqrt{5}$, and $2/\sqrt{35}$. Since a shape-three increment has variance $3/4$, conditioning $(2(X+Y)^2 - 5/2)/\sqrt{15}$ gives $(2X^2 - 1)/\sqrt{15}$. This equals $p_{2,2}(X)/\sqrt{5}$, and at $X = 1$ it is $1/\sqrt{15}$.

Carry forward. The exact cocycle permits successive increments. Compactness holds for every positive increment; Schatten membership requires $pt > 2$.

Source and scope. VI Theorem 8.1, "Polynomial martingale law," and Proposition 8.2, "Cocycle and compactness." Degrees through 60; a rank-61 truncation at increment three has exact omitted norm $\sigma_{61} \approx 0.00957$.

PAPER VI / 10 **LESSON 78**

A continuous coherent orbit resolves identity



$$\psi_{\alpha,u,\eta}(y) = e^{i\eta(y-u/2)} g_\alpha(y-u), \qquad \frac{1}{2\pi}\int_{\mathbb{R}^2} |\langle \psi_{\alpha,u,\eta}, f\rangle|^2 \, du\, d\eta = \|f\|_2^2$$

Read the figure. Translation moves the window; modulation oscillates its complex amplitude. Only real parts are drawn on the left. The right integrates the coherent-transform energy of $f = g_2$ over a position strip, including every modulation frequency. Its approach to one illustrates the continuous frame normalization. Three displayed states alone do not form the identity resolution.

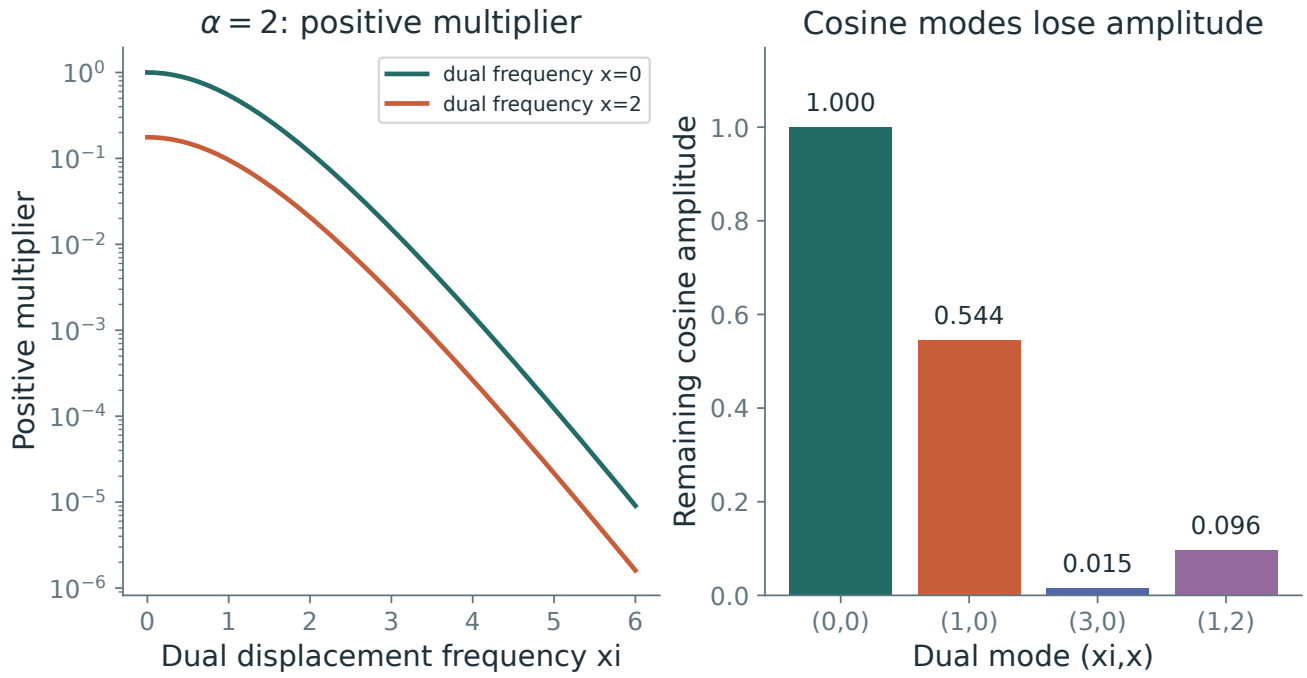
Work an example. For $f = g_2$, the frame energy density is $p_{2,2}(u)\rho_4(\eta)$. Integrating frequency removes its normalized factor. In the strip $|u| \le \log 3$, the logistic endpoints are $1/4$ and $3/4$. The Beta$(2,2)$ CDF is $3v^2 - 2v^3$, so the captured energy is exactly $11/16$.

Carry forward. An overlap kernel becomes a coherent transform and a reproducing kernel when the full normalized orbit is used.

Source and scope. VI Theorems 9.1 and 9.2, "Cross-shape coherent overlap" and "Continuous tight frame." Shape two; strip energy uses an exact Beta CDF with frequency integrated on all $\mathbb{R}$.

PAPER VI / 11 **LESSON 79**

Positive smoothing can have unstable inversion



$$\widehat{\mathcal{B}}_\alpha(\xi,x)=\frac{|\Gamma(\alpha+i\xi)|^2}{\Gamma(\alpha)^2}\operatorname{sech}^{2\alpha}(x/2)>0, \qquad \widetilde{F}=\mathcal{B}_\alpha * F$$

Read the figure. The multiplier stays positive while shrinking quickly along either dual coordinate. The bars show its action on four cosine modes: convolution preserves each mode and multiplies its amplitude by the displayed number. Therefore exact information survives algebraically, but recovering a small attenuated mode requires amplifying any error attached to it.

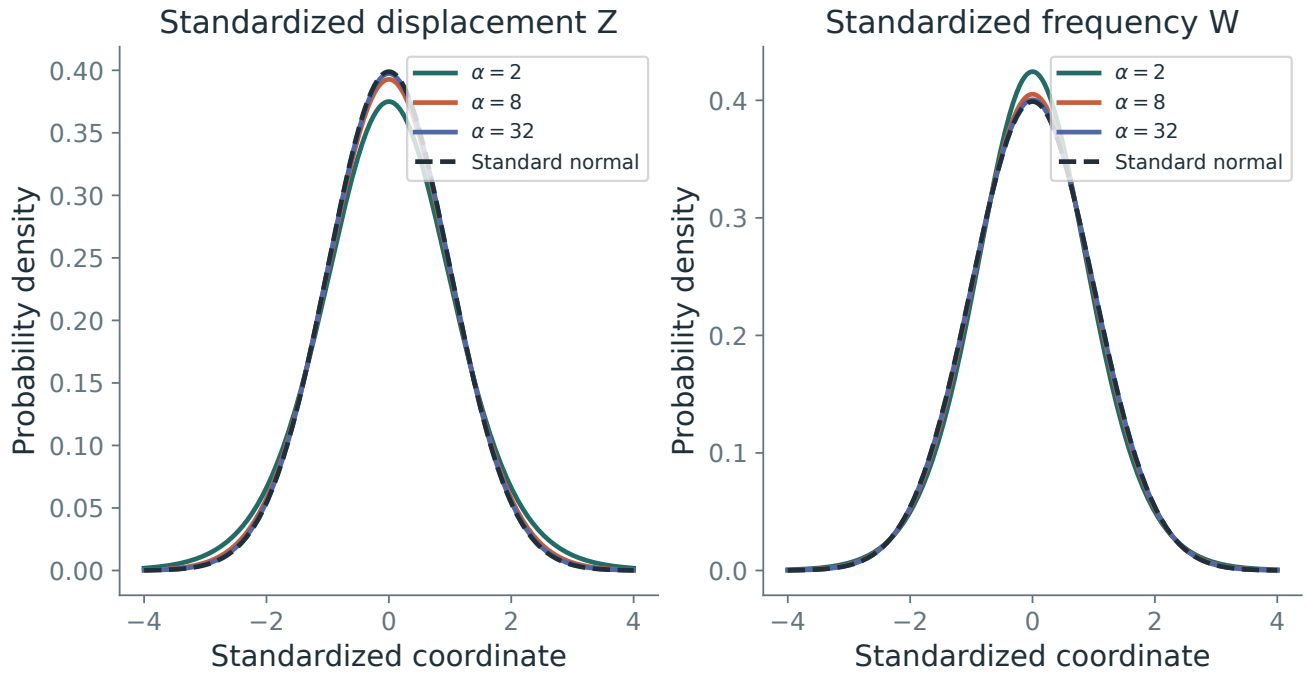
Work an example. At shape two, $\widehat{\mathcal{B}}_2(1,0)=2\pi/\sinh\pi\approx 0.544058$. The mode $(3,0)$ retains only $30\pi/\sinh(3\pi)\approx 0.015212$, requiring inverse amplification about 65.7. For mode $(1,2)$, the additional factor is $\operatorname{sech}^4(1)$, reducing its amplitude to about 0.095960. The constant mode retains amplitude one.

Carry forward. Injectivity is an exact uniqueness statement. Stable numerical recovery requires an additional regularization or restricted function class.

Source and scope. VI Theorem 10.1, "Exact Berezin factorization," and Corollary 10.2, "Injectivity and ill-posed inversion." Bounded cosine symbols illustrate attenuation; the L^2 inverse statement is the source theorem.

PAPER VI / 12 **LESSON 80**

Rescale shape toward a Gaussian heat kernel



$$Z_\alpha = \sqrt{\alpha/2}\, H_\alpha, \quad W_\alpha = \sqrt{2/\alpha}\, \Omega_\alpha \implies N(0,1), \qquad S_\alpha F \longrightarrow e^{\Delta/2} F$$

Read the figure. The two panels use different rescalings because unscaled displacement narrows while frequency broadens. Both normalized laws approach the same standard normal curve. At finite shape, the position variance is still slightly above one; frequency variance is exactly one. Matching a limiting curve does not remove the higher finite-shape cumulants or establish a function-space convergence theorem.

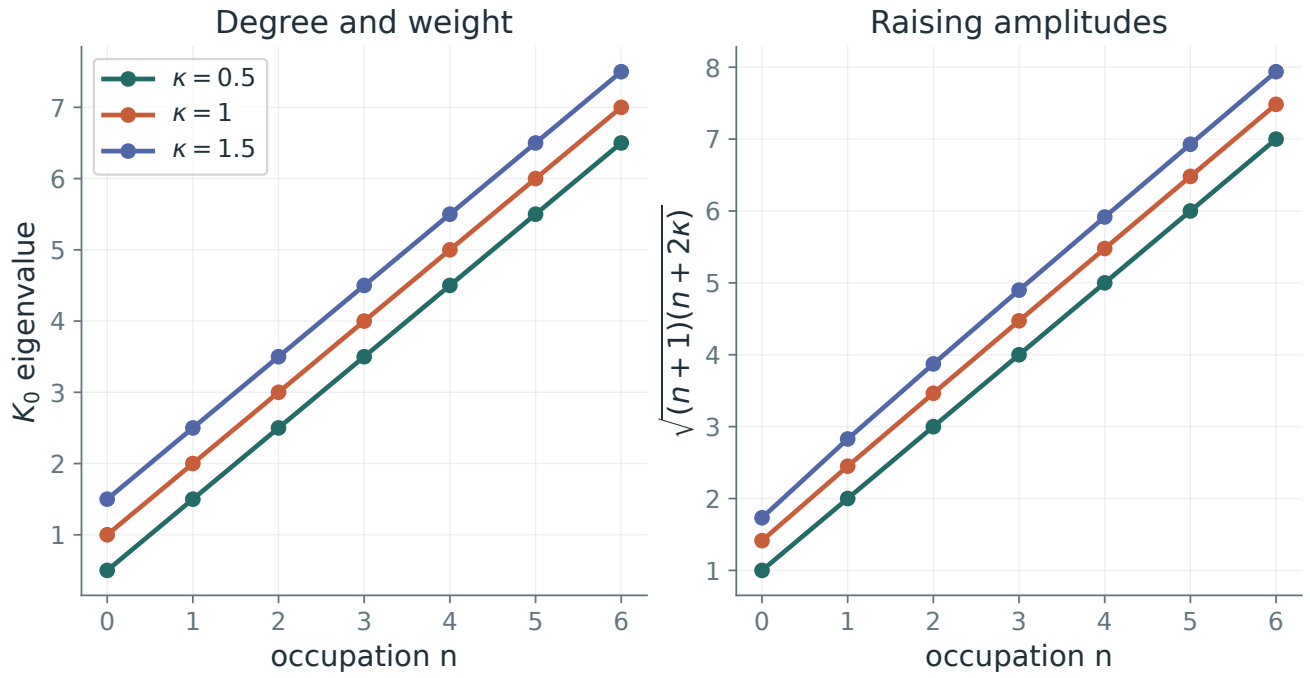
Work an example. At shape two, $\mathrm{Var}(Z_2) = 2\psi_1(2) \approx 1.289868$, while $\mathrm{Var}(W_2) = 1$. At shape 32, the first variance is about 1.015788. The rescaled two-dimensional multiplier at dual mode $(1,1)$ is then about 0.365956, approaching the heat multiplier e^{-1}. For a Gaussian test symbol $e^{-|z|^2/2}$, the limiting smoothed value is $\frac{1}{2}e^{-|z|^2/4}$.

Carry forward. The natural rescaling gives independent standard-normal marginals and the two-dimensional heat operator as the large-shape limit.

Source and scope. VI Theorem 11.1, "Gaussian marginal limits," and Corollary 11.2, "Heat-operator limit." Exact finite-shape densities; tail bounds recorded. All-Schwartz-seminorm convergence belongs to the source proof, not the plotted comparison.

Paper VII / 01 **LESSON 81**

A ladder begins with a positive shape



$$K_0|n\rangle = (n+\kappa)|n\rangle, \qquad K_+|n\rangle = \sqrt{(n+1)(n+2\kappa)}\,|n+1\rangle$$

Read the figure. Read the left panel vertically: an occupation label selects a weight eigenvalue. Changing the positive shape shifts that entire ladder. The right panel reads the same labels as raising amplitudes. Those coefficients determine how neighboring degrees are joined, rather than merely naming them. The curves are computed from the defining representation, with no fitted model. These two pieces of data are the input to every tensor construction in this volume.

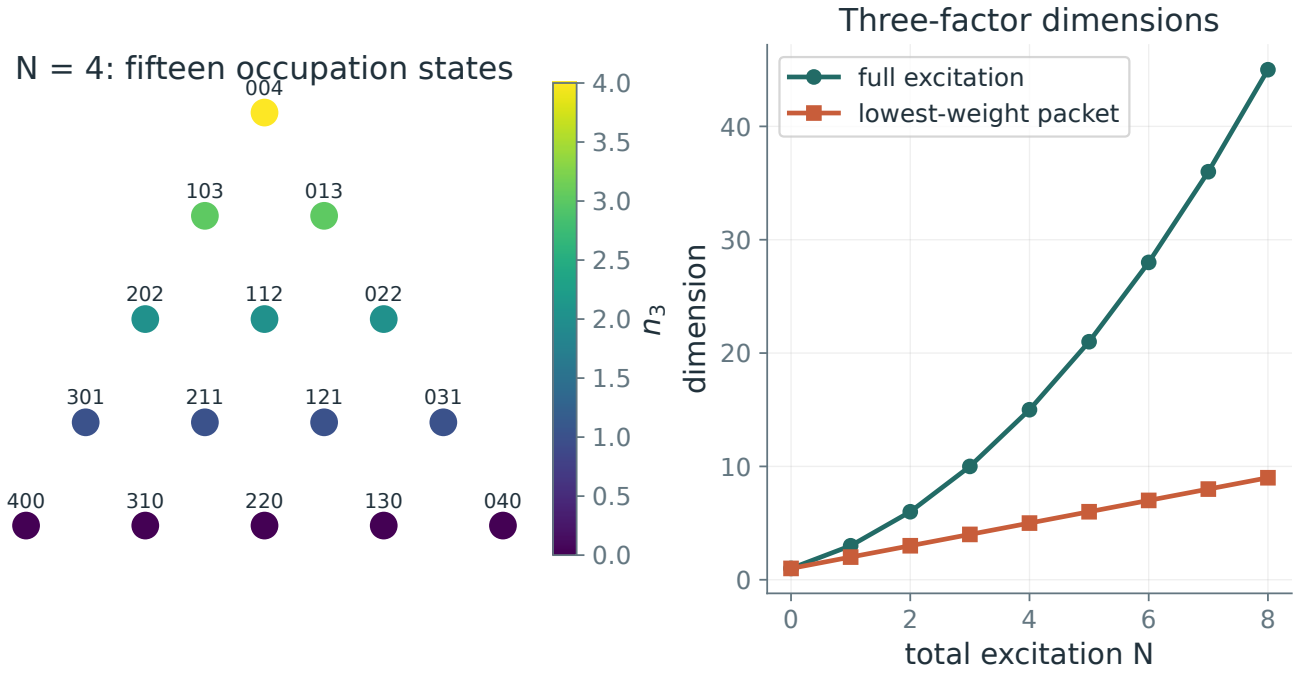
Work an example. Set $\kappa = 1/2$ and start at degree $n = 2$. Its weight is 2.5, while its raising coefficient is $\sqrt{3 \cdot 3} = 3$. Thus $K_+|2\rangle = 3|3\rangle$ in the algebraic ladder. This coefficient is an operator amplitude, not a probability. A normalized physical transition would require its own state and dynamics. The example explains why later Casimir matrices retain products of ladder amplitudes.

Carry forward. Keep the degree label, weight eigenvalue, and transition amplitude as three distinct quantities.

Source and scope. VII, Chapter 1, Definition 1.1, *Positive shape packet*, source lines 219–243. Direct representation formulas; positive κ, nonnegative integer degree, finite-support vectors.

Paper VII / 02 **LESSON 82**

Project a large excitation simplex



$$\dim H_N^{(3)} = \binom{N+2}{2}, \qquad \dim M_N^{(3)} = N+1$$

Read the figure. Each point on the left is one occupation triple with the same total excitation. The three digits give its exact address, and color records the third occupation. The plot contains fifteen points because weak compositions count the ambient basis. On the right, compare that full count with the dimension of the new lowest-weight kernel. The smaller curve counts an exact subspace. It does not mean that a few occupation states were discarded by sampling.

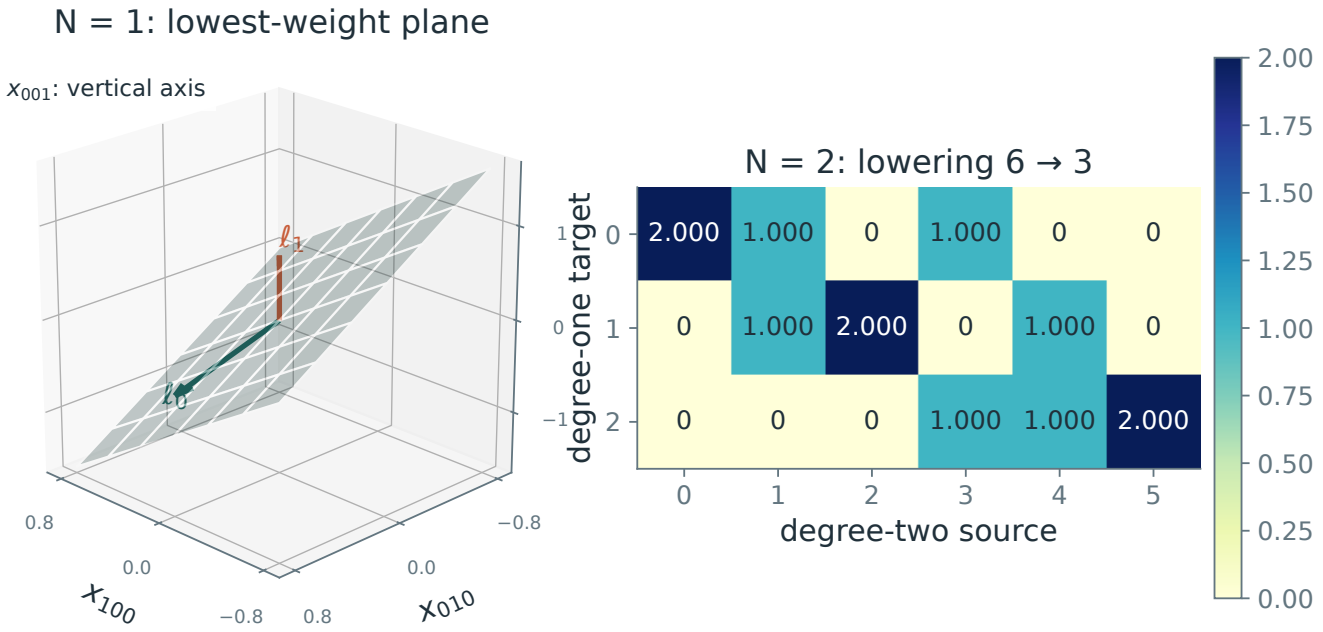
Work an example. At $N = 4$, the full space has $\binom{6}{2} = 15$ basis states. The lowering map targets degree three, whose full dimension is ten. Its full row rank therefore leaves a five-dimensional kernel. A subsequent recoupling matrix needs 5×5 entries, even though its defining projector was constructed in fifteen dimensions. At $N = 0$, both spaces have dimension one, so the reduction also respects the initial degree.

Carry forward. Compression comes from an operator kernel, with its dimension proved before any numerical atlas is chosen.

Source and scope. VII, Chapter 2, Proposition 2.1 and Theorem 2.2. The explicit full-row-rank proof used here is VIII, Theorem 3.1, specialized at $q = 1$.

Paper VII / 03 **LESSON 83**

See the lowest-weight plane



$$M_N = \ker(K_-^{[3]}|_{H_N}), \qquad N = 1: \quad x_{100} + x_{010} + x_{001} = 0$$

Read the figure. The three-dimensional view is coefficient space. Its axes are amplitudes of three occupation basis states, rather than spatial coordinates of particles. The shaded plane is the exact lowering kernel for three half-shapes at one excitation. Two arrows show an orthonormal atlas inside that plane. The right panel advances one degree and shows the rectangular lowering matrix. The next kernel is again selected by an equation, not by the apparent proximity of points in a picture.

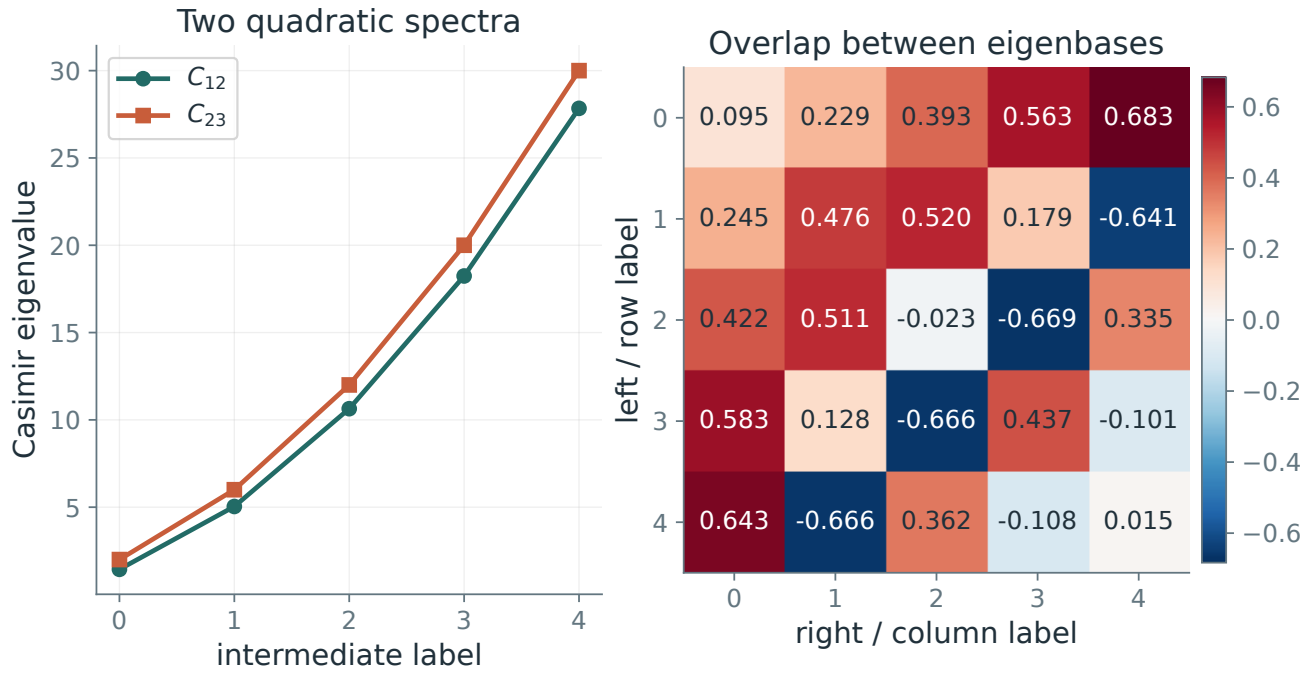
Work an example. At degree one, $(1, 1, -2)/\sqrt{6}$ lies in the plane because its coefficients sum to zero. The vector $(1, -1, 0)/\sqrt{2}$ also lies there, and their inner product vanishes. At degree two, the displayed 3×6 lowering map has a three-dimensional nullspace. The generated frame satisfies its lowering equation to floating-point roundoff. This residual checks this frame; the rank argument proves the general dimension.

Carry forward. A basis is a choice inside the kernel; the kernel is the mathematical object being represented.

Source and scope. VII, Chapter 2, *Fixed excitation and the lowest-weight projector*, lines 259–343; Chapter 5, the one-excitation construction. Newly computed plane and matrix.

Paper VII / 04 **LESSON 84**

Two observables select two atlases



$$\lambda_j^{ab} = (\kappa_a + \kappa_b + j)(\kappa_a + \kappa_b + j - 1), \qquad \mathcal{R} = L^{\mathsf{T}} R$$

Read the figure. The left curves are the spectra of two intermediate Casimirs. Their labels record how two neighboring shape factors are coupled. The right panel is the overlap of their complete eigenbases in the same lowest-weight space. A spectrum gives the addresses of an atlas, while the overlap tells how coordinates move between atlases. Eigenvalues alone do not determine that movement. The signed entries retain the phase convention of the selected real eigenvectors.

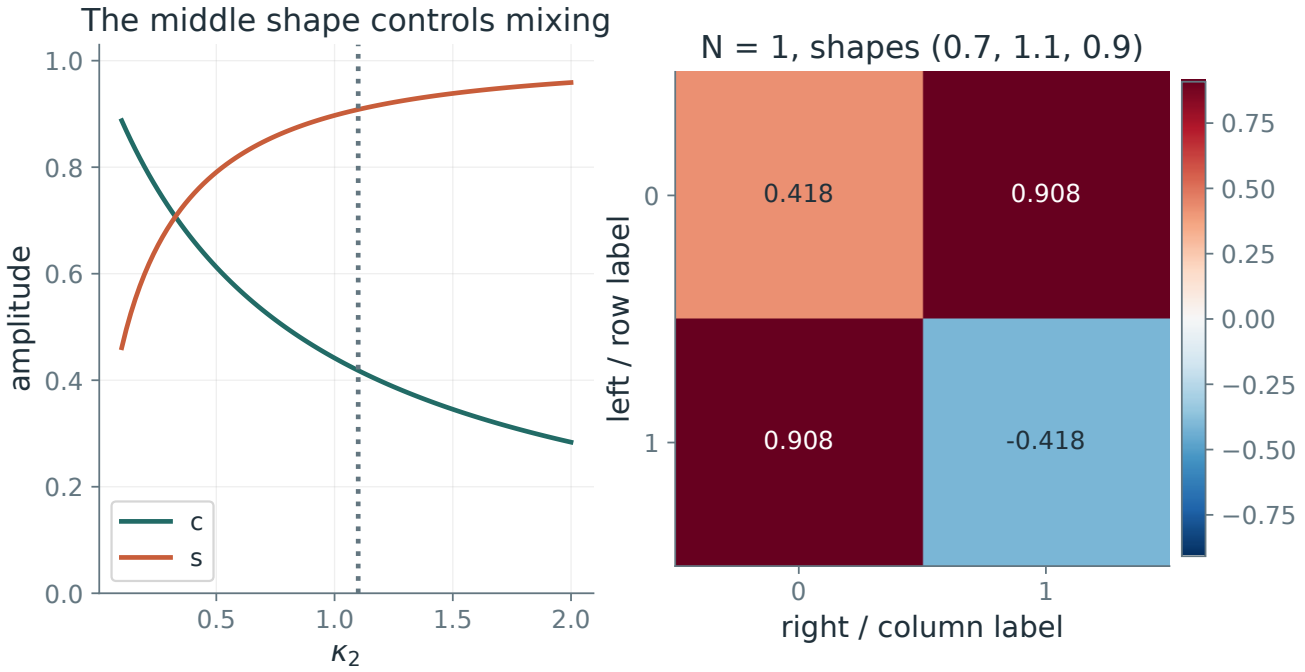
Work an example. Use shapes $(0.7, 1.1, 0.9)$ and $N = 4$. The left pair begins at $1.8(0.8) = 1.44$, and the right pair begins at $2(1) = 2$. Both spectra contain five entries because the multiplicity dimension is five. The program restricts each Casimir, orders its eigenvalues, and computes the displayed overlap. It separately compares those eigenvalues with the formula and checks orthogonality. These are complementary numerical checks of the chosen example.

Carry forward. The shared space supports reconstruction; the different intermediate observables support different coordinate descriptions.

Source and scope. VII, Chapter 3, Proposition 3.1; Chapter 4, Definition 4.1 and Theorem 4.2. Pair-spectrum identification is a classical representation-theoretic input.

Paper VII / 05 **LESSON 85**

The middle shape controls a beam splitter



$$\mathcal{R}_1 = \begin{pmatrix} c & s \\ s & -c \end{pmatrix}, \qquad c^2 = \frac{\kappa_1\kappa_3}{(\kappa_1+\kappa_2)(\kappa_2+\kappa_3)}, \quad s^2 = 1 - c^2$$

Read the figure. Hold the outer shapes fixed and move along the middle-shape axis. The first curve is the retained-channel amplitude, and the second is the transferred-channel amplitude in the declared real gauge. Their squares always sum to one. The right panel freezes the curve at one shape triple and displays the full signed transform. Its negative entry is needed for orthogonality. Reading the same numbers as unsigned probabilities would erase the operation that makes exact synthesis possible.

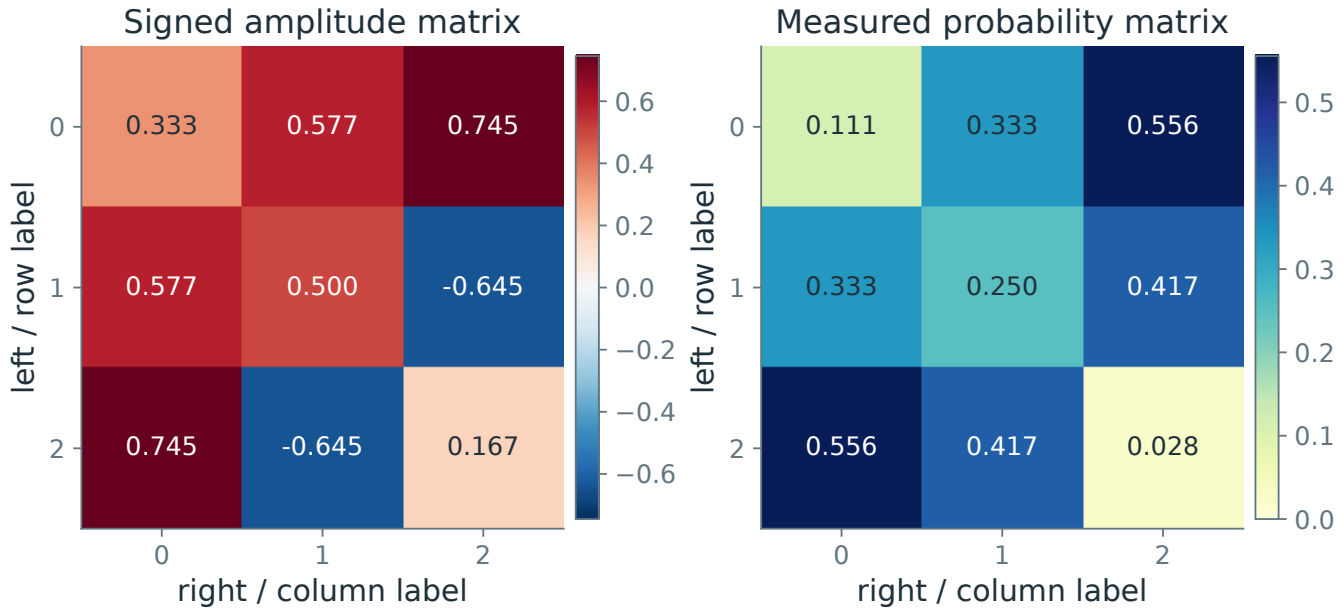
Work an example. For $(\kappa_1, \kappa_2, \kappa_3) = (0.7, 1.1, 0.9)$, the denominator is $1.8 \cdot 2 = 3.6$. Hence $c^2 = 0.175$ and $s^2 = 0.825$, giving $c \approx 0.41833$ and $s \approx 0.90830$. The independent Casimir construction reproduces this matrix. Applying the overlap and then its transpose recovers every two-channel amplitude vector. Squaring entries instead produces a measured channel with a different role.

Carry forward. The exact low-degree formula links a continuous shape choice to a finite reversible coordinate transform.

Source and scope. VII, Chapter 5, *One excitation as a shape beam splitter*, source lines 452–510. Exact formula checked against the newly computed pair-Casimir overlap.

Paper VII / 06 **LESSON 86**

An exact three-channel transform



$$\mathcal{R}_2 = \begin{pmatrix} 1/3 & 1/\sqrt{3} & \sqrt{5}/3 \\ 1/\sqrt{3} & 1/2 & -\sqrt{15}/6 \\ \sqrt{5}/3 & -\sqrt{15}/6 & 1/6 \end{pmatrix}, \qquad P_{jm} = |\mathcal{R}_2(j,m)|^2$$

Read the figure. Read the left matrix as amplitudes and the right matrix as probabilities after measurement. The two negative amplitudes participate in cancellations, while the probability matrix contains only non-negative entries. Rows and columns of the amplitude matrix are orthonormal. Rows and columns of the probability matrix sum to one. Both panels describe the same exact half-shape example, but they support different operations. The displayed decimals are visual labels for the exact radicals in the central formula.

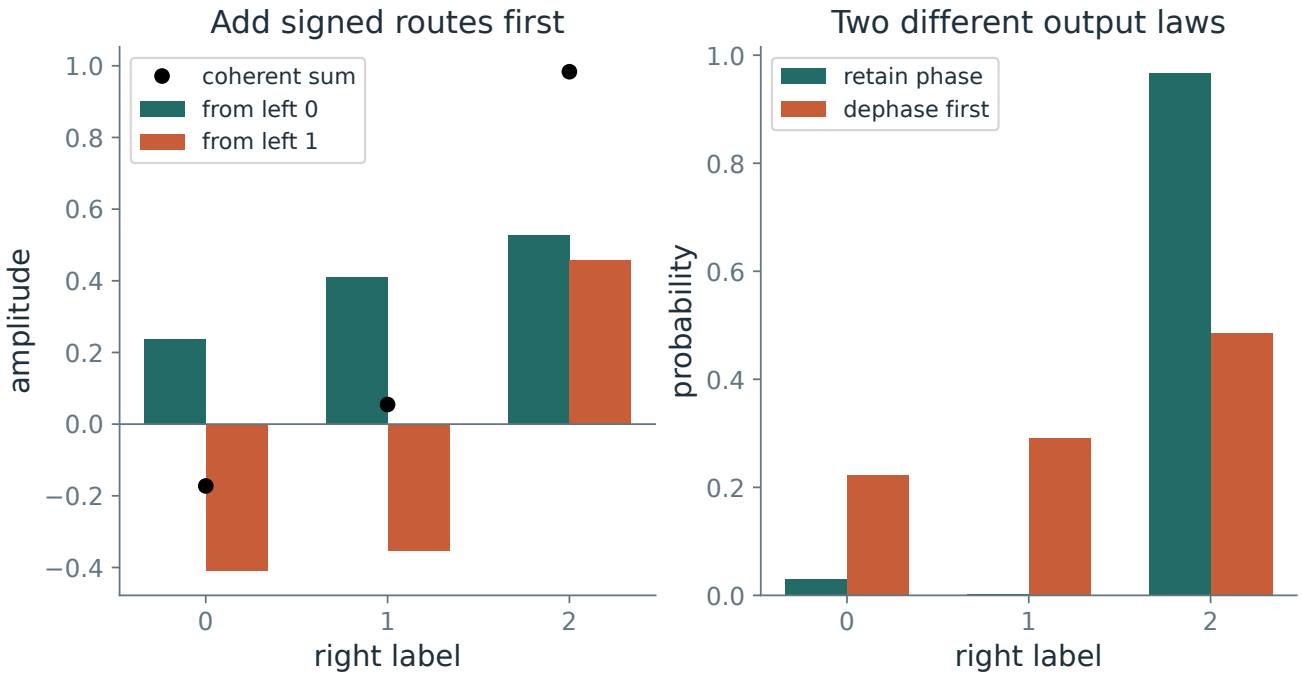
Work an example. The first amplitude row has squared norm $1/9 + 1/3 + 5/9 = 1$. Its probability row is therefore $(1/9, 1/3, 5/9)$. For the first two amplitude rows, positive and negative products cancel, giving inner product zero. The generated Casimir overlap agrees with the complete radical matrix. Checking just the first probability row would confirm one normalization, while the full orthogonality check confirms reversible reconstruction across all three channels.

Carry forward. Keep the exact signed matrix available even when the application eventually requests only measured probabilities.

Source and scope. VII, Chapter 6, *An exact three-channel example*, source lines 512–559, equal shapes $1/2$ and $N = 2$.

Paper VII / 07 **LESSON 87**

Phase changes a measured output



$$b_m = \sum_j \mathcal{R}_{jm} a_j, \qquad |b_m|^2 \text{ and } \sum_j |\mathcal{R}_{jm}|^2 |a_j|^2 \text{ need not agree}$$

Read the figure. The left bars are the two signed contributions reaching each target channel. The black points are their coherent sums. The right panel compares measuring those sums with dephasing the input first and then using the squared-amplitude channel. Both output laws are normalized, yet they differ because only one retains the cross terms between routes. This is a concrete reason to separate a reversible coordinate transform from a stochastic measurement kernel in the packet record.

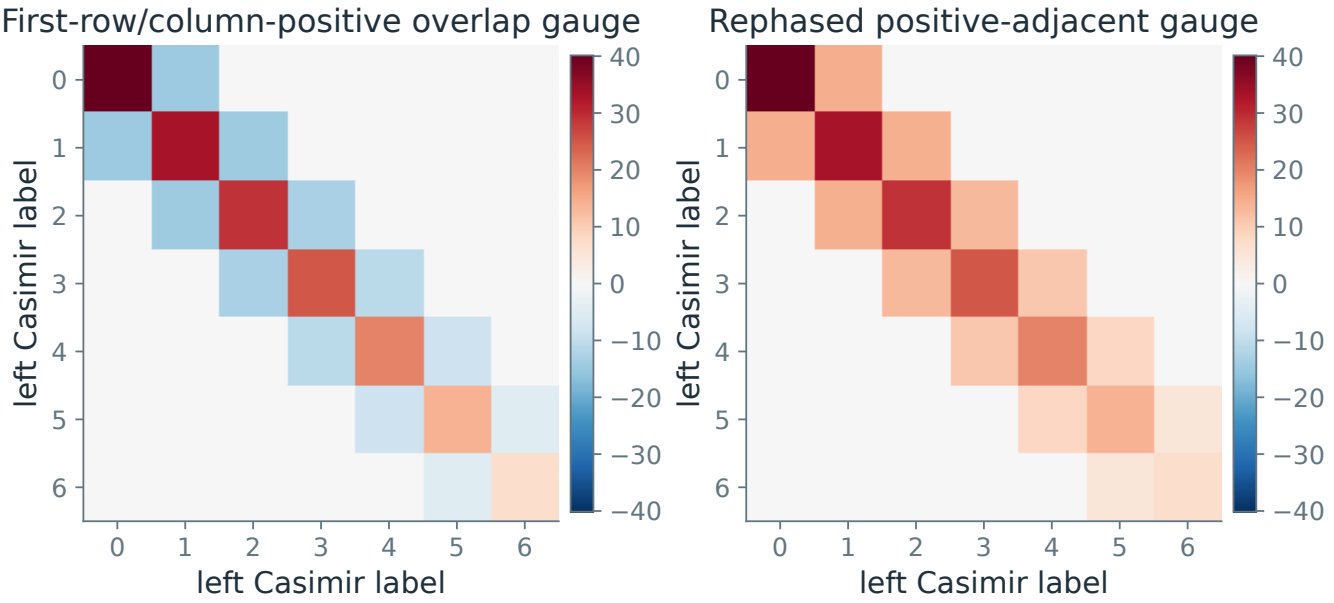
Work an example. Start in the exact three-channel example with $a = (1, -1, 0)/\sqrt{2}$. At target label zero, the coherent amplitude is $(1/3 - 1/\sqrt{3})/\sqrt{2}$. Its squared magnitude is approximately 0.02977. If the input is dephased first, the corresponding probability is $(1/9 + 1/3)/2 = 2/9$. The probability difference comes from interference. It is not a failure of normalization, and the signed matrix itself still has its exact inverse.

Carry forward. Amplitude addition occurs before squaring in coherent synthesis; a dephased channel has already lost those cross terms.

Source and scope. VII, Chapters 9 and 11, measurement interpretation and Boundary 11.1. Newly worked superposition using the exact Chapter 6 matrix.

Paper VII / 08 **LESSON 88**

A positive recurrence needs its own gauge



$$J = \mathcal{R}\ \mathrm{diag}(\lambda_m)\mathcal{R}^{\mathsf{T}}, \qquad S = \mathrm{diag}(s_j):\ (SJS)_{j,j+1} = |J_{j,j+1}|$$

Read the figure. Both panels represent the same opposing Casimir. In the left panel, the overlap convention makes its first row and column positive. The resulting adjacent Casimir entries can be negative. The right panel changes the signs of left-atlas vectors so every adjacent entry is positive. The zero pattern and eigenvalues remain unchanged. This distinction matters when a scalar three-term recurrence is presented as a Jacobi recurrence with positive neighboring coefficients.

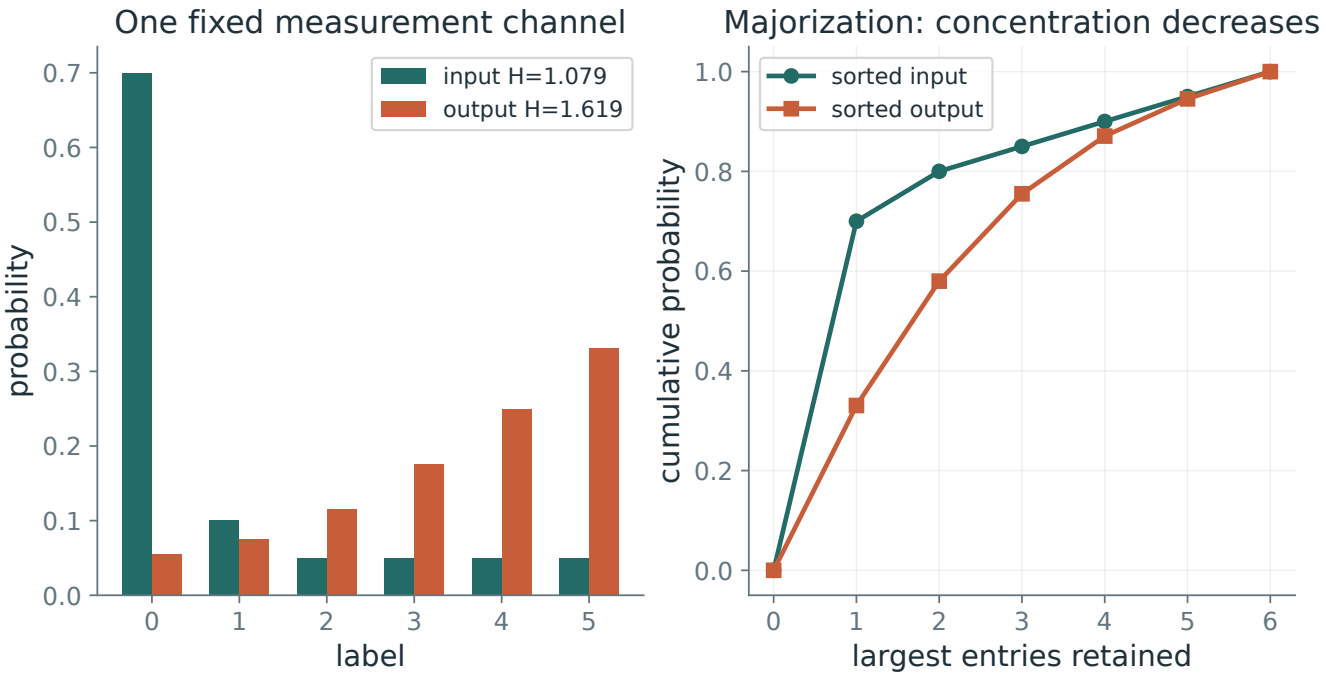
Work an example. For three half-shapes at $N = 1$, the printed overlap has $J_{01} = -\sqrt{3}/2$. It cannot simultaneously have the same signed coordinates and a positive adjacent coefficient. Set $s_0 = 1$, then choose $s_{j+1} = s_j\,\mathrm{sign}(J_{j,j+1})$. The rephased overlap is $S\mathcal{R}$, and its recurrence uses SJS. The displayed seven-channel example checks the tridiagonal zero pattern and the rephased matrix eigen-equation separately.

Carry forward. A gauge changes coordinates; state it explicitly before assigning signs to recurrence coefficients.

Source and scope. VII, Chapter 7, Theorem 7.1, read with the corrected row-sign convention. Irreducible tridiagonality is a classical Racah input; the displayed finite matrices are newly checked.

Paper VII / 09 **LESSON 89**

A fixed measured channel spreads a law



$$P_{jm} = |\mathcal{R}_{jm}|^2, \qquad H(pP) \geq H(p), \qquad H(p) = -\sum_j p_j \log p_j$$

Read the figure. The bars compare one input law with its output under one fixed squared-overlap matrix. The right panel sorts both distributions before adding their largest entries. The output curve lies below the input curve until both reach total mass one. That is the finite concentration order behind the entropy statement. The comparison is between input and output at a fixed kernel. It does not compare unrelated kernels or promise that entropy rises when a shape parameter is changed.

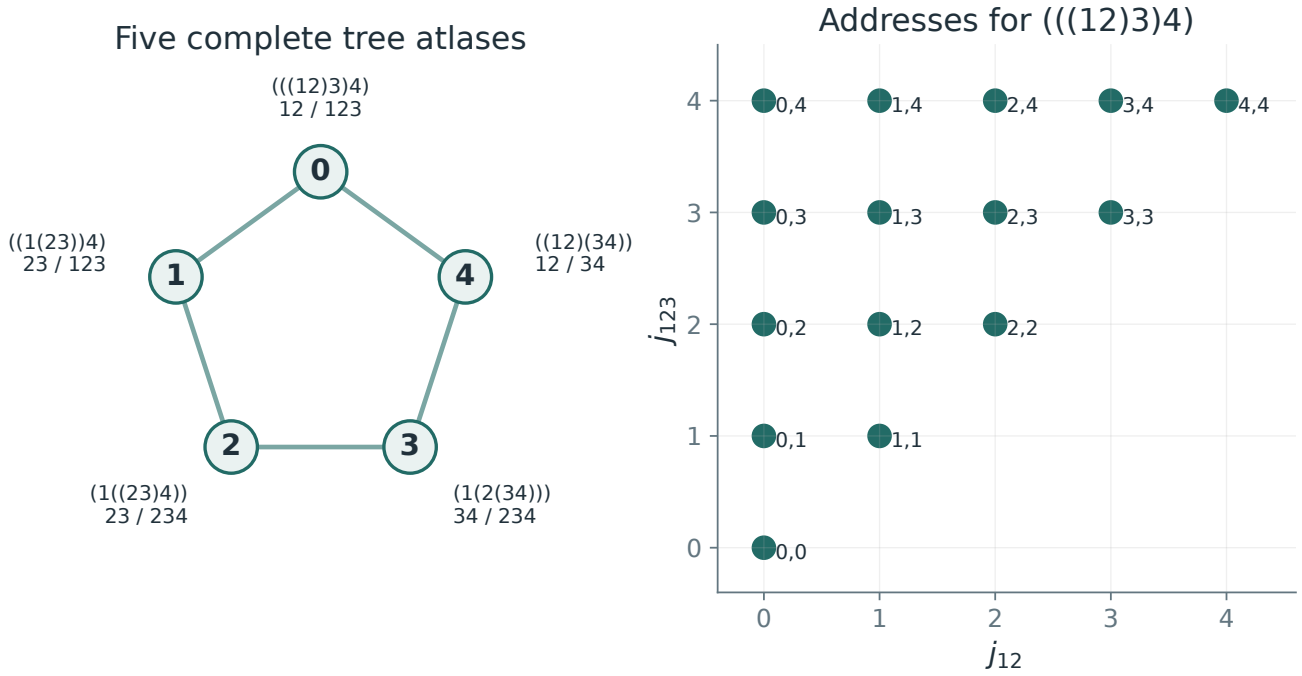
Work an example. At $N = 5$, use shapes $(0.7, 1.1, 0.9)$ and the input $(0.7, 0.1, 0.05, 0.05, 0.05, 0.05)$. The code computes its six-channel measured output directly. Each row and column of the kernel sums to one, and the output entropy exceeds the input entropy. Concavity applied with the column weights proves the inequality for every probability law. No random sampling is needed for that theorem.

Carry forward. Bistochasticity gives a universal fixed-channel entropy law, while particular mixing rates remain properties of the chosen kernel.

Source and scope. VII, Chapter 9, Theorem 9.1; Chapter 10, Theorem 10.1. Natural logarithms give entropy in nats; zero terms use $0 \log 0 = 0$.

Paper VII / 10 **LESSON 90**

Tree coordinates have joint addresses



$$\dim M_N^{(4)} = \binom{N+2}{2}, \qquad (((12)3)4): \quad 0 \le j_{12} \le j_{123} \le N$$

Read the figure. Each vertex on the left names a binary bracketing of four factors. The two block labels beneath it name the commuting intermediate Casimirs used by that tree. The right panel shows their joint integer addresses for the first tree. These addresses fill a triangular lattice rather than an unconstrained square. An atlas is complete only when all compatible addresses occur in the same final lowest-weight space. The graph explains which coordinate transforms connect neighboring bracketings.

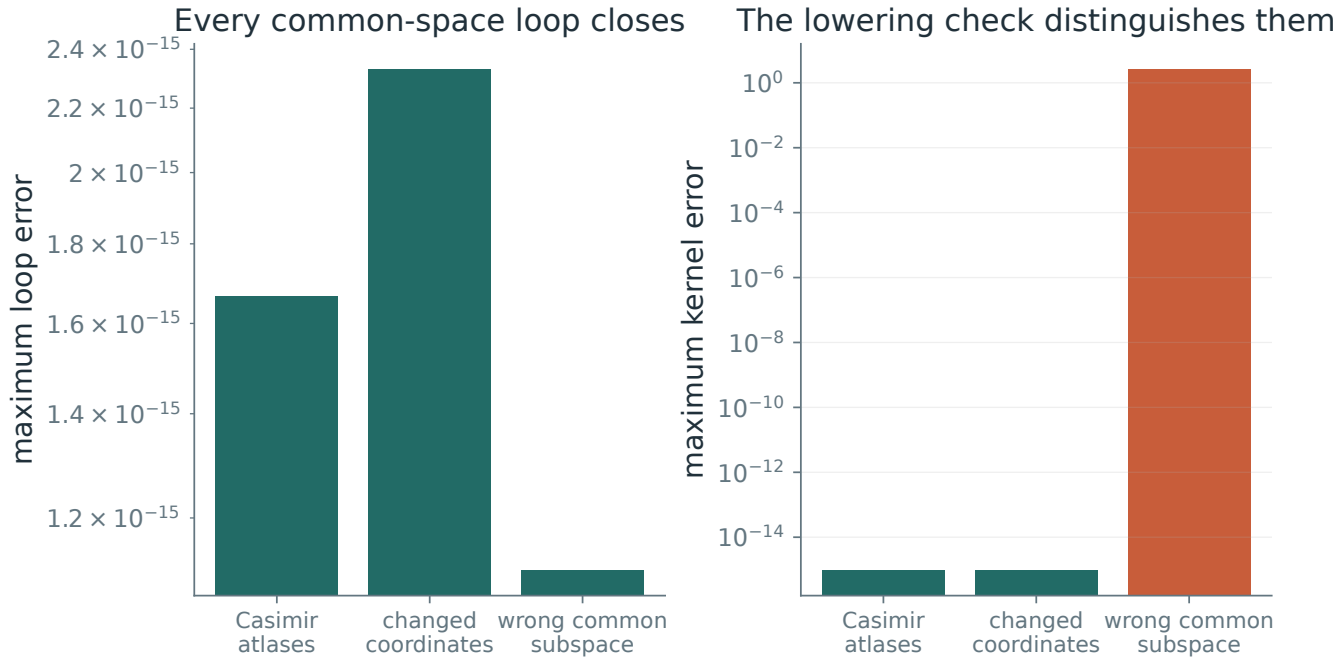
Work an example. At $N = 4$, there are fifteen addresses. With shapes $(0.55, 0.8, 1.05, 1.3)$, the address $(j_{12}, j_{123}) = (1, 3)$ gives intermediate shapes 2.35 and 5.4. Their ordinary Casimir eigenvalues are 3.1725 and 23.76. The numerical joint eigenbasis recovers the full triangular address set and diagonalizes both operators. Dimension, address completeness, and diagonalization each test a different part of this construction.

Carry forward. A joint spectrum supplies a finite address system for a tree, rather than just a list of separate eigenvalues.

Source and scope. VII, Chapter 12, *Five complete coupling trees* and Proposition 12.1; plotted addresses are extracted from newly computed joint eigenbases.

Paper VII / 11 **LESSON 91**

What a pentagon check actually certifies



$$U_{r,r+1} = B_r^{\mathsf{T}} B_{r+1}, \qquad U_{01}U_{12}U_{23}U_{34}U_{40} = I$$

Read the figure. The left bars show that three constructions all close their common-space overlap loop. The first uses the intended Casimir atlases. The second changes coordinates consistently at every vertex. The third uses a common subspace that fails the intended lowering equation. The right bars reveal that difference. The loop theorem remains exact, but its telescoping proof cannot independently distinguish the intended projector from every consistently shared alternative. The plotted log scale displays roundoff and a large failure together.

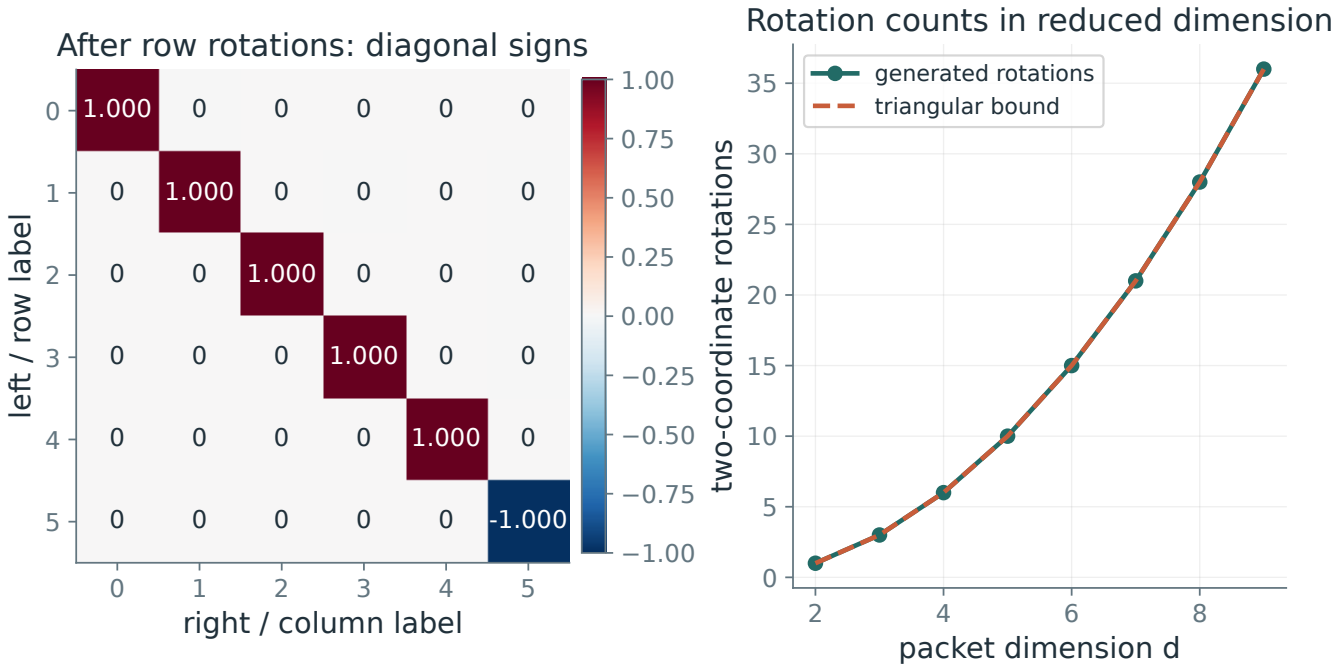
Work an example. For four factors at $N = 2$, the intended packet dimension is six inside a ten-dimensional excitation space. Five complete orthonormal bases of a common six-dimensional subspace always telescope. This remains true after consistent orthogonal coordinate changes. Choosing six ambient coordinate vectors also produces a closing loop, yet their lowering residual exceeds one. Thus the loop check passes while the separate kernel check rejects the wrong subspace.

Carry forward. Pair overlap closure with kernel, dimension, spectrum, and eigen-equation checks when validating an associator implementation.

Source and scope. VII, Chapter 13, Theorem 13.1, with its implementation-test interpretation corrected. Newly constructed deterministic negative control, coordinate-change seed 73011.

Paper VII / 12 **LESSON 92**

Compile in the reduced dimension



$$\mathcal{R} = G_1^{\mathsf{T}} \cdots G_L^{\mathsf{T}} D, \qquad L \le d(d-1)/2, \qquad D_{jj} \in \{-1, 1\}$$

Read the figure. The left panel is the signed diagonal remaining after row rotations eliminate entries below the overlap's diagonal. Reversing those rotations reconstructs the original transform. The right panel compares generated rotation counts with the triangular worst-case bound as the packet dimension grows. Each rotation touches only two coordinate slots. This compiler uses the multiplicity dimension, so its index set is smaller than the original tensor excitation space that defined the projector.

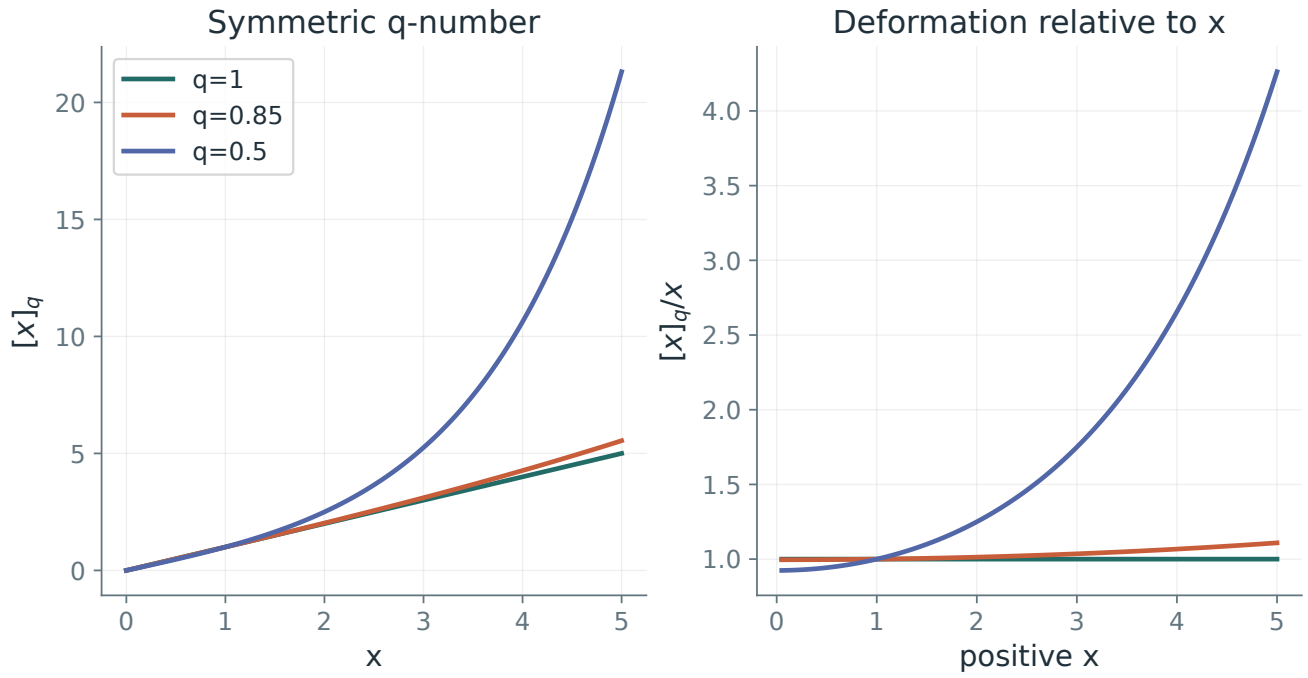
Work an example. At $N = 5$ for three factors, the packet dimension is $d = 6$ and the bound is fifteen rotations. The program records each Givens matrix, reduces the overlap to diagonal signs, and reconstructs it in reverse order. The residual is checked against the original overlap. This gives a finite algebraic circuit for the example. It does not assert nearest-neighbor hardware locality, minimum circuit depth, or an optimal gate count for a particular device.

Carry forward. Reduction defines the working coordinates; rotation factorization supplies an exact reconstruction procedure in those coordinates.

Source and scope. VII, Chapter 15, Theorem 15.1, *Givens packet compilation*; Chapter 16, *Projector-resolved Racah transform*. Direct finite linear algebra and new bounded checks.

Paper VIII / 01 **LESSON 93**

Replace a linear number by a q-number



$$[x]_q = \frac{q^x - q^{-x}}{q - q^{-1}} = \frac{\sinh(x\theta)}{\sinh\theta}, \qquad q = e^{-\theta}, \quad [x]_1 = x$$

Read the figure. The left panel shows the symmetric q-number at three positive deformation choices. The ordinary linear coordinate is recovered at one. The right panel divides by the positive input, making the relative deformation visible. This convention is symmetric under replacing q by its reciprocal, even though the ordered coproduct later retains directional q-weights. A scalar convention must be fixed before formulas from different quantum-algebra sources are compared.

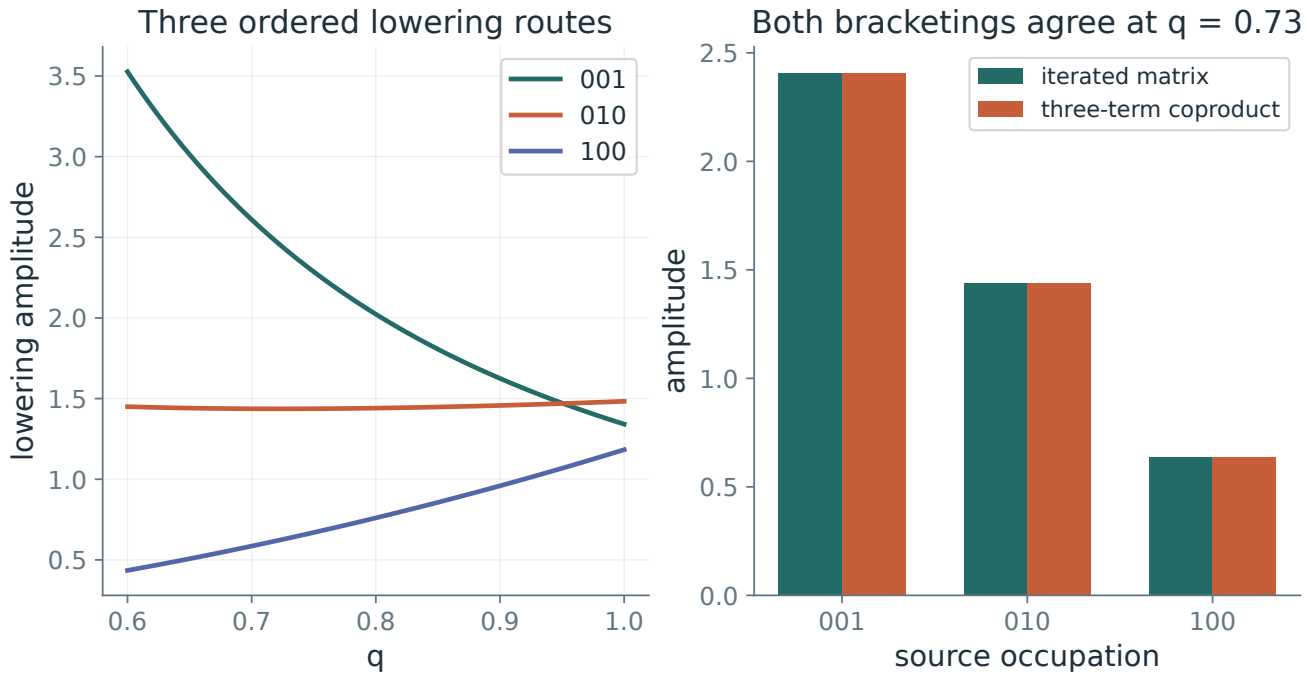
Work an example. At $q = 1/2$, $[2]_q = 2.5$ and $[3]_q = 5.25$, while $[1]_q = 1$. Thus the half-shape ladder's raising amplitude at degree one becomes $\sqrt{[2]_q[2]_q} = 2.5$. At $q = 1$, that coefficient is two. The stable implementation uses the hyperbolic expression near one and the exact continuous value at one. Positive x always gives a positive q-number in the declared real range.

Carry forward. Deforming the scalar ladder coefficients preserves the positive shape construction while changing its degree-dependent geometry.

Source and scope. VIII, Chapter 1, Definitions 1.1–1.2 and Proposition 1.3. Real range $0 < q \leq 1$; q=1 is defined by continuity.

Paper VIII / 02 **LESSON 94**

The coproduct routes lowering events



$$\Delta K_- = K_- \otimes q^{K_0} + q^{-K_0} \otimes K_-, \qquad (\Delta \otimes I)\Delta = (I \otimes \Delta)\Delta$$

Read the figure. Each curve on the left corresponds to lowering a different occupied factor at total degree one. The labels follow the declared composition order. Their unequal weights come from the q-powers assigned to factors before and after the lowering event. On the right, an explicit three-term expansion agrees with the iterated matrix implementation. This tests coassociative routing in a small transparent case. Coassociativity concerns bracketings of the same ordered factors, rather than freely permuting those factors.

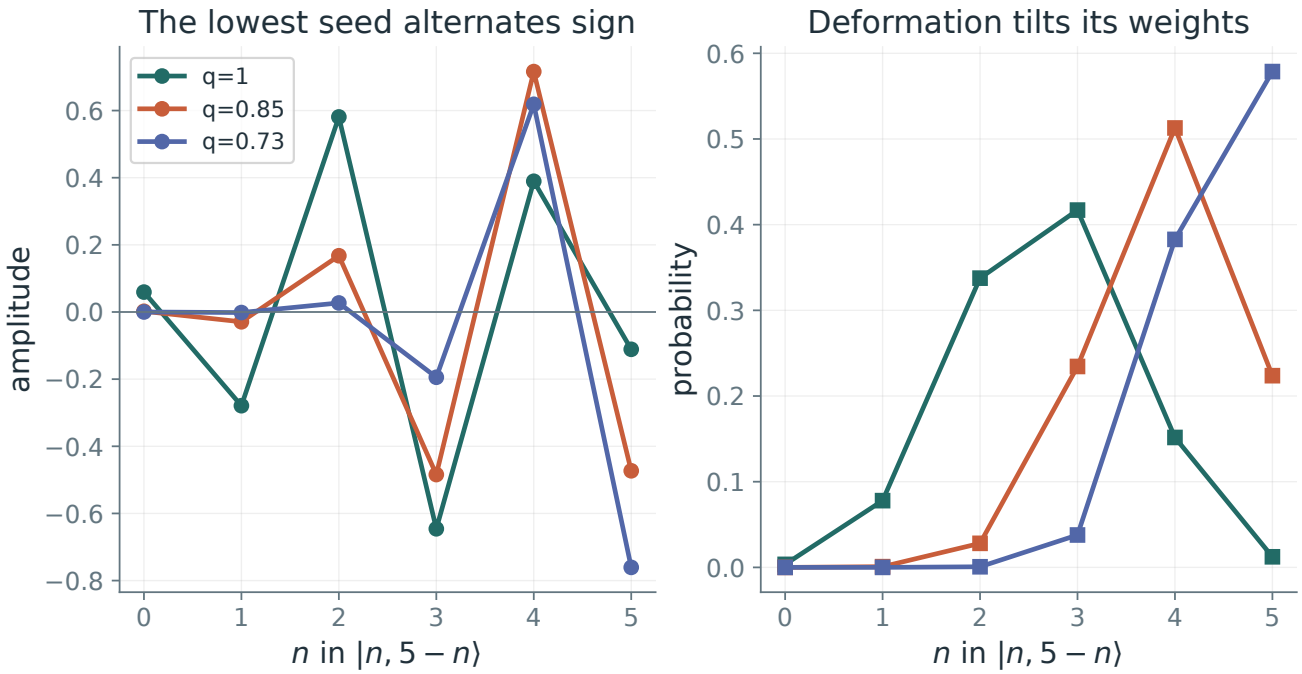
Work an example. At shapes $(0.7, 1.1, 0.9)$ with $q = 0.73$, the $|001\rangle$ route has coefficient $q^{-(0.7+1.1)}\sqrt{[1.8]_q}$. The route from $|010\rangle$ has coefficient $q^{-0.7+0.9}\sqrt{[2.2]_q}$, and the $|100\rangle$ route has $q^{1.1+0.9}\sqrt{[1.4]_q}$. Both coproduct bracketings produce exactly these three terms. Their values also match the freshly built lowering row.

Carry forward. Preserve the tensor order and q-number convention when constructing block observables or comparing formulas.

Source and scope. VIII, Chapter 2, Theorem 2.1, *Coassociative packet routing*, source lines 293–327. Direct expansion and new degree-one matrix comparison.

Paper VIII / 03 **LESSON 95**

A q-Hahn seed keeps signs and weights



$$\frac{c_{n+1}}{c_n} = -q^{-(N-1+\kappa_1+\kappa_2)}\sqrt{\frac{[N-n]_q[2\kappa_2+N-n-1]_q}{[n+1]_q[2\kappa_1+n]_q}}$$

Read the figure. The left panel retains the alternating phases of the one-dimensional lowest-weight seed. The right panel squares those same coefficients and exposes the q-dependent weight tilt. Both come from a solved lowering equation. Changing q alters the distribution without changing the six available occupation labels. The normalized vectors have total probability one. Identifying general coupled coefficients with scalar q-Hahn polynomials is an additional classical representation-theoretic input.

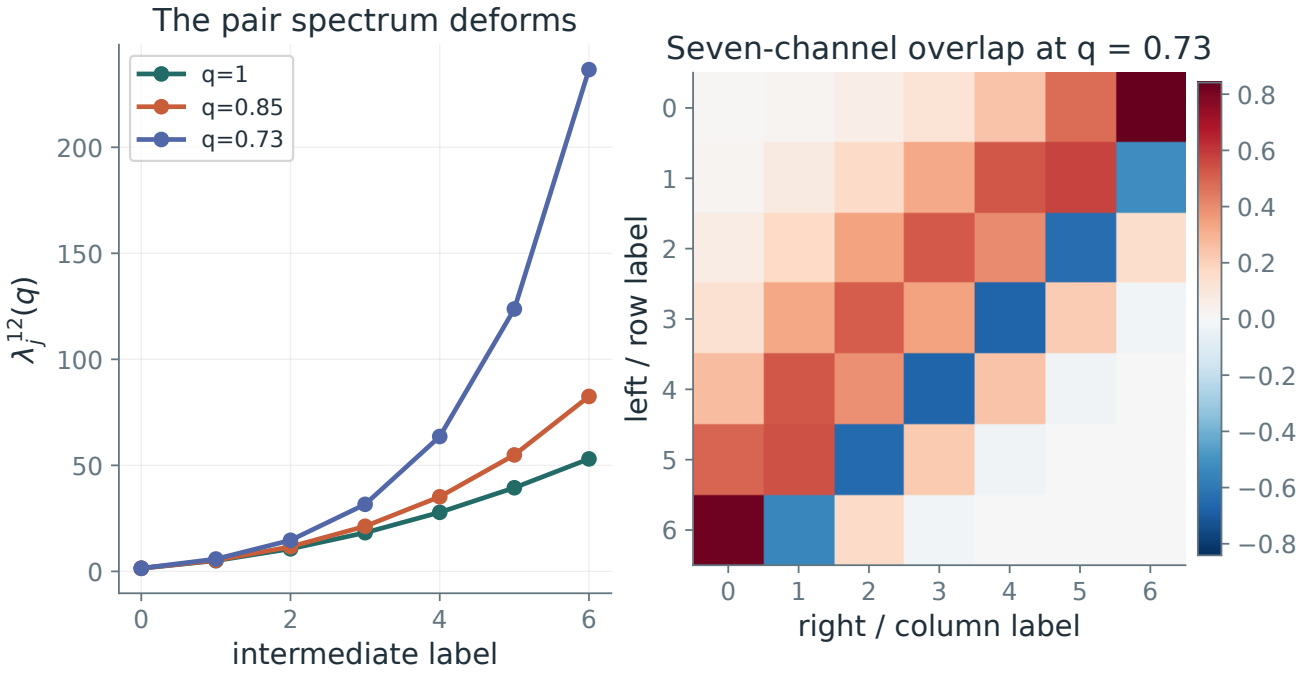
Work an example. Take $N = 5$ and shapes $(0.7, 1.1)$. Starting with $c_0 = 1$, apply the displayed ratio five times, then normalize. At $q = 0.73$, the resulting vector is annihilated by the two-factor lowering matrix. It also agrees up to its overall sign with a separately computed nullspace vector. The ratio derives the seed analytically; the two numerical checks confirm its implementation at this input. The plotted squared weights are not inferred from a fitted probability model.

Carry forward. The signed seed supports synthesis, and its square supports a weight description; neither representation should replace the other silently.

Source and scope. VIII, Chapter 4, Theorem 4.1, *Explicit q-Hahn lowest packet*, source lines 407–474. New recurrence and nullspace comparisons at three q choices.

Paper VIII / 04 **LESSON 96**

Deform both a spectrum and an atlas



$$\lambda_j^{ab}(q) = [\kappa_a + \kappa_b + j]_q[\kappa_a + \kappa_b + j - 1]_q, \qquad \mathcal{R}_N(q) = L_N(q)^{\mathsf{T}} R_N(q)$$

Read the figure. The left curves follow one pair's intermediate eigenvalues as q changes. On the right, the complete overlap at one q value records how the left and right Casimir atlases mix. The packet dimension remains seven throughout this example. The changed colors describe coordinate geometry on a fixed-size object, rather than a change in the number of channels. Spectral agreement and overlap orthogonality are checked separately.

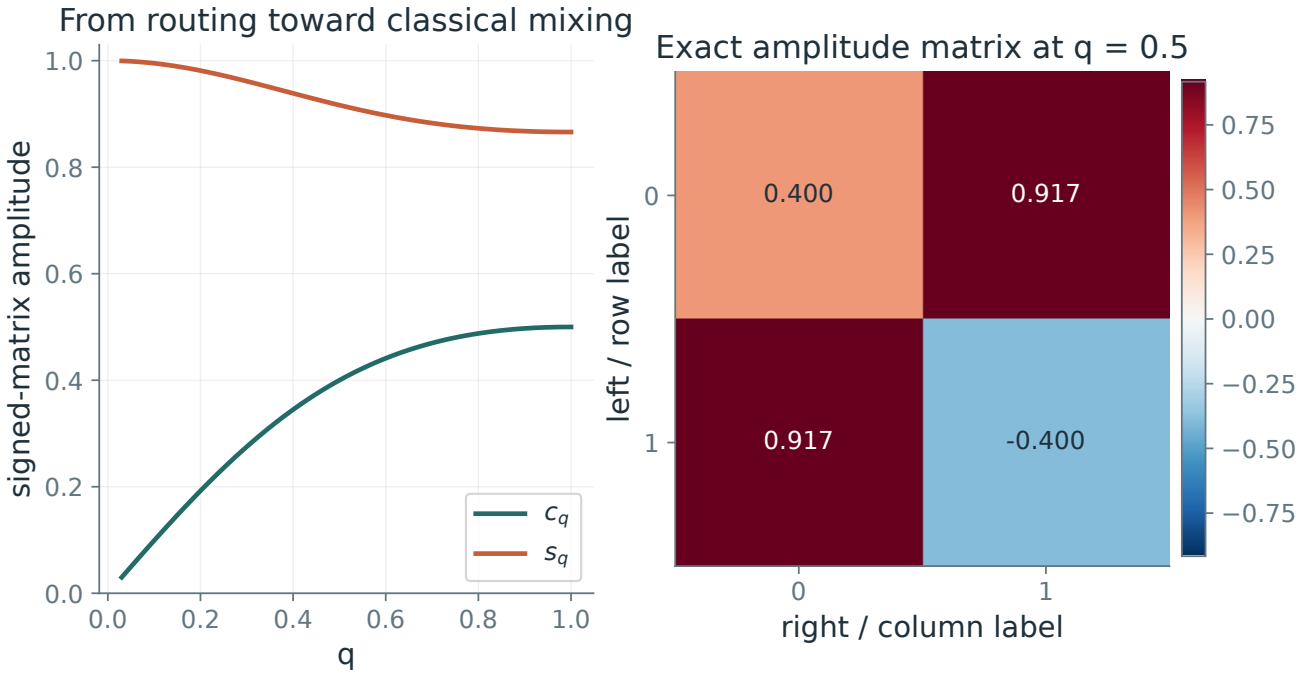
Work an example. For $N = 6$, shapes $(0.7, 1.1, 0.9)$ and $q = 0.73$, build the full degree-six lowering map, compute its seven-dimensional kernel, and restrict both pair Casimirs. Their ordered eigenvectors define the overlap. The code compares the left eigenvalues with the displayed q-number formula and checks $\mathcal{R}^{\mathsf{T}}\mathcal{R} = I$. This is a finite matrix construction. The exact scalar q-Racah parameter and weight map is kept as a separate comparison obligation.

Carry forward. The matrix module is usable before an explicit scalar normalization formula is supplied, provided its evidence is described at that level.

Source and scope. VIII, Chapter 5, Theorem 5.1 and *Two intermediate q-Casimir atlases*. Classical pair-spectrum/q-Racah inputs; the plotted matrix is newly computed.

Paper VIII / 05 **LESSON 97**

An exact q-coordinate reaches a swap



$$\mathcal{R}_q = \begin{pmatrix} c_q & s_q \\ s_q & -c_q \end{pmatrix}, \qquad c_q = \frac{q}{1+q^2}, \quad s_q = \frac{\sqrt{1+q^2+q^4}}{1+q^2}$$

Read the figure. Read the amplitude curves from small q toward one. The diagonal amplitude rises from zero to one half, while the transferred amplitude approaches $\sqrt{3}/2$. The right panel displays the complete signed transform at the midpoint q value. Its limit at zero is a routing swap. This is an exact limit for this normalized two-channel model. The unnormalized q-number operators themselves do not have a uniform finite limit at zero.

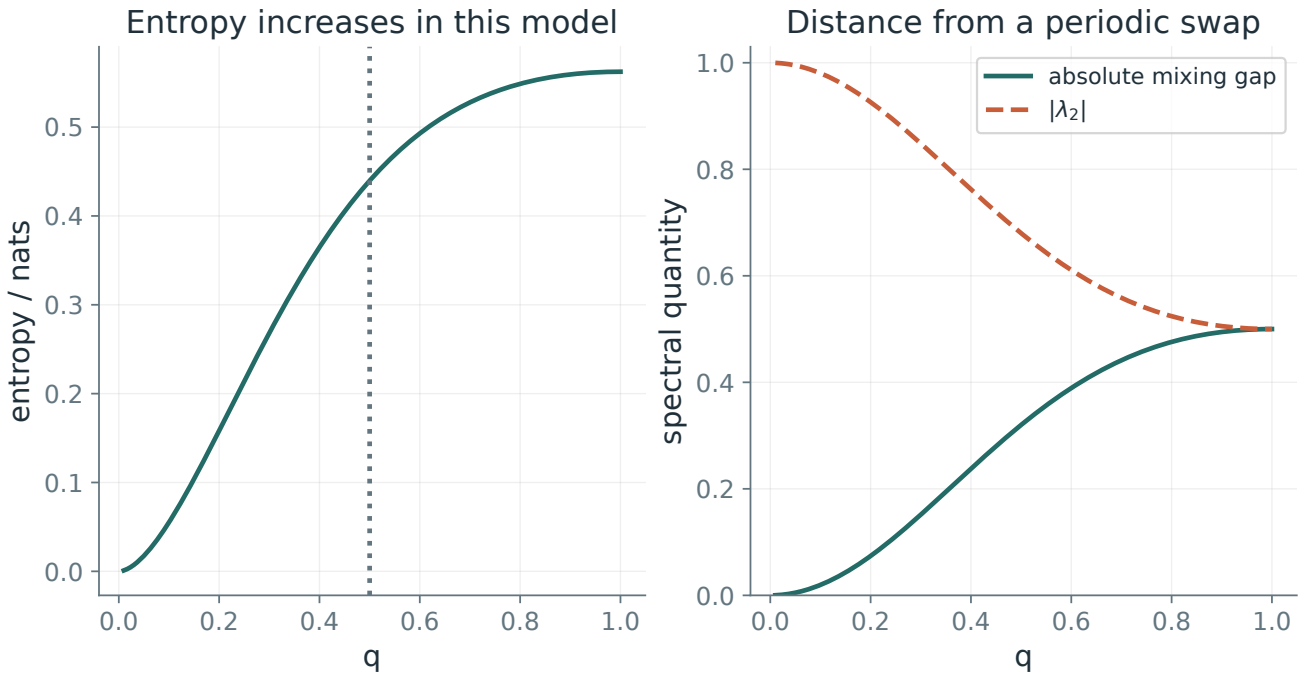
Work an example. At $q = 0.5$, $c_q = 0.4$ and $s_q = \sqrt{0.84} \approx 0.916515$. Their squares sum to one, and the lower-right sign makes the two columns orthogonal. The numerical pair-Casimir construction matches this matrix at four q values. At $q = 1$, it recovers the classical half-shape beam splitter. At a very small positive q, the closed expression approaches the swap matrix directly, avoiding an ill-conditioned large-degree operator construction.

Carry forward. State the normalization and tested model before promoting a visually sparse q endpoint into a general routing theorem.

Source and scope. VIII, Chapter 6, Theorem 6.1, *Closed two-channel q-Racah transform*, half-shapes and $N = 1$. Routing concerns this closed formula only.

Paper VIII / 06 **LESSON 98**

Two-channel mixing has a monotone gap



$$p(q) = \frac{q^2}{(1+q^2)^2}, \qquad \lambda_2 = 2p - 1, \qquad \mathrm{gap}_{\mathrm{abs}} = 1 - |\lambda_2| = 2p$$

Read the figure. The left curve is the binary entropy of one measured row. The right panel separates the absolute mixing gap from the magnitude of the other eigenvalue. Small q is close to a periodic swap, whose second eigenvalue has magnitude one. Moving toward q=1 reduces that magnitude and increases the absolute gap. The word absolute matters: a negative second eigenvalue still produces an oscillating mode, and its distance from one alone is not the mixing rate used here.

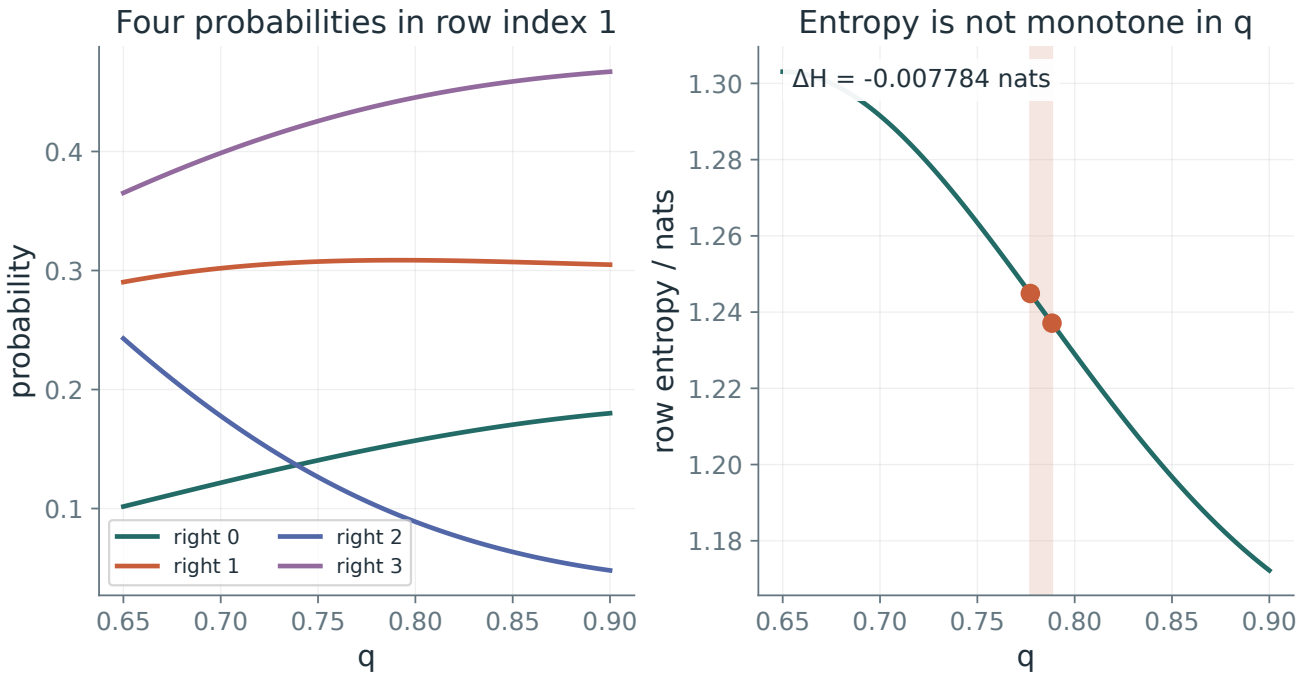
Work an example. At $q = 0.5$, the measured matrix has rows $(0.16, 0.84)$ and $(0.84, 0.16)$. Its second eigenvalue is -0.68, its absolute gap is 0.32, and its row entropy is approximately 0.43967 nats. The smaller row probability increases only to $1/4$ over the declared interval. Binary entropy is increasing there, which proves the model's q-monotonicity without relying on the plotted grid.

Carry forward. The exact one-excitation model has a monotone deformation law; higher multiplicity requires its own analysis.

Source and scope. VIII, Chapter 7, Theorem 7.2, *Monotone one-excitation mixing*. Equal half-shapes, $N = 1$, $0 < q \leq 1$, absolute spectral gap.

Paper VIII / 07 **LESSON 99**

Higher-level row entropy can decrease



$$H_1(q) = -\sum_m |\mathcal{R}_3(q)_{1m}|^2 \log |\mathcal{R}_3(q)_{1m}|^2, \qquad H_1(q_1) - H_1(q_0) \approx -0.007784$$

Read the figure. The left panel follows the four probabilities of the second measured row, using zero-based row index one. The right panel computes their entropy and highlights two nearby q values. The curve decreases between them. Every individual kernel remains bistochastic, so each still obeys the input-to-output entropy inequality. The decrease compares two different kernels' row laws. It therefore refutes universal entropy monotonicity in q without contradicting the fixed-channel theorem.

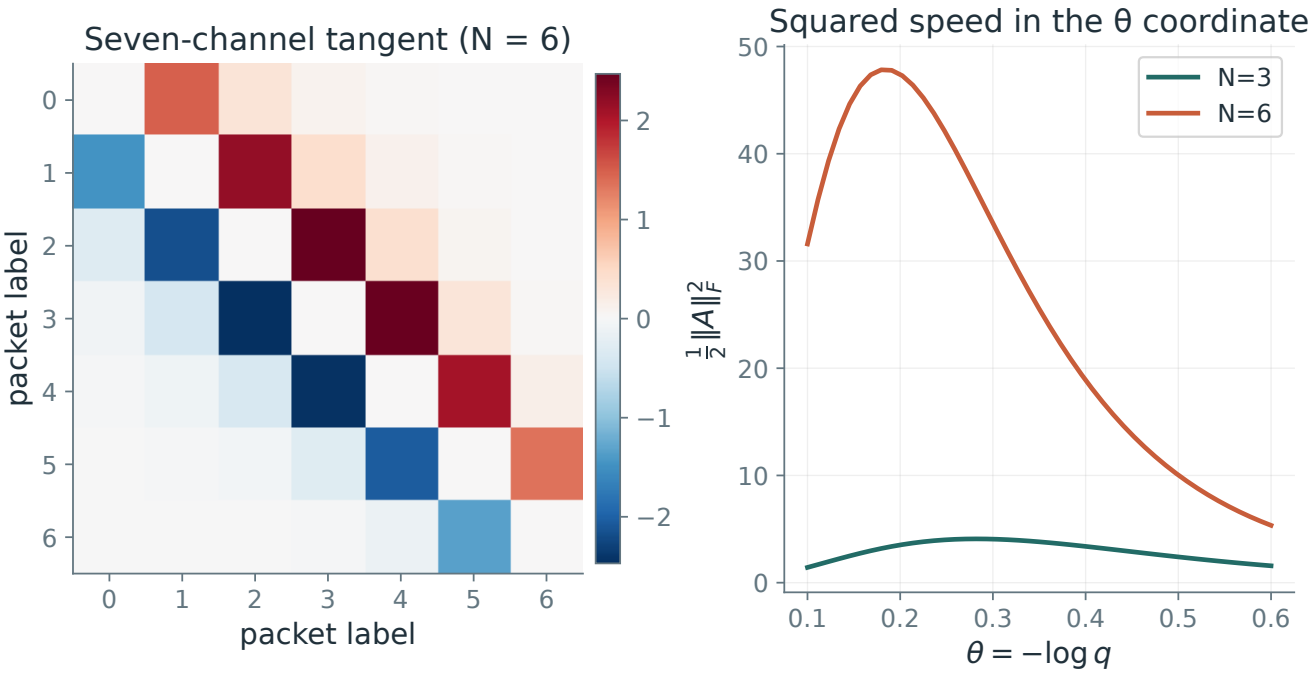
Work an example. For $N = 3$ and three half-shapes, take $q_0 = 307/395 \approx 0.777215$ and $q_1 = 1557/1975 \approx 0.788354$. The entropies are approximately 1.244882 and 1.237098 nats. Their difference is negative by about 0.007784. The guide recomputes both matrices in double precision from the q-coproduct. A separate full-space implementation records a decreasing interval from $q = 0.78$ to 0.80. These are bounded numerical witnesses, not interval proof certificates or a classification of all deformation behavior.

Carry forward. A negative control defines the theorem boundary as precisely as a successful example defines its mechanism.

Source and scope. VIII, Chapter 7, Boundary 7.3, *No universal entropy monotonicity in q*. New endpoint witness in vii_viii_audit.json and separately saved independent full-space evidence.

Paper VIII / 08 **LESSON 100**

Differentiate a complete coordinate transform



$$A(\theta) = \mathcal{R}(\theta)^{\mathsf{T}}\partial_\theta \mathcal{R}(\theta), \qquad A^{\mathsf{T}} = -A, \quad \partial_\theta \mathcal{R} = \mathcal{R}A$$

Read the figure. The left matrix is the skew tangent generator for the seven-channel transform at $N = 6$. Opposite entries have opposite signs, and diagonal entries vanish. The right curves measure squared speed for two excitation levels in the same $\theta = -\log q$ coordinate. This quantity concerns sensitivity of the complete atlas overlap, rather than entropy of its measured rows. Its size depends on parameterization, while constant orthogonal changes of atlas preserve the Frobenius coefficient.

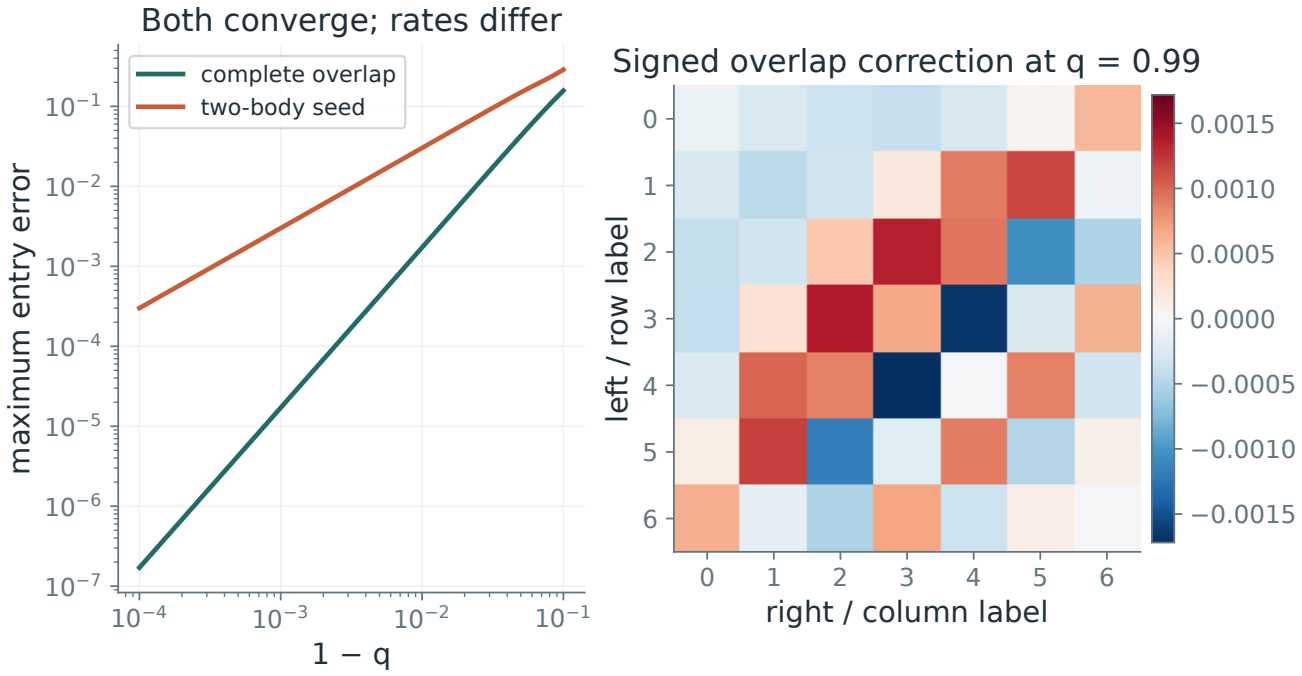
Work an example. At $\theta = 0.35$, compute the overlaps at $\theta \pm 2 \times 10^{-5}$, align their real sign conventions, and form a central difference. Before projecting to a skew matrix, the code checks the raw generator's symmetric residual. It also checks the tangent equation afterward. This avoids treating an explicitly antisymmetrized output as independent evidence of skewness. Analytically, differentiating $\mathcal{R}^{\mathsf{T}}\mathcal{R} = I$ proves the exact skew law in a smooth gauge.

Carry forward. A deformation tangent is meaningful only after the atlas conventions are made continuous along the chosen coordinate.

Source and scope. VIII, Chapter 8, Theorem 8.1, *Skew deformation generator*. New finite-difference diagnostics; derivative step and raw residual recorded in the audit.

Paper VIII / 09 **LESSON 101**

Approach the classical atlas carefully



$$[x]_q = x + O((\log q)^2), \qquad \mathcal{R}_N(q) \longrightarrow \mathcal{R}_N(1) \quad \text{in a matched sign gauge}$$

Read the figure. Both curves on the left tend toward zero error as q approaches one. One compares complete recoupling overlaps, and the other compares normalized two-body seed vectors. Their rates differ here. The right panel retains the signed overlap correction at $q = 0.99$. The q-number's even hyperbolic expansion does not by itself establish the same rate for every seed or coordinate choice, because the coproduct also carries directional q-powers.

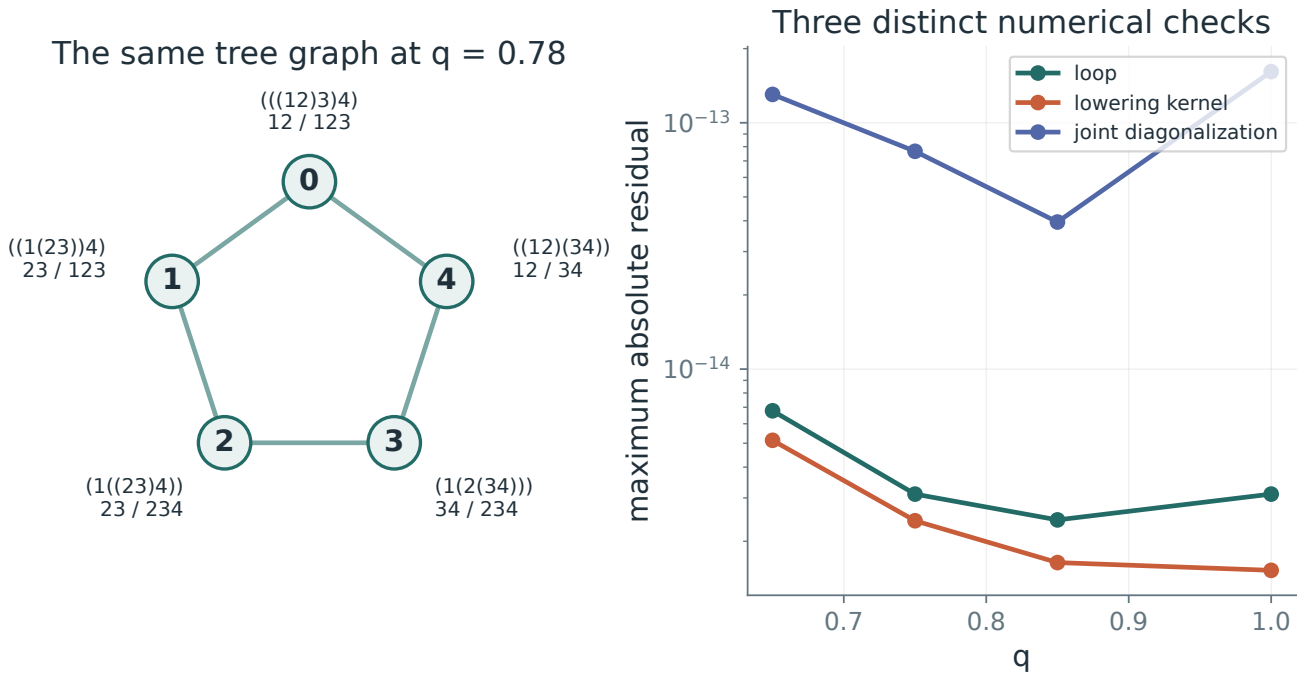
Work an example. For $N = 6$ and shapes $(0.7, 1.1, 0.9)$, compute the q=1 overlap as the reference. Align row and column signs before taking entry differences at nearby q. The seed comparison uses the two-body degree-five vector for shapes $(0.7, 1.1)$. Both finite comparisons converge over the displayed range. They verify these numerical examples and conventions. The continuity argument is supplied by the finite matrix construction and its nondegenerate spectral data.

Carry forward. Match atlases before measuring a limit, and distinguish an operator coefficient expansion from an entire reconstructed object's convergence rate.

Source and scope. VIII, Chapter 9, *Classical and routing limits*, source lines 751–763. New q-grid comparisons at fixed positive shapes; no universal rate asserted.

Paper VIII / 10 **LESSON 102**

q-trees need more than loop closure



$$U_{r,r+1}(q) = B_r(q)^{\mathsf{T}} B_{r+1}(q), \qquad U_{01}U_{12}U_{23}U_{34}U_{40} = I \quad \text{(indices modulo 5)}$$

Read the figure. The five vertices still represent the same ordered planar bracketings after deformation. Each now uses q-Casimirs on contiguous blocks. The right panel plots three separate diagnostics: common-space loop closure, annihilation by total lowering, and joint diagonalization. Their residuals remain small in the displayed finite tests. They answer different questions. Combining them gives more information than calling the closing overlap loop alone a certificate of every label, phase, and projector convention.

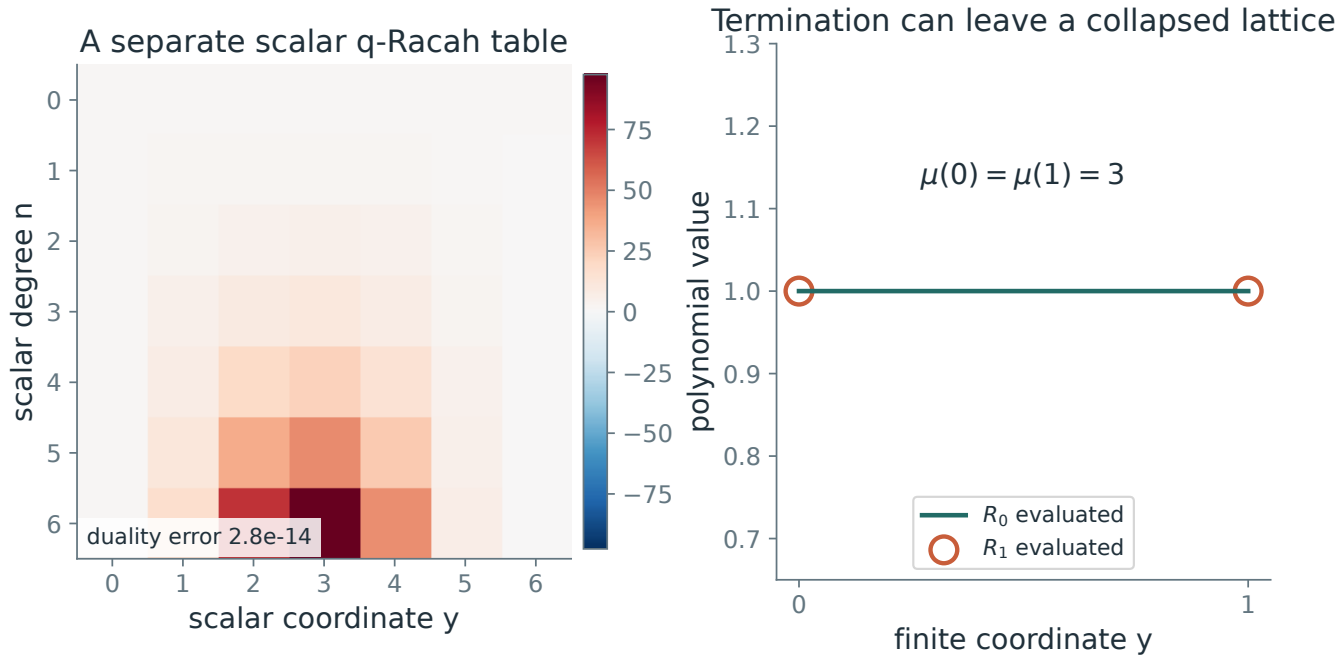
Work an example. At four factors and $N = 3$, the multiplicity dimension is ten. For q values 0.65, 0.75, 0.85, and one, the code constructs every joint atlas and composes its five overlaps. It separately tests commuting intermediate operators and the displayed kernel and diagonalization residuals. Consistent coordinate changes would still leave the loop equal to identity. A future stronger local-associator check would compare independently constructed q-Racah edge blocks with these global overlaps before composing them.

Carry forward. Keep structural operator checks alongside loop checks when the same data construction could make closure automatic.

Source and scope. VIII, Chapter 10, Theorem 10.1, *Finite q-pentagon certificate*, with corrected interpretation. Four-factor inputs and residuals recorded separately.

Paper VIII / 11 **LESSON 103**

A scalar table is a separate comparison



$$R_n(\mu_{\gamma,\delta}(y);\alpha,\beta,\gamma,\delta \mid q) = R_y(\mu_{\alpha,\beta}(n);\gamma,\delta,\alpha,\beta \mid q)$$
$$\mu_{u,v}(t) = q^{-t} + uvq^{t+1}$$

Read the figure. The left panel is generated from the terminating scalar q-hypergeometric expression, with independent scalar parameters. Exchanging degree and coordinate together with the parameter pairs gives the recorded duality agreement. This table has not been identified entry by entry with the shape-Casimir overlap. The right panel gives a finite-support counterexample: the two lattice points coincide, and two evaluated polynomial rows coincide. A denominator truncation condition alone therefore cannot guarantee a positive orthogonal family.

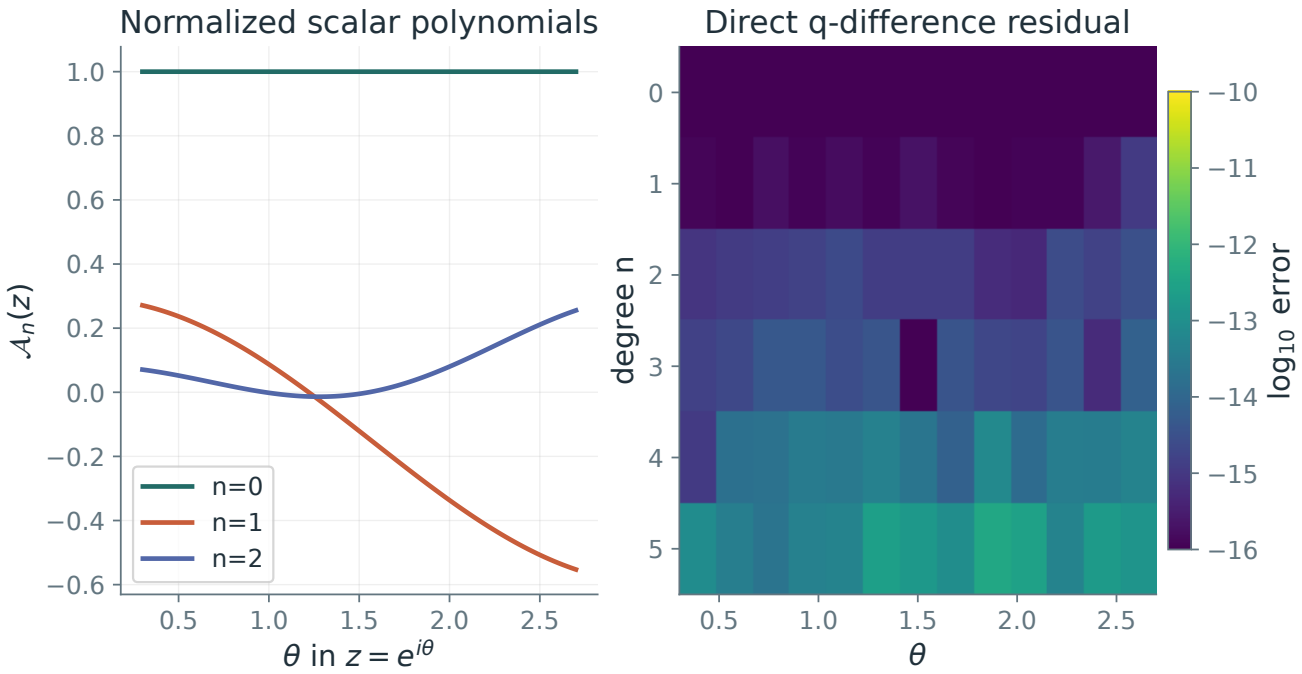
Work an example. Set $N = 1$, $q = 1/2$, $\alpha = \beta = 1/2$, $\gamma = 4$, and $\delta = 1$. Although $\gamma q = q^{-N}$, both lattice values are three. The finite formula gives $R_0 = 1$ and $R_1(\mu) = 6 - (5/3)\mu$, so both row vectors are $(1,1)$. Their inner product under positive weights is $w_0 + w_1 > 0$. This exact rational witness separates termination, nondegeneracy, and positivity. The complete shape-to-scalar map still needs base, parameters, weights, norms, and phases.

Carry forward. Scalar identities can be verified independently while a matrix-to-polynomial normalization comparison remains explicit unfinished work.

Source and scope. VIII, Chapter 13, Theorem 13.1; Chapter 19, first open direction. Scalar sums require $0 < q < 1$ and nonzero finite denominator factors; $q = 1$ is a separate limit. The collapsed-lattice witness uses exact rational arithmetic.

Paper VIII / 12 **LESSON 104**

Check a shifted Askey–Wilson operator



$$\mathcal{L}\mathcal{A}_n = (q^{-n} + abcdq^{n-1})\mathcal{A}_n, \qquad \mathcal{L} = D_q + (1 + abcd/q)I$$

Read the figure. The left curves are normalized terminating Askey–Wilson polynomials on the continuous unit-circle coordinate. The right panel substitutes six degrees into the q-difference equation at thirteen nonsingular points. The residual scale shows numerical agreement. The eigenvalue uses the shifted operator: D_q is the two-difference part, while the scalar identity term has been added. Omitting that shift would change the eigenvalue convention and make the comparison inconsistent.

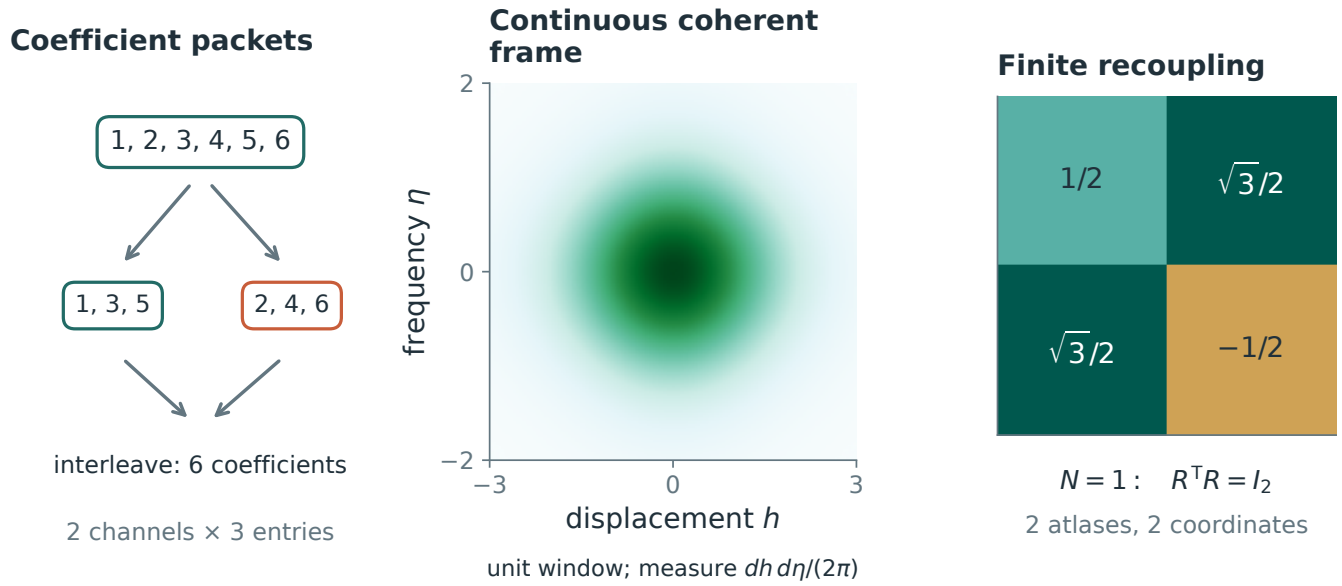
Work an example. Take $q = 0.7$ and $(a, b, c, d) = (0.2, 0.3, -0.25, 0.4)$. At degree two, the shifted eigenvalue is $q^{-2} + abcdq \approx 2.036616$. Evaluate the finite polynomial at z, qz, and z/q, then apply the declared operator coefficients away from their poles. The program compares this result with the eigenvalue times the unshifted polynomial value. This checks a classical scalar identity. It does not construct a continuous-series unitary packet transform or its spectral measure.

Carry forward. A continuous variable in a scalar polynomial is a bridge to further analysis, not an already completed continuous-series transform.

Source and scope. VIII, Chapter 14, Theorem 14.1, *Askey-Wilson eigenfunction law*. Scalar sums require $0 < q < 1$, nonzero finite denominator factors, and nonsingular operator points; $q = 1$ is a separate limit. Classical identity, newly evaluated on the declared grid.

SYNTHESIS / 01 **LESSON 105**

Three reconstruction contracts



$$\mathcal{S}_M \mathcal{A}_M = I, \qquad \mathcal{V}_g^* \mathcal{V}_g = I, \qquad R^{\mathsf{T}} R = I_{N+1}$$

Read the figure. The series uses three different coordinate spaces. Coefficient packets partition an index set. A normalized coherent window analyzes a function over a continuous phase plane. Casimir atlases analyze a finite multiplicity space. Each has an exact synthesis map, although its coefficients, measure, and admissible range differ. The middle panel plots coherent coefficient intensity $|A|^2$ for a log-Gamma window with shape $3/2$.

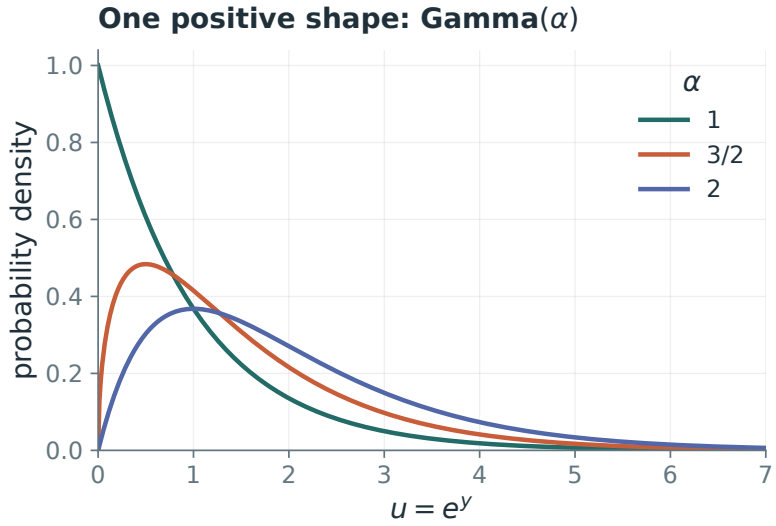
Work an example. Split $(1,2,3,4,5,6)$ into $(1,3,5)$ and $(2,4,6)$, then interleave to recover all six entries. At $N = 1$, the displayed recoupling matrix sends $(1,0)$ to $(1/2, \sqrt{3}/2)$; its transpose recovers the input. In the continuous case, the unit-window Moyal identity integrates squared coefficients with measure $dh\, d\eta\,/\,(2\pi)$ to recover the input norm.

Carry forward. Identify the coordinate space and its synthesis rule before transporting an identity.

Source and scope. I: exact polyphase reconstruction; VI: continuous tight frame; VII–VIII: finite reconstruction. Analytic frame identities come from the corrected shape core; the diagram does not identify these three transform ranges.

SYNTHESIS / 02 **LESSON 106**

Arithmetic parameters become a shape



Arithmetic → ladder

$a = 3/4,\ \beta = 1/2$
$\alpha = 1, \quad \kappa = 1/2$
positive kernel domain

$a = 2,\ \beta = 2$
$\alpha = 3/2, \quad \kappa = 3/4$
principal arithmetic parameters

$a = 3/2,\ \beta = 1$
$\alpha = 2, \quad \kappa = 1$
another admissible shape

$$\alpha = \frac{2a-1}{\beta} = 2\kappa, \qquad K_+|n\rangle = \sqrt{(n+1)(n+\alpha)}\,|n+1\rangle$$

Read the figure. The arithmetic scale exponent fixes a positive Gamma shape. The same shape enters the log-Gamma window and the ordinary positive ladder after setting $\kappa = \alpha/2$. This is a precise parameter dictionary across IV–VII. The curves show Gamma densities in the variable $u = e^y$, so their normalization uses du, whereas the window density uses dy.

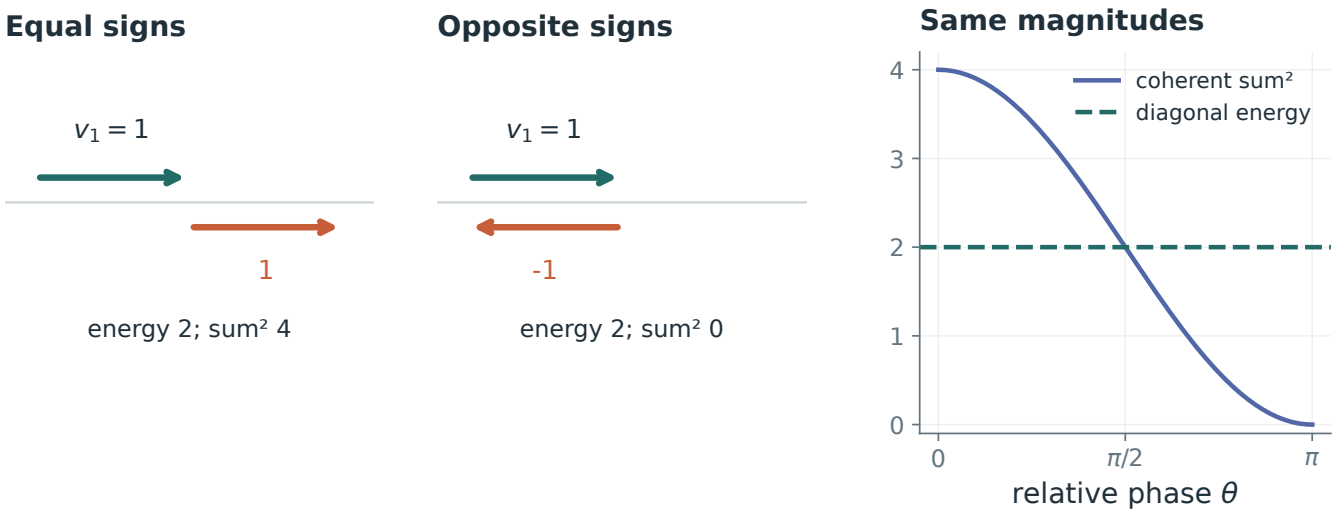
Work an example. Take $a = 2$ and $\beta = 2$. Then $\alpha = 3/2$, $\kappa = 3/4$, and the first two raising coefficients are $\sqrt{3/2}$ and $\sqrt{5}$. Taking $a = 3/4$, $\beta = 1/2$ instead gives $\alpha = 1$: the positive kernel is admissible because $a > 1/2$. The original absolutely convergent signed series requires $a > 1$, so that second choice belongs to the positive branch.

Carry forward. One shape links the formulas; each realization retains its own domain and measure.

Source and scope. IV–V: $\alpha = (2a-1)/\beta$; V–VI: normalized log-Gamma windows and ladder; VII: $\alpha = 2\kappa$. The bridge concerns the finite-span Lie-algebra formulas, not a new global-group integration theorem.

SYNTHESIS / 03 **LESSON 107**

A diagonal lift removes arithmetic signs



$$E = \sum_n |v_n|^2, \qquad |v_1 + v_2|^2 = 4\cos^2(\theta/2) \quad (v_1 = 1,\ v_2 = e^{i\theta})$$

Read the figure. Time averaging the arithmetic amplitude retains its diagonal packet energy. Its squared Möbius factor is positive, but the original signed sum uses information that this diagonal contraction removes. The illustration varies a relative phase while holding both component magnitudes fixed. The energy stays at two, while the coherent sum ranges from four to zero. A full Gram kernel may retain other phase relations; the loss here is the specified diagonal operation.

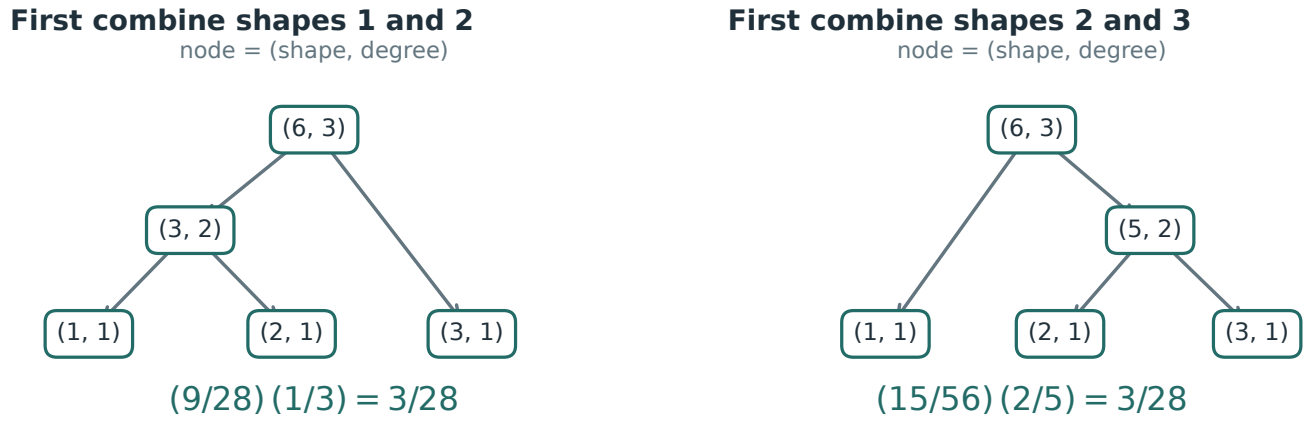
Work an example. For $(v_1, v_2) = (1, 1)$, the energy is two and the squared sum is four. For $(1, -1)$, the energy remains two and the squared sum is zero. Therefore identical positive diagonal data cannot determine the signed amplitude. This exact two-component witness explains why the positive Gamma, frame, and semigroup results do not supply the principal Möbius cancellation estimate.

Carry forward. Record which phases an averaging or measurement operation discards.

Source and scope. IV: exact time-average identity; I–VI: signed-coherence boundary; VII–VIII: measured versus coherent recoupling. This finite phase illustration is not an arithmetic counterexample or an estimate for Möbius sums.

SYNTHESIS / 04 **LESSON 108**

A binary refinement becomes a tree



$$\left(C^{\mathbf{s}}_{n,\mathbf{r}}\right)^2 = \frac{n!\prod_j (s_j)_{r_j}}{(\sum_j s_j)_n \prod_j r_j!}, \qquad \sum_j r_j = n$$

Read the figure. Shape addition produces normalized two-child coefficients. Multiplying them down a refinement tree cancels every intermediate factorial and Pochhammer factor. The remaining expression depends only on leaf shapes and degrees. Nodes show both numbers: a shape is not an excitation degree. This coefficient cancellation is the shape-level analogue of composing coordinate changes across recoupling trees; the two constructions use different coefficient systems.

Work an example. Choose shapes $(1,2,3)$, total degree three, and leaf degrees $(1,1,1)$. The left route has squared factors $9/28$ and $1/3$; the right route has $15/56$ and $2/5$. Both products are $3/28$, hence both positive amplitude coefficients equal $\sqrt{3/28}$. Enumerating all ten degree-three leaf compositions gives squared coefficients summing exactly to one. This verifies the displayed example independently of a tree drawing.

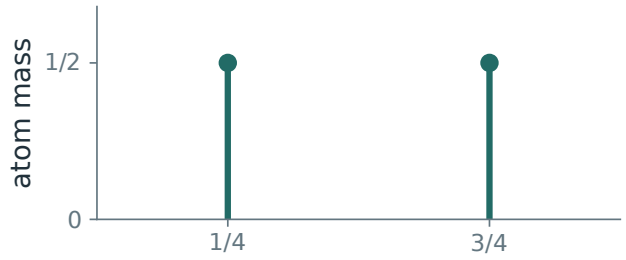
Carry forward. Cancel intermediate normalization factors before interpreting a refinement as tree independent.

Source and scope. VI: two-child refinement and Dirichlet-multinomial extension; VII–VIII: common-space tree atlases. Exact rational checks cover the stated three-child example; general cancellation is the generating-function identity in the corrected shape core.

SYNTHESIS / 05 **LESSON 109**

Positivity needs a specified measure

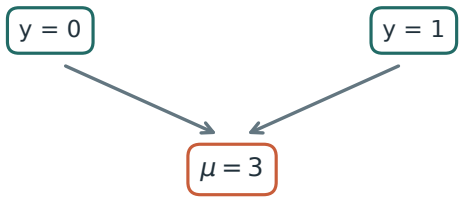
A specified positive measure



1	1/2
1/2	5/16

$\det G = 1/16 > 0$

A terminating scalar expression



$R_0 = (1, 1), \qquad R_1 = (1, 1)$

$$\sum_y w_y R_0(y) R_1(y) = 1$$

for any normalized positive weights

$$G_{ij} = \int x^{i+j}\, d\nu(x), \qquad \gamma q = q^{-N} \text{ alone does not imply positive orthogonality}$$

Read the figure. A positive measure makes its moment matrix a Gram matrix: every quadratic form is an integral of a squared polynomial. This mechanism underlies III's positive spectral branch. A terminating scalar q-Racah expression is a separate construction. Nonzero denominators make its values defined, but do not ensure a distinct lattice, positive weights, or nonzero orthogonal norms. The right panel shows two labels landing on the same lattice point.

Work an example. For the illustrative measure $\nu = \frac{1}{2}\delta_{1/4} + \frac{1}{2}\delta_{3/4}$, the first moment matrix has entries $1, 1/2, 5/16$ and determinant $1/16$. In VIII's exact degenerate example, take $N = 1$, $q = 1/2$, $\alpha = \beta = 1/2$, $\gamma = 4$, $\delta = 1$. Then $\mu(0) = \mu(1) = 3$ and $R_0 = R_1 = (1, 1)$. Their inner product equals one for any normalized positive weights.

Carry forward. Check the lattice, weight, norms, parameter dictionary, and phases separately.

Source and scope. III: positive moment measure; VIII: scalar formulas, corrected by C11–C12. The left measure is a two-atom illustration, not the infinite arithmetic measure. The scalar counterexample is evaluated exactly with nonzero finite denominators.

SYNTHESIS / 06 LESSON 110

Match the evidence to the question

Three indexed claims, three different questions

Source row	Concrete calculation / target	Ledger status
I · theorem.002	6 coefficients → 2 × 3 packets F(1/3) = 181/81 in both routes	Lean draft present (partial source link)
VIII · theorem.011	q = 1/2: c² = 4/25, s² = 21/25 c²+s² = 1; 5-point float check	queued
V · conjecture.021	For every ε > 0: |cₖ|²/Eₖ ≤ Cε k^ε no such uniform bound produced here	conjectural goal

Exact algebra decides the displayed identity. Floating residuals decide a bounded implementation check.

Kernel acceptance requires a proof term and its successful build. A claim record supplies neither.

$$c_{1/2}^2 = \frac{4}{25}, \qquad s_{1/2}^2 = \frac{21}{25}, \qquad c_{1/2}^2 + s_{1/2}^2 = 1$$

Read the figure. Three source rows ask different questions. The coefficient example compares finite reconstruction routes. The q-matrix example checks exact normalization and floating orthogonality at specified inputs. The coherence conjecture requires one constant for each positive exponent, uniformly over depth. A finite calculation preserves that distinction: it answers a bounded question without weakening the quantifiers of another claim.

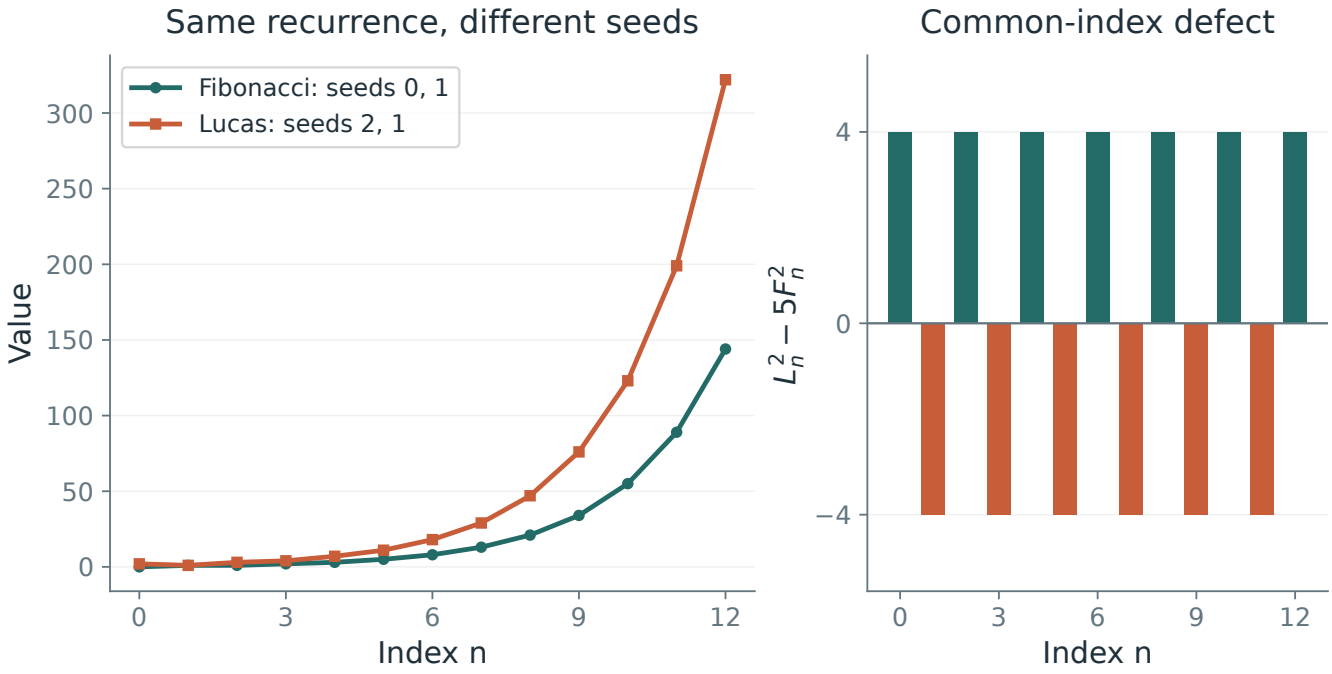
Work an example. For I.theorem.002, evaluate the six-term polynomial at $z = 1/3$ directly and through two residue packets: both give $181/81$. For VIII.theorem.011 at $q = 1/2$, the squared coefficients sum to one exactly; five floating-point inputs also have orthogonality residual below 10^{-14}. The ledger marks these rows partial and queued, respectively. V.conjecture.021 remains conjectural. No Lean kernel build is performed by these calculations.

Carry forward. Attach each result to its input, arithmetic domain, source row, and verification method.

Source and scope. Preserved claim index: I.theorem.002, VIII.theorem.011, V.conjecture.021, with full IDs in the computation JSON. Status labels come from the retrieved ledger snapshot; they are not a claim that all later formalization has been searched exhaustively.

SEQUENCES / 01 **LESSON 111**

Two seeds, one Fibonacci recurrence



$$F_{n+2} = F_{n+1} + F_n, \quad L_{n+2} = L_{n+1} + L_n, \quad L_n^2 - 5F_n^2 = 4(-1)^n$$

Read the figure. The two families share the same recurrence and have different seeds: $(F_0, F_1) = (0, 1)$ and $(L_0, L_1) = (2, 1)$. The right panel uses the same index in both families. Its alternating defect stays exactly four in magnitude.

Work an example. At $n = 7$, $F_7 = 13$ and $L_7 = 29$. Thus $29^2 - 5 \cdot 13^2 = 841 - 845 = -4$. Comparing terms at different indices would destroy this identity.

Carry forward. A recurrence operator and its initial state are separate parts of the sequence specification.

Source and scope. OEIS A000045 and A000032, indexed from zero. Exact recurrence and common-index identity; the plotted prefix ends at $n = 12$.

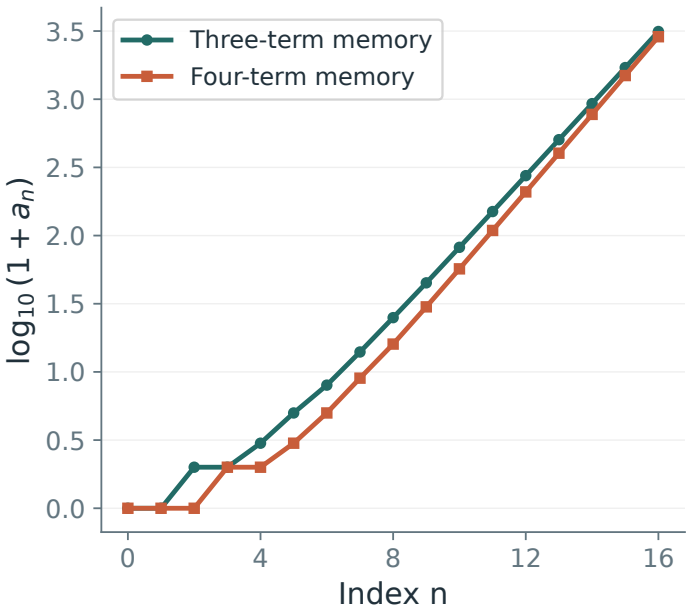
SEQUENCES / 02 **LESSON 112**

Longer recurrence memory

Fix the seeds before iterating

	n=0	1	2	3
Tribonacci	0	0	1	1
Tetranacci	0	0	0	1

Growth on a labeled log scale



$$T_n = T_{n-1} + T_{n-2} + T_{n-3}, \qquad Q_n = \sum_{j=1}^{4} Q_{n-j}$$

Read the figure. The seed table fixes the OEIS convention. Tribonacci starts $0, 0, 1$; tetranacci starts $0, 0, 0, 1$. The curves use $\log_{10}(1 + a_n)$ so that zeros and rapidly growing terms fit together. The transform changes the plotted scale, not the integer sequence.

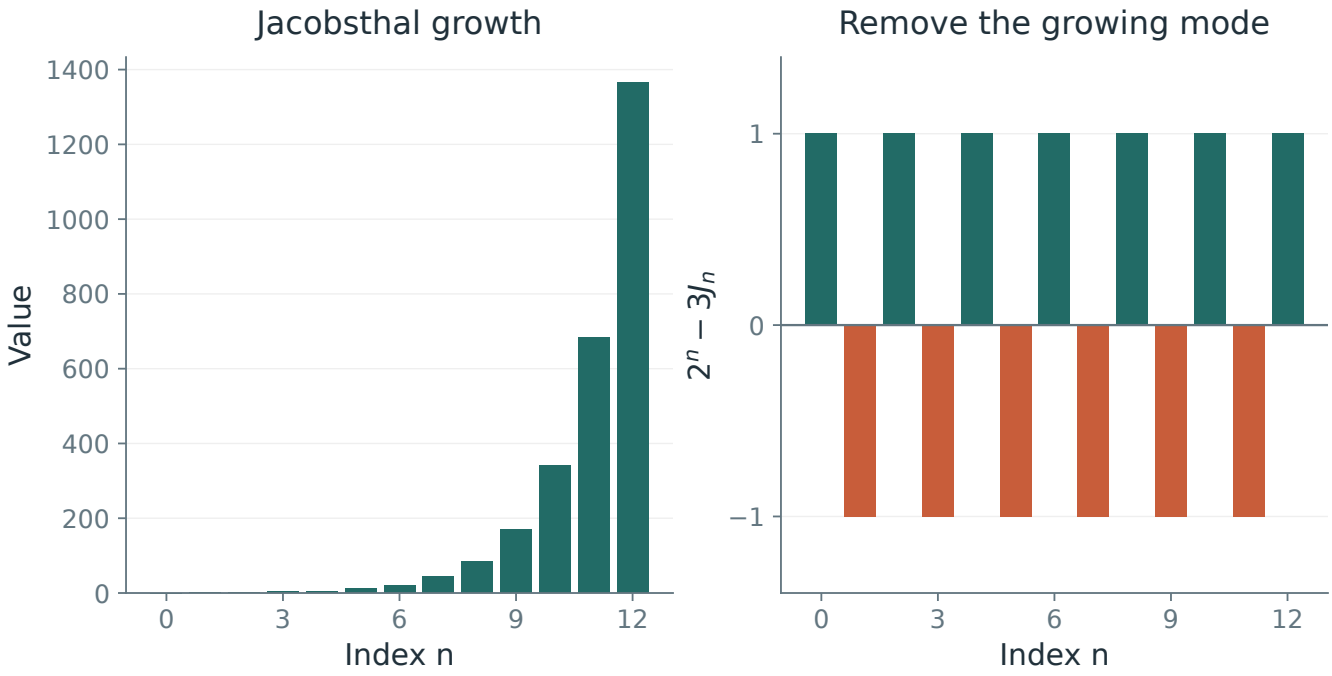
Work an example. Tribonacci gives $T_5 = 2 + 1 + 1 = 4$. Tetranacci gives $Q_7 = 4 + 2 + 1 + 1 = 8$. The recurrence first applies at $n = 3$ for T and $n = 4$ for Q.

Carry forward. These finite-memory recurrences have three and four feedback taps. The seed length must match the memory.

Source and scope. OEIS A000073 and A000078, both indexed from zero. Exact integer terms through $n = 16$; logarithmic ordinate explicitly labeled.

SEQUENCES / 03 **LESSON 113**

Jacobsthal separates two modes



$$J_0 = 0, \quad J_1 = 1, \quad J_{n+2} = J_{n+1} + 2J_n = \frac{2^{n+2} - (-1)^{n+2}}{3}$$

Read the figure. The rising bars are Jacobsthal numbers. The right panel removes their growing mode: $2^n - 3J_n = (-1)^n$. What remains is an alternating mode of constant magnitude. Both modes belong to the same second-order recurrence.

Work an example. At $n = 6$, $J_6 = 21$ and $2^6 - 3 \cdot 21 = 1$. At $n = 7$, $J_7 = 43$ and $2^7 - 3 \cdot 43 = -1$.

Carry forward. A recurrence can combine growth and oscillation. Splitting the modes explains the parity correction.

Source and scope. OEIS A001045, indexed from zero. Direct closed form and exact recurrence agree for $0 \le n \le 18$.

SEQUENCES / 04 **LESSON 114**

A Pell pair shares one unit

One unit, two integer coordinates

n	x(n)	y(n)	norm
0	1	0	1
1	2	1	1
2	7	4	1
3	26	15	1
4	97	56	1
5	362	209	1
6	1351	780	1
7	5042	2911	1

x(n+1) = 2x(n) + 3y(n)
y(n+1) = x(n) + 2y(n)

(7, 4) → (26, 15)

determinant = 1
norm x² − 3y² = 1

$$x_n + y_n\sqrt{3} = (2+\sqrt{3})^n, \qquad x_n^2 - 3y_n^2 = 1$$

Read the figure. The table keeps both coordinates at the same index. Multiplication by $2+\sqrt{3}$ advances the pair using the displayed integer update. Its determinant is one, and it preserves the quadratic norm. The zero-index pair is $(1,0)$.

Work an example. Starting from $(x_2, y_2) = (7,4)$ gives $(x_3, y_3) = (2\cdot 7 + 3\cdot 4, 7 + 2\cdot 4) = (26,15)$. The norm is $26^2 - 3\cdot 15^2 = 1$.

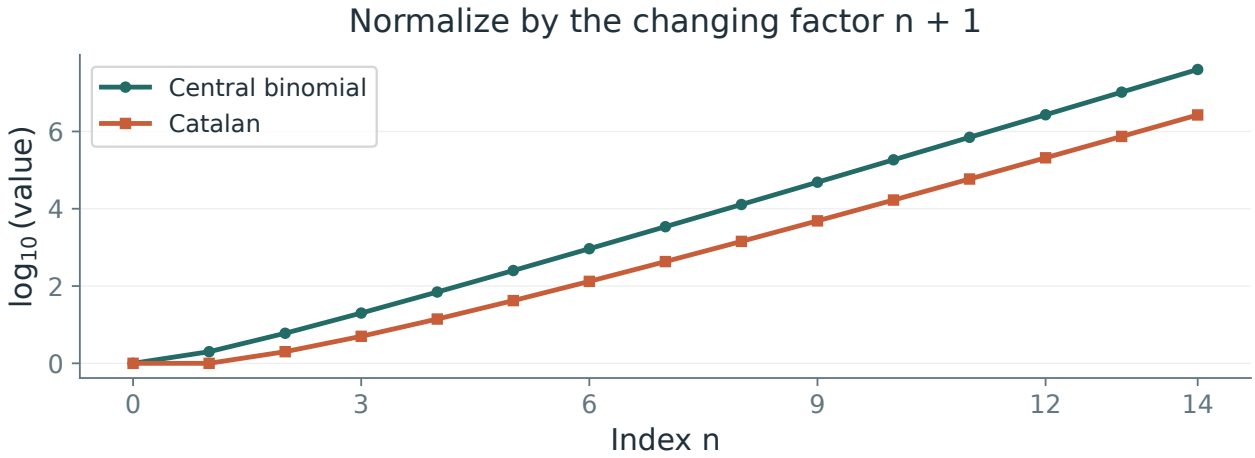
Carry forward. A shared recurrence state can retain an exact invariant while both coordinates grow.

Source and scope. OEIS A001075 and A001353, indexed from zero. Integer matrix iteration and the norm are checked through $n = 18$.

SEQUENCES / 05 **LESSON 115**

Normalize central binomial coefficients

	0	1	2	3	4	5	6
Binomial	1	2	6	20	70	252	924
Divide by	1	2	3	4	5	6	7
Catalan	1	1	2	5	14	42	132



$$B_n = \binom{2n}{n}, \qquad C_n = \frac{B_n}{n+1}$$

Read the figure. Each table column shows one central binomial coefficient and its Catalan normalization. The curves extend the comparison through index fourteen on a base-ten logarithmic axis. Division by $n+1$ is exact here and gives an integer at every index.

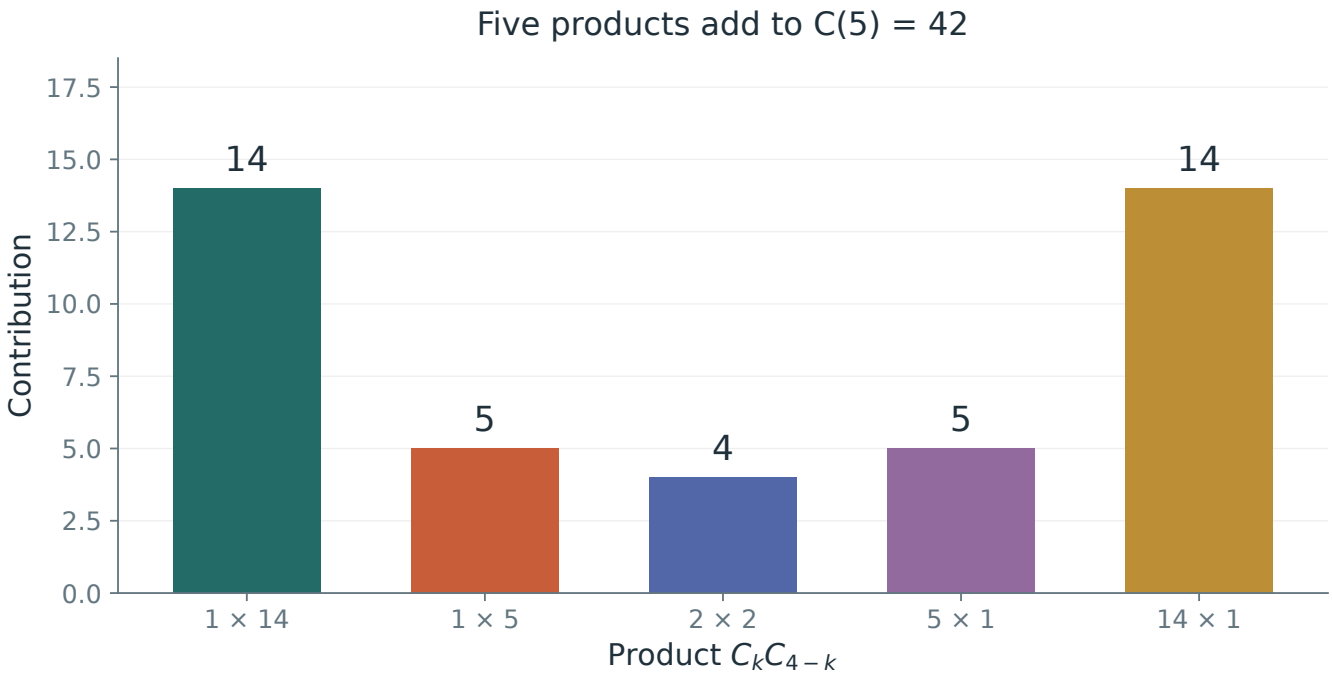
Work an example. For $n = 4$, $B_4 = \binom{8}{4} = 70$ and $C_4 = 70/5 = 14$. For $n = 5$, $252/6 = 42$. The divisor changes with the index.

Carry forward. Normalization is an operator on coefficients. It need not be a fixed convolution or a constant tap weight.

Source and scope. OEIS A000984 and A000108, indexed from zero. Binomial formulas and integrality checked through $n = 18$.

SEQUENCES / 06 **LESSON 116**

Catalan convolution rebuilds the next term



$$C_{n+1} = \sum_{k=0}^{n} C_k C_{n-k}, \qquad C(z) = 1 + zC(z)^2$$

Read the figure. The five bars are the five products contributing to C_5. The input indices add to four, and their sum supplies the next coefficient. Here $C(z) = \sum_{n\geq 0} C_n z^n$ is an ordinary generating function.

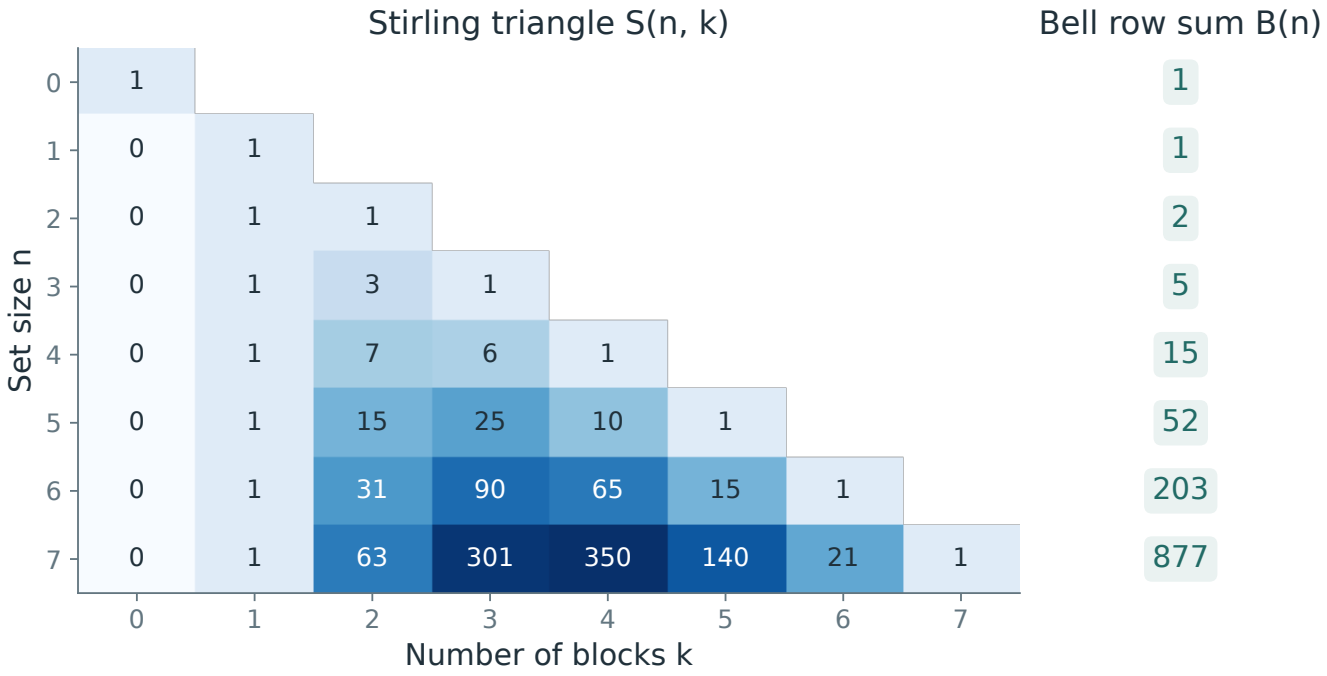
Work an example. The contributions are $1 \cdot 14$, $1 \cdot 5$, $2 \cdot 2$, $5 \cdot 1$, and $14 \cdot 1$. Their sum is $14 + 5 + 4 + 5 + 14 = 42 = C_5$.

Carry forward. A nonlinear generating-function equation becomes an exact convolution identity among coefficients.

Source and scope. OEIS A000108. All convolution identities with $0 \leq n \leq 17$ are checked against the binomial definition.

SEQUENCES / 07 **LESSON 117**

Bell numbers are Stirling row sums



$$B_n = \sum_{k=0}^{n} S(n,k), \qquad \sum_{n\geq 0} B_n \frac{t^n}{n!} = \exp(e^t - 1)$$

Read the figure. Each matrix row contains Stirling numbers of the second kind, counting partitions into k nonempty blocks. Summing across the row gives the Bell number at its right. The generating function is exponential, so its coefficient is $B_n/n!$.

Work an example. The fifth row contains $0, 1, 15, 25, 10, 1$. Its sum is $52 = B_5$. Equivalently, apply the Stirling transform to the constant input sequence $1, 1, 1, \ldots$.

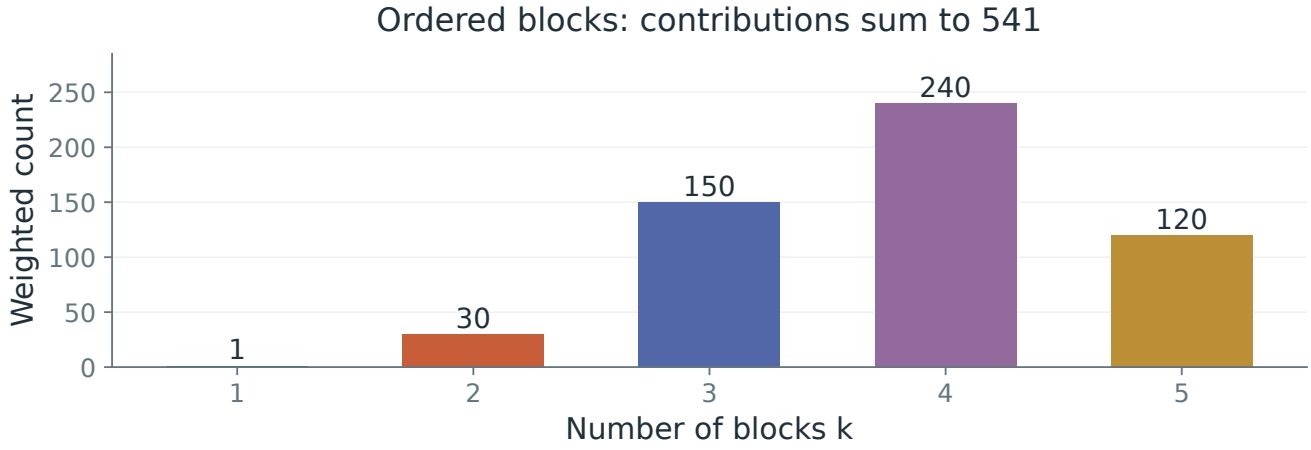
Carry forward. A triangular transform uses all relevant input positions. It is not automatically a fixed-length tap filter.

Source and scope. OEIS A000110. Stirling recurrence and an independent binomial Bell recurrence agree through $n = 18$; the figure shows rows zero through seven.

SEQUENCES / 08 **LESSON 118**

Factorial weights order the blocks

	1	2	3	4	5
S(5, k)	1	15	25	10	1
k!	1	2	6	24	120
Product	1	30	150	240	120



$$A_n = \sum_{k=0}^{n} k! S(n,k), \qquad \sum_{n\geq 0} A_n \frac{t^n}{n!} = \frac{1}{2 - e^t}$$

Read the figure. The same Stirling row now receives factorial weights. Ordering k blocks gives $k!$ arrangements. The upper table shows the factors at $n = 5$; the bars show their products. The sum is the ordered Bell, or Fubini, number.

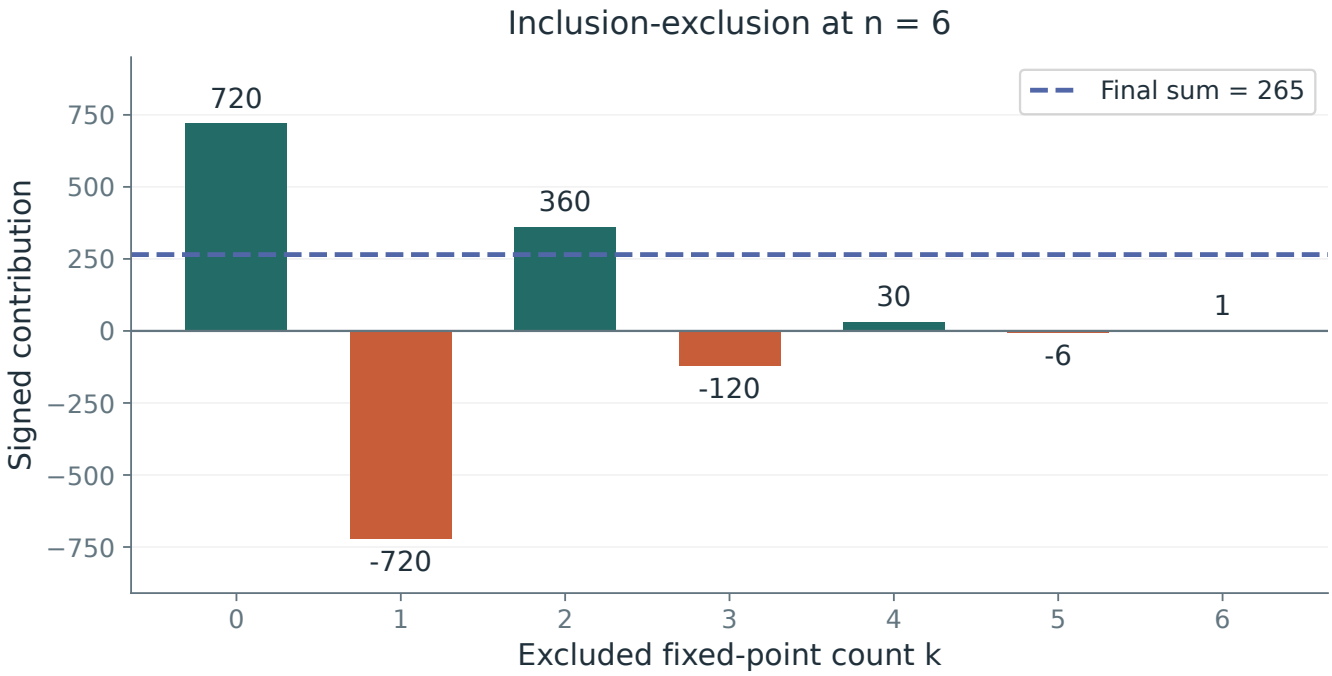
Work an example. At $n = 5$, the weighted contributions are $1, 30, 150, 240, 120$, totaling 541. The unweighted row sums to only 52. The weights encode a different combinatorial operation.

Carry forward. Changing the transform's input from one to $k!$ changes the output family while retaining the same triangular kernel.

Source and scope. OEIS A000670 and A000142, indexed from zero. Integer Stirling sums and an independent ordered-partition recurrence agree through $n = 18$.

SEQUENCES / 09 **LESSON 119**

Derangements show signed cancellation



$$D_n = n! \sum_{k=0}^{n} \frac{(-1)^k}{k!}, \qquad D_n = (n-1)(D_{n-1} + D_{n-2}) \quad (n \geq 2)$$

Read the figure. Positive and negative bars are the inclusion-exclusion contributions at $n = 6$. Their large magnitudes cancel to a smaller integer. The dashed line records the final sum rather than an individual contribution. Here $D_0 = 1$ and $D_1 = 0$.

Work an example. The sum is $720 - 720 + 360 - 120 + 30 - 6 + 1 = 265$. The recurrence independently gives $D_6 = 5(44 + 9) = 265$.

Carry forward. Signed transforms must retain cancellation. Magnitudes alone do not determine the result.

Source and scope. OEIS A000166. Factorial sum, variable-coefficient recurrence, and brute-force permutation counts through $n = 8$ agree; exact formulas checked through $n = 18$.

SEQUENCES / 10 **LESSON 120**

Secant and tangent interleave

Even degrees belong to secant

	deg 0	deg 2	deg 4	deg 6	deg 8	deg 10
Secant number	1	1	5	61	1385	50521
Divide by	1	2	24	720	40320	3628800

Odd degrees belong to tangent

	deg 1	deg 3	deg 5	deg 7	deg 9	deg 11
Tangent number	1	2	16	272	7936	353792
Divide by	1	6	120	5040	362880	39916800

$$\sum_{n\ge 0} E_n \frac{t^n}{n!} = \sec t + \tan t, \quad E_{2m} = s_m, \quad E_{2m+1} = \tau_m$$

Read the figure. The coefficient table separates even and odd positions of the Euler up/down family. Even positions are positive secant numbers. Odd positions are tangent numbers. The factorial row makes clear that these are exponential-generating-function numbers, not ordinary Taylor coefficients.

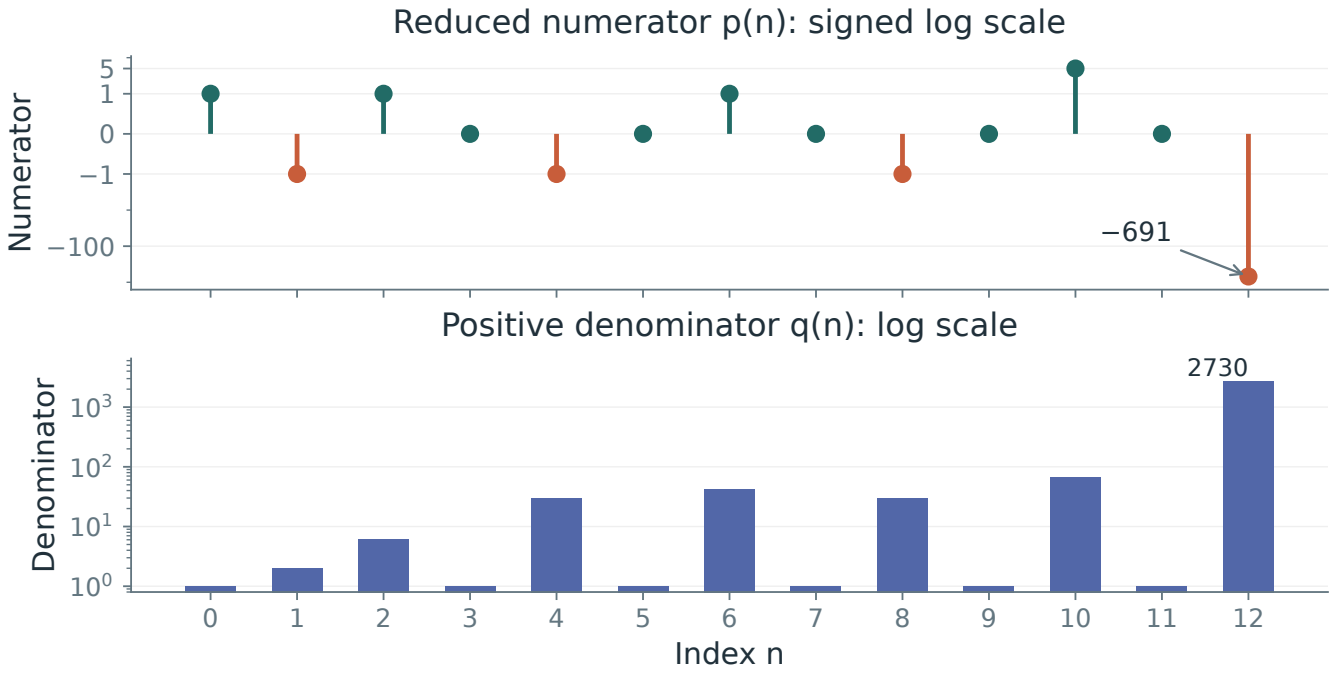
Work an example. At degree four, $E_4 = 5$ contributes $5t^4/4!$ to secant. At degree five, $E_5 = 16$ contributes $16t^5/5!$ to tangent. The first tangent entry corresponds to degree one.

Carry forward. Parity packets can identify familiar functions, provided the factorial normalization and sequence offset are kept.

Source and scope. OEIS A000111, A000364, and A000182. The tangent entry has OEIS initial index one; τ_m denotes its degree-$2m+1$ value. Exact series checked through degree eighteen.

SEQUENCES / 11 **LESSON 121**

Bernoulli data need both coordinates



$$\frac{t}{e^t-1}=\sum_{n\ge 0} B_n \frac{t^n}{n!}, \qquad B_n=\frac{p_n}{q_n}, \quad q_n>0$$

Read the figure. The top panel shows signed numerators on a symmetric logarithmic scale. The lower panel shows positive denominators on a logarithmic scale. Fractions are reduced. A zero Bernoulli number is stored as $0/1$, and this guide uses $B_1=-1/2$.

Work an example. At $n=10$, $p_{10}=5$ and $q_{10}=66$, so $B_{10}=5/66$. Its Taylor coefficient is $(5/66)/10!$. At $n=12$, $B_{12}=-691/2730$.

Carry forward. An OEIS integer numerator sequence does not by itself specify the rational family or its generating-function coefficient.

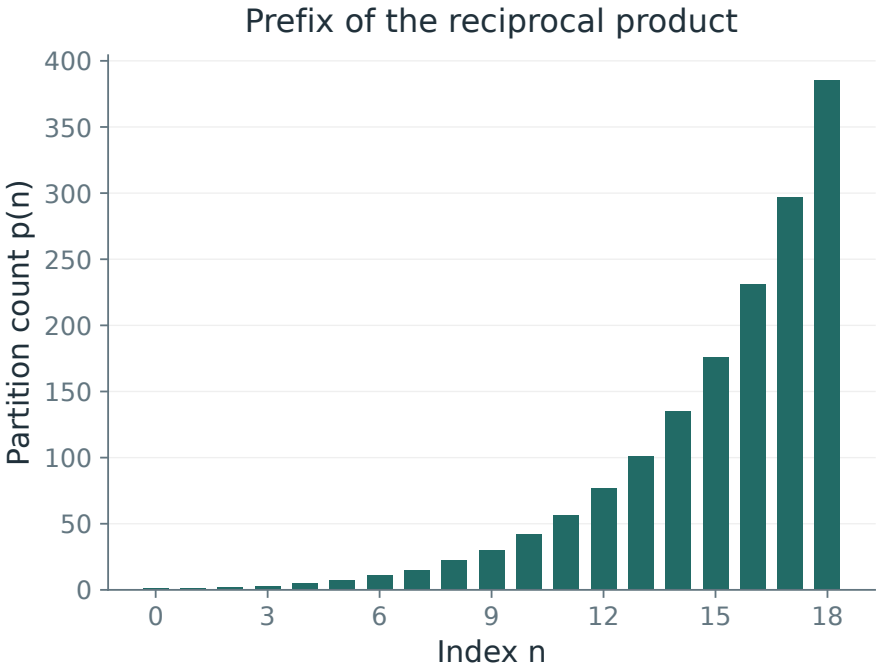
Source and scope. OEIS A027641 and A027642, indexed from zero. Exact rational recurrence and multiplication by $(e^t-1)/t$ checked through degree eighteen.

SEQUENCES / 12 **LESSON 122**

Partitions multiply reciprocal factors

Five choices of multiplicities

Partitions of 4
4
3 + 1
2 + 2
2 + 1 + 1
1 + 1 + 1 + 1



$$P(z) = \prod_{j \geq 1} \frac{1}{1 - z^j} = \sum_{n \geq 0} p(n) z^n$$

Read the figure. A factor indexed by j chooses how many parts of size j occur. The left table lists the five partitions of four. The right bars show the first nineteen partition numbers. This is an ordinary generating function with integer coefficients.

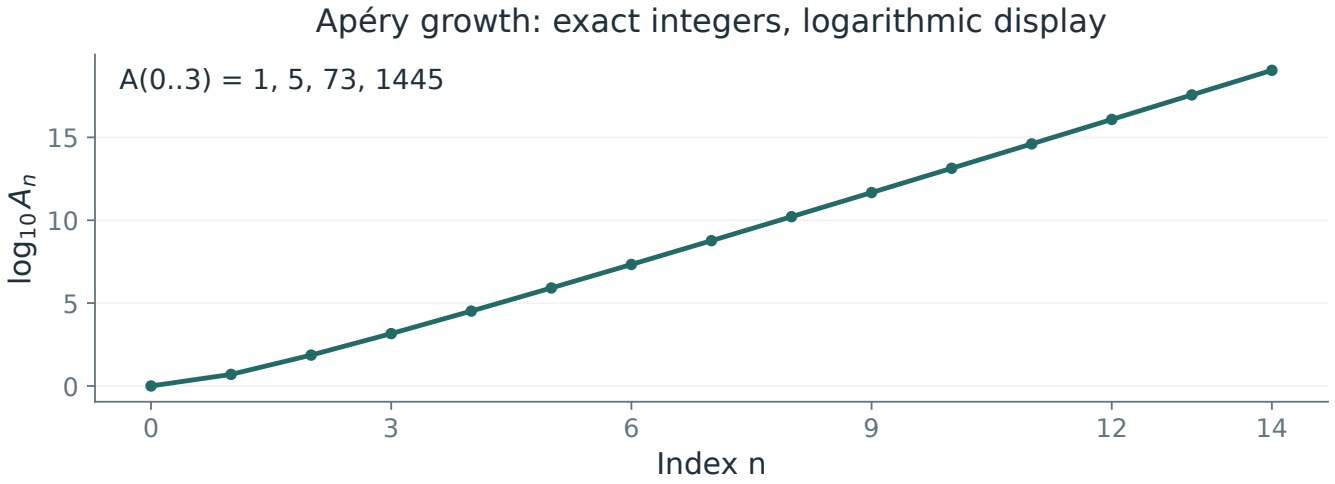
Work an example. The partitions of four are 4, $3+1$, $2+2$, $2+1+1$, and $1+1+1+1$. Thus $p(4) = 5$. To find coefficients through degree eighteen, only factors with $j \leq 18$ are needed.

Carry forward. Reciprocal factors turn independent multiplicities into a coefficient-counting product. The finite prefix can be reconstructed exactly.

Source and scope. OEIS A000041. Product coefficients computed by integer dynamic programming, independently checked by partition enumeration through $n = 10$.

SEQUENCES / 13 **LESSON 123**

Apéry uses taps that depend on the index



n = 2: 535 × 73 − 8 × 5 = 39015

39015 ÷ 27 = 1445

$$(n+1)^3 A_{n+1} = (2n+1)(17n^2+17n+5)A_n - n^3 A_{n-1}$$

Read the figure. The prefix annotation begins the Apéry sequence defined by $A_n = \sum_{k=0}^{n} \binom{n}{k}^2 \binom{n+k}{k}^2$. The curves show its growth through index fourteen on a base-ten logarithmic scale. The lower diagram evaluates the recurrence at $n = 2$.

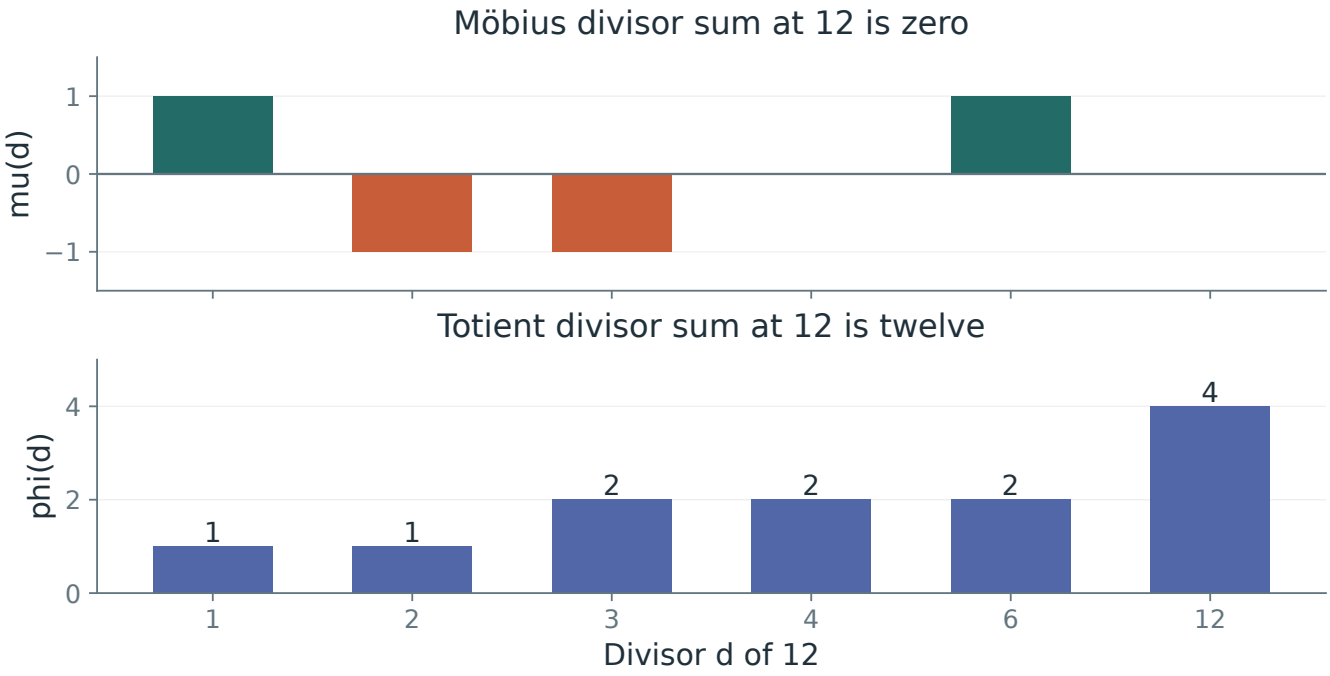
Work an example. Using $A_1 = 5$ and $A_2 = 73$ gives $27A_3 = 535 \cdot 73 - 8 \cdot 5 = 39015$. Therefore $A_3 = 1445$. The recurrence applies for $n \geq 1$, with $A_0 = 1$.

Carry forward. This is a three-term recurrence with polynomial coefficients. Its weights change with n, so it is not a constant-tap filter.

Source and scope. OEIS A005259. Exact binomial sums and the displayed polynomial-coefficient recurrence agree for $1 \leq n \leq 17$.

SEQUENCES / 14 **LESSON 124**

Divisor convolution changes the address rule



$$\sum_{d\mid n}\mu(d)=\mathbf{1}_{n=1}, \qquad \sum_{d\mid n}\varphi(d)=n$$

Read the figure. The figure places the six divisors of twelve in matching columns. Möbius contributions sum to zero; totient contributions sum to twelve. The address rule is divisibility. This differs from the additive index splitting used by ordinary power-series convolution.

Work an example. For $n=12$, $\mu(1),\mu(2),\mu(3),\mu(4),\mu(6),\mu(12)$ are $1,-1,-1,0,1,0$. The totient values are $1,1,2,2,2,4$. Their sums are zero and twelve.

Carry forward. Choose the convolution law before identifying a transform. Divisor packets and residue packets organize different relations.

Source and scope. OEIS A008683 and A000010, both indexed from one. Prime-factor definitions and both divisor sums checked for $1\le n\le 60$.

SEQUENCES / 15 **LESSON 125**

One binary statistic creates three families

Binary addresses 0 through 7

	0	1	2	3	4	5	6	7
Binary	0000	0001	0010	0011	0100	0101	0110	0111
Weight	0	1	1	2	1	2	2	3
Parity	0	1	1	0	1	0	0	1
Gould	1	2	2	4	2	4	4	8

Binary addresses 8 through 15

	8	9	10	11	12	13	14	15
Binary	1000	1001	1010	1011	1100	1101	1110	1111
Weight	1	2	2	3	2	3	3	4
Parity	1	0	0	1	0	1	1	0
Gould	2	4	4	8	4	8	8	16

$$w(n) = \operatorname{popcount}(n), \quad t(n) = w(n) \bmod 2, \quad g(n) = 2^{w(n)}$$

Read the figure. Each column has a four-bit address, its binary weight, its Thue–Morse parity, and its Gould value. Reading a final zero bit preserves weight; reading a final one adds one. Parity toggles and the Gould value doubles in the latter case.

Work an example. The address $13 = 1101_2$ has weight three, so $t(13) = 1$ and $g(13) = 8$. Address $12 = 1100_2$ has weight two, parity zero, and Gould value four.

Carry forward. The same state statistic can feed several exact outputs. Binary refinement gives simple even and odd channel recurrences.

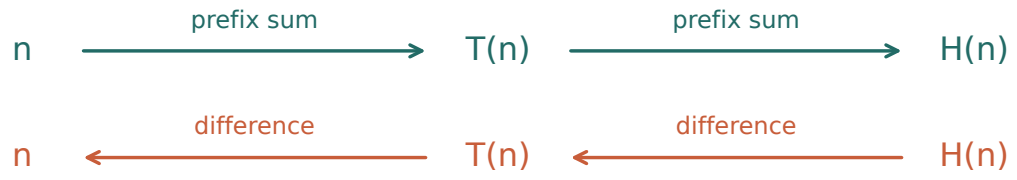
Source and scope. OEIS A000120, A010060, and A001316, indexed from zero. Binary formulas and even/odd recurrences checked for $0 \le n \le 63$; figure shows zero through fifteen.

SEQUENCES / 16 **LESSON 126**

Sums and differences form a polynomial ladder

Common indices: n = 1 through 6

	1	2	3	4	5	6
n	1	2	3	4	5	6
Triangular	1	3	6	10	15	21
Tetrahedral	1	4	10	20	35	56
Square	1	4	9	16	25	36
Cube	1	8	27	64	125	216



$$T_n = \sum_{j=1}^{n} j, \quad H_n = \sum_{j=1}^{n} T_j, \quad \Delta T_n = n, \quad \Delta H_n = T_n$$

Read the figure. The upper table follows positive integers into triangular and tetrahedral numbers. Squares and cubes occupy the lower rows for comparison. The arrows reverse prefix sums by backward differences, $\Delta f_n = f_n - f_{n-1}$. All plotted values use their displayed common index.

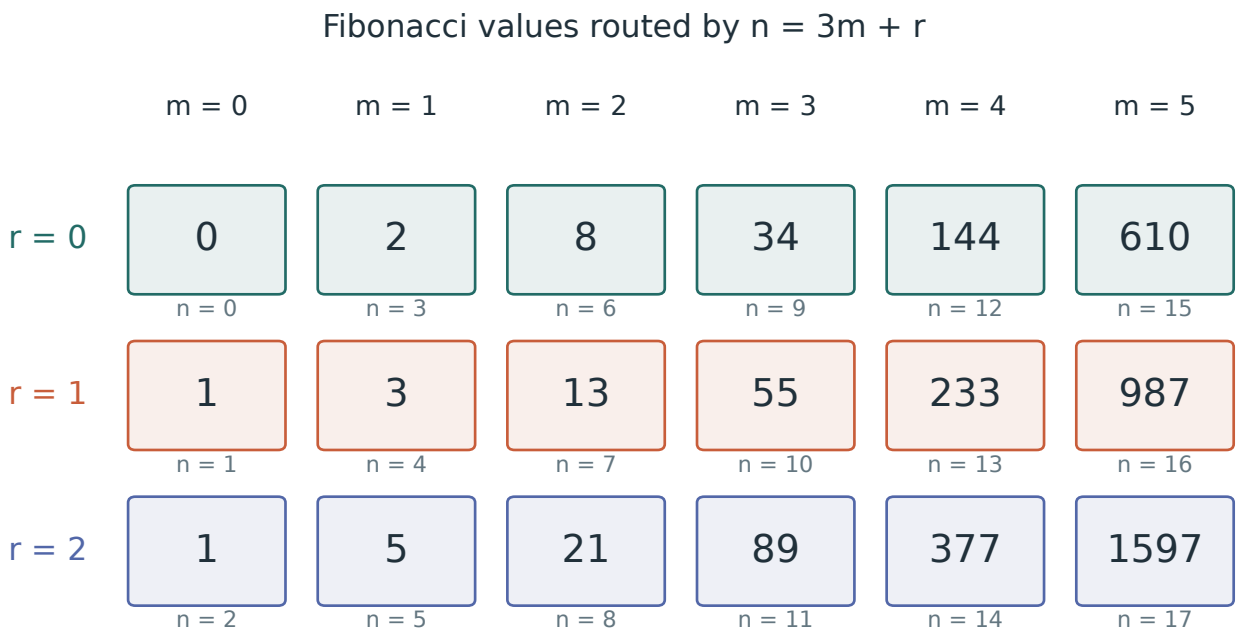
Work an example. At $n = 4$, $T_4 = 10$ and $H_4 = 20$. The differences are $10 - 6 = 4$ and $20 - 10 = 10$. Separately, $4^2 - 3^2 = 7$ and $4^3 - 3^3 = 37$.

Carry forward. Prefix summation raises polynomial degree; differencing lowers it. These are exact operators with boundary values at zero; the displayed difference identities apply for $n \geq 1$.

Source and scope. OEIS A000027, A000217, A000292, A000290, and A000578. Positive integers start at one; the other four families include index zero. Identities checked through $n = 18$.

POLYPHASE / 01 **LESSON 127**

Split Fibonacci into three actual streams



$$F_{3,r}(u) = \sum_{m \geq 0} F_{3m+r} u^m, \qquad r = 0, 1, 2$$

Read the figure. The large numbers are Fibonacci coefficients, not exponent labels. Each column advances one step inside a channel, which advances three steps in the original sequence. The smaller label underneath records the original index. The three colors together account for every index from zero to seventeen.

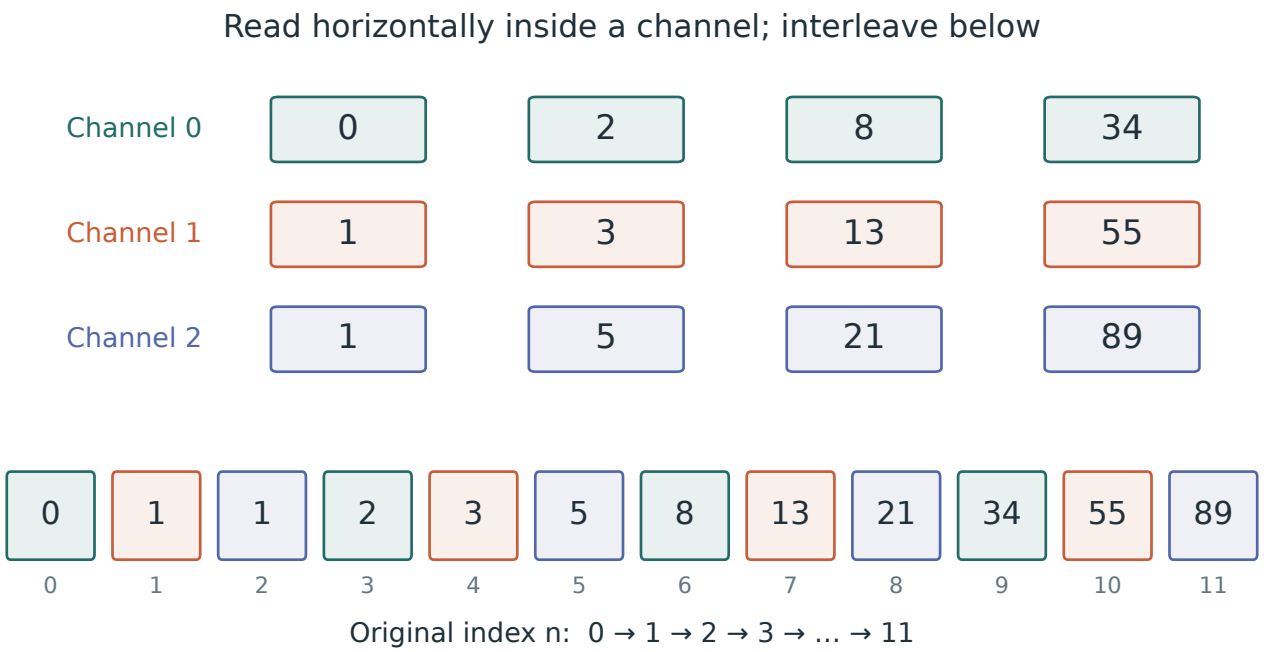
Work an example. The first channel begins $0, 2, 8, 34, 144, 610$. The second begins $1, 3, 13, 55, 233, 987$, and the third begins $1, 5, 21, 89, 377, 1597$. Thus the coefficient of u^4 in channel two is $F_{14} = 377$.

Carry forward. Declare the starting index before splitting a sequence. Here $F_0 = 0$, $F_1 = 1$, and channel indices start at $m = 0$.

Source and scope. Fibonacci: OEIS A000045. Exact integer coefficients; the displayed prefix ends at index seventeen. The splitting definition is valid for the full formal series.

POLYPHASE / 02 **LESSON 128**

Weave the three streams back together



$$\sum_{n\geq 0} F_n z^n = F_{3,0}(z^3) + zF_{3,1}(z^3) + z^2F_{3,2}(z^3)$$

Read the figure. Read the top rows horizontally to see each internal stream. Read the lower row in increasing original index to see the reconstruction. Its colors repeat zero, one, two. Synthesis restores both the coefficient and the place where it belongs.

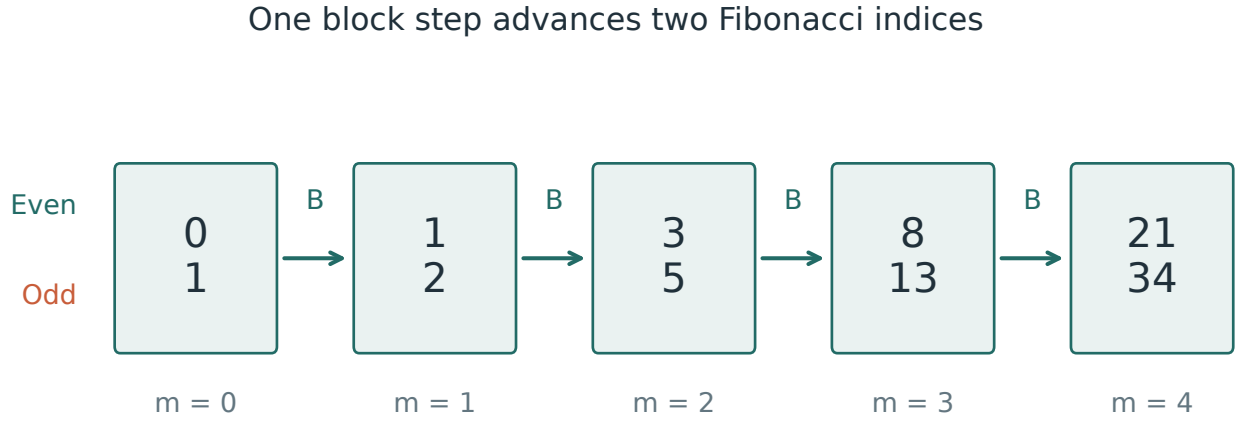
Work an example. The channel terms $2u$, $3u$, and $5u$ become $2z^3$, $3z^4$, and $5z^5$. Interleaving the four displayed terms from each channel produces precisely the first twelve Fibonacci coefficients, ending with $F_{11} = 89$.

Carry forward. Splitting followed by synthesis is a change of coordinates. It does not smooth, average, or estimate the sequence.

Source and scope. OEIS A000045; Paper I, exact polyphase reconstruction. Equality follows coefficient by coefficient from the unique division $n = 3m + r$. The numerical example is finite.

POLYPHASE / 03 **LESSON 129**

Two Fibonacci channels share one denominator



$$B : (x, y) \mapsto (x + y,\ x + 2y)$$

$$E(u) = \frac{u}{1 - 3u + u^2}, \quad O(u) = \frac{1 - u}{1 - 3u + u^2}, \quad B = \begin{pmatrix} 1 & 1 \\ 1 & 2 \end{pmatrix}$$

Read the figure. Each box is the adjacent pair (F_{2m}, F_{2m+1}). The same block matrix advances every box by two original indices. Both channel series therefore obey the same second-order recurrence, although they have different starting coefficients.

Work an example. The initial pair is $(0, 1)$. Applying B gives $(1, 2)$, then $(3, 5)$, then $(8, 13)$. Consequently $E = 0 + u + 3u^2 + 8u^3 + \cdots$ and $O = 1 + 2u + 5u^2 + 13u^3 + \cdots$.

Carry forward. A shared recurrence does not imply identical channels. Initial values and numerator data retain the residue information.

Source and scope. OEIS A000045. Here $B = T^2$ for $T = \left(\begin{smallmatrix} 0 & 1 \\ 1 & 1 \end{smallmatrix}\right)$. The denominator is a formal-series identity, equivalently a rational identity near zero.

POLYPHASE / 04 **LESSON 130**

Every Fibonacci stride has a jump recurrence

Fibonacci jump data: choose stride M, then initial values

Stride M	Trace L(M)	Determinant	g(0) = F(1)	g(1) = F(M+1)	g(2) = F(2M+1)
1	1	-1	1	1	2
2	3	1	1	2	5
3	4	-1	1	3	13
4	7	1	1	5	34
5	11	-1	1	8	89
6	18	1	1	13	233

$$g_m = F_{Mm+r}, \qquad g_{m+2} = L_M g_{m+1} - (-1)^M g_m \quad (M \geq 1)$$

Read the figure. Each table row chooses a stride M. The trace of T^M is the Lucas number L_M, while its determinant is $(-1)^M$. The last three columns use the same starting offset $r = 1$ and show the two initial values and the next value.

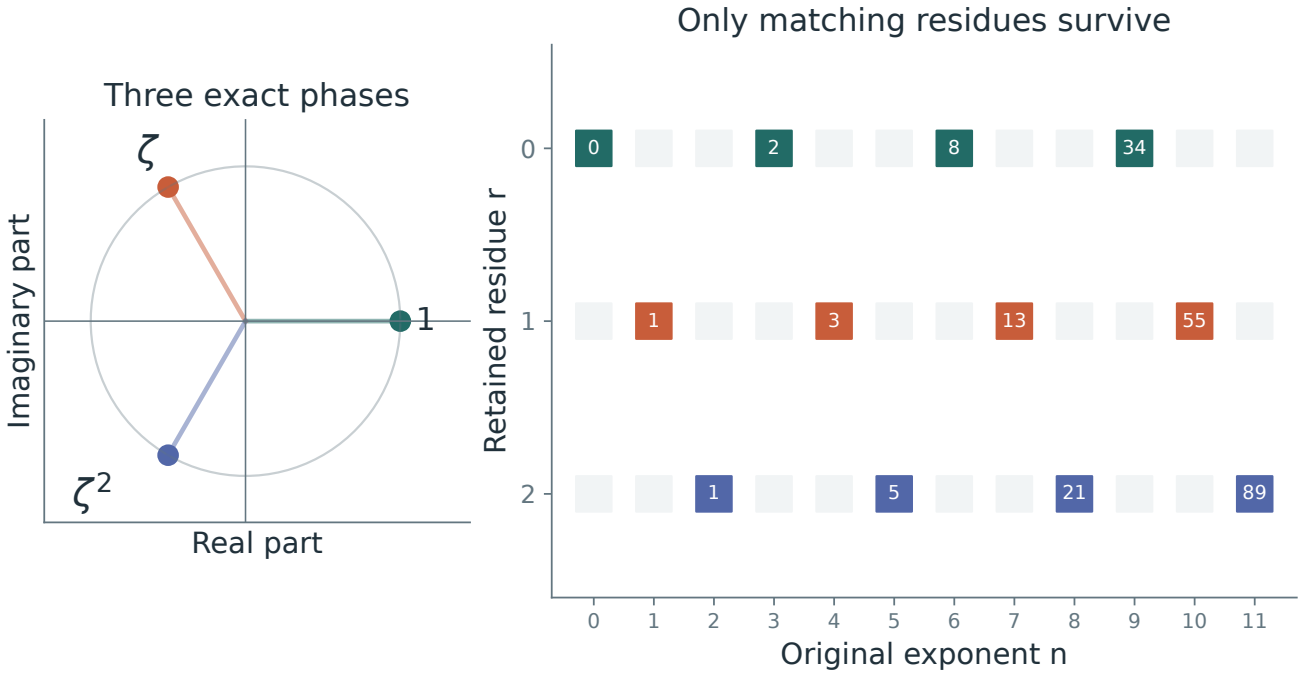
Work an example. For $M = 3$, start with $g_0 = F_1 = 1$ and $g_1 = F_4 = 3$. Since $L_3 = 4$ and the determinant is -1, the next value is $4 \cdot 3 + 1 = 13 = F_7$. For $M = 4$, the sign changes: $7 \cdot 5 - 1 = 34$.

Carry forward. The stride determines the recurrence. The starting offset determines $g_0 = F_r$ and $g_1 = F_{M+r}$. A residue channel uses $0 \leq r < M$.

Source and scope. OEIS A000045 and A000032, with $L_0 = 2$, $L_1 = 1$. Here M is a positive integer and $m, r \geq 0$. The formula follows from Cayley–Hamilton for T^M; the table displays strides one through six at offset one.

POLYPHASE / 05 **LESSON 131**

Complex phases select one residue



$$z^r F_{M,r}(z^M) = \frac{1}{M} \sum_{j=0}^{M-1} \zeta^{-rj} F(\zeta^j z), \qquad \zeta = e^{2\pi i/M}$$

Read the figure. The triangle places the three cube roots of unity in the complex plane. The selection grid shows the resulting coefficient mask: an exponent survives in exactly one row. Individual evaluations can be complex even when the original coefficients and the reconstructed residue series are real.

Work an example. At $M = 3$, the coefficient $F_7 = 13$ survives the selector for $r = 1$ because $7 - 1$ is divisible by three. The sum of its three phase factors is three. For $r = 0$ or $r = 2$, those phase factors sum to zero.

Carry forward. This selector uses a characteristic-zero field containing the required roots of unity, here the complex numbers. Address splitting itself needs no such extension.

Source and scope. Paper I, roots-of-unity filters; M is a positive integer and $0 \le r < M$. OEIS A000045 supplies the example. Exact cancellation is checked in $\mathbb{Q}[\zeta]/(\zeta^2 + \zeta + 1)$, not inferred from floating-point cancellation.

POLYPHASE / 06 **LESSON 132**

Refine even and odd into six coefficient streams

Refine modulus 2 by 3: each child retains real coefficients

		j = 0	j = 1	j = 2
Even parent	ell = 0 → child 0	0 n = 0	8 n = 6	144 n = 12
Even parent	ell = 1 → child 2	1 n = 2	21 n = 8	377 n = 14
Even parent	ell = 2 → child 4	3 n = 4	55 n = 10	987 n = 16
Odd parent	ell = 0 → child 1	1 n = 1	13 n = 7	233 n = 13
Odd parent	ell = 1 → child 3	2 n = 3	34 n = 9	610 n = 15
Odd parent	ell = 2 → child 5	5 n = 5	89 n = 11	1597 n = 17

$$F_{2,r}(u) = \sum_{\ell=0}^{2} u^{\ell} F_{6,r+2\ell}(u^3), \qquad r = 0, 1$$

Read the figure. The parent color identifies even or odd original indices. The child address is $r + 2\ell$, so the even parent has children zero, two, four and the odd parent has children one, three, five. Each child row lists three actual Fibonacci coefficients.

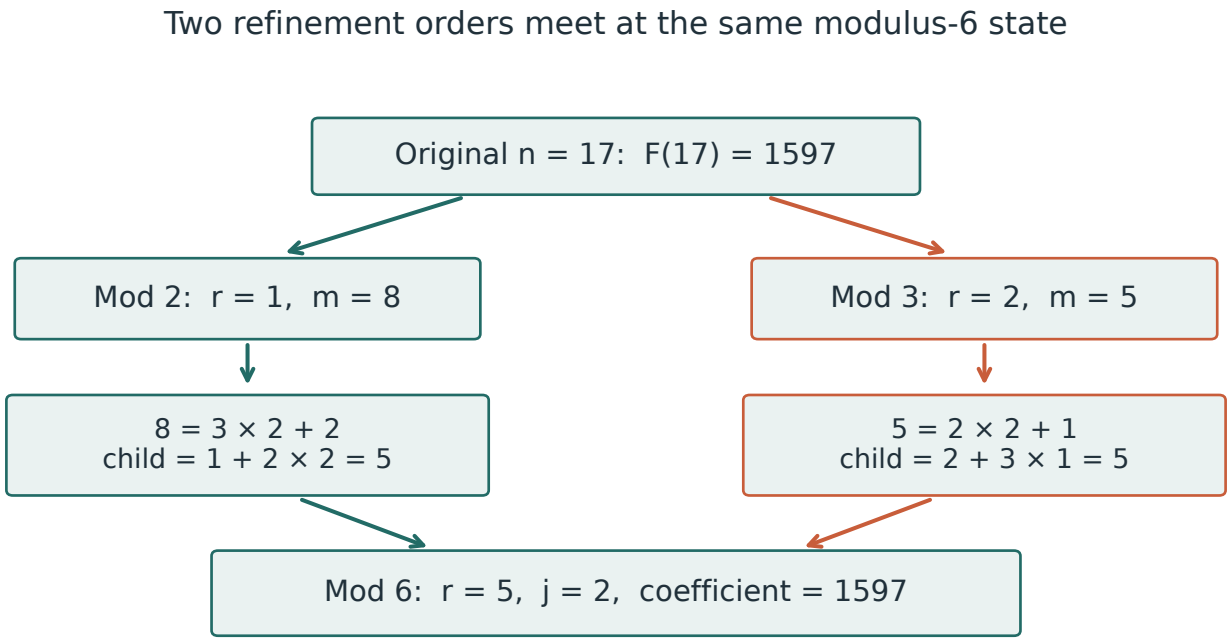
Work an example. Inside the even parent, coefficient 55 occurs at internal index five: $F_{10} = 55$. Splitting $5 = 3 \cdot 1 + 2$ sends it to child four at index one. Its reconstructed exponent is $6 \cdot 1 + 4 = 10$.

Carry forward. A child address alone is insufficient. Carry its internal index and the factor u^{ℓ} through the refinement.

Source and scope. OEIS A000045; Paper I parent–child refinement. The rows use exact values through F_{17}; the identity follows from splitting the parent index $m = 3j + \ell$.

POLYPHASE / 07 **LESSON 133**

Different refinement orders reach the same coefficient



$$17 = 2(3 \cdot 2 + 2) + 1 = 3(2 \cdot 2 + 1) + 2 = 6 \cdot 2 + 5$$

Read the figure. Follow the left path through modulus two and the right path through modulus three. The intermediate residues differ. Both paths arrive at the same modulus-six address, with the same internal index and the same Fibonacci coefficient.

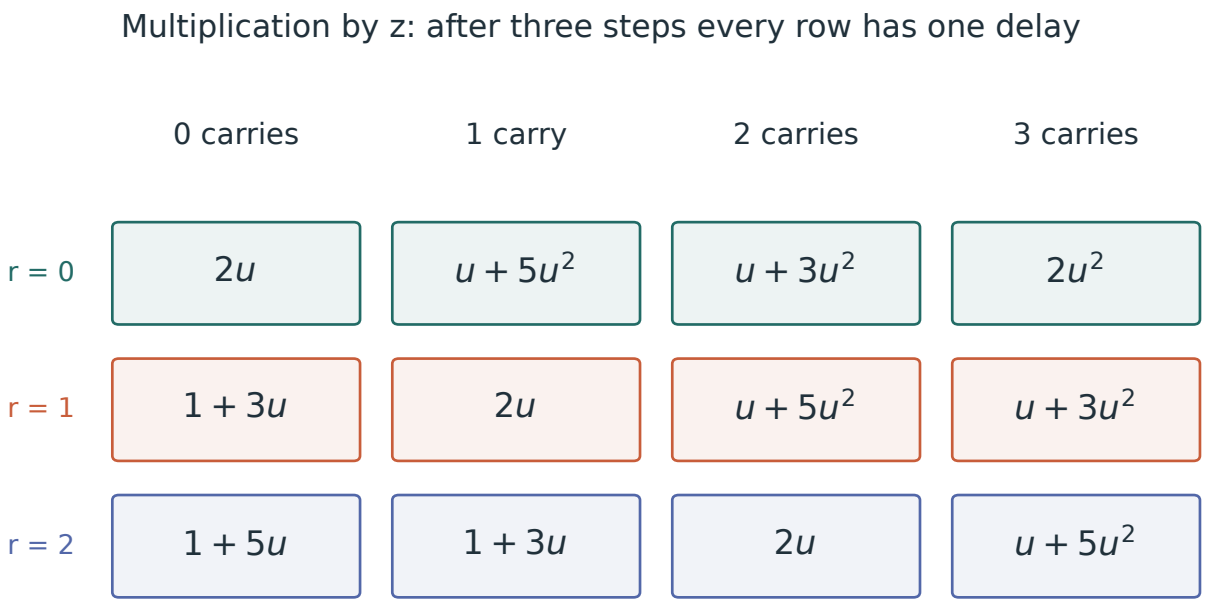
Work an example. Left: $17 = 2 \cdot 8 + 1$, then $8 = 3 \cdot 2 + 2$, giving child $1 + 2 \cdot 2 = 5$. Right: $17 = 3 \cdot 5 + 2$, then $5 = 2 \cdot 2 + 1$, giving child $2 + 3 \cdot 1 = 5$. Both retain $F_{17} = 1597$.

Carry forward. Refinement orders agree after the address permutation is accounted for. Their intermediate labels need not agree.

Source and scope. Paper I refinement identity, illustrated with OEIS A000045. The two routes are exact Euclidean division; the full coefficient check uses indices zero through seventeen.

POLYPHASE / 08 **LESSON 134**

Three carries produce one block delay



$$C_3(u) = \begin{pmatrix} 0 & 0 & u \\ 1 & 0 & 0 \\ 0 & 1 & 0 \end{pmatrix}, \qquad C_3(u)^3 = uI_3$$

Read the figure. Columns show successive multiplication by z for the finite Fibonacci polynomial $P = z + z^2 + 2z^3 + 3z^4 + 5z^5$. Rows keep the three residue addresses. After three carries, every packet has returned to its row and acquired exactly one block delay.

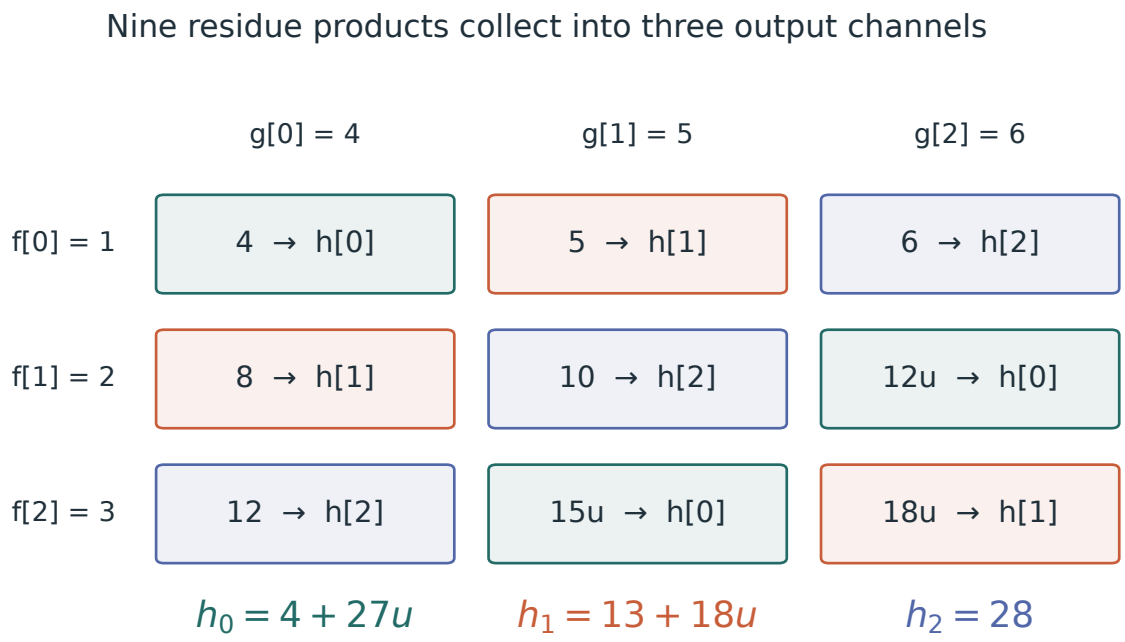
Work an example. Initially the packets are $(2u, 1+3u, 1+5u)$. One carry gives $(u+5u^2, 2u, 1+3u)$. Three carries give $(2u^2, u+3u^2, u+5u^2)$, which synthesize to z^3P.

Carry forward. Wrapping adds a power of u. It does not silently erase the coefficient at the end of a displayed prefix.

Source and scope. Paper I intertwining law. The matrix identity is algebraic over a polynomial ring; the displayed six-coefficient example retains its full output support.

POLYPHASE / 09 **LESSON 135**

Polynomial multiplication has visible residue carries



$$h_t(u) = \sum_{\substack{0 \le r,s < M \\ r+s \equiv t \pmod M}} u^{\lfloor (r+s)/M \rfloor} f_r(u) g_s(u)$$

Read the figure. Each cell multiplies one residue coefficient from $f = 1 + 2z + 3z^2$ by one from $g = 4 + 5z + 6z^2$. Its color records the output residue. The cells beyond the diagonal wrap to a lower residue and carry a factor of u.

Work an example. At modulus three, the product packets are $h_0 = 4 + 27u$, $h_1 = 13 + 18u$, and $h_2 = 28$. They synthesize to $4 + 13z + 28z^2 + 27z^3 + 18z^4$, exactly the ordinary polynomial product.

Carry forward. Residue convolution must retain carry factors. Multiplying only equal-address channels omits cross terms.

Source and scope. Worked finite-polynomial example over the integers. The general formula follows from $r + s = M\lfloor (r+s)/M \rfloor + (r + s \bmod M)$ in a commutative coefficient ring.

POLYPHASE / 10 **LESSON 136**

An exponential generating function changes the weights

One sequence, two coefficient conventions

Original n	OGF coefficient F(n)	EGF coefficient F(n)/n!	Residue / index
0	0	0	0 / m=0
1	1	1	1 / m=0
2	1	1/2	0 / m=1
3	2	1/3	1 / m=1
4	3	1/8	0 / m=2
5	5	1/24	1 / m=2
6	8	1/90	0 / m=3
7	13	13/5040	1 / m=3

$$\sum_{n\geq 0} \frac{a_n z^n}{n!} = \sum_{r=0}^{M-1} z^r \sum_{m\geq 0} \frac{a_{Mm+r}}{(Mm+r)!} (z^M)^m$$

Read the figure. The same Fibonacci values appear on both sides of the table. Ordinary generating-function coefficients retain the integers. Exponential generating-function coefficients divide by the factorial of the original index before channel routing. The denominator does not reset inside a channel.

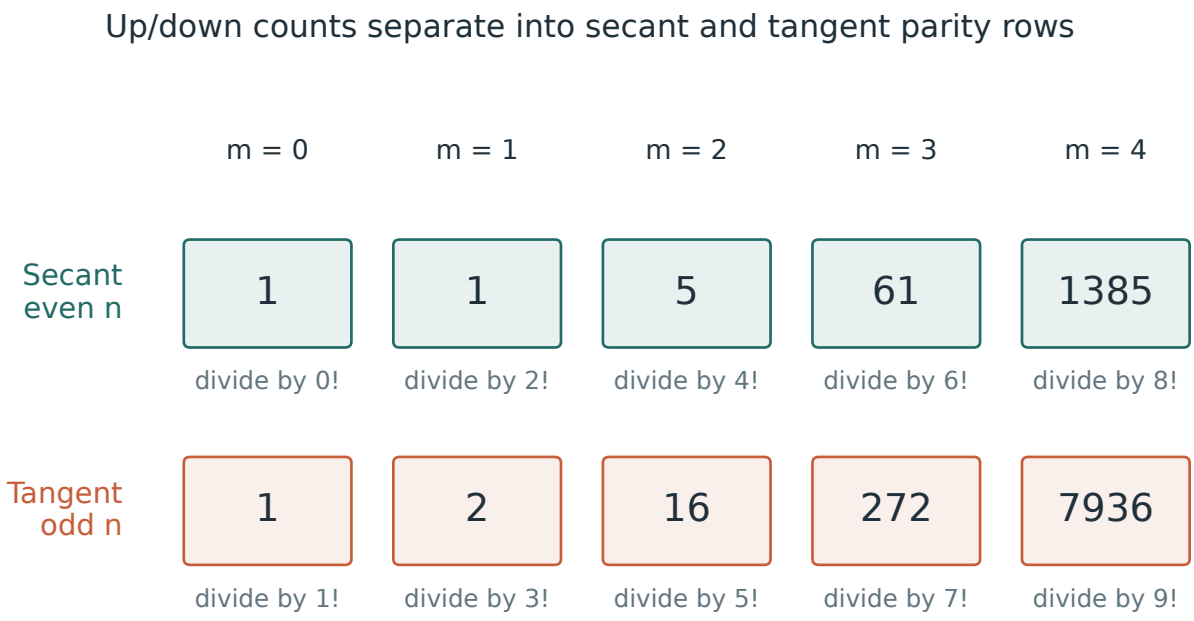
Work an example. The even coefficient $F_6 = 8$ becomes $8/6! = 1/90$ in the exponential series, at channel index three. Dividing by 3! instead would give $4/3$, a different series. The odd coefficient $F_7 = 13$ becomes $13/5040$.

Carry forward. State whether a channel holds sequence values or normalized series coefficients. This choice changes every operator using those coefficients.

Source and scope. OEIS A000045 supplies the values. Exact rational normalization; the reconstruction formula is a coefficient identity over a characteristic-zero field. It is not a claim that the channel itself is an EGF in u.

POLYPHASE / 11 **LESSON 137**

Parity separates secant and tangent counts



$$\sec z = \sum_{m\geq 0} \frac{A_{2m} z^{2m}}{(2m)!}, \qquad \tan z = \sum_{m\geq 0} \frac{A_{2m+1} z^{2m+1}}{(2m+1)!}$$

Read the figure. The combined up/down stream A_n splits into a secant row and a tangent row. The figure displays the integer counts, with the factorial denominator underneath each value. Thus the parity split is applied to the coefficients of $\sec z + \tan z$ with their original-index normalization intact.

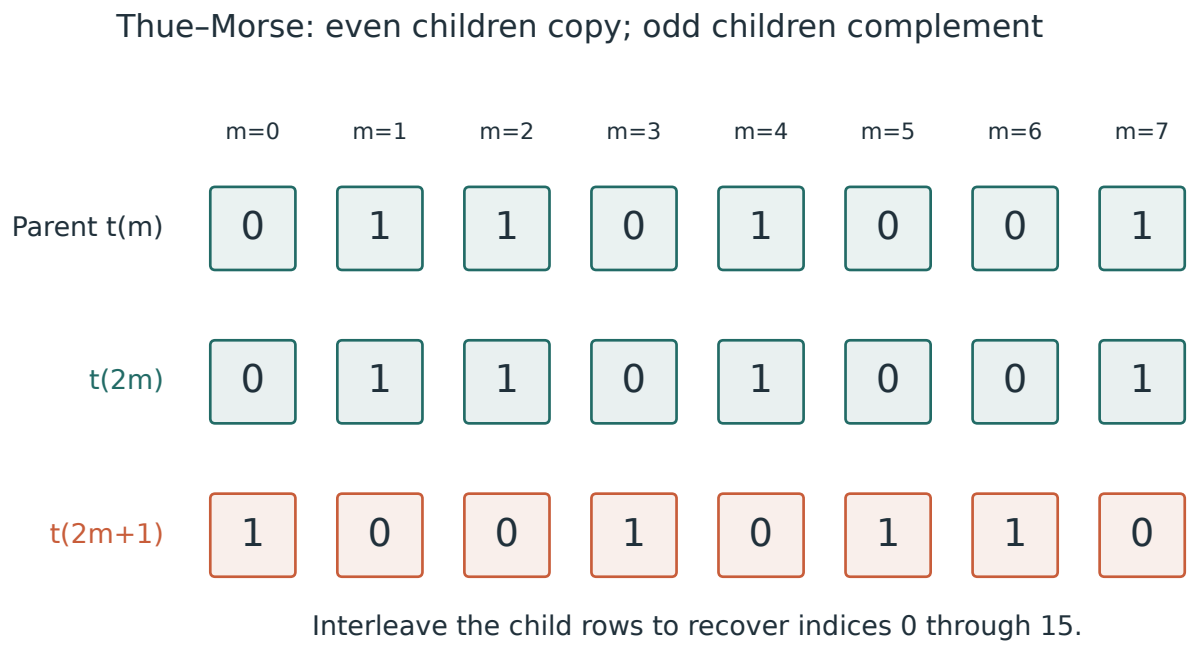
Work an example. At internal index two, the secant term is $5z^4/4!$ and the tangent term is $16z^5/5!$. The tangent row starts $1, 2, 16, 272, 7936$ at exponents $1, 3, 5, 7, 9$. These are positive counts, not signed Euler numbers.

Carry forward. The tangent OEIS sequence starts at native index one. Here its first term is explicitly reindexed to channel index $m = 0$.

Source and scope. OEIS A000111, A000364, A000182. The finite check independently divides the formal sine and cosine series and compares counts through exponent eleven.

POLYPHASE / 12 **LESSON 138**

Thue–Morse refines by copying and complementing



$$t(2m) = t(m), \quad t(2m+1) = 1 - t(m), \quad T(z) = (1-z)T(z^2) + \frac{z}{1-z^2}$$

Read the figure. Each parent bit creates two children. Its even child copies the parent, while its odd child complements it. The two-row child bank reconstructs the first sixteen bits when interleaved. No statistical fitting is involved: the binary digit rule determines every entry.

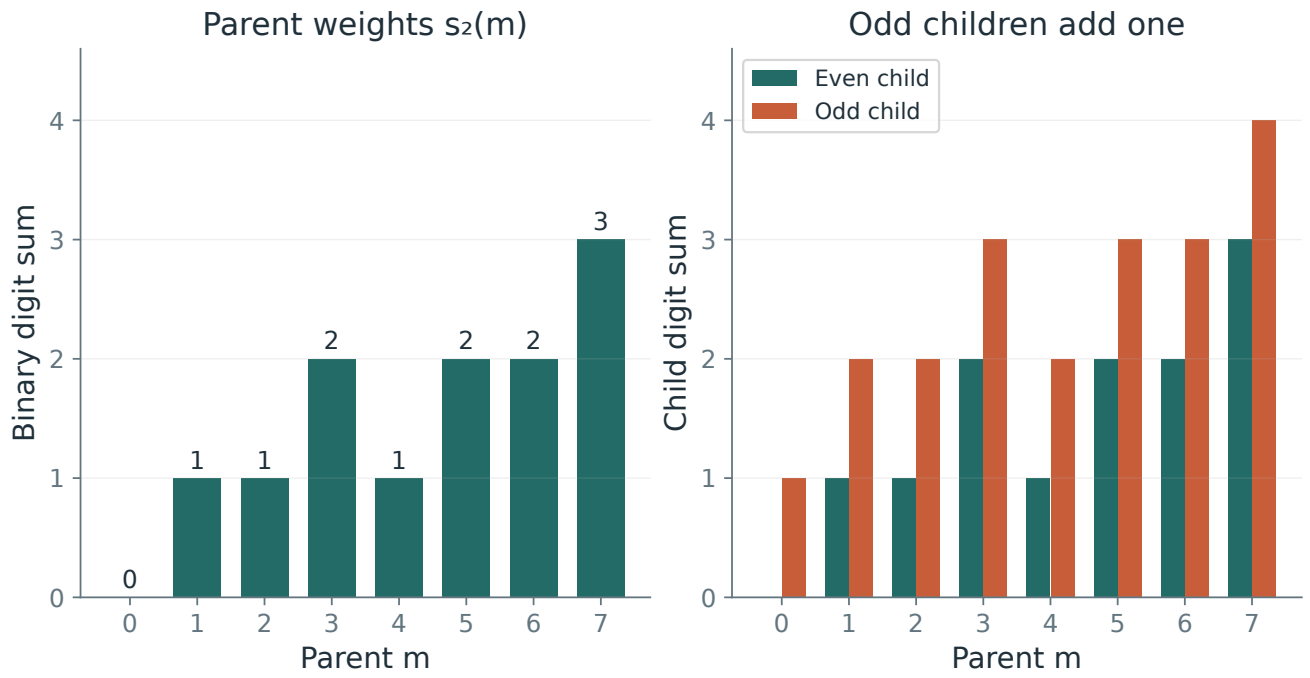
Work an example. For $m = 5$, the binary expansion is 101 and its digit sum is two, so $t(5) = 0$. Its children are $t(10) = 0$ and $t(11) = 1$. In the generating identity, the complement contributes the constant stream $1/(1-z^2)$.

Carry forward. A refinement operator may be affine. Omitting the constant term changes the odd channel.

Source and scope. OEIS A010060, offset zero. $t(n)$ is the binary digit sum modulo two. The universal recurrence follows by appending a binary zero or one; exact checks cover $0 \le n < 256$.

POLYPHASE / 13 **LESSON 139**

Binary weight keeps the affine increment



$$s_2(2m) = s_2(m), \quad s_2(2m+1) = s_2(m) + 1, \quad W(z) = (1+z)W(z^2) + \frac{z}{1-z^2}$$

Read the figure. The left bars show the binary weights of eight parents. On the right, even children preserve each height and odd children add one. These are integer digit counts. Reducing their values modulo two recovers the previous lesson's Thue–Morse bits.

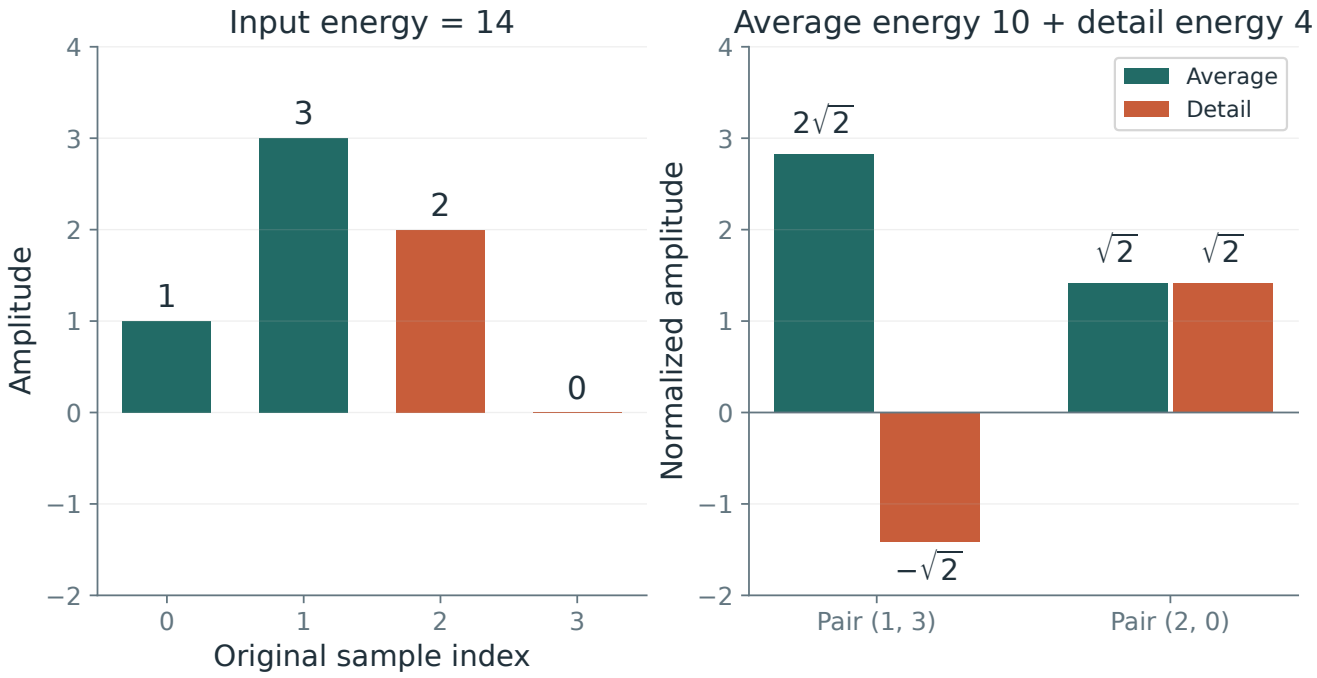
Work an example. The parent $m = 7$ has binary form 111, so its weight is three. Appending zero gives $14 = 1110$ with weight three. Appending one gives $15 = 1111$ with weight four. The odd increment is visible in every pair.

Carry forward. An affine update becomes linear on the augmented state $(s_2(m), 1)^T$. The odd update matrix is $\left(\begin{smallmatrix} 1 & 1 \\ 0 & 1 \end{smallmatrix}\right)$.

Source and scope. OEIS A000120, offset zero. The recurrence and generating identity follow from binary appending. Exact checks cover $0 \le n < 256$; the bars display only parents zero through seven.

POLYPHASE / 14 **LESSON 140**

A Haar bank preserves average and detail together



$$\begin{pmatrix} a \\ d \end{pmatrix} = \frac{1}{\sqrt{2}} \begin{pmatrix} 1 & 1 \\ 1 & -1 \end{pmatrix} \begin{pmatrix} x \\ y \end{pmatrix}, \qquad x^2 + y^2 = a^2 + d^2$$

Read the figure. Group the four input amplitudes into adjacent pairs. The right bars show the normalized average and detail channels for each pair. A negative detail is meaningful: it records which member of the pair is larger. Keeping both channels permits the inverse transform.

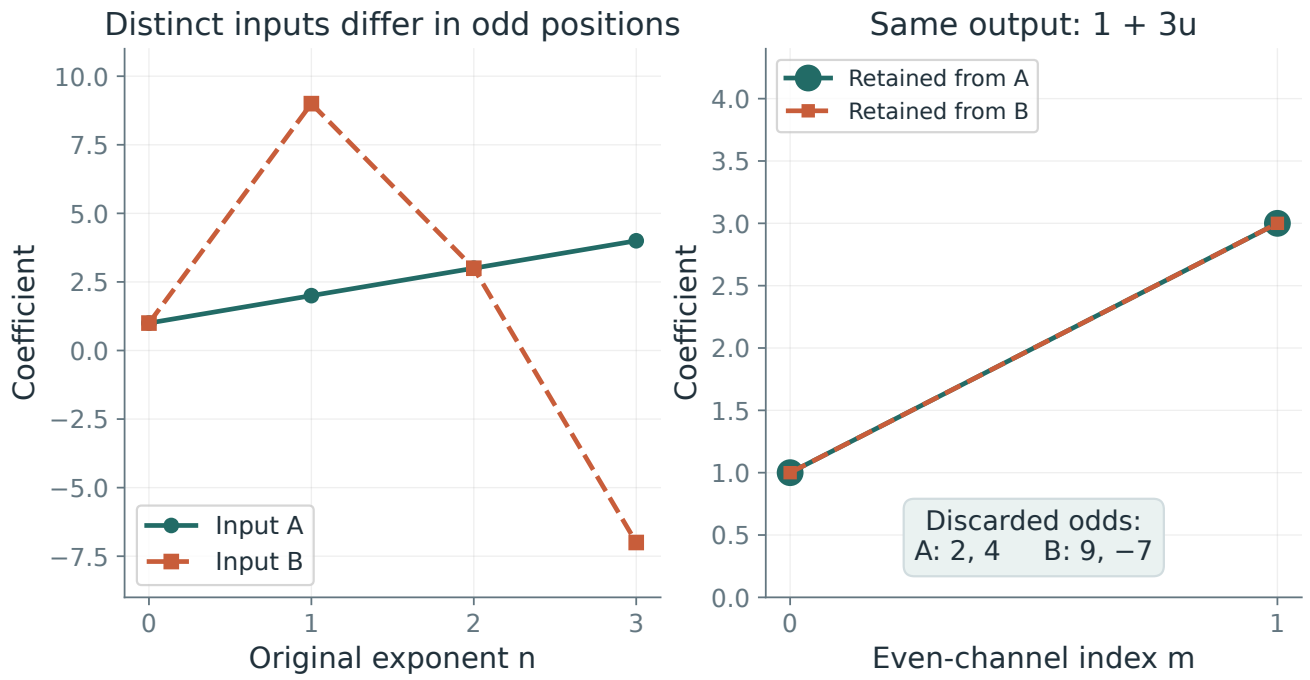
Work an example. For $(1, 3, 2, 0)$, the averages are $(2\sqrt{2}, \sqrt{2})$ and the details are $(-\sqrt{2}, \sqrt{2})$. Their energies are ten and four, totaling the original energy fourteen. Inverting the first pair gives $x = (a + d)/\sqrt{2} = 1$ and $y = (a - d)/\sqrt{2} = 3$.

Carry forward. These are normalized filtering taps on paired amplitudes. They are distinct from recurrence coefficients or an unnormalized arithmetic mean.

Source and scope. Exact Haar two-channel teaching example over $\mathbb{R}$; amplitudes lie in $\mathbb{Q}(\sqrt{2})$. The plotted bars are numerical renderings of the stated exact algebraic values.

POLYPHASE / 15 **LESSON 141**

One retained channel cannot identify the original



$$\mathcal{R}_{2,0}(1+2z+3z^2+4z^3) = \mathcal{R}_{2,0}(1+9z+3z^2-7z^3) = 1+3u$$

Read the figure. The two input polynomials share their even coefficients but differ at both odd positions. The right panel overlays the identical retained channel. The missing odd channel prevents the two inputs from being distinguished after projection.

Work an example. Their difference is $7z - 11z^3$, whose even channel is zero. Full two-channel routing would retain odd channels $2 + 4u$ and $9 - 7u$ and would reconstruct each input exactly. Discarding those channels loses this distinction.

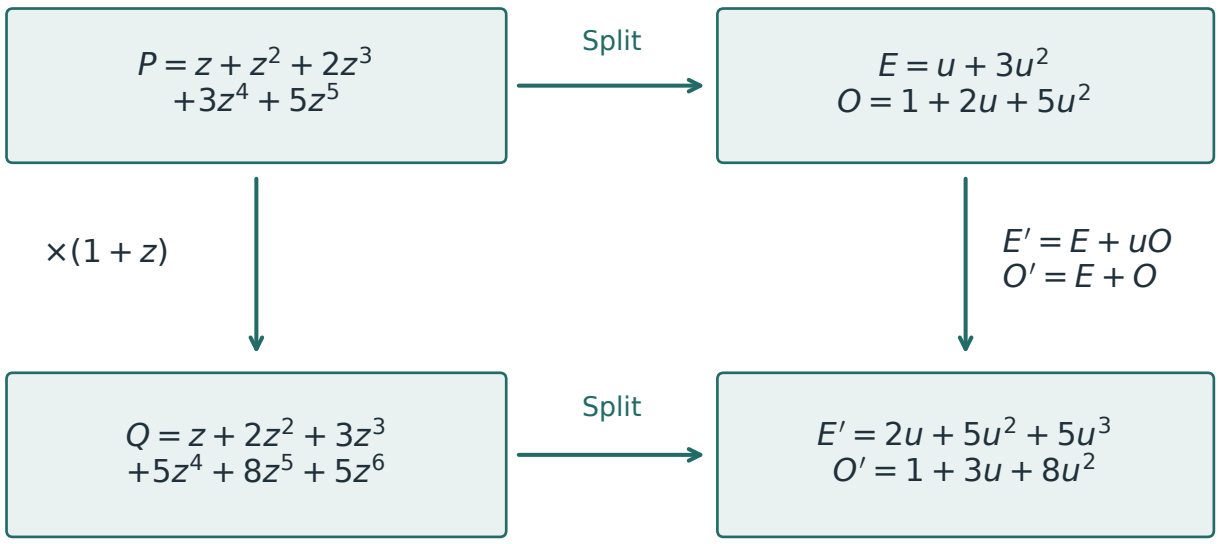
Carry forward. Exact routing is reversible only while the complete channel state is retained. A projection needs a separate recovery hypothesis.

Source and scope. Explicit finite counterexample over the integers. This proves noninjectivity of retaining only the even channel, rather than estimating reconstruction quality on a sample.

POLYPHASE / 16 **LESSON 142**

A complete operation agrees along both routes

A full finite operation agrees before or after channel splitting



$$\mathcal{R}_2((1+z)P) = \begin{pmatrix} 1 & u \\ 1 & 1 \end{pmatrix} \mathcal{R}_2(P), \qquad \mathcal{S}_2\mathcal{R}_2 = I$$

Read the figure. Follow either side of the square. The left route operates on the scalar polynomial first and then splits it. The right route splits first and applies the channel matrix. The two bottom states encode exactly the same seven output coefficients.

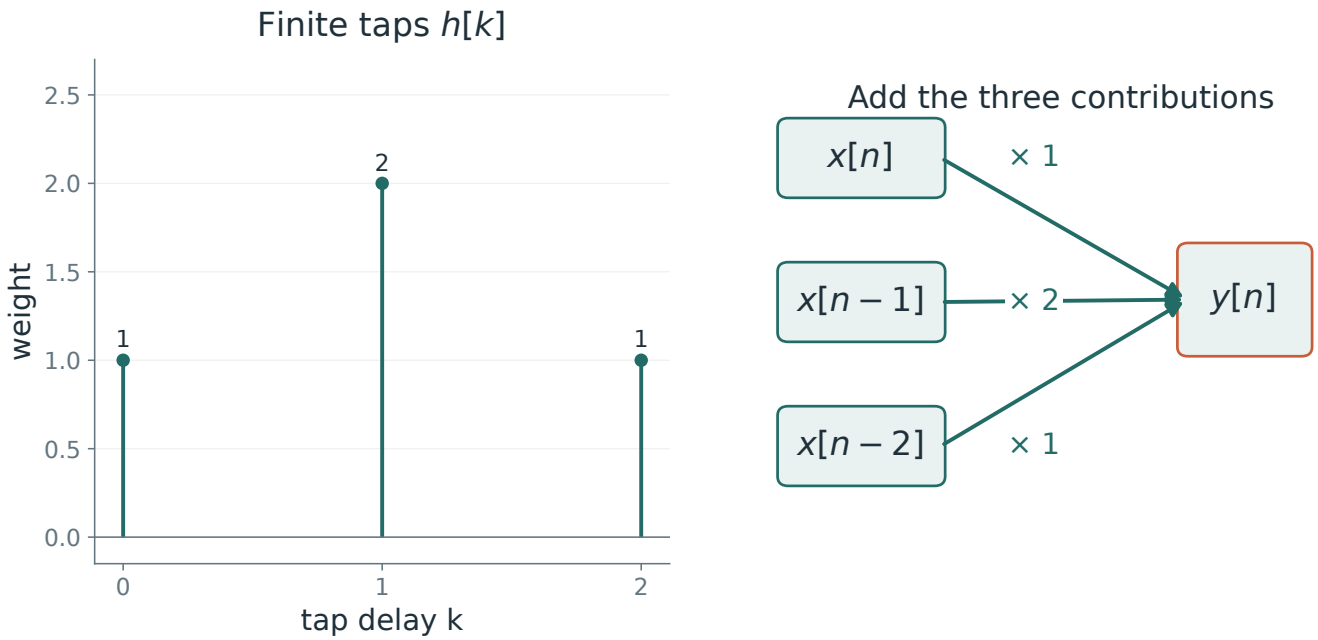
Work an example. For $P = z + z^2 + 2z^3 + 3z^4 + 5z^5$, the input channels are $E = u + 3u^2$, $O = 1 + 2u + 5u^2$. The output channels are $E' = 2u + 5u^2 + 5u^3$, $O' = 1 + 3u + 8u^2$. Their synthesis ends with $5z^6$, retained from the finite input boundary.

Carry forward. A complete contract declares the input support, channel convention, operator, and output support. Equality of those states is the check.

Source and scope. Paper I intertwining, worked on a finite prefix of OEIS A000045. The universal matrix identity follows from the two-phase carry; exact integer checks retain the whole output polynomial.

TAPS / T01 **LESSON 143**

Read a tap as a delayed contribution



$$y[n] = \sum_{k=0}^{L-1} h[k]x[n-k], \qquad h = (1,2,1), \quad x[n] = 0 \ (n < 0)$$

Read the figure. The stem height is a weight, and its horizontal position is a delay. The right panel applies the three weights to three different input samples before adding. A tap specifies which delayed value contributes and with what weight.

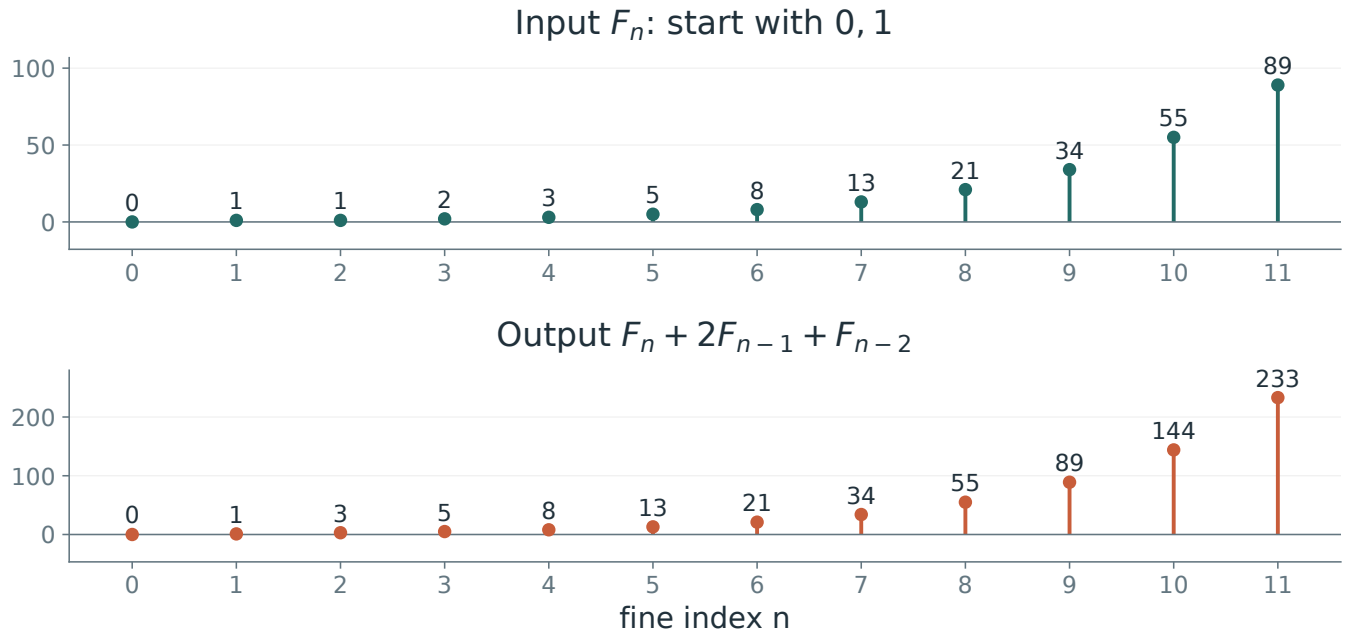
Work an example. At $n = 5$, the three inputs are $x[5], x[4], x[3]$. Their contribution is $x[5] + 2x[4] + x[3]$. At $n = 0$, the two delayed inputs are zero under our causal convention.

Carry forward. Keep the weight, the delay, and the input sample separate.

Source and scope. New worked FIR example. Integer indices $n \geq 0$; every input is zero at negative indices. The finite tap list has length $L = 3$. This convention applies throughout the tap atlas.

TAPS / T02 **LESSON 144**

Execute the taps on Fibonacci numbers



$$F_0 = 0,\ F_1 = 1, \qquad y[n] = F_n + 2F_{n-1} + F_{n-2}$$

Read the figure. Read the two rows at the same fine index. The input follows its recurrence, while the output comes from a separate weighted convolution. The output is larger because two nearby values contribute in addition to the current value.

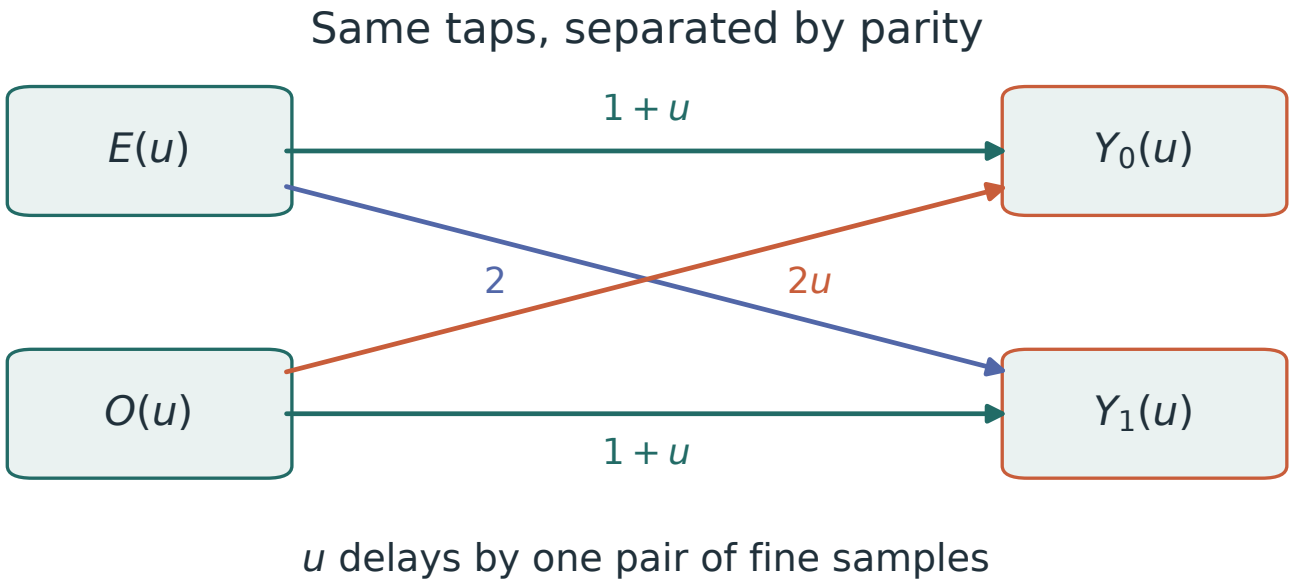
Work an example. At $n = 5$, the result is $5 + 2 \cdot 3 + 2 = 13$. At $n = 11$, it is $89 + 2 \cdot 55 + 34 = 233$. The first twelve displayed outputs are computed with integers, including the zero-extended initial positions.

Carry forward. A sequence recurrence and an applied tap filter are different operations.

Source and scope. Fibonacci convention $F_0 = 0, F_1 = 1$; OEIS A000045 as verified in the sequence atlas. New tap example. Indices 0–11; exact inputs and outputs are recorded in `evidence/tap_checks.json`.

TAPS / T03 **LESSON 145**

Turn three taps into a two-phase matrix



$$\begin{pmatrix} Y_0 \\ Y_1 \end{pmatrix} = \begin{pmatrix} 1+u & 2u \\ 2 & 1+u \end{pmatrix} \begin{pmatrix} E \\ O \end{pmatrix},$$
$$E = \sum_{m\geq 0} x[2m]u^m, \quad O = \sum_{m\geq 0} x[2m+1]u^m$$

Read the figure. Each arrow is one matrix entry. The same-phase contributions use $1+u$, and the cross-phase contributions differ by a coarse delay. Here u shifts an entire pair of fine samples, so it must not be read as a single fine-sample delay.

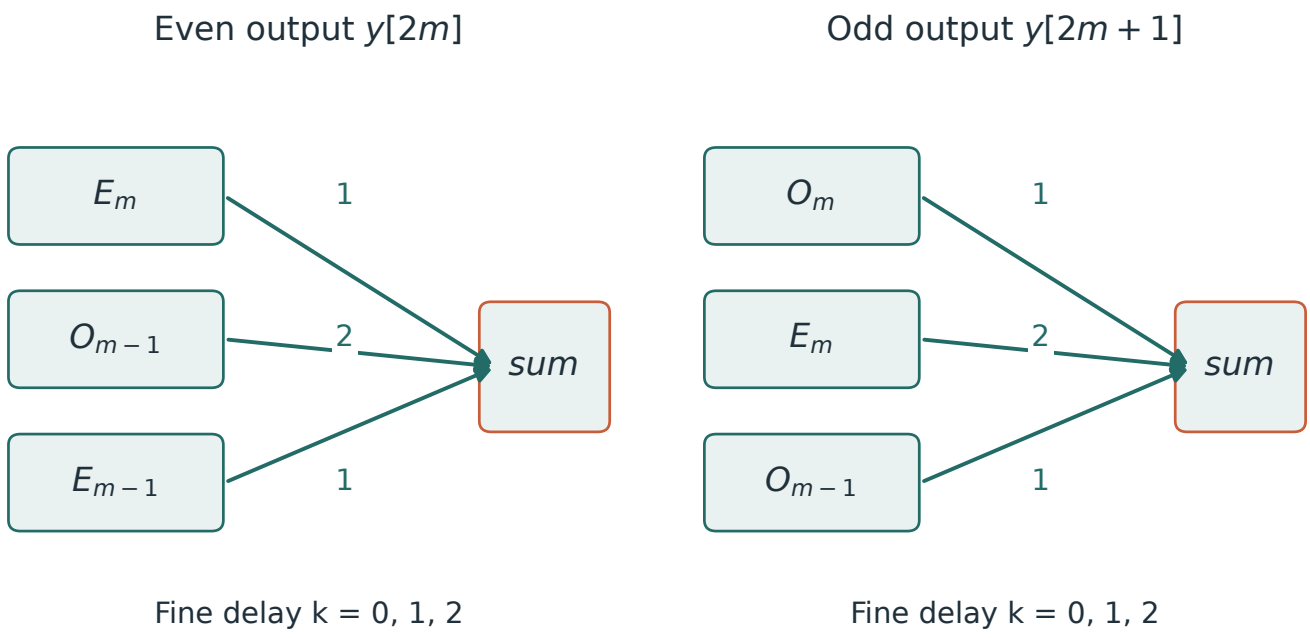
Work an example. The even output is $E_m + 2O_{m-1} + E_{m-1}$. The odd output is $O_m + 2E_m + O_{m-1}$. Summing each channel as an ordinary generating function gives the displayed matrix exactly.

Carry forward. Polyphase representation reorganizes the original convolution.

Source and scope. PSC Paper V, Theorem 4.2 and Corollary 4.5, specialized to $M = 2$ and $h = (1, 2, 1)$; new exact derivation. Rows are output phases, columns are input phases. Causal zero extension fixes the initial positions.

TAPS / T04 **LESSON 146**

Locate the delay when a tap wraps a block



$$y[2m] = E_m + 2O_{m-1} + E_{m-1}, \qquad y[2m+1] = O_m + 2E_m + O_{m-1}$$

Read the figure. Follow the middle tap in both panels. Subtracting one from the even fine index reaches the odd phase of the previous block. Subtracting one from the odd fine index reaches the even phase of the current block. That single index calculation explains the asymmetry.

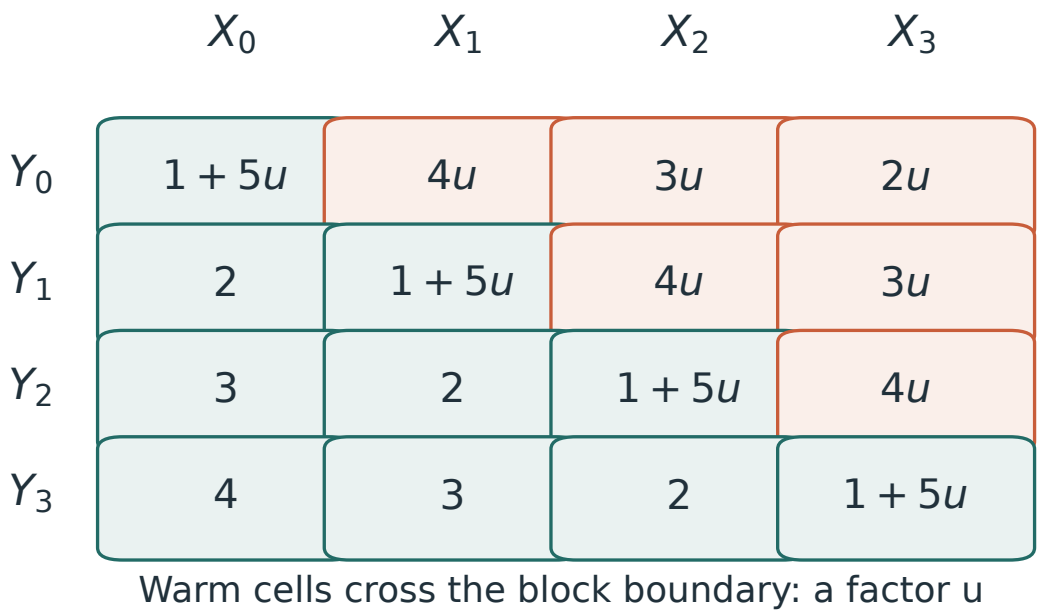
Work an example. For $m = 2$, $y[4]$ reads $x[4], x[3], x[2]$, whereas $y[5]$ reads $x[5], x[4], x[3]$. The first middle contribution has a factor u in its generating function; the second does not.

Carry forward. Assign a coarse delay only after solving the fine-index equation.

Source and scope. PSC Paper V, Theorem 4.2. New per-tap expansion of the matrix in T03. The labels E_m, O_m denote phase coefficients, while $E(u), O(u)$ denote their OGFs.

TAPS / T05 **LESSON 147**

Route a finite filter through four phases



Warm cells cross the block boundary: a factor u

$$P_{rs}(u) = \sum_{\substack{k\geq 0 \\ 0\leq Mk+r-s<L}} h[Mk+r-s]u^k, \qquad 0 \leq r,s < M$$

Read the figure. Rows are output phases and columns are input phases. For the five taps $(1,2,3,4,5)$, a same-phase contribution combines tap zero with tap four. Warm cells cross the block boundary and therefore carry one coarse delay.

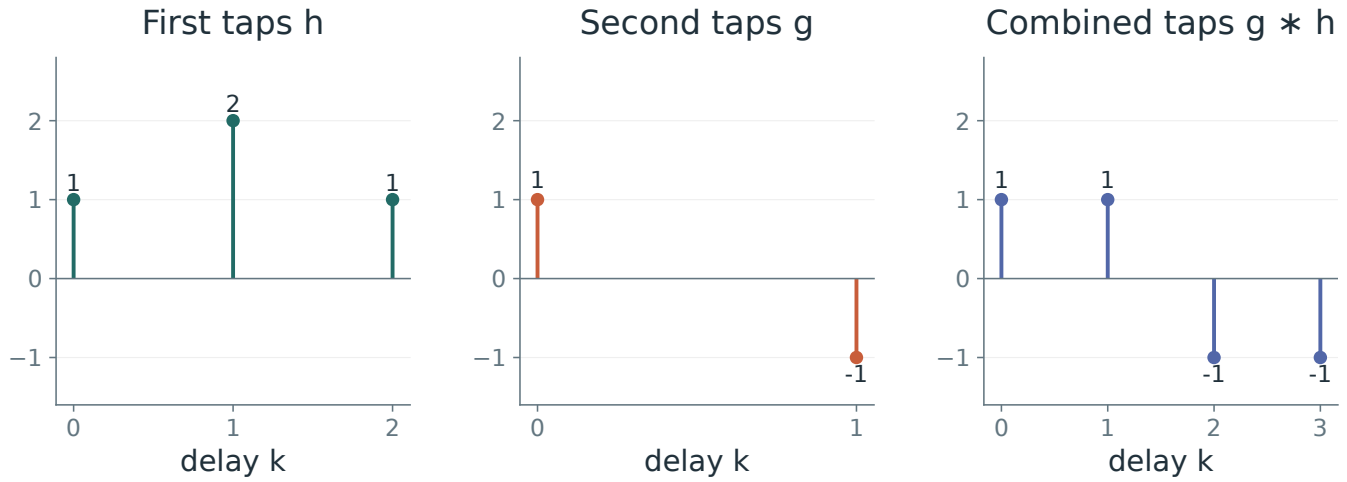
Work an example. At $M = 4$, the first row is $(1+5u, 4u, 3u, 2u)$. For example, $y[4m]$ receives $4x[4m-3] = 4X_{1,m-1}$ from tap three. That contribution belongs to column one and has coefficient $4u$.

Carry forward. The index equation supplies every matrix entry for any finite tap length.

Source and scope. PSC Paper V, Theorem 4.2, Corollary 4.5, and Example 4.6. The plotted matrix uses $M = 4, L = 5$. Exact routing also checked for moduli 2–6 and tap lengths 1–9; these finite tests verify the implementation.

TAPS / T06 **LESSON 148**

Compose filters before or after phase splitting



$$P_2(g) \cdot P_2(h) = P_2(g * h)$$

Composition is exact in either representation

$$h = (1,2,1), \quad g = (1,-1), \quad g * h = (1,1,-1,-1), \qquad P_2(g)P_2(h) = P_2(g * h)$$

Read the figure. The combined tap list is the convolution of the two finite lists. The bottom identity describes the same composition after splitting into even and odd channels. Matrix multiplication retains the delays that are easy to lose in a verbal description.

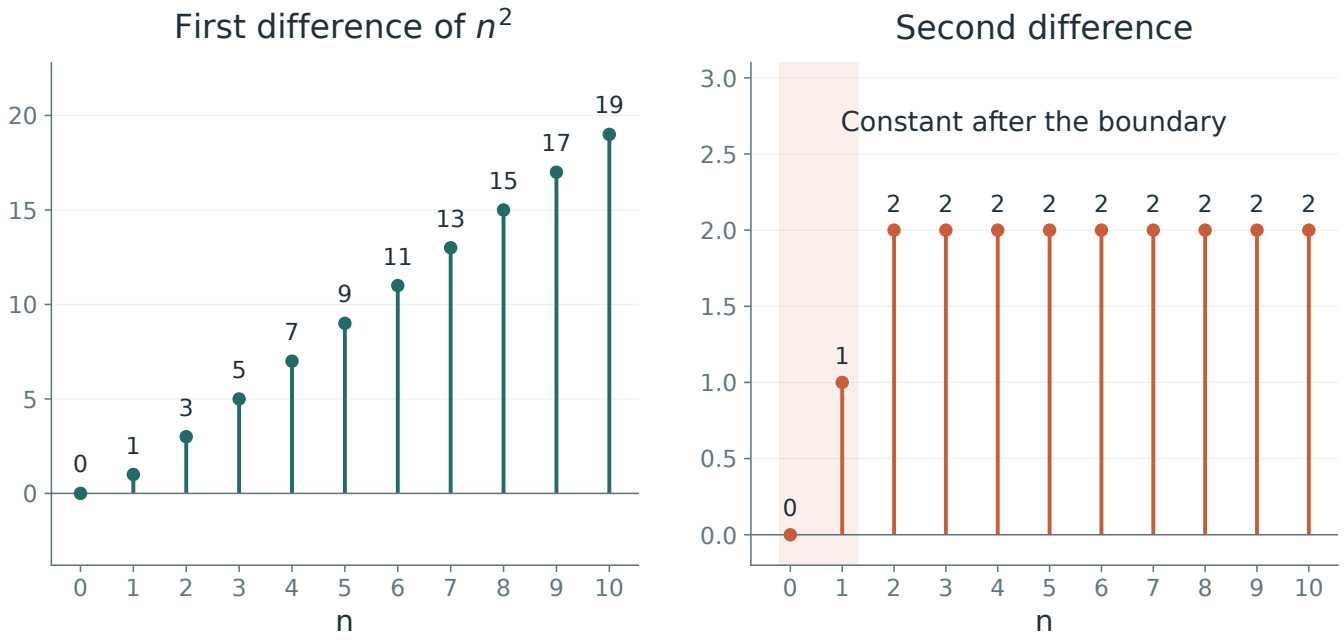
Work an example. The combined fine-delay polynomial is $(1-z)(1+2z+z^2) = 1+z-z^2-z^3$. Its two-phase matrix is $\left(\begin{smallmatrix} 1-u & u-u^2 \\ 1-u & 1-u \end{smallmatrix}\right)$, obtained independently by routing the four combined taps.

Carry forward. Composition is represented faithfully in both coefficient and phase coordinates.

Source and scope. PSC Paper V, Proposition 4.4 and Corollary 4.5; new signed-filter example. The rightmost matrix acts first. Exact polynomial convolution and exact matrix multiplication agree in the check ledger.

TAPS / T07 **LESSON 149**

Use signed taps as finite differences



$$\Delta x[n] = x[n] - x[n-1], \qquad \Delta(n^2) = 2n - 1 \ (n \geq 1), \quad \Delta^2(n^2) = 2 \ (n \geq 2)$$

Read the figure. The first signed filter turns a quadratic sequence into an increasing linear sequence. Applying it again gives a constant after the initial boundary. The shaded positions show why a polynomial identity on unrestricted integer arguments is not automatically the zero-extended causal identity at the start.

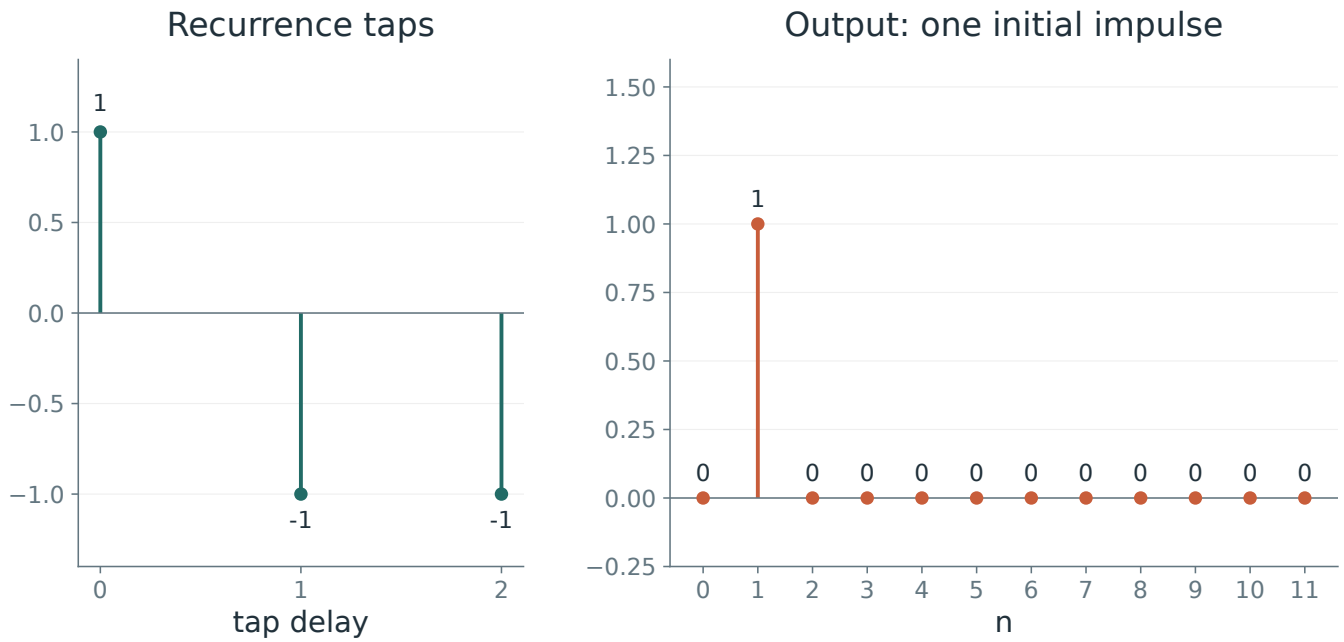
Work an example. At $n = 3$, $9 - 4 = 5$. A second difference gives $5 - 3 = 2$. At $n = 1$, the causal second difference is 1, because the missing negative-index input was defined to be zero.

Carry forward. State the boundary before calling a filter an annihilator.

Source and scope. New exact finite-difference example, tap list $(1, -1)$, input $x[n] = n^2$ for $n \geq 0$. Indices 0–10 checked exactly. This lesson does not claim a finite constant-coefficient annihilator for arbitrary sequences.

TAPS / T08 **LESSON 150**

Let recurrence taps expose initial data



$$(1 - z - z^2)F(z) = z, \qquad F(z) = \sum_{n \geq 0} F_n z^n, \qquad ((1, -1, -1) * F)[n] = \delta_{n,1}$$

Read the figure. The negative taps subtract the two previous Fibonacci values. Every recurrence position cancels, but the initial value $F_1 = 1$ survives as one impulse. The generating-function numerator records precisely that surviving initial information.

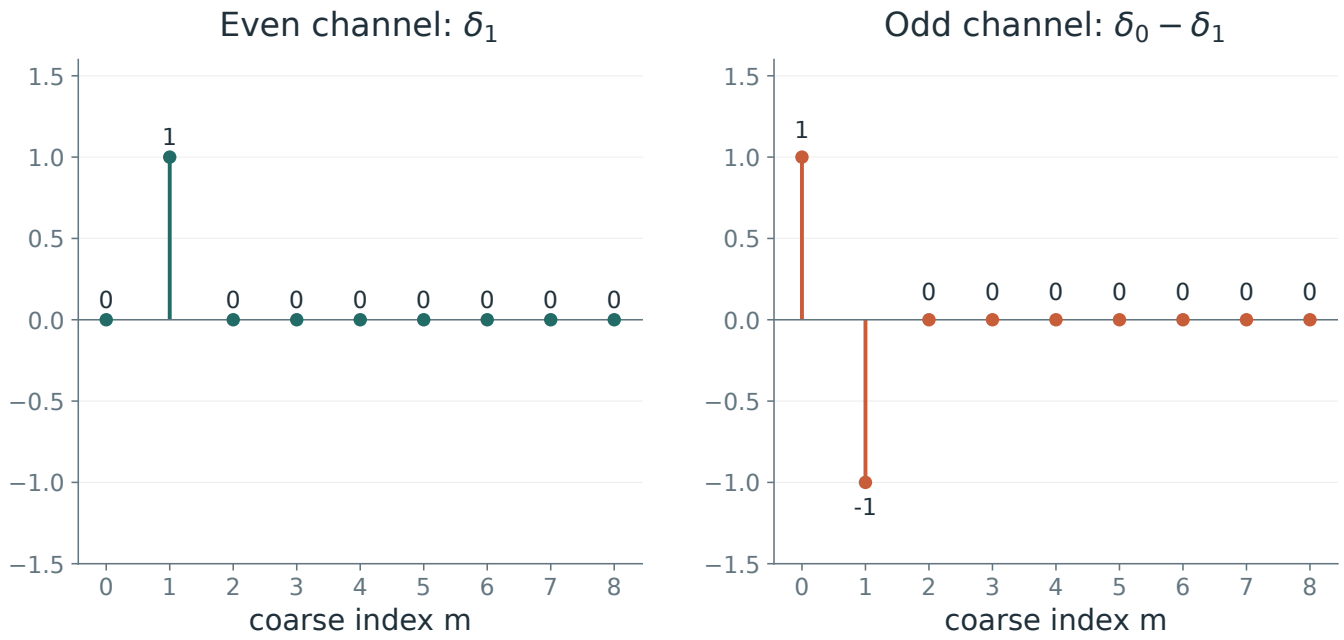
Work an example. At $n = 4, 3 - 2 - 1 = 0$. At $n = 1, 1 - 0 - 0 = 1$. Thus the filter annihilates the recurrence tail while leaving the initial impulse visible. Here $\delta_{n,j}$ is one at $n = j$ and zero otherwise.

Carry forward. An initial numerator is part of the exact recurrence representation.

Source and scope. Fibonacci recurrence with causal zero extension; new tap presentation. Twenty-four coefficients checked exactly. The polynomial $1 - z - z^2$ uses the fine-delay variable z, unlike the coarse variable u in T09.

TAPS / T09 **LESSON 151**

Give the two Fibonacci phases different numerators



$$E(u) = \frac{u}{1 - 3u + u^2}, \qquad O(u) = \frac{1 - u}{1 - 3u + u^2}, \qquad E_m = F_{2m},\ O_m = F_{2m+1}$$

Read the figure. The two phase channels share a recurrence denominator, but their initial impulses differ. Applying the taps $(1, -3, 1)$ gives one impulse in the even channel and two signed impulses in the odd channel. Those residuals are the two displayed numerators.

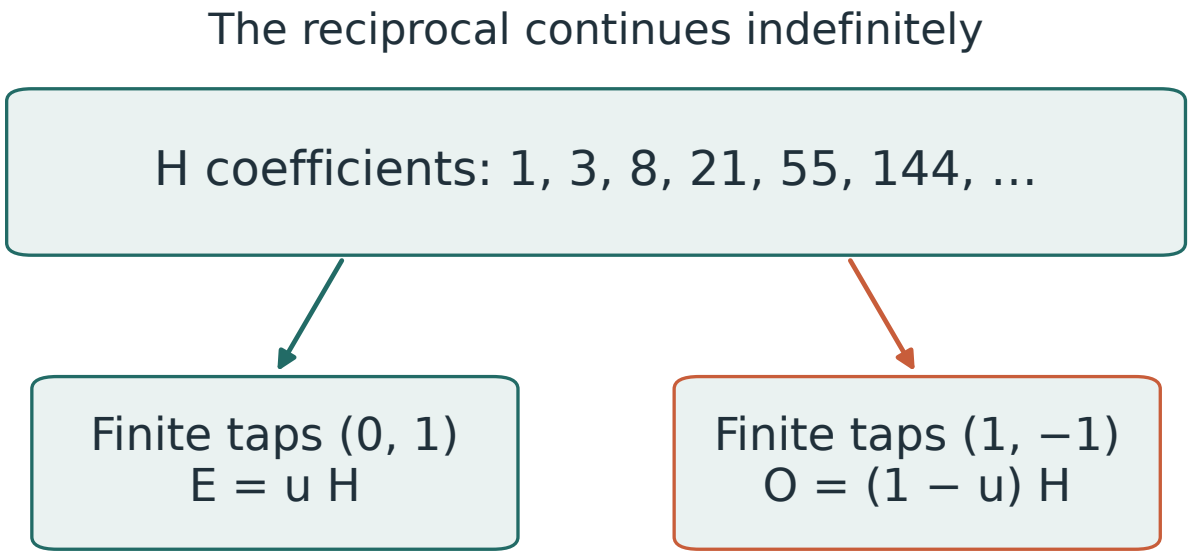
Work an example. The first even terms are $0, 1, 3, 8$, giving residuals $0, 1, 0, 0$. The first odd terms are $1, 2, 5, 13$, giving $1, -1, 0, 0$. The coarse recurrence holds from $m = 2$ onward in both channels.

Carry forward. Shared denominator does not mean identical phase initialization.

Source and scope. Fibonacci phase extraction and exact recurrence calculation. Twenty-four coefficients in each channel checked. Residual notation: δ_1 and $\delta_0 - \delta_1$ on the coarse index.

TAPS / T10 **LESSON 152**

Separate finite taps from an infinite reciprocal response



$$H(u) = \frac{1}{1 - 3u + u^2} = 1 + 3u + 8u^2 + 21u^3 + \cdots, \qquad E = uH, \quad O = (1-u)H$$

Read the figure. The long row is an infinite impulse response. The two boxes below it are finite numerator tap lists acting on that response. The denominator taps are finite too, but taking their reciprocal creates a response with infinitely many nonzero coefficients.

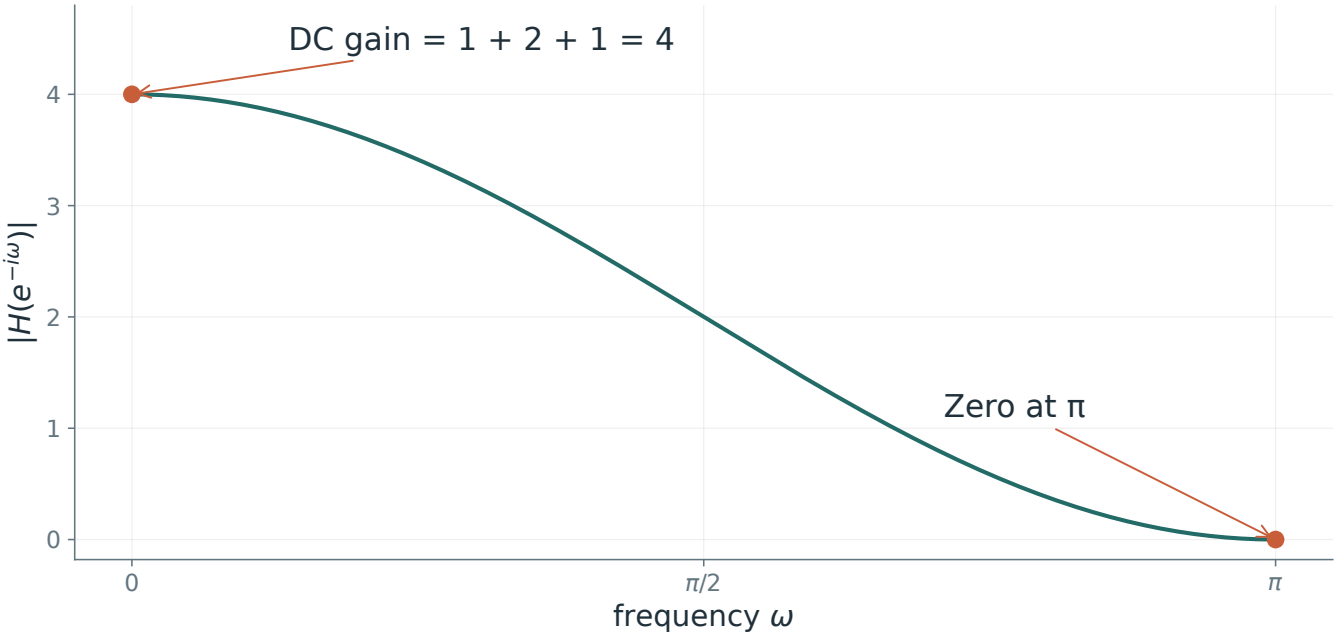
Work an example. The even numerator $(0, 1)$ shifts the response to $0, 1, 3, 8, \ldots$. The odd numerator $(1, -1)$ subtracts successive response coefficients to give $1, 2, 5, 13, \ldots$. Applying $(1, -3, 1)$ directly to H leaves δ_0.

Carry forward. Finite numerator and denominator polynomials do not make their reciprocal FIR.

Source and scope. New formal-OGF reconstruction of T09. Twenty-four coefficients checked exactly. The reciprocal identity is formal around $u = 0$; the plate makes no claim about convergence at every complex value of u.

TAPS / T11 **LESSON 153**

Read frequency response from the tap polynomial



$$H(e^{-i\omega}) = 1 + 2e^{-i\omega} + e^{-2i\omega}, \qquad |H(e^{-i\omega})| = 4\cos^2(\omega/2)$$

Read the figure. The tap polynomial becomes a frequency response by substituting a unit complex delay. Its value at zero frequency is the sum of the weights. The endpoint at π cancels because adjacent samples alternate signs there.

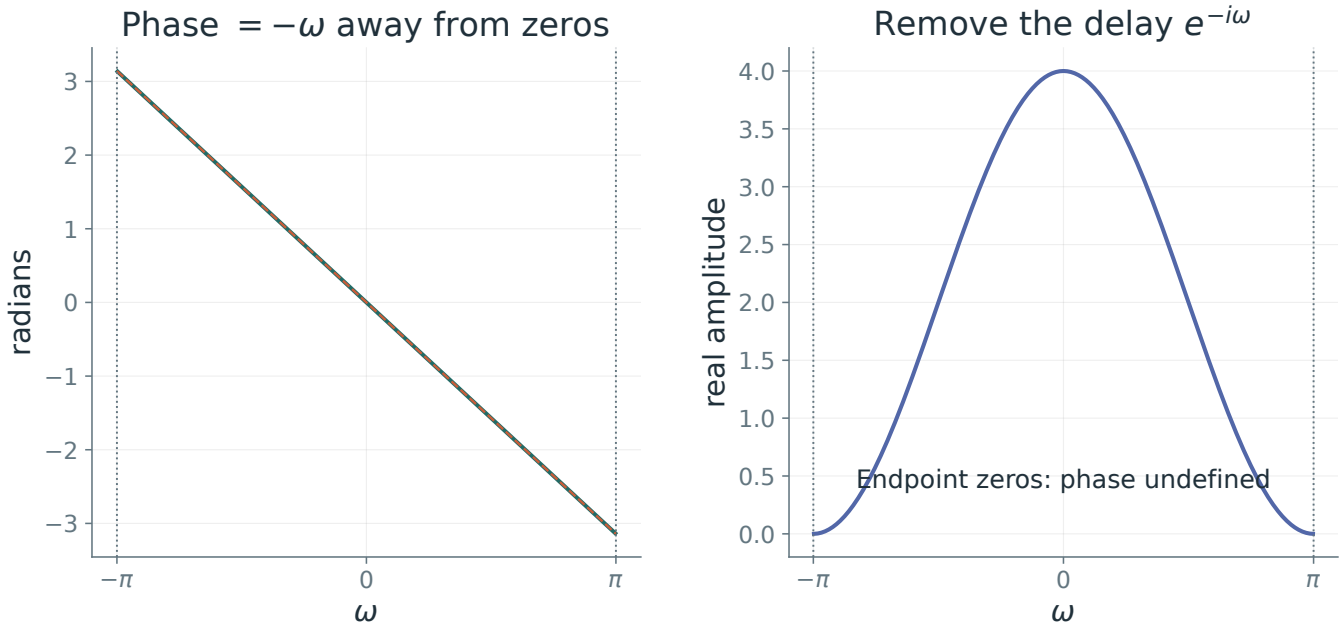
Work an example. A constant input is multiplied by $1 + 2 + 1 = 4$ away from its causal starting boundary. At $\omega = \pi$, the three contributions are $1, -2, 1$ and sum to zero. The plotted curve agrees with the exact magnitude formula on the stated grid.

Carry forward. A frequency curve describes these taps; it is not a performance guarantee.

Source and scope. New FIR frequency example. NumPy complex128 on 801 samples of $[0, \pi]$. The endpoint and DC identities are algebraic; the sampled error is recorded separately. No ideal anti-aliasing claim is made.

TAPS / T12 **LESSON 154**

Expose the delay carried by symmetric taps



$$H(e^{-i\omega}) = e^{-i\omega}(2 + 2\cos\omega), \qquad \arg H(e^{-i\omega}) = -\omega \quad (-\pi < \omega < \pi)$$

Read the figure. The symmetric taps factor into one sample of delay and a nonnegative real amplitude. Removing the delay leaves the second panel. At the endpoint zeros the complex number vanishes, so its phase is undefined rather than a meaningful continuation of the plotted straight line.

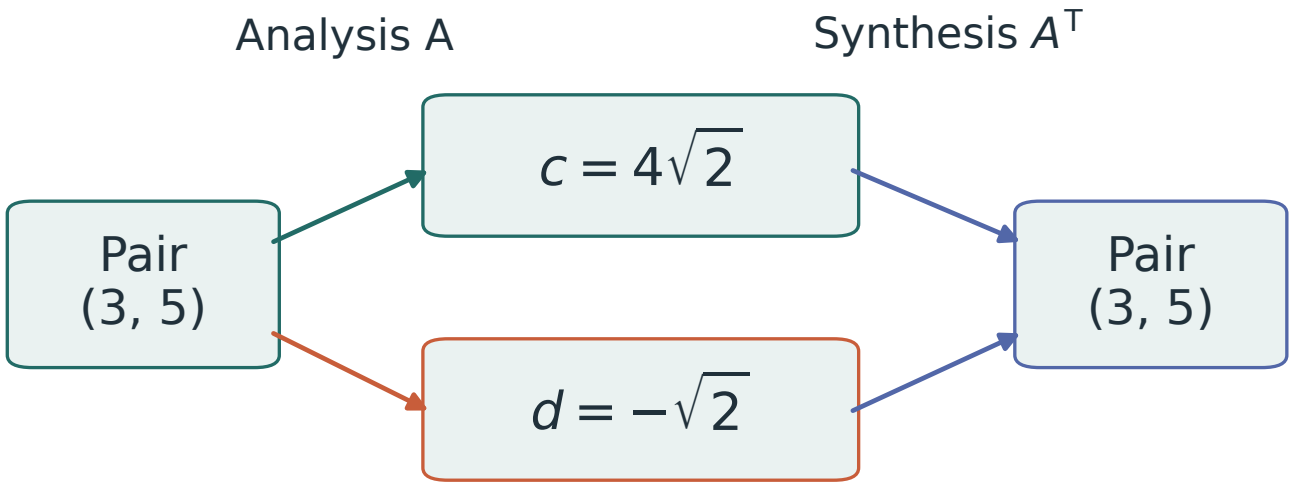
Work an example. At $\omega = \pi/2$, the amplitude is 2 and the delayed response is $-2i$. More generally, a symmetric list of length L factors a delay $(L-1)/2$; the remaining real factor may change sign, introducing phase jumps.

Carry forward. Linear phase needs its sign and zero conventions stated.

Source and scope. New symmetric FIR example. The displayed formula is exact. The numerical phase check uses 801 interior samples and excludes $\pm\pi$. A phase value supplied by floating-point arithmetic at a zero is not used as evidence.

TAPS / T13 **LESSON 155**

Reconstruct exactly with Haar analysis and synthesis



$$c = (3+5)/\sqrt{2}, \quad d = (3-5)/\sqrt{2}$$

$$A = \frac{1}{\sqrt{2}}\begin{pmatrix} 1 & 1 \\ 1 & -1 \end{pmatrix}, \qquad \begin{pmatrix} c_m \\ d_m \end{pmatrix} = A \begin{pmatrix} x[2m] \\ x[2m+1] \end{pmatrix}, \qquad A^{\mathsf{T}}A = I$$

Read the figure. Analysis combines one nonoverlapping pair into a normalized sum and difference. Synthesis reverses that change of coordinates. This plate fixes the pair convention explicitly, avoiding the extra shifts that appear under other convolution-and-decimation conventions.

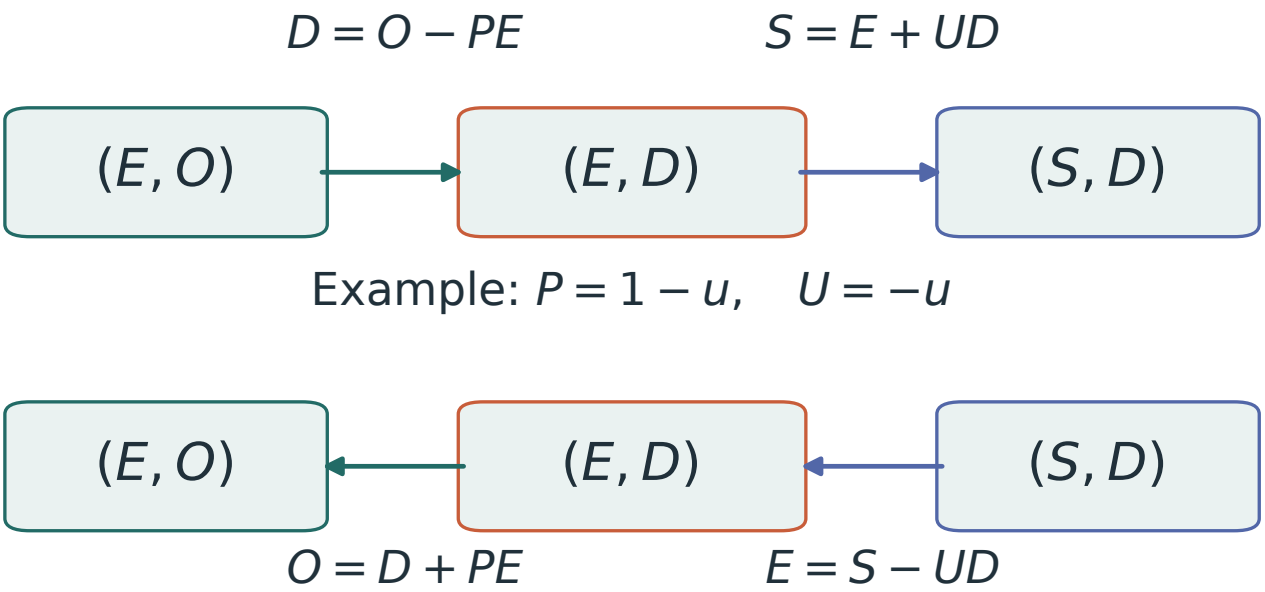
Work an example. The pair $(3,5)$ gives $(c,d) = (4\sqrt{2}, -\sqrt{2})$. Reconstruction yields $((c+d)/\sqrt{2}, (c-d)/\sqrt{2}) = (3,5)$. Both the normalization and the difference sign are necessary.

Carry forward. Perfect reconstruction is an operator identity with a fixed convention.

Source and scope. Standard Haar pair transform, independently verified by direct matrix algebra. Exact sum/difference witnesses cover all 121 integer pairs in $[-5,5]^2$, with the common square-root factor canceled symbolically.

TAPS / T14 **LESSON 156**

Reverse signed prediction and update steps



$$D = O - PE, \quad S = E + UD, \qquad E = S - UD, \quad O = D + PE$$

Read the figure. Forward lifting first predicts the odd channel from the even channel, then updates the even channel using the residual. Reverse lifting undoes those two steps in the opposite order. Neither step needs an inverse filter for P or U.

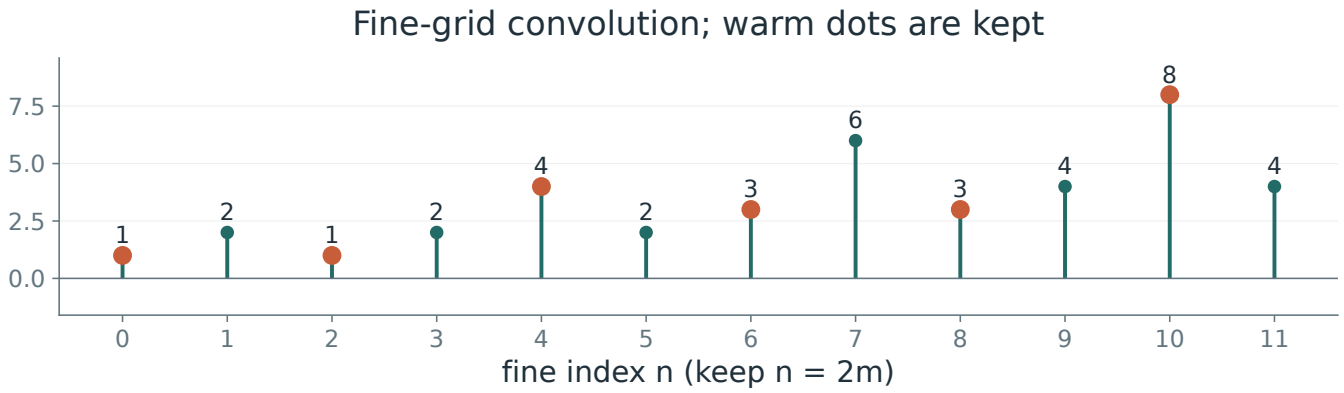
Work an example. Use the signed causal taps $P = 1 - u$ and $U = -u$. The combined matrix is $\left(\begin{smallmatrix} 1+u-u^2 & -u \\ -1+u & 1 \end{smallmatrix}\right)$ and has determinant one. Any finite predict and update polynomials admit the displayed algebraic reversal.

Carry forward. Invertibility comes from the triangular steps, not from a special predictor.

Source and scope. New exact lifting example over rational coefficients. Negative coarse indices are zero in both directions. Sixteen signed filter-pair witnesses checked with integers and fractions. Streaming use must retain the histories needed by both filters.

TAPS / T15 **LESSON 157**

Resample at rate three over two by exact routing



output m	0	1	2	3	4	5
phase r	0	2	1	0	2	1
input ℓ	0	0	1	2	2	3
tap weight	1	1	2	1	1	2
output y[m]	1	1	4	3	3	8

$$y[m] = \sum_n h[2m - 3n]x[n] = \sum_{k \geq 0} h_{r_m}[k]x[\ell_m - k],$$
$$r_m = 2m \bmod 3, \quad \ell_m = \lfloor 2m/3 \rfloor$$

Read the figure. First insert two zeros between input samples, convolve on the fine grid, and keep every second result. The table expresses those same kept values through three tap phases: $h_r[k] = h[3k + r]$. The phase selector changes with the output index.

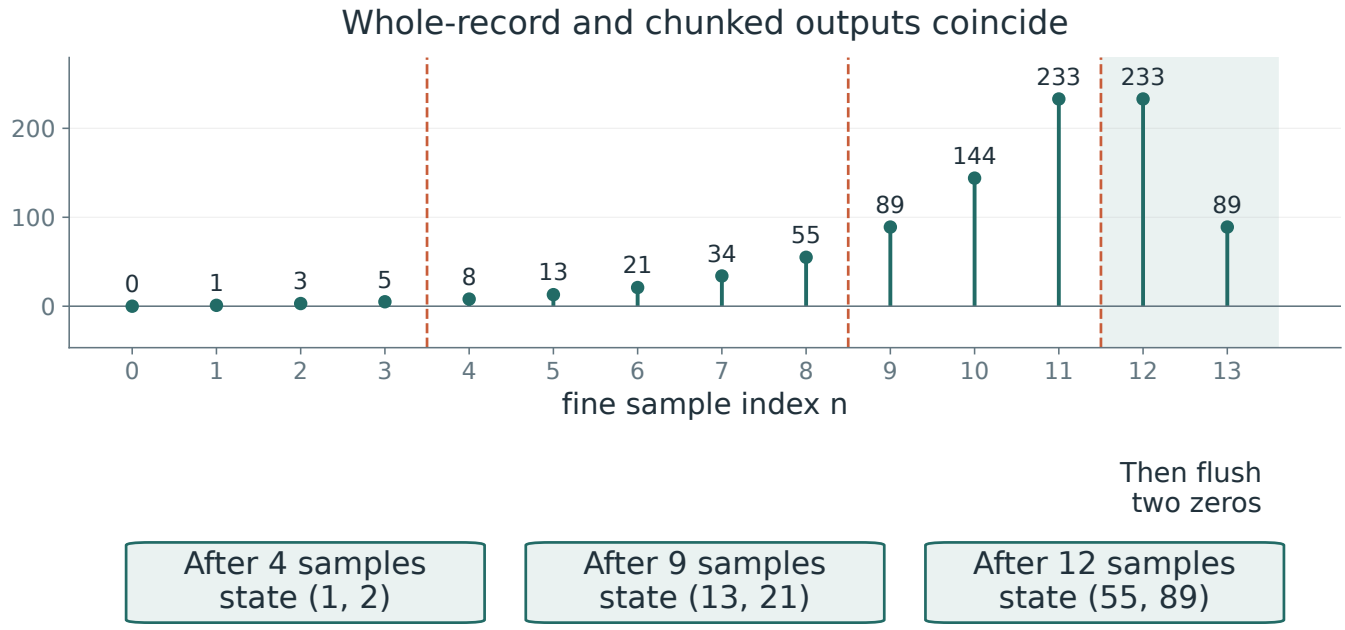
Work an example. For $x = (1, 2, 3, 4)$ and $h = (1, 2, 1)$, the selected phases are $0, 2, 1, 0, 2, 1$. The six outputs are $(1, 1, 4, 3, 3, 8)$. Each method includes the full finite convolution tail.

Carry forward. Rational rate conversion can be implemented without materializing inserted zeros.

Source and scope. New small-filter 3/2 example. Exact zero insertion, convolution, downsampling, and phase routing agree. The filter demonstrates indexing only; no passband, stopband, or alias-suppression specification is claimed.

TAPS / T16 **LESSON 158**

Carry the needed state across chunk boundaries



direct-form FIR state: $L-1$ previous input samples, $\quad y_{\text{chunks}}[n] = y_{\text{whole}}[n]$

Read the figure. The dashed lines mark chunk boundaries, not restarts of the filter. The lower boxes hold the two input samples needed by the next chunk. The shaded tail is produced by an explicit two-zero flush after the final real sample.

Work an example. For $(1, 2, 1)$, after twelve Fibonacci samples the saved state is $(55, 89)$, oldest first. Feeding zero twice produces tail outputs 233 and 89. Resetting state at an interior chunk boundary would lose delayed contributions.

Carry forward. Boundary handling is part of the mathematical execution contract.

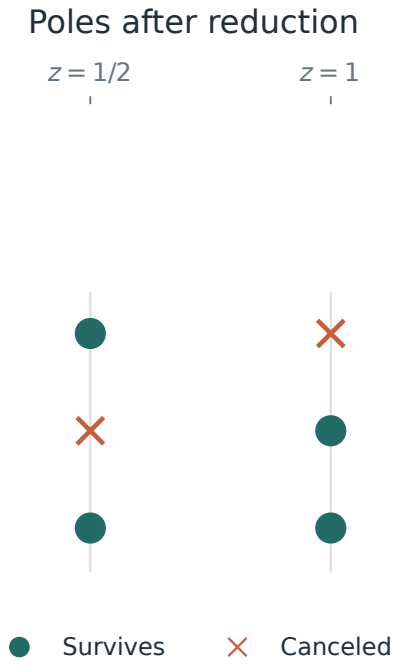
Source and scope. New direct-form FIR streaming example. Twenty signed-filter cases cover lengths 1–5, four chunk partitions, and complete flushed tails. The $L-1$ rule describes this implementation, rather than a universal lower bound on every filter realization.

BRIDGE / 01 **LESSON 159**

Seeds choose which modes survive

Same recurrence, different seeds

Seeds	Numerator	Coefficients
(1, 2)	$1 - z$	2^n
(1, 1)	$1 - 2z$	1
(0, 1)	z	$2^n - 1$



$$a_{n+2} = 3a_{n+1} - 2a_n, \qquad A(z) = \frac{a_0 + (a_1 - 3a_0)z}{(1 - z)(1 - 2z)}$$

Read the figure. Every row uses the same recurrence denominator. The seeds change its numerator, which can cancel a denominator factor. Filled marks are poles that remain after reducing the rational function; crosses mark factors that cancel. The two candidate modes are 1 and 2^n.

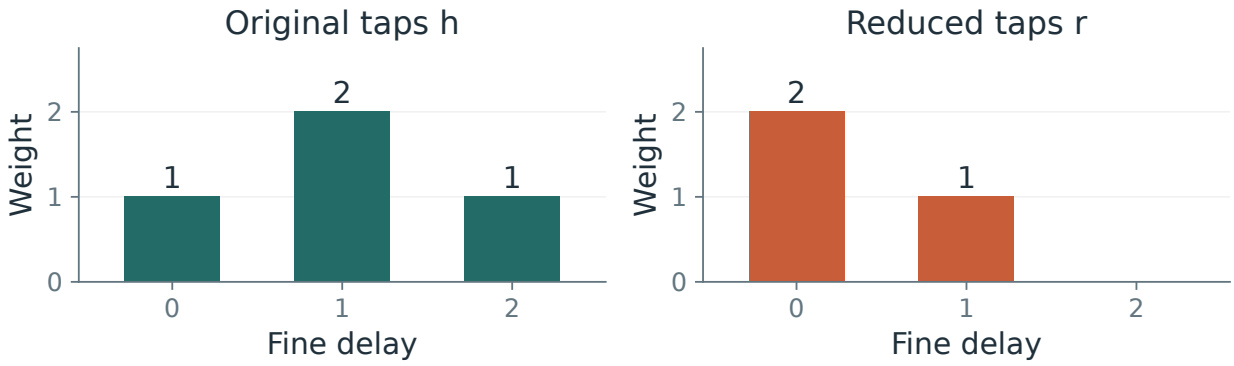
Work an example. Seeds $(1, 2)$ give numerator $1 - z$, leaving $A(z) = 1/(1 - 2z)$ and coefficients 2^n. Seeds $(1, 1)$ instead cancel $1 - 2z$, leaving the constant sequence. Seeds $(0, 1)$ retain both modes and give $2^n - 1$.

Carry forward. A recurrence denominator lists candidate modes. The numerator determines which are present in the specified sequence.

Source and scope. New elementary rational-series example, $n \geq 0$. Numerator residuals and all three mode formulas are checked through index eighteen. Cancellations are exact; this is not a robustness claim for perturbed seeds or hidden states.

BRIDGE / 02 **LESSON 160**

Compile taps against an exact recurrence



	0	1	2	3	4	5	6	7
Three taps	0	1	3	5	8	13	21	34
Two taps	0	2	3	5	8	13	21	34
Correction	0	-1	0	0	0	0	0	0
Corrected	0	1	3	5	8	13	21	34

$$D = 1 - z - z^2, \quad F = z/D, \quad h = (1+z)^2 = (2+z) - D,$$
$$hF = (2+z)F - z$$

Read the figure. The top panels compare the original three taps with a shorter list. The table shows why the shorter list needs an initial correction: its output differs at index one. Subtracting that impulse makes every coefficient agree, including the causal boundary. Here $F_n = 0$ for $n < 0$.

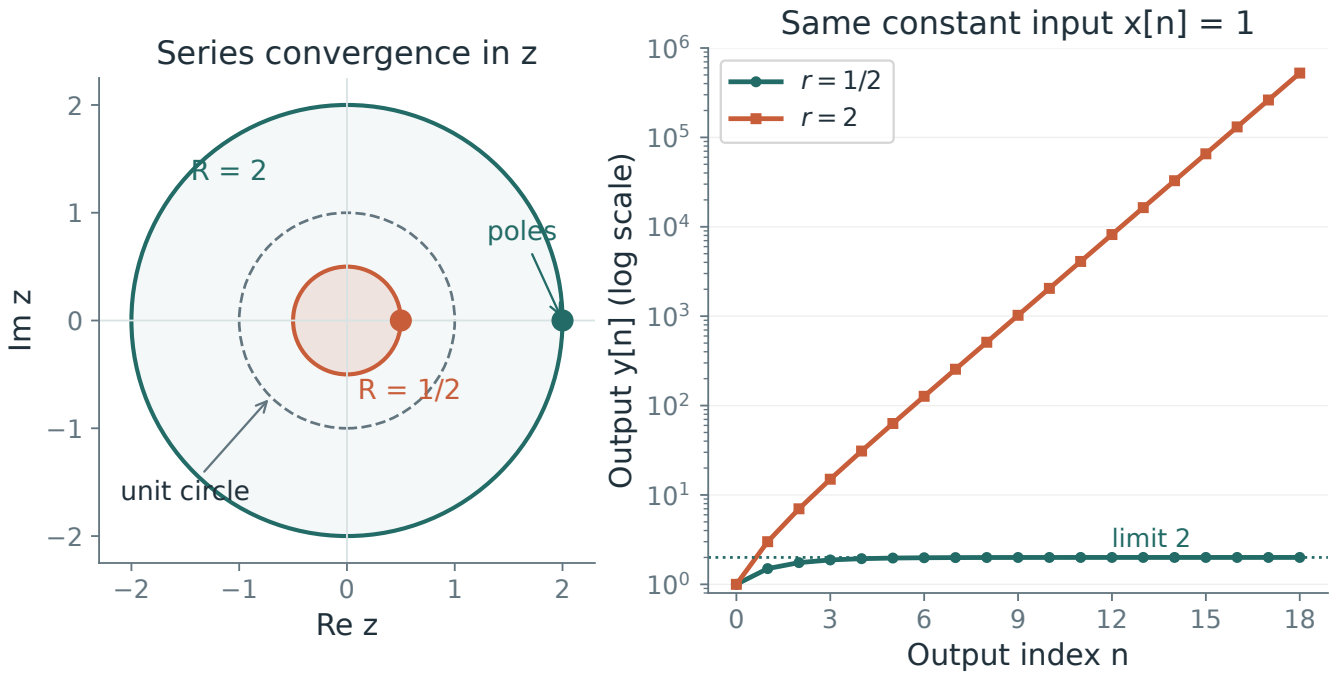
Work an example. The reduced formula is $y_n = 2F_n + F_{n-1} - \delta_{n,1}$. At $n = 1$, it gives $2 - 1 = 1$; at $n = 5$, it gives $2 \cdot 5 + 3 = 13$. If $DF = N$ and polynomial division gives $h = qD + r$, then $hF = rF + qN$.

Carry forward. The recurrence can simplify an operator while its numerator carries the remaining boundary contribution.

Source and scope. OEIS A000045, $F_0 = 0, F_1 = 1$, with new exact polynomial algebra. The coefficient check runs through index eighteen; finite-input tails are checked with $N = DF$, including terminal residuals. The reduction is for this recurrence input; it does not replace the original filter on arbitrary signals.

BRIDGE / 03 **LESSON 161**

A formal reciprocal need not be a stable filter



$$H_r(z) = \frac{1}{1 - rz} = \sum_{n \geq 0} r^n z^n, \qquad |z| < 1/|r| \quad (r \neq 0)$$

Read the figure. The disks show where each causal series converges. The dashed unit circle lies inside the disk for $r = 1/2$ and outside it for $r = 2$. The right panel applies both responses to the same bounded input $x[n] = 1$ and uses a logarithmic output axis.

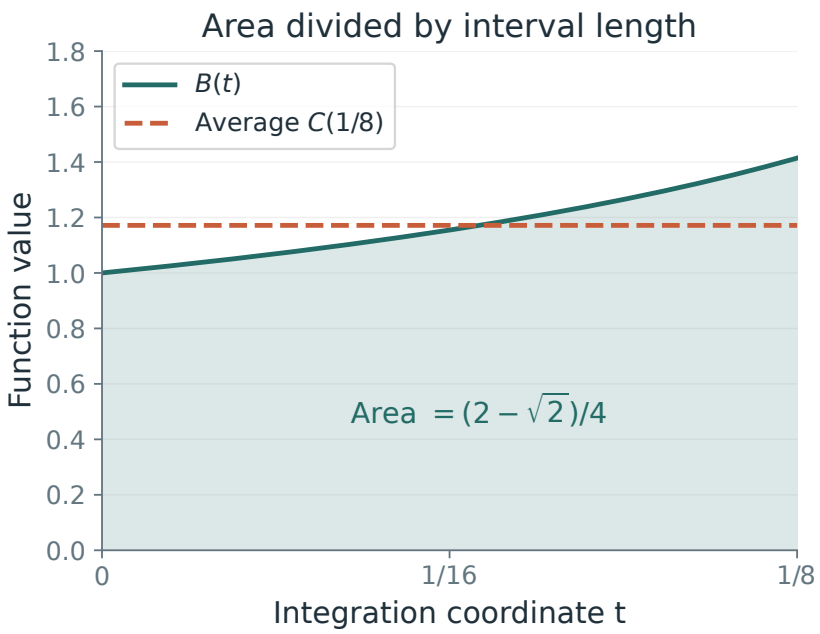
Work an example. For $r = 1/2$, $y_n = 2 - 2^{-n}$ tends to two, and every bounded input satisfies $|y_n| \leq 2\|x\|_\infty$. For $r = 2$, $y_n = 2^{n+1} - 1$ grows without bound even though the input stays one.

Carry forward. A formal-series identity, an analytic convergence domain, and bounded-input stability have distinct contracts.

Source and scope. New causal geometric-response examples, $n \geq 0$, with zero input at negative indices. Exact rational convolutions checked through index eighteen. The unstable rational expression can be evaluated on the unit circle, but its causal Fourier series there does not converge.

BRIDGE / 04 **LESSON 162**

Coefficient division becomes an area average



Integration divides by the new exponent

n	b(n)	÷(n + 1)	c(n)
0	1	1	1
4	70	5	14
5	252	6	42

C(0) = 1 by removal

$$B(z) = \frac{1}{\sqrt{1-4z}}, \qquad C(z) = \frac{1}{z}\int_0^z B(t)\,dt = \frac{1-\sqrt{1-4z}}{2z}$$

Read the figure. The shaded area under the central-binomial generating function is divided by the interval length. The dashed line is that average, the Catalan generating function at $z = 1/8$. The table shows the coefficient operation: integrating raises the exponent and divides by $n+1$; dividing by z restores its address.

Work an example. At index four, $70z^4$ integrates to $14z^5$, then becomes $14z^4$ after division by z. At $z = 1/8$, the area is $(2-\sqrt{2})/4$, so its average is $4-2\sqrt{2}$.

Carry forward. An index-dependent coefficient normalization can come from a familiar continuous operator.

Source and scope. OEIS A000984 and A000108; new elementary integral derivation. The square-root branch equals one at zero, $C(0) = 1$ by removal, and the analytic identities hold on $|z| < 1/4$. Coefficient identities also hold over formal rational series; exact checks cover indices zero through eighteen.

OPERATOR / 01 **LESSON 163**

Transport the operator with the normalization

Same stationary taps act in different coefficient coordinates

	n = 0	n = 1	n = 2	n = 3	n = 4	n = 5
Counts a_n	1	1	1	1	1	1
Count FIR $(Ha)_n$	1	0	0	0	0	0
Taylor $b_n = (Na)_n$	1	1	1/2	1/6	1/24	1/120
Taylor FIR $(Hb)_n$	1	0	-1/2	-1/3	-1/8	-1/30
Pullback $(N^{-1}HNa)_n$	1	0	-1	-2	-3	-4

Count FIR EGF: 1 | Taylor FIR series: $(1-z)e^z$

$$(Na)_n = \frac{a_n}{n!}, \qquad (Hb)_n = \sum_{k=0}^{\min(K,n)} h_k b_{n-k},$$

$$(N^{-1}HNa)_n = \sum_{k=0}^{\min(K,n)} h_k (n)_k a_{n-k}, \qquad (n)_k = \frac{n!}{(n-k)!}$$

Read the figure. The same stationary taps $(1,-1)$ are applied in two different coefficient coordinates. The top pair uses integer counts; the middle pair uses Taylor coefficients. Returning the latter output to count coordinates gives the bottom row. Its operator has index-dependent weights, rather than the original stationary taps.

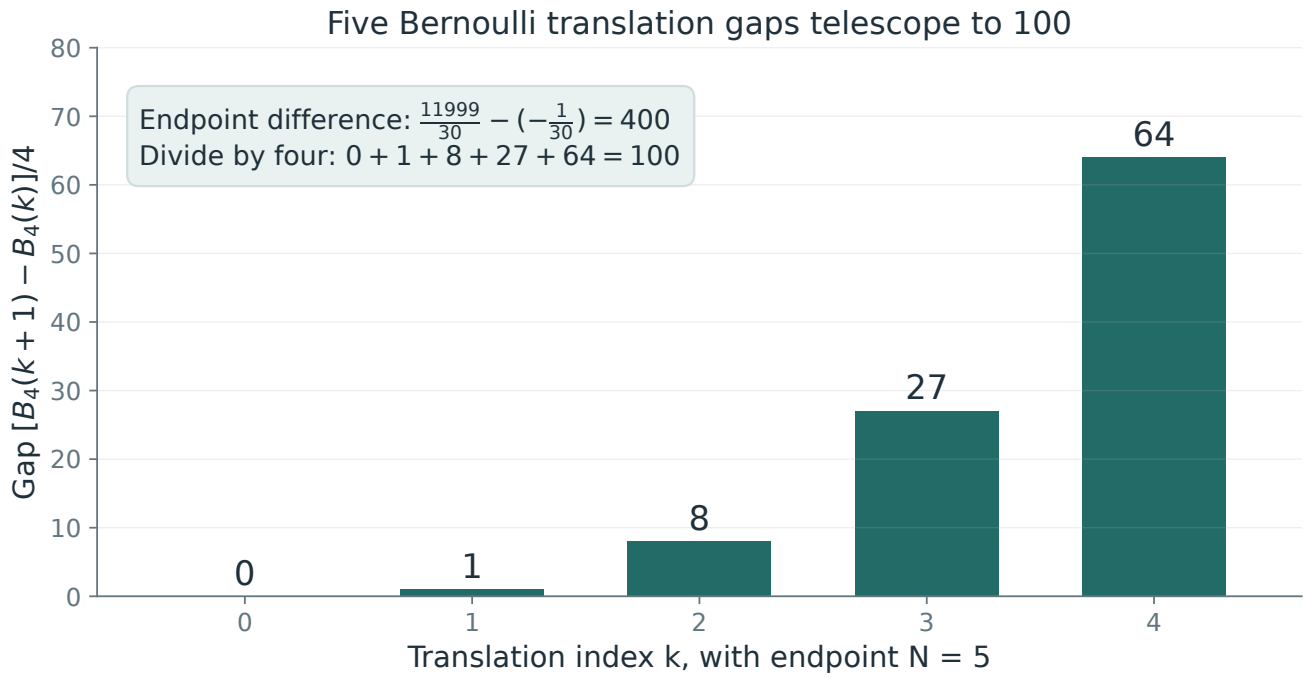
Work an example. Start with $a_n = 1$ for all $n \geq 0$, so $b_n = 1/n!$ and the EGF is e^z. Filtering the counts gives $(1,0,0,\ldots)$ and EGF 1. Filtering the Taylor coefficients gives $(1-z)e^z$. Its count coordinates are $1-n$, beginning $1,0,-1,-2,\ldots$.

Carry forward. A stationary Taylor FIR pulls back to counts as $N^{-1}HN$. Applying the same stationary weights in both coordinates is a different operation.

Source and scope. Exact formal coefficient identity over $\mathbb{Q}$, $\mathbb{R}$, or $\mathbb{C}$; $n, K \geq 0$ are integers and $h_0, \ldots, h_K$ are finite taps. Counts transported in the opposite direction use NHN^{-1} with weights $h_k/(n)_k$ for $n \geq k$. Prefixes are not finite input cutoffs.

OPERATOR / 02 **LESSON 164**

Bernoulli resolves a discrete antiderivative



$$B_4(x) = x^4 - 2x^3 + x^2 - \frac{1}{30}, \qquad B_4(x+1) - B_4(x) = 4x^3,$$
$$\frac{B_4(N) - B_4(0)}{4} = \sum_{k=0}^{N-1} k^3 \qquad (N \geq 0)$$

Read the figure. Each bar is a forward translation gap divided by four. The taps compare the polynomial at arguments $k+1$ and k; they do not shift its order or its Taylor-coefficient index. Adding the five visible gaps cancels all interior endpoint values. The two remaining Bernoulli endpoints determine the sum.

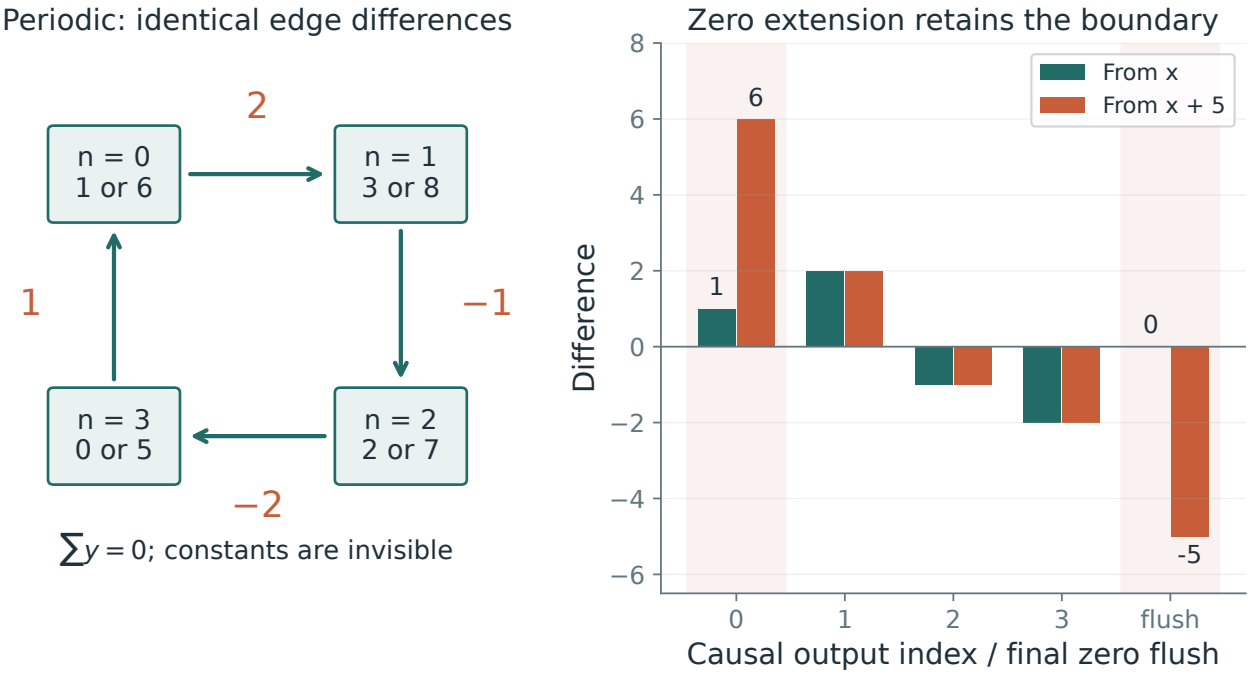
Work an example. For $N = 5$, the gaps are $0, 1, 8, 27, 64$, totaling 100. Also $B_4(5) = 11999/30$ and $B_4(0) = -1/30$, so their difference is 400. Division by four recovers exactly the same sum.

Carry forward. Translation taps can turn a special function into an exact discrete primitive. Its additive constant disappears under differencing.

Source and scope. Bernoulli-polynomial normalization from Paper I and sequence lesson S11, with $B_1 = -1/2$. Expanding the stated polynomial proves its difference identity for every real or complex x; telescoping proves the integer sum. Exact sample checks cover $0 \leq N \leq 50$.

OPERATOR / 03 **LESSON 165**

The boundary changes what an inverse can recover



$$D_{\mathrm{per}}x[n] = x[n] - x[(n-1) \bmod 4], \quad \ker D_{\mathrm{per}} = \langle \mathbf{1} \rangle, \quad \operatorname{im} D_{\mathrm{per}} = \left\{ y : \sum_{n=0}^{3} y[n] = 0 \right\}$$

Read the figure. The periodic cycle places two possible amplitudes at every node. Both inputs give the same edge differences because adding a constant changes no periodic difference. The causal panel uses the same taps $(1, -1)$ with zero extension. Its initial output and flushed tail retain the boundary information.

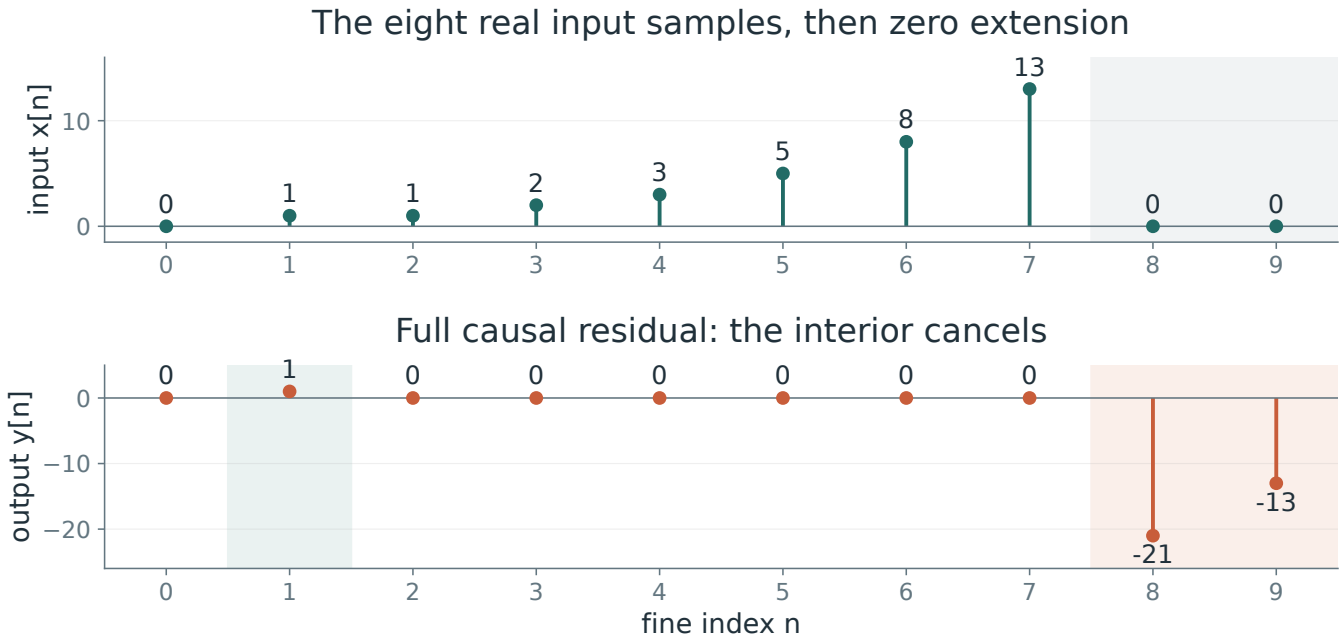
Work an example. The four-value inputs $(1, 3, 2, 0)$ and $(6, 8, 7, 5)$ both have periodic output $(1, 2, -1, -2)$. Their causal outputs, including one zero flush, are $(1, 2, -1, -2, 0)$ and $(6, 2, -1, -2, -5)$. In the periodic problem, fixing $x[0] = 1$ reconstructs the first input uniquely.

Carry forward. A periodic inverse requires zero-sum output and one initial value. Causal summation instead recovers the zero-extended input from its full difference stream.

Source and scope. Exact four-periodic linear algebra over $\mathbb{Q}$ or $\mathbb{R}$. In the causal panel each four-value vector is zero outside indices 0–3; adding five affects those stored values only. Equal periodic differences force a constant difference, while telescoping gives the zero-sum condition.

CAPSTONE / 01 **LESSON 166**

A finite record leaves endpoint impulses



$$(1 - z - z^2)P_N(z) = z - F_N z^N - F_{N-1} z^{N+1}, \qquad N \geq 2$$

Read the figure. The record is $x = (0, 1, 1, 2, 3, 5, 8, 13)$ at indices zero through seven, with zero elsewhere. Apply the causal taps $(1, -1, -1)$ and retain all ten output positions. The green strip marks the surviving seed. The warm strip marks the two impulses created by ending the record.

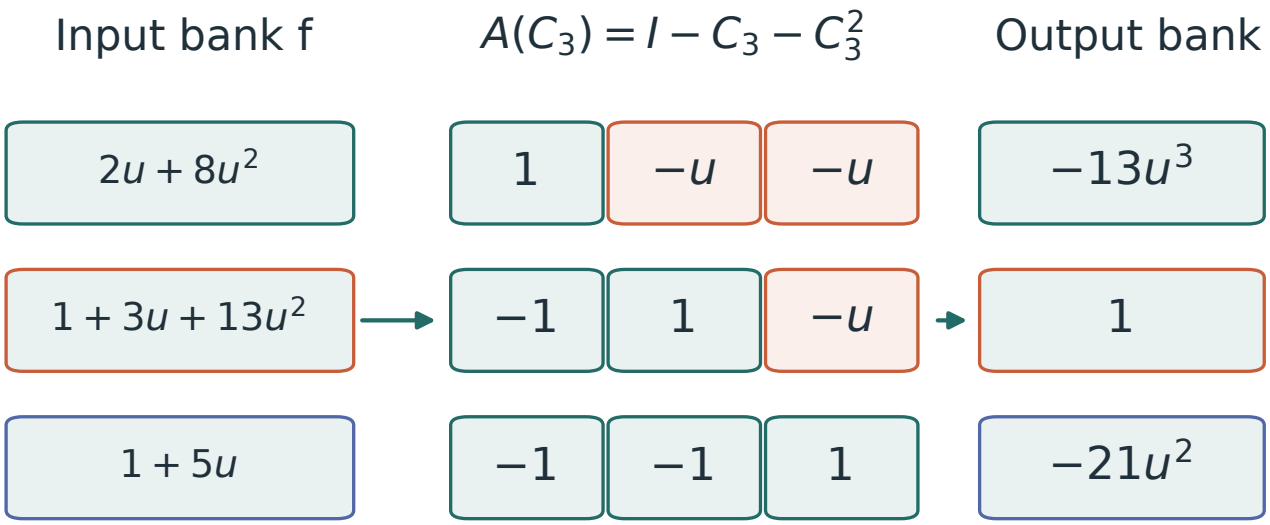
Work an example. Write $P_8(z) = \sum_{n=0}^{7} F_n z^n$. Interior coefficients cancel by the Fibonacci recurrence. At index eight, the input has ended, so the output is $0 - 13 - 8 = -21$. At index nine it is $0 - 0 - 13 = -13$. Thus the complete output is $z - 21z^8 - 13z^9$.

Carry forward. A finite cutoff has a boundary residual even when every interior recurrence step is exact.

Source and scope. Direct coefficient derivation, $P_N = \sum_{n=0}^{N-1} F_n z^n$, $F_0 = 0, F_1 = 1$. OEIS A000045 supplies the record. Exact finite checks cover $N = 2$–20; the displayed general identity follows by collecting coefficients, not by extrapolating those checks.

CAPSTONE / 02 **LESSON 167**

Transfer the whole residual into three channels



$$A(C_3) = \begin{pmatrix} 1 & -u & -u \\ -1 & 1 & -u \\ -1 & -1 & 1 \end{pmatrix}, \qquad A(C_3)f = \begin{pmatrix} -13u^3 \\ 1 \\ -21u^2 \end{pmatrix}$$

Read the figure. Split the same eight input values into residues zero, one, and two. Each box holds an ordinary generating polynomial in the internal index. The matrix represents $A(z) = 1 - z - z^2$. Its factors of u retain the coarse delay when a fine tap crosses a block boundary. Rows are output phases; columns are input phases.

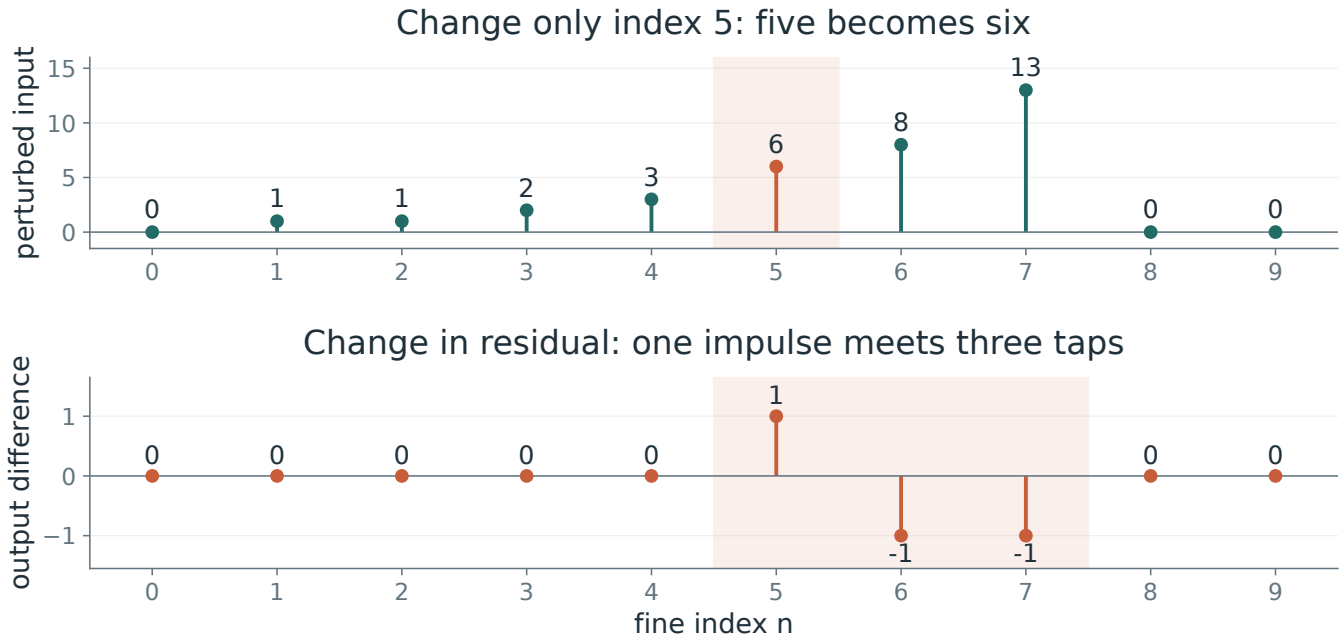
Work an example. The input bank is $f = (2u + 8u^2, 1 + 3u + 13u^2, 1 + 5u)^T$. In row zero, subtracting u times the other two channels leaves $-13u^3$. Synthesis of the output bank gives $-13z^9 + z - 21z^8$, precisely the scalar output in C01.

Carry forward. Scalar filtering and full packet filtering agree, including the endpoint impulses.

Source and scope. Direct carry calculation, $A(C_3) = I - C_3 - C_3^2$, with $u = z^3$ under synthesis. Exact integer polynomial arithmetic checks the complete three-channel result and all ten synthesized output coefficients. No channel is discarded.

CAPSTONE / 03 **LESSON 168**

An interior perturbation has its own signature



$$Q = P_8 + z^5, \qquad A(z)(Q - P_8) = z^5 - z^6 - z^7$$

Read the figure. Change only the sample at index five from five to six. The top row shows that changed record. The bottom row shows the change in the filtered output, not the full output. A single input impulse meets three taps and therefore changes three consecutive residual positions. The seed and endpoint residuals stay unchanged.

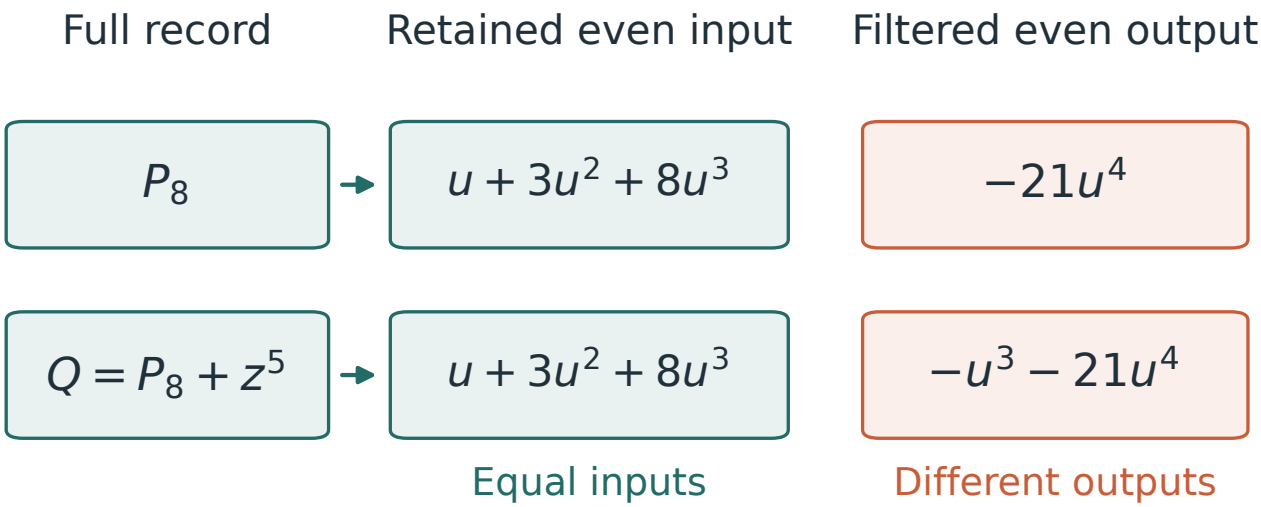
Work an example. At index five, the perturbed output is $6 - 3 - 2 = 1$. At index six it is $8 - 6 - 3 = -1$, and at index seven it is $13 - 8 - 6 = -1$. The full output becomes $z + z^5 - z^6 - z^7 - 21z^8 - 13z^9$.

Carry forward. Distinguish an interior model defect from the declared finite-record boundary.

Source and scope. Exact one-sample perturbation experiment over the integers. The identity follows by linearity of multiplication by $A(z)$. This example identifies the consequences of its specified change; an arbitrary residual alone does not decide whether data or an assumed recurrence model is wrong.

CAPSTONE / 04 **LESSON 169**

A discarded channel returns through the next operation



The discarded odd coefficient re-enters an even output.

$$\mathcal{R}_{2,0}(Q - P_8) = 0, \qquad \mathcal{R}_{2,0}\big(A(z)(Q - P_8)\big) = -u^3$$

Read the figure. Switch from C02's three-phase bank to the modulus-two observation retaining even indices only. The two records from C03 have identical observed inputs. After the same filter, their even outputs differ at index six. A contribution from the discarded odd sample has crossed into a retained output.

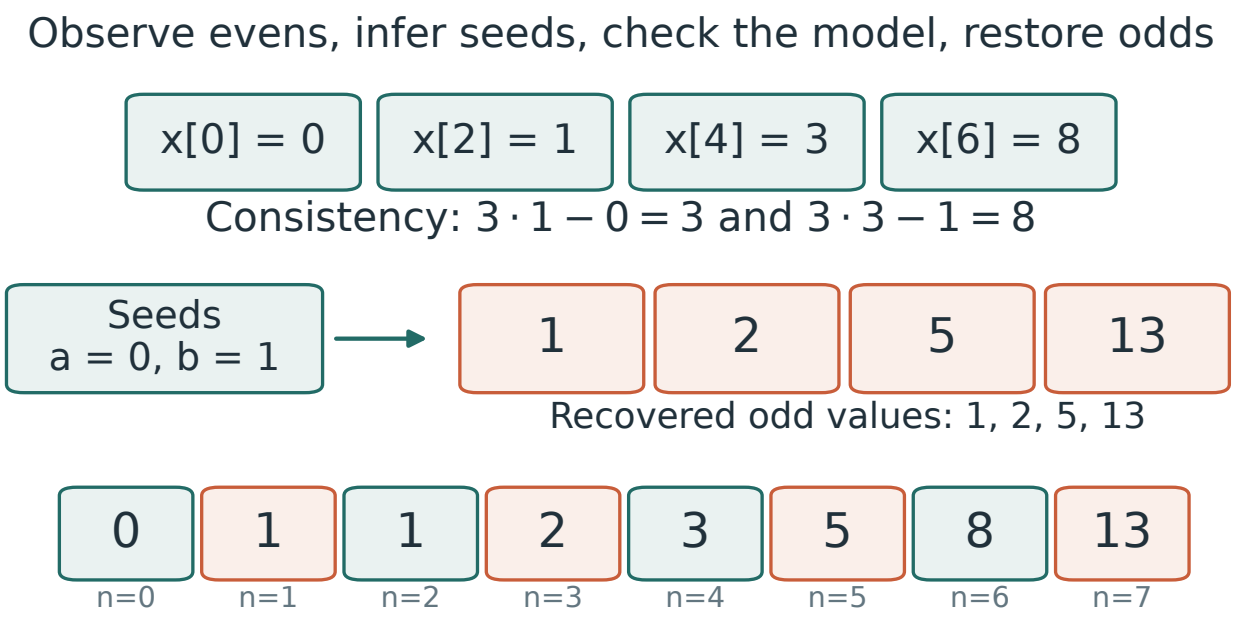
Work an example. Both retained inputs are $u + 3u^2 + 8u^3$. For P_8, the retained output is $-21u^4$. For Q, it is $-u^3 - 21u^4$. The coefficient of u^3 changes because the tap $-z$ carries the perturbation at index five to index six.

Carry forward. A projection must retain the information needed by the next operator.

Source and scope. Explicit finite counterexample, with $u = z^2$ under synthesis: no map U on even input channels can satisfy $\mathcal{R}_{2,0}(A(z)P) = U(\mathcal{R}_{2,0}P)$ for every finite integer polynomial P. Equal arguments would force equal values. This does not rule out recovery under an additional model.

CAPSTONE / 05 **LESSON 170**

Repair with a declared recurrence model



$$E_m = x[2m], \qquad a = E_0, \quad b = E_1 - E_0,$$
$$E_2 = 3E_1 - E_0, \qquad E_3 = 3E_2 - E_1$$

Read the figure. Keep the modulus-two observation, and require the eight-value record to obey $x[n+2] = x[n+1] + x[n]$ for $n = 0, \ldots, 5$, with unknown seeds (a, b). The first two even observations determine those seeds. The remaining two must pass the displayed consistency checks. The model then supplies the missing odd values.

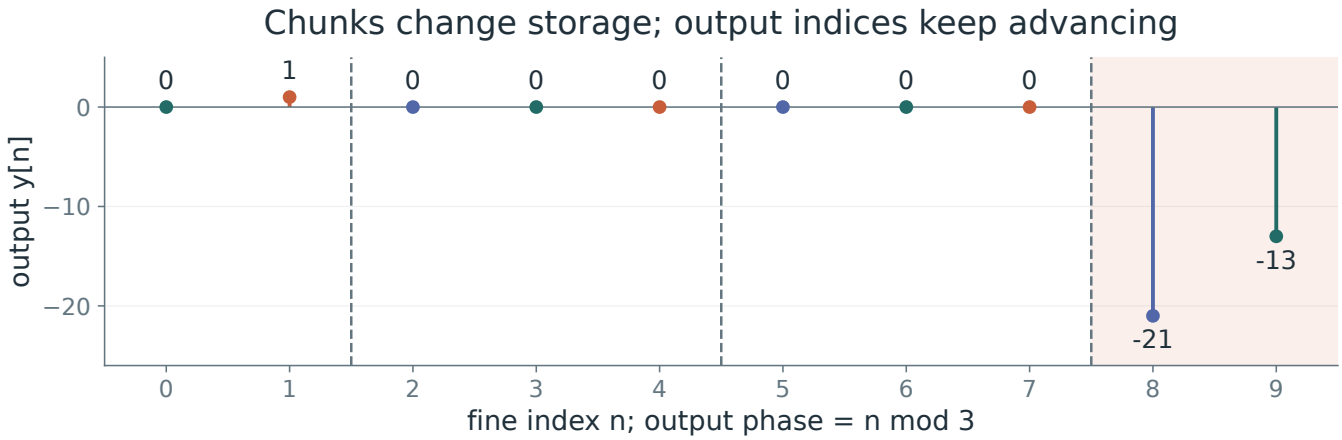
Work an example. For $E = (0, 1, 3, 8)$, the inferred seeds are $(0, 1)$. The checks give $3 \cdot 1 - 0 = 3$ and $3 \cdot 3 - 1 = 8$. Rebuilding from the seeds gives odd values $(1, 2, 5, 13)$ and restores C01's record. The perturbed Q has the same observations but lies outside this recurrence family.

Carry forward. A recovery hypothesis changes what the retained coordinates can identify.

Source and scope. Direct finite-state derivation: the even values are $(a, a+b, 2a+3b, 5a+8b)$. The two checks are necessary and sufficient for a unique completion inside this length-eight recurrence family. Exact tests cover 49 integer seed pairs and 196 inconsistent observation cases. No claim of recovery for arbitrary records or noisy observations is made.

CAPSTONE / 06 **LESSON 171**

Keep the history and the phase clock



After 2 inputs	After 5 inputs	After 8 inputs	Two-zero flush
history (0, 1)	history (2, 3)	history (8, 13)	-21 at phase 2
next phase 2	next phase 2	next phase 2	-13 at phase 0

$$S_n = (x[n-2], x[n-1];\ n \bmod 3), \qquad y[n] = x[n] - x[n-1] - x[n-2]$$

Read the figure. Return to the modulus-three output bank and execute the same filter in chunks of lengths two, three, and three. Before processing fine index n, the state holds the two preceding samples and the phase receiving $y[n]$. Dashed lines are chunk boundaries. The shaded tail comes from two explicit zero inputs after the last real sample.

Work an example. After eight inputs, the history is $(8, 13)$ and the next index is eight, phase two. The first zero gives -21 in phase two. The next gives -13 at index nine, phase zero. Continuing the clock yields output banks $(0, 0, 0, -13)$, $(1, 0, 0)$, and $(0, 0, -21)$, exactly as in C02.

Carry forward. A chunk boundary changes storage, while the filter history and global address continue.

Source and scope. Exact direct-form streaming and output routing, with zero history initially. All 128 positive chunk compositions of this eight-value record are checked against whole-record convolution and routing, including the two-zero flush. The stated history describes this implementation; resetting the phase clock changes output addresses even if the arithmetic samples remain correct.

Sequence, channel, and tap conventions

The three atlases contain 48 illustrated lessons. They connect sequence definitions with exact coefficient channels and finite operations. Each sequence retains its own starting index and normalization.

Convention	How to read the new lessons
Ordinary series	$A(z) = \sum_{n \geq 0} a_n z^n$. The coefficient is a_n.
Exponential series	$A(z) = \sum_{n \geq 0} a_n z^n / n!$. The sequence value is $n!$ times the coefficient.
Residue channels	$A_{M,r}(u) = \sum_{m \geq 0} a_{Mm+r} u^m$, with $0 \leq r < M$. The variable u advances one coarse block.
Finite taps	$y_n = \sum_k h_k a_{n-k}$. Negative sample indices are zero in the causal tap examples.
Recurrence taps	Applying a finite annihilating kernel can leave an initial-condition residual. Its reciprocal response can have infinitely many terms.
Refinement masks	A mask routes a finer-scale representation. Its reconstruction contract is stated separately from an arbitrary convolution filter.

OEIS identifications. Thirty official OEIS records were read from the export dated 7 October 2026, pinned to commit `2ce625d68f85e35e26e15c0d9681f69280c095e7`. The source package retains names, offsets, first eight indexed terms, entry revisions, and extraction hashes. The dated records identify the sequences; the displayed transforms have their own derivations and checks.

Related project source. The finite convolution and polyphase transfer examples also use *Projector-Resolved Seed Calculus V*, Section 4, Theorem 4.2, Proposition 4.4, Corollary 4.5, and Example 4.6. That source writes coarse delays as z^{-m}; these new lessons use u^m. The underlying delay operation is the same.

Reading sequence. Follow the sequence atlas for definitions and transforms, the polyphase atlas for exact routing, and the tap atlas for execution. These are applications of the coefficient language introduced in the foundations, with additional examples from combinatorics and signal processing.

Evidence. The source records, author checks, independent exact computations, and final page inspection are separate records. Finite computations corroborate the implementations in their stated ranges. No new Lean certificate, universal constant-coefficient recurrence for all sequences, or historical novelty claim is made by this addition.

Closing bridges and capstone. Thirteen further lessons connect seeds to surviving modes, carry taps through coefficient normalization, use Bernoulli translation differences, and distinguish causal from periodic inversion. The capstone follows one eight-term Fibonacci record through its complete residual, three channels, a local defect, discarded-channel obstruction, model-constrained repair, and streaming phase state. Their elementary derivations and bounded exact checks are recorded separately.

Notation and source map

Notation	Meaning in this guide
M, r, m	Coefficient modulus, residue address, and internal coefficient index.
a, β, k	Arithmetic decay, positive scale exponent, and nonnegative integer depth. In the Bernoulli–Hurwitz sections, a instead labels the declared translation argument.
q in I–IV	Integer character modulus. Use the actual modulus for the character's zero set.
α, γ	Positive continuous shapes. Arithmetic shape is $\alpha = (2a-1)/\beta$.
κ	Positive ladder label; the ordinary shape bridge is $\kappa = \alpha/2$.
q in VIII	Real deformation parameter $0 < q \leq 1$, with $q = 1$ the ordinary limit.
N	Total excitation in VII–VIII; a numerical cutoff elsewhere is labeled explicitly.
ν, E_k	Positive arithmetic moment measure and its moments. A signed companion is distinguished explicitly.
h, η	Real translation and modulation coordinates in ambiguity formulas.
$\mathcal{R}, P$	Signed orthogonal recoupling overlap and its entrywise squared measured channel.

In VIII.11, $\alpha, \beta, \gamma, \delta$ are local scalar q-Racah parameters. In VIII.12, a, b, c, d are local scalar Askey–Wilson parameters. Their roles differ from the arithmetic and continuous-shape notation above.

The source releases are the eight *Projector Generated Special Functions* archives collected in the first consolidation. Source notes name the paper and claim or construction. The source package includes the guide scripts, computed figure files, per-chapter computation checks, source hashes, correction register, and the 173-record special-function claim index.

The original series contains 431 PDF pages and 212 distinct archived vector figures. This guide uses newly prepared lesson figures and explanatory examples. The eight original releases and the 38-page consolidated manuscript are included in this collection under `series/` and in its collected reader. The earlier registry is contextual evidence, not an additional numbered volume.

Reproduction. Run the figure scripts, then compile `main.tex` three times with XeLaTeX. The packaged README gives commands and dependency versions. The computation records identify exact finite checks, floating-point residuals, quadrature tolerances, and declared truncation bounds. Visual inspection and mathematical review are recorded separately.